Pivotal role of GABAergic neurons of the basolateral amygdala in relaying hippocampal and serotonergic information

Marco Bocchio

St. John's College

MRC Brain Network Dynamics Unit

Department of Pharmacology

University of Oxford

This dissertation is submitted for the degree of

Doctor of Philosophy

Trinity Term 2016

To the pillars of my life

My parents, my brother, Teresa

"Share your knowledge.

It is a way to achieve immortality."

— Dalai Lama XIV

"The more I read,

the more I acquire,

the more certain I am

that I know nothing."

— Voltaire

Declaration

I hereby declare that the contents of this dissertation are original and have not been submitted in whole or in part for consideration for any other degree or qualification in this, or any other University. This dissertation contains less than 50,000 words including appendices, references and tables and has less than 250 figures.
All the results presented are the results of my own work, with the following exceptions.

Dr. Michäel Bazelot and I equally contributed to the project described in Chapter 2. Dr. Bazelot performed recordings, analysed the data and prepared panels for the experiments represented in Figure 2.6, Figure 2.7, Figure 2.8D, Figure 2.10, Figure 2.11, Figure 2.12, Figure 2.14A-G. He also collected part of the data shown in Figure 2.15.

Dr. Yu Kasugai performed anatomical analyses that produced the following figures in Chapter 2: Figure 2.5, Figure 2.8A-C, Figure 2.14H-I.

Lydia Oikonomidis and Dr. Stephen McHugh performed the fear conditioning experiments and analysed the data shown in Figure 3.4 and Figure 3.5A. Additionally, Lydia Oikonomidis performed, under my day-to-day supervision, immunohistochemical staining, stereological counting and analysed the data shown in Figure 3.5D-F.

Giulia Fucsina performed, under my day-to-day supervision, all the recordings that produced the data shown in Figure 3.11, together with some recordings for Figure 3.9. She also contributed to the analysis of these data.

Dr. Simon Fisher and Dr. Vladyslav V Vyazovskiy performed experiments and analysed data shown in Figure 4.4A-D.

The work carried out during my DPhil has given rise to the following articles.

Published

Bocchio M, Fisher SP, Unal G, Ellender TJ, Vyazovskiy VV & Capogna M. Sleep and serotonin modulate paracapsular nitric oxide synthase expressing neurons of the amygdala. eNeuro, *in press*.

Bocchio M & Capogna M (2014). Oscillatory substrates of fear and safety. Neuron 83:753–755.

Bazelot M*, **Bocchio M***, Kasugai Y, Dodson PD, Ferraguti F, Fischer D & Capogna M (2015). Hippocampal theta input to the amygdala shapes feedforward inhibition to gate heterosynaptic plasticity. Neuron 87:1290–1303. *co-first authors

Bocchio M, Fucsina G, Oikonomidis L, McHugh SB, Bannerman DM, Sharp T & Capogna M (2015). Increased serotonin transporter expression reduces fear and recruitment of parvalbumin interneurons of the amygdala. Neuropsychopharmacology 40:1–38.

Bocchio M, McHugh SB, Bannerman DM, Sharp T & Capogna M (2016). Serotonin, amygdala and fear: assembling the puzzle. Front. Neural Circuits 10:10:24.

Unpublished

Sengupta A**, Bocchio M**, Bannerman DM, Sharp T & Capogna M. Control of amygdala circuits by 5-HT neurons via glutamate and 5-HT co-transmission, *in revision*.

Bocchio M*, Nabavi S* & Capogna M. Synaptic plasticity and network oscillations in amygdala circuits for the storage and retrieval of emotional memories, *submitted*. *co-first authors

18/10/2016
Marco Bocchio

Acknowledgements

You wouldn't be reading this thesis if it weren't for the support, teaching and inspiration I received from innumerable wonderful people, both during my DPhil and during the journey that led me to it.

First of all, my gratitude goes to my supervisor, Prof. Marco Capogna, who chose me as DPhil candidate for his lab. He has been an amazing guide and friend in extremely difficult times. Thanks to his kind, careful and encouraging supervision, I never lost motivation or passion for research.

Sincere thanks to Prof. Peter Somogyi for the unprecedented support he provided to me and to our lab in these years, as well as for embodying an inspiring example of scientific integrity and passion for research.

The research I carried out during these years has greatly benefited from the collaboration with outstanding scientists. I thank Prof. David Bannerman, Dr. Stephen McHugh, Prof. Trevor Sharp, Dr. Paul Dodson, Dr. Vladyslav Vyazovskiy, Dr. Simon Fisher and Dr. Tommas Ellender for exceptional scientific contributions, feedbacks on data and helpful discussions, and for reading parts of my thesis. I also thank Prof. Francesco Ferraguti, and Dr. Yu Kasugai for extraordinary experimental work, and for solving my doubts on neuroanatomy. It was a pleasure and an honour to work with you all.

My deepest gratitude goes to Prof. Paul Bolam and Dr. Stephen McHugh for feedbacks on my work throughout my DPhil, and for carefully proofreading my thesis.

In addition, I thank Prof. Pete Magill and Prof. Peter Brown for precious support in the last months of my DPhil.

I am grateful to Dr. David Dupret for helpful hints for my future steps, and to Dr. Andy Sharott and Dr. Tim Viney for helpful feedbacks and discussions.

I am indebted to Katharine Whitworth, Jane Janson, Liz Norman and Ben Micklem for the impressive and patient technical support they provided.

During these years, I had the privilege to meet awesome people that helped me cope with the precarious situation of our lab without losing enthusiasm. I thank them for helpful scientific discussions, but especially for being great friends I could always count on: Abhilasha Joshi, Minas Salib, Dr. Michäel Bazelot, Ayesha Sengupta, Alexei Bygrave, Dimitrios Kotzadimitriou, Vasileios Eftychidis, Gunes Unal, Barbara Zonta, Anna-Kristin Kaufmann, Dr. Linda Katona, Lydia Oikonomidis, Giulia Fucsina, Dr. Stephanie Trouche, Dr. Vitor Lopes Dos Santos.

Thank you to all my friends for holding on to me in these four challenging years, despite I could not always find time for them.

This thesis is dedicated to my parents, Daniela and Paolo, my brother Andrea, and to (Dr.!) Teresa for all the love and support they have given me. I would not be here if it wasn't for you.

Abstract

The amygdala is a brain structure located in the temporal lobe that coordinates a wide range of emotional behaviours, in particular fear responses. Neuroimaging studies in humans have shown that in patients with post-traumatic stress disorder (PTSD) and phobias the amygdala is hyper-responsive to emotional stimuli. Thus, deciphering the neuronal mechanisms through which the amygdala orchestrates fear responses may improve treatments for pathological fear. In the last decades it has become evident from rodent experiments that neuronal circuits of the basolateral nucleus of the amygdala (BLA) control the acquisition and retrieval of fear memories. This is achieved through precise control of glutamatergic principal neuron (PN) activity by the release of γ-aminobutyric acid (GABA) from distinct populations of inhibitory neurons. Notably, the firing of BLA neurons is moulded by a vast array of extrinsic structures, namely sensory areas of the cortex, regions involved in memory processing and subcortical neuromodulatory afferents. However, the cellular mechanisms enabling the modulation of BLA circuits by afferent regions are still poorly understood.

The modulation of BLA circuits by the hippocampus and by the neuromodulator serotonin (5-HT) is of particular interest because these pathways may be of clinical importance. Nonetheless, these inputs have received little attention using circuit-based approaches. To fill this gap, I used a combination of *ex vivo* recordings from brain slices, *in vivo* recordings from anaesthetised mice, optogenetics, pharmacology, behavioural tests and immunohistochemistry. These experiments reveal that GABAergic neurons of the BLA are key nodes through which hippocampus and 5-HT modulate the excitability of PNs, the main output of the BLA. Specifically, optogenetic activation of ventral hippocampus pyramidal cells axons recruits BLA GABAergic interneurons that provide feedforward inhibition onto PNs. However, activation of hippocampal axons at theta frequency triggers a $GABA_B$-dependent depression of feedforward inhibition, creating time windows in which the induction of synaptic plasticity of parallel excitatory pathways is facilitated.

Furthermore, GABAergic interneurons expressing parvalbumin (PV) are a prominent target of the 5-HT action in the BLA. 5-HT depolarizes these cells via $5\text{-}HT_{2A}$ receptors, enhancing PN inhibition. Remarkably, in mice overexpressing the 5-HT transporter (5-HTT), an animal model of a genetic 5-HTT variation occurring in humans, PV+ interneurons display reduced depolarization by 5-HT and diminished recruitment by fear memory recall.

Finally, I report a novel GABAergic neuron type of the BLA that expresses high levels of neuronal nitric oxide synthase (nNOS). These cells are instead hyperpolarized by 5-HT via $5\text{-}HT_{1A}$ receptors, representing the first example of a BLA inhibitory neuron inhibited by this neuromodulator. Assessment of their c-Fos immunoreactivity showed that nNOS+ cells are active during sleep but not during wakefulness. Since 5-HT is highly released during the latter but not the former vigilance state, its hyperpolarizing action on nNOS+ cells provides a putative mechanism through which these cells are activated in a brain state-dependent fashion.

My results demonstrate that hippocampus and 5-HT influence BLA microcircuits via prominent action on GABAergic cells. Notably, 5-HT appears to exert GABAergic cell type-specific actions, suggesting that studying the impact of extrinsic pathways on defined amygdala neuron types can be decisive to comprehend the neural circuits controlling emotional learning.

Contents

LIST OF FIGURES XVI

LIST OF TABLES XVIII

LIST OF ABBREVIATIONS XIX

CHAPTER 1 GENERAL INTRODUCTION 1

1.1 THE AMYGDALA AND FEAR CONDITIONING 3

1.2 AMYGDALOID SUBDIVISIONS 4

1.3 CYTOARCHITECTURE AND PHYSIOLOGY OF THE BLA 6

1.3.1 GABAergic interneurons 7

1.4 DEVELOPMENTAL ORIGINS OF BLA NEURONS 10

1.5 MECHANISMS OF GABAERGIC TRANSMISSION 12

1.5.1 $GABA_A$ receptors 13

1.5.2 $GABA_B$ receptors 15

1.6 AFFERENT CONNECTIVITY OF THE BLA 17

1.6.1 Sensory inputs 17

1.6.2 Inputs from areas involved in memory processing 18

1.6.3 Subcortical neuromodulatory inputs 19

1.7 EFFERENT CONNECTIVITY OF THE BLA 19

1.7.1 Intra-amygdaloid outputs 19

1.7.2 Extra-amygdaloid outputs 20

1.8 BLA CIRCUIT DYNAMICS UNDERLYING FEAR CONDITIONING 22

1.9 SYNAPTIC PLASTICITY IN BLA CIRCUITS 24

1.9.1 General mechanisms of synaptic plasticity 25

1.9.2 Long-term synaptic plasticity in BLA circuits 31

1.10 NEURONAL OSCILLATIONS IN BLA AND INTERCONNECTED STRUCTURES 35

1.10.1 Theta oscillations *35*

1.10.2 Gamma oscillations *37*

1.11 AIMS OF THIS THESIS 38

CHAPTER 2 HIPPOCAMPAL MODULATION OF BASAL AMYGDALA CIRCUITS VIA FEEDFORWARD INTERNEURONS 39

2.1 INTRODUCTION 39

2.2 MATERIALS AND METHODS 41

2.2.1 Animals *41*

2.2.2 Expression of ChR2 in vCA1 pyramidal cells *41*

2.2.3 In vivo recordings *42*

2.2.4 Analysis of in vivo recordings *43*

2.2.5 Ex vivo recordings and analysis *44*

2.2.6 Histological processing *48*

2.2.7 Statistical analyses *52*

2.2.8 Drugs *52*

2.3 RESULTS 53

2.3.1 Differential firing of BA PNs and INs during theta oscillations in vivo *53*

2.3.2 Theta stimulation of vCA1 pyramidal cell axons inhibits BA PNs and activates INs in vivo *56*

2.3.3 Theta stimulation of vCA1 axons drives feedforward inhibition in BA PNs *60*

2.3.4 Cellular dynamics evoked by theta stimulation of vCA1 axons *67*

2.3.5 Theta stimulation of vCA1 axons gates heterosynaptic plasticity in BA PNs *74*

2.4 DISCUSSION 77

CHAPTER 3 IMPACT OF SEROTONIN TRANSPORTER OVEREXPRESSION ON FEAR AND BASAL AMYGDALA PARVALBUMIN INTERNEURONS 85

3.1 INTRODUCTION 85

3.1.1 5-HT innervation of BLA neurons *85*

3.1.2 Impact of genetic variations of the 5-HT transporter on the BLA and fear learning 90

3.2 MATERIALS AND METHODS 92

3.2.1 Animals 92

3.2.2 Fear conditioning 92

3.2.3 Fear conditioning data analysis 93

3.2.4 Ex vivo recordings 94

3.2.5 Analysis of ex vivo recordings 95

3.2.6 Immunohistochemistry 96

3.2.7 Quantification of c-Fos+ and PV+ neurons 97

3.2.8 Statistical analyses 97

3.2.9 Drugs 98

3.3 RESULTS 99

3.3.1 5-HTT overexpression leads to impaired PV+ IN activation by fear memory 99

3.3.2 5-HTT overexpression leads to impaired 5-HT excitation of PV+ INs 102

3.3.3 5-HTT overexpression causes reduced 5-HT-evoked inhibitory drive onto PNs 106

3.3.4 Impaired 5-HT$_{2A}$ function underlies deficit in 5-HT-evoked inhibition of PNs 111

3.3.5 5-HTT overexpression causes deficient 5-HT modulation of PN firing 113

3.4 DISCUSSION 114

CHAPTER 4 BIDIRECTIONAL MODULATION OF PARACAPSULAR NITRIC OXIDE SYNTHASE EXPRESSING NEURONS BY SLEEP AND SEROTONIN 119

4.1 INTRODUCTION 119

4.2 MATERIALS AND METHODS 121

4.2.1 Animals 121

4.2.2 Ex vivo recordings 122

4.2.3 Analysis of ex vivo recordings 123

4.2.4 EEG Recordings and Sleep deprivation 123

4.3 HISTOLOGICAL PROCEDURES 126

4.3.1 Immunohistochemistry *126*

4.3.2 Quantification of overlap between neurochemical markers *127*

4.3.3 Drugs *128*

4.3.4 Statistical analyses *128*

4.4 RESULTS 129

4.4.1 Neurochemical profile of nNOS+ type I neurons of the BLA *129*

4.4.2 Anatomical and electrophysiological features of paracapsular nNOS+ type I neurons *131*

4.4.3 Sleep activates pc-nNOS+ neurons *135*

4.4.4 5-HT inhibits pc-nNOS+ neurons *138*

4.5 DISCUSSION 141

CHAPTER 5 GENERAL DISCUSSION AND FUTURE DIRECTIONS 147

5.1 MAIN FINDINGS AND IMPLICATIONS 147

5.2 TECHNICAL LIMITATIONS AND FUTURE DIRECTIONS 151

5.2.1 Achieving more physiological stimulations of afferent pathways of the BLA *152*

5.2.2 Achieving temporally-precise read-out of BLA neuronal activity *153*

5.2.3 Achieving temporally-precise manipulation of BLA neuronal activity *155*

5.2.4 Probing the interplay between hippocampal and 5-HT inputs to the BLA *156*

5.3 CONCLUSION 157

REFERENCES 159

List of figures

Figure 1.1. Defined pathways to and from the amygdala that modulate specific behaviours. 2
Figure 1.2. Nuclei of the rat amygdaloid complex. 5
Figure 1.3 Nuclear subdivisions, GABAergic cell density and information flow in the mouse amygdala. 6
Figure 1.4. Neurochemically-defined GABAergic neurons of the rodent BLA. 8
Figure 1.5. Connectivity between BLA PNs and IN populations in rodents. 9
Figure 1.6 Schematic of the developmental origins of amygdala neurons. 11
Figure 1.7. Subcellular localization and function of $GABA_B$ receptors. 16
Figure 1.8 Basolateral amygdala and central amygdala connectivity 20
Figure 1.9. Activity of PV+ and SOM+ INs of the BLA during fear conditioning. 23
Figure 1.10. Model of AMPA trafficking during LTP and LTD 29
Figure 1.11. Long-term synaptic plasticity related to conditioned fear in the basolateral amygdaloid complex. 34
Figure 1.12 Increased theta oscillations in CA1 and LA of rats during fear memory retrieval 36
Figure 2.1. Clustering of PNs and INs and histologically verified positions of fibre optic tip and recorded neurons. 54
Figure 2.2. Differential firing frequencies of PNs and INs during theta epochs. 55
Figure 2.3. Responses to high frequency stimulation of vCA1 pyramidal cell soma or axons expressing ultrafast ChR2/YFP. 57
Figure 2.4 Optical TBS of hippocampal axons inhibits PNs and triggers firing in INs of the BA *in vivo*. 58
Figure 2.5. CA1 pyramidal cells axons form asymmetric synapses onto both INs and PNs of the BA. 59
Figure 2.6 Activation of hippocampal inputs provides feedforward inhibition of BA principal neurons. 62
Figure 2.7 Optogenetic stimulation of vCA1 axons evokes heterogeneous responses in BA PNs. 63
Figure 2.8. ITCs receive excitatory inputs from vCA1 pyramidal cells. 64
Figure 2.9. Optical TBS of hippocampal axons transiently inhibits PNs and triggers firing in INs ex vivo. 65
Figure 2.10. High intensity TBS of vCA1 axons transiently depresses the firing of PNs in a $GABA_B$ receptor manner, and reliably activates INs *ex vivo*. 66
Figure 2.11. Synaptic dynamics evoked by TBS in BA PNs and INs. 68
Figure 2.12. Blockade of GABA reuptake evokes depression of feedforward inhibition in PNs with vCA1-evoked $GABA_A$ receptor only IPSPs. 69
Figure 2.13. Optical stimulation of vCA1 axons with firing pattern of a vCA1 pyramidal cell recapitulates synaptic dynamics evoked by TBS. 70
Figure 2.14. Presynaptic $GABA_B$ receptors at BA IN-PN synapses mediate depression of feedforward inhibition 72
Figure 2.15. TBS of hippocampal inputs gates LTP of LA-BA synapses. 75
Figure 2.16. Blockade of $GABA_A$ receptors does not unmask LA-BA PN LTP, and TBS of vCA1 axons does not evoke vCA1-BA PN LTP. 76
Figure 2.17 Model of the vCA1-BA circuit. 76

Figure 3.1. 5-HT innervation of the mouse amygdala. 85
Figure 3.2. 5-HT innervation and 5-HT receptor expression of BLA neurons. 88
Figure 3.3. Reduced fear-evoked BLA theta oscillations in 5-HTTOE mice. 91
Figure 3.4. WT and 5-HTTOE mice freezing levels during fear memory retrieval. 99
Figure 3.5. Increased 5-HTT expression leads to reduced fear recruitment of PV+ INs of the BLA. 101
Figure 3.6. 5-HT-evoked depolarization of PV+ INs of the BA is impaired in 5-HTTOE mice. 104
Figure 3.7. Direct 5-HT depolarization of PV+ INs via 5-HT_{2A} receptors 105
Figure 3.8. Indirect 5-HT inhibition of PNs is impaired in 5-HTTOE mice. 107
Figure 3.9. 5-HT promotes indirect inhibition of BA PNs of the primarily through 5-HT_{2A} receptors. 109
Figure 3.10. Impairment of 5-HT facilitation of GABA release leads to reduced hyperpolarization of PNs. 110
Figure 3.11. 5-HT_{2A}-mediated inhibition of PNs is impaired in 5-HTTOE mice. 112
Figure 3.12. Increased 5-HTT expression alters the output of BA PNs. 113
Figure 3.13. Model of amygdala circuit alterations in 5-HTTOE mice. 114
Figure 4.1. Neurochemical profile and localisation of nNOS+ type I neurons of the BLA. 130
Figure 4.2. Anatomical features of pc-nNOS+ neurons 132
Figure 4.3. Electrophysiological features of pc-nNOS+ neurons 134
Figure 4.4. pc-nNOS+ neurons are activated during sleep 137
Figure 4.5. 5-HT inhibits pc-nNOS+ neurons. 139
Figure 4.6. Direct hyperpolarization of pc-nNOS+ neurons by 5-HT via 5-HT_{1A} receptors 140

List of tables

Table 1.1. Main GABAergic classes of the rodent BLA and some of their characteristics. 8
Table 3.1. 5-HT receptor types expressed in the BLA and their function 89
Table 3.2. Electrophysiological membrane properties of PV+ INs recorded from WT and 5-HTTOE mice. 103
Table 3.3. Electrophysiological differences between BA PNs and PV+ INs. 103
Table 3.4. Overexpression of the 5-HTT does not alter electrophysiological membrane properties of BA PNs 108
Table 4.1. Electrophysiological parameters of pc-nNOS+ neurons..... 135

List of abbreviations

A

ACSF	artificial cerebrospinal fluid
AHP	after-hyperpolarization

B

BA	basal amygdala
BLA	basolateral amygdala
BM	basomedial amygdala
BSA	bovine serum albumin

C

CaMKII	calcium/calmodulin-dependent protein kinase II
CB	calbindin
CCK	cholecystokinin
CeA	central amygdala
CeL	centrolateral amygdala
CeM	centromedial amygdala
ChR2	Channelrhodopsin-2
CR	calretinin
CS	conditioned stimulus
CV	coefficient of variation

D

DIC	differential interference contrast
DRN	dorsal raphe nuclei

E

Erk	extracellular signal-regulated kinase
EC	external capsule
EEG	electroencephalogram

E_{IPSC}	reversal potential of the inhibitory postsynaptic current
EMG	electromyography
EPSC	excitatory postsynaptic current
EPSP	excitatory postsynaptic potential

F

fAHP	fast after-hyperpolarization
FFT	fast Fourier transform
FRIL	freeze-fracture replica immunolabelling

G

GABA	γ-aminobutyric acid
GFP	green fluorescent protein
GIRK	G protein-coupled inwardly rectifying potassium channels

H

HPC	hippocampus
5-HT	5-hydroxytriptamine, serotonin
5-HTT	serotonin transporter
5-HTTKO	serotonin transporter knock-out mice
5-HTTLPR	serotonin transporter-linked polymorphic region
5-HTTOE	serotonin transporter overexpressing mice

I

IC	intermediate capsule
IEI	inter-event interval
IN	interneuron
IPSC	inhibitory postsynaptic current
IPSP	inhibitory postsynaptic potential
ISI	inter-spike interval
ITC	intercalated cell

L

LA	lateral amygdala
LFP	local field potential
LTP	long-term potentiation

M

MAPK	mitogen-activated protein kinase
mGluR	metabotropic glutamate receptor
mPFC	medial prefrontal cortex

N

NA	numerical aperture
NK1	neurokinin-1 receptor
nNOS	neuronal nitric oxide synthase
NPY	neuropeptide Y
NREM	non rapid eye movement sleep

P

PB	phosphate buffer
PBS	phosphate-buffered saline
PFA	paraformaldehyde
PKA	protein kinase A
PKC	protein kinase C
PKMζ	protein kinase Mζ
PSP	postsynaptic potential
PSTH	peri-stimulus time histogram
PTSD	post-traumatic stress disorder
PV	parvalbumin

R

REM	rapid eye movement
R_{in}	input resistance
RT	room temperature

S

SD	sleep deprivation
SDS	sodium dodecyl sulphate
SEM	standard error of the mean
SOM	somatostatin
SSRI	selective serotonin reuptake inhibitor
STDP	spike-timing-dependent plasticity
SWA	slow wave activity

T

T-BS	tris-buffered saline
TBS	theta burst stimulation
TeA	temporal association cortex
TEM	transmission electron microscopy

U

US	unconditioned stimulus

V

VGAT	vesicular γ-aminobutyric acid transporter
VIP	vasoactive intestinal peptide
V_m	membrane potential

W

WT	wild-type

Y

YFP	yellow fluorescent protein

Chapter 1 General introduction

We all remember more vividly emotionally significant experiences compared to dull ones, regardless of whether they are pleasant or traumatic. For example, listening to a song can instil feelings towards a person or a context we associate the song with. From an evolutionary perspective, affectively arousing events are exceptionally engraved in memory because they are likely to carry information that is precious for survival or reproductive success. Several theories have tried to explain the neural mechanisms leading to the strengthening of emotionally-relevant memories. Among these, the 'emotional tagging' theory (Bergado et al., 2011) proposes that affective experiences activate the amygdala, a brain structure located in the temporal lobe, which in turns modulates synaptic plasticity in areas encoding declarative memories, such as the hippocampus (Vouimba et al., 2007).

Understanding the neural mechanisms of emotional memory formation and storage is critical because recall of emotional memories can become maladaptive. In anxiety disorders and post-traumatic stress disorder (PTSD), excessive fear or anguish can be triggered by objects (or contexts) in the absence of an actual threat, significantly impacting people's lives. The amygdala appears to be a promising target for therapeutic efforts aimed at ameliorating pathological fear. In fact, besides its modulation of hippocampal-dependent memories, the amygdala is a crucial site for storage and retrieval of emotional memories.

In humans, lesions of the amygdala reduce or abolish perception of innate fear and associative fear learning (Adolphs et al., 1995, 1999; Bechara et al., 1995; LaBar et al., 1995; Young et al., 1995). Accumulating evidence from electrophysiological and behavioural rodent studies suggests that synaptic interactions between amygdala neurons control the association

between an aversive (or appetitive) stimulus to a neutral cue (Duvarci and Paré, 2014; Gründemann and Lüthi, 2015; Janak and Tye, 2015). However, amygdala circuits do not work independently, but via dynamic interactions with several other brain structures with which they are wired (Pitkänen, 2000; Freese and Amaral, 2009). As a result, emotional memories, leading to defensive or appetitive behavioural responses, rely on the interplay between the amygdala and regions such as the hippocampus (HPC), the medial prefrontal cortex (mPFC), the nucleus accumbens, the periacqueductal gray and the hypothalamus (Figure 1.1; Janak and Tye, 2015; Tovote et al., 2015).

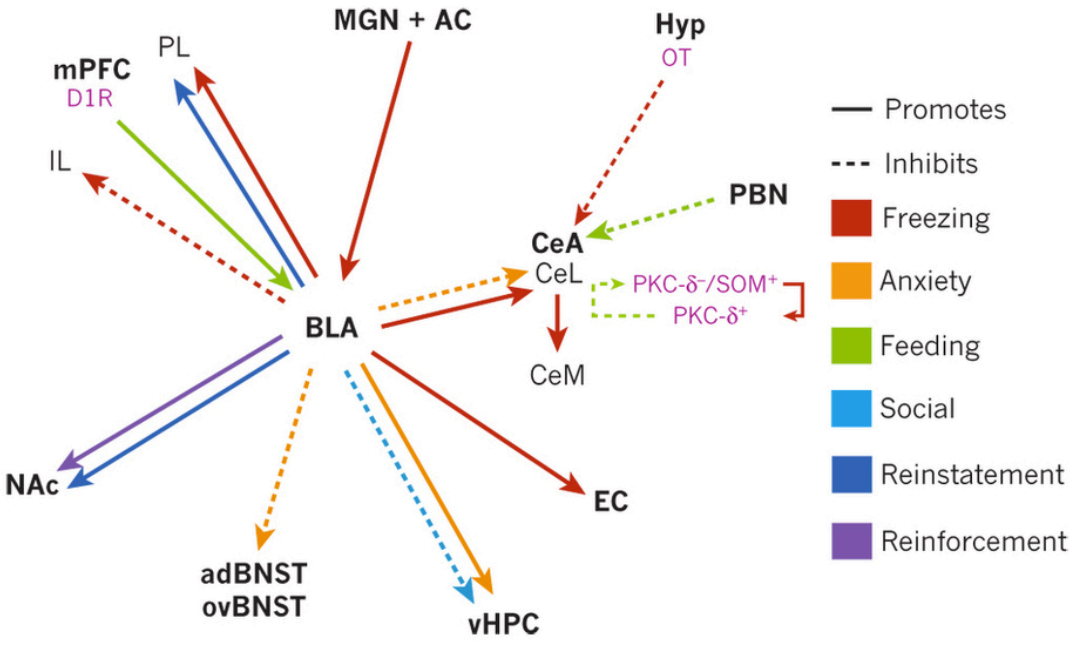

Figure 1.1. Defined pathways to and from the amygdala that modulate specific behaviours.
Simplified schematic depicting amygdala afferent and efferent pathways that have been shown to promote or inhibit certain behaviours. For simplicity, projections that are anatomically or electrophysiologically defined but have not been shown to have a causal relationship with behaviour are omitted. AC, auditory cortex; adBNST, anterodorsal bed nucleus of the stria terminalis; CeA, central nucleus of the amygdala; CeL, lateral CeA; CeM, medial CeA; D1R, dopamine 1 receptor; EC, entorhinal cortex; Hyp, hypothalamus; IL, infralimbic; MGN, medial geniculate nucleus; mPFC, medial prefrontal cortex; NAc, nucleus accumbens; OT, oxytocin; ovBNST, oval nucleus of the BNST; PBN, parabrachial nucleus; PKC, protein kinase C; PL, prelimbic; SOM, somatostatin; vHPC, ventral hippocampus. From Janak and Tye, 2015.

Hence, unravelling the mechanisms through which amygdala neurons interact with each other and with cells located in other brain areas can significantly contribute to our understanding of how the brain encodes aversive information. Crucially, the past decades of neuropharmacological research did not lead to major breakthroughs for the treatment of

mental illnesses, including pathological anxiety and fear (Hyman, 2014). Reprogramming of dysfunctional fear and anxiety circuits, which involve amygdala neurons, represents a promising road forward to achieve better treatments for anxiety disorders and PTSD (Tye, 2014).

1.1 The amygdala and fear conditioning

A widely used paradigm to study emotional learning in the laboratory is Pavlovian fear conditioning, in which an initially neutral cue (conditioned stimulus, CS; a visual cue, a tone, an odour or a context) is paired with a noxious unconditioned stimulus (US) such as a mild footshock. The *acquisition* of an associative fear memory during this *training* session causes the presentation of the CS only during the *test* (or *fear retrieval*) session to elicit fear responses. The *expression* of conditioned fear is assessed by measuring skin conductance responses in humans (Ressler and Mayberg, 2007). In rodents, fear expression is evaluated by measuring the time spent freezing (Bolles, 1970), which is a stereotypic defensive behaviour (defined as the absence of movement apart from respiration) that occurs in response to perceived danger or threat (LeDoux, 2000). Alternatively, fear memories are probed via the fear-potentiated startle paradigm, which gauges the startle reflex elicited by a sudden loud noise. This reflex is exaggerated in the presence of a cue (a light or tone) that has previously been paired with footshock (Davis et al., 1993).

Data collected from human experiments support the idea that the amygdala is a key brain area that encodes fear memories. Unilateral or bilateral amygdala damage leads to strong deficits in fear conditioning (Bechara et al., 1995; LaBar et al., 1995). Additionally, functional neuroimaging experiments have shown that the human amygdala is activated during both presentation of fearful faces (Morris et al., 1996) and fear conditioning (LaBar et

al., 1998; Büchel et al., 1999). Rodent studies have clarified that the basolateral nucleus of the amygdala (BLA) is essential for both fear memory acquisition and expression, because lesion of this nucleus either before training or before fear memory retrieval reduce fear responses during the test session (LeDoux et al., 1990b; Campeau and Davis, 1995; Cousens and Otto, 1998). It is important to keep in mind, however, that the BLA does not only regulate fear responses, but also other behaviours such as anxiety (Tye et al., 2011; Felix-Ortiz et al., 2013) and reward processing (Gore et al., 2015; Namburi et al., 2015), suggesting it may play a more general role in determining stimulus valence.

1.2 Amygdaloid subdivisions

Based on cytoarchitecture, immunohistochemical analyses and afferent/efferent projections, the amygdala has been subdivided in several nuclei (Figure 1.2). The most widely adopted classification for rodents encompasses the BLA, often subdivided into lateral (LA) and basal (BA) nuclei, the basomedial amygdala (BM), the central amygdala (CeA), which includes the centrolateral (CeL) and centromedial (CeM) nuclei, intercalated cells (ITCs) surrounding the BLA, the medial amygdala and the cortical amygdala (Pitkänen, 2000; Sah et al., 2003). The BLA, CeA and ITCs have received particular attention, mainly due to their unambiguous involvement in fear conditioning (Duvarci and Paré, 2014). While the BLA displays a cortex-like cytoarchitecture (McDonald, 1984), the CeA and the ITCs between BLA and CeA are considered a ventrocaudal extension of the striatum (McDonald, 1982a).

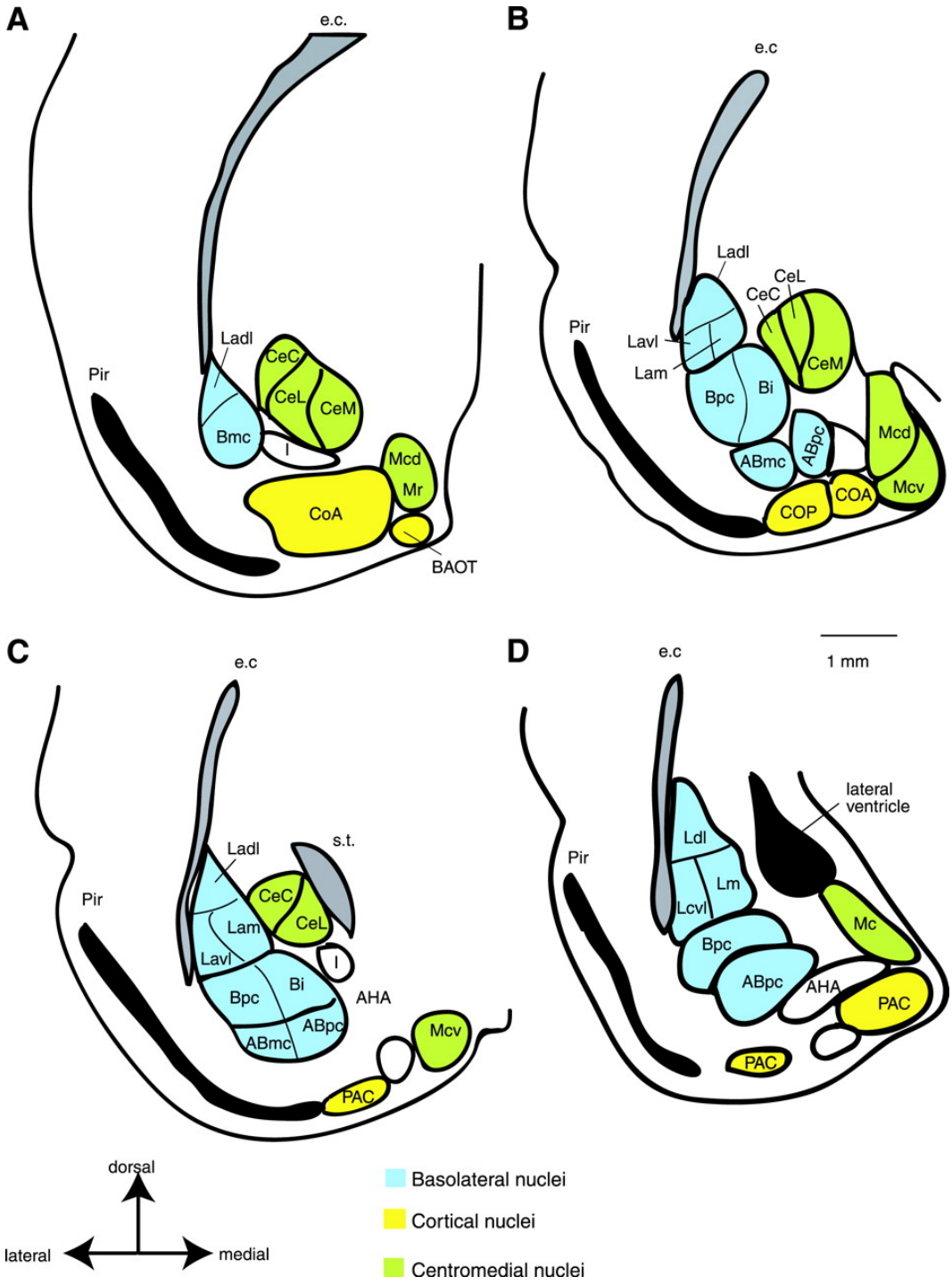

Figure 1.2. Nuclei of the rat amygdaloid complex.
Coronal sections are drawn from rostral (*A*) to caudal (*D*). Areas in blue form part of the basolateral group, areas in yellow are the cortical group, and areas in green form the centromedial group. ABmc, accessory basal magnocellular subdivision; ABpc, accessory basal parvicellular subdivision; Bpc, basal nucleus magnocellular subdivision; e.c., external capsule; Ladl, lateral amygdala medial subdivision; Lam, lateral amygdala medial subdivision; Lavl, lateral amygdala ventrolateral subdivision; Mcd, medial amygdala dorsal subdivision; Mcv, medial amygdala ventral subdivision; Mr, medial amygdala rostral subdivision; Pir, piriform cortex; s.t., stria terminalis. From Sah et al., 2003.

1.3 Cytoarchitecture and physiology of the BLA

The BLA is delimited by two fibre bundles: the external capsule laterally, separating BLA from cortex, and the intermediate capsule medially, separating the BLA from the central amygdala (CeA). Both BLA subdivisions, LA and BA, are formed for ~80% by glutamatergic principal neurons (PNs) and for ~20% by interneurons (INs) releasing γ-aminobutyric acid (GABA; McDonald, 1982b; Figure 1.3).

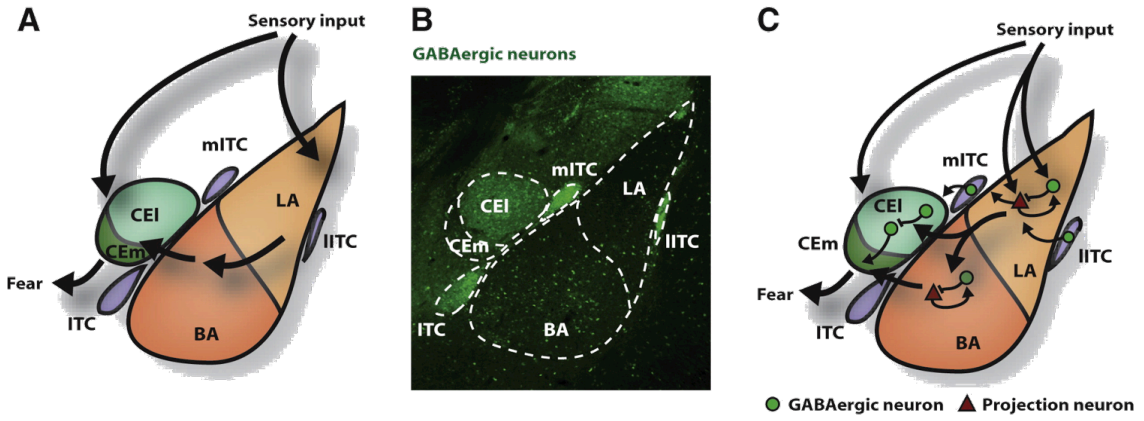

Figure 1.3 Nuclear subdivisions, GABAergic cell density and information flow in the mouse amygdala.
A, Scheme of the basic organization and overall flow of information within the amygdaloid complex. LA, lateral amygdala; BA, basal amygdala; CEl, latero-capsular subdivision of the central amygdala; CEm, medial subdivision of the central amygdala; mITC, medial intercalated cell cluster; lITC, lateral intercalated cell cluster. **B**, Coronal brain slice stained for the 67 kD isoform of the enzyme glutamic acid decarboxylase (GAD67) illustrating the distribution of GABAergic neurons across the amygdaloid complex. **C**, Simplified scheme of the organization and function of inhibitory INs in amygdaloid nuclei. In the LA and BA, local INs are part of feedforward and feedback circuits and control projection neuron output. lITCs and mITCs relay feedforward inhibition to the BLA and CeA, respectively. CEm output neurons are under inhibitory control originating in CEl. Intrinsic CEl inhibition may also participate in controlling CEl output. From Ehrlich et al., 2009.

The PNs are pyramidal-like projection neurons with spiny dendrites (McDonald, 1982b). Their axons innervate other brain regions distally and, through collaterals, other PNs and INs locally (McDonald, 1982b; Millhouse and DeOlmos, 1983). *In vivo,* PNs fire at low rates (usually <1 Hz), with higher activity during sleep than wake (Paré and Gaudreau, 1996). During behaviour, subsets of PNs display dramatic phasic increases in firing rate following presentation of sensory, noxious and/or aversive stimuli (Beyeler et al., 2016). *Ex vivo*, when

depolarized with current injections, they display adapting firing and broad (~1 ms half-width in whole-cell mode) action potentials (Sosulina et al., 2006).

1.3.1 GABAergic interneurons

The activity of PNs is tightly coordinated by the release of GABA from BLA INs, which are characterized by mostly aspiny dendrites and widely branching local axons (McDonald, 1982b; Millhouse and DeOlmos, 1983). BLA INs provide feedforward inhibition to PNs and act as gatekeepers of synaptic plasticity because depression of feedforward inhibition is necessary to induce long-term potentiation (LTP) at excitatory synapses onto PNs (Watanabe et al., 1995; Bissière et al., 2003; Tully et al., 2007; Morozov et al., 2011). As with cortical (Ascoli et al., 2008) and HPC INs (Klausberger and Somogyi, 2008), BLA INs are heterogeneous and can be classified in several ways. A widely used method of IN categorisation involves their neurochemical examination, and particularly the expression of different Ca^{2+} binding proteins or neuropeptides (Figure 1.4 and Table 1.1).

Notably, INs expressing different neurochemical markers often display distinct intrinsic membrane properties, brain state-dependent firing and innervation of subcellular compartments of postsynaptic neurons (Figure 1.5; Muller et al., 2006, 2007a; Woodruff and Sah, 2007a; Jasnow et al., 2009; Bienvenu et al., 2012; Manko et al., 2012). Two BLA IN populations have received particular attention so far: the parvalbumin (PV)-expressing INs, accounting for ~50% of the of BLA INs (McDonald and Mascagni, 2001a), and somatostatin (SOM)-expressing, accounting for 11-18% (McDonald and Mascagni, 2002). The PV+ INs are more abundant in the BA (McDonald and Mascagni, 2001a) and target the perisomatic region of PNs (Bienvenu et al., 2012; Wolff et al., 2014).

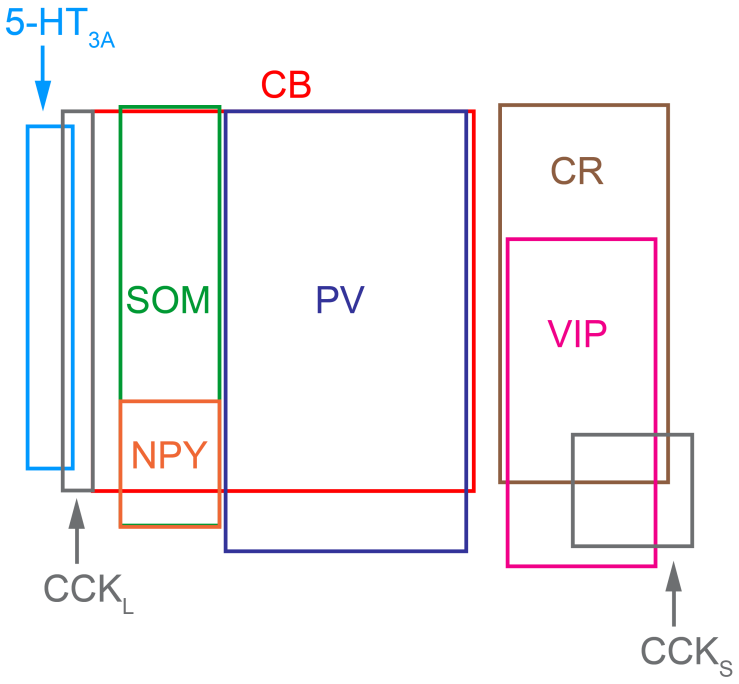

Figure 1.4. Neurochemically-defined GABAergic neurons of the rodent BLA. Schematic diagram representing abundance and overlap of main neurochemical markers for GABAergic neurons in the rodent BLA.
Abbreviations:
CB: calbindin;
CCK: cholecystokinin;
CCK_L large CCK+ cells;
CCK_S: small CCK+ cells;
CR: calretinin
NPY: neuropeptide Y;
PV: parvalbumin;
SOM: somatostatin;
VIP: vasoactive intestinal peptide.
Adapted from Mascagni and McDonald, 2007 and Truitt et al., 2009.

Table 1.1. Main GABAergic classes of the rodent BLA and some of their characteristics.
Abbreviations: CB: calbindin; CB1R: cannabinoid 1 receptor; CCK: cholecystokinin; NPY: neuropeptide Y; PN: principal neuron; PV: parvalbumin; SOM: somatostatin; VIP: vasoactive intestinal peptide.

Immunohistochemical markers	% of BLA interneurons	Known cell types	Known postsynaptic targets in BLA	Activity during fear conditioning	References
PV (high overlap with CB)	~50%	Basket; axo-axonic; AStria projecting	PN; PV; SOM (perisomatic region)	Inhibited during US, excited during CS (on average)	(McDonald and Mascagni, 2001a, 2004; Muller et al., 2005, 2006; Rainnie et al., 2006; Woodruff and Sah, 2007a, 2007b; Bienvenu et al., 2012; Wolff et al., 2014)
SOM (high overlap with CB)	11-18%	Dendrite-projecting INs; Long-range projection neurons	PN (mostly distal dendrites, few proximal dendrites and somata); PV; VIP; SOM	Inhibited during US and CS (on average)	(McDonald, 1989; McDonald and Mascagni, 2002; Muller et al., 2007a; Wolff et al., 2014)
NPY (high overlap with CB and SOM)	3-6%	Neurogliaform; long-range projection neurons	PN (mostly proximal dendrites, but also soma)	Unknown	(McDonald, 1989; Manko et al., 2012; McDonald et al., 2012)
CCK/CB1R (some overlap with CB, minor overlap with 5-HT3A)	~4%	Large CCK	PN, CCK (perisomatic region)	Unknown	(McDonald and Mascagni, 2001b; Mascagni and McDonald, 2003; Jasnow et al., 2009; Trouche et al., 2013)
VIP (high overlap with CR, some overlap with CCK)	~10%	Small CCK; VIP (CCK-)	PN (soma and distal dendrites), CB, VIP	Unknown	(Mascagni and McDonald, 2003; Muller et al., 2003)
5-HT3A (but CCK-negative)	6-12%	Unknown	Unknown	Unknown	(Mascagni and McDonald, 2007)

In vivo, PV+ INs fire at higher rates than PNs (Muller et al., 2006; Bienvenu et al., 2012). *Ex vivo*, they often display a fast-spiking phenotype upon depolarization, with high rates (up to ~100 Hz) of short (~0.5 ms half-width) action potentials and little adaptation (Rainnie et al., 2006).

In contrast, SOM+ INs innervate the distal dendrites of PNs (Muller et al., 2007a) and display longer spikes than PV+ INs (Wolff et al., 2014). Most of the PV+ and SOM+ INs, together with large INs expressing cholecystokinin (CCK) and many neurons releasing neuropeptide Y (NPY), co-express calbindin (CB; McDonald and Mascagni, 2001a, 2002; Mascagni and McDonald, 2003). The CB+ INs represent the largest class of BLA INs, accounting for ~60% of all GABAergic cells (McDonald and Mascagni, 2001a).

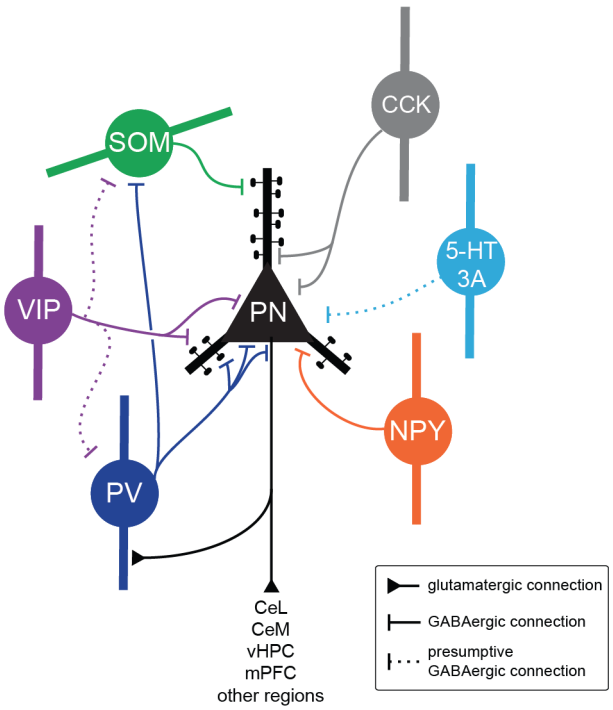

Figure 1.5. Connectivity between BLA PNs and IN populations in rodents.
PV+ INs target the perisomatic region of PNs (soma, proximal dendrites, axon initial segment), but also inhibit SOM+ INs, disinhibiting PNs distal dendrites. VIP+ INs inhibit PN soma and proximal dendrites. As they have been shown to inhibit high numbers of calbindin-expressing (CB+) INs, and the majority of CB+ INs are either PV+ or SOM+, VIP+ INs could target PV+ and/or SOM+ INs, disinhibiting specific PN subcellular compartments, but this has not been demonstrated. The VIP-negative CB1R+ population of CCK+ INs (also known as large CCK+ INs) target the perisomatic region of PNs. Although it is likely that CCK-negative 5-HT_{3A}+ INs contact PNs, this has not been shown experimentally. A subset of NPY+ INs (neurogliaform cells) have been shown to inhibit PN soma and proximal dendrites.

Another major population of BLA GABAergic neurons is formed by calretinin (CR)-expressing INs, which include cells that also express vasointestinal peptide (VIP), together with small CCK+ neurons (most of which are also VIP+; Mascagni and McDonald, 2003). In neocortex, VIP+ INs deliver prominent inhibition to SOM+ INs, and therefore promote disinhibition of pyramidal cells dendrites (Pfeffer et al., 2013). In the BLA, VIP+ INs have

been shown to target PNs and CB+ INs (Muller et al., 2003). As most of BLA PV+ and SOM+ INs co-express CB, their inhibition by VIP+ INs is likely, but not yet demonstrated. In addition to local INs, feedforward inhibition onto BLA PNs is driven by ITCs located in external and intermediate capsules that surround the BLA (Millhouse, 1986; Asede et al., 2015; Bienvenu et al., 2015).

Crucially, the heterogeneity of GABAergic neurons of the BLA has been poorly explored compared to other brain regions (Capogna, 2014). As a result, our knowledge of the functional specialisation of defined GABAergic cell types is still limited. To understand the principles of operation of the BLA, it is critical to gain insights on: (1) synaptic interactions between distinct GABAergic populations; (2) subtypes of SOM+ INs; (3) physiological role of CCK+ and VIP+ INs; (4) neurochemical identity and function of neuronal nitric oxide synthase (nNOS)-expressing cells, which are abundant in HPC and neocortex (Tricoire and Vitalis, 2012); (5) long-range projecting GABAergic neurons (McDonald et al., 2012; McDonald and Zaric, 2015).

1.4 Developmental origins of BLA neurons

Recent advances in genetic fate mapping approaches have shed light on a remarkable developmental logic governing the emergence of defined cortical neuron types. Understanding the developmental origins of amygdala neurons could strengthen our understanding of amygdala circuits in health and disease.

Genetic fate mapping studies using Dbx1-Cre mice suggest that the PNs of the BLA derive from the ventral pallium (Bielle et al., 2005; Hirata et al., 2009). Since, the CeA displays morphological features resembling the striatum (McDonald, 1982a) and the striatum contains Isl1+ neurons deriving from the ventral lateral ganglionic eminence (vLGE; Stenman

et al., 2003), it was hypothesized that CeA neuron would also derive from the vLGE (Swanson and Petrovich, 1998). Indeed, using Isl1-Cre mice, Waclaw et al. identified CeA neurons originating from the vLGE (Waclaw et al., 2010).

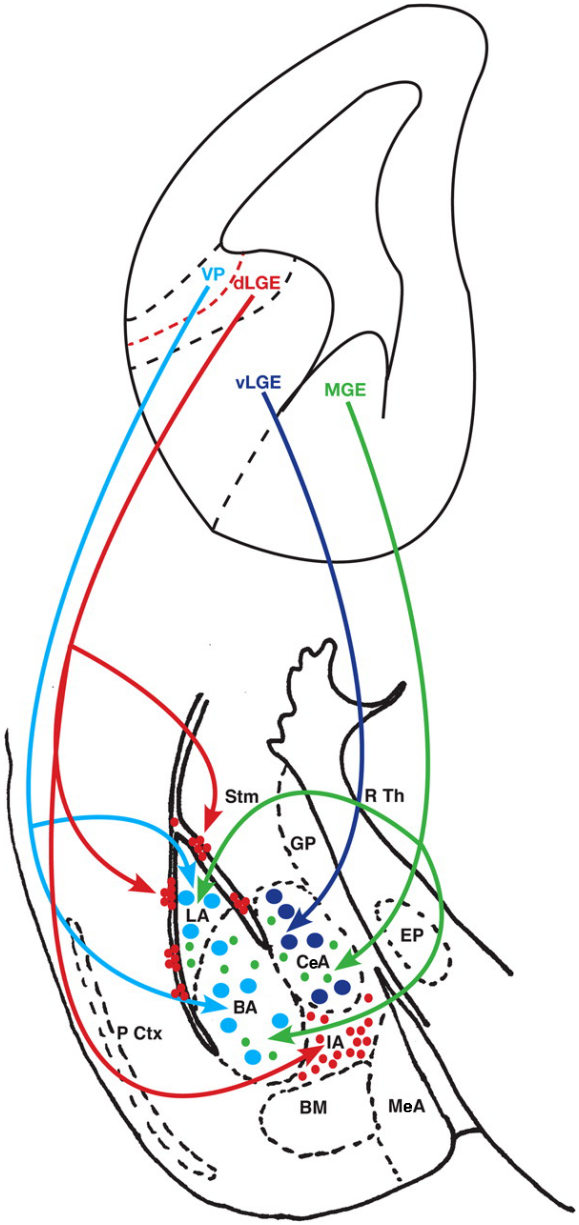

Figure 1.6 Schematic of the developmental origins of amygdala neurons.
The ventral pallium (VP; in blue) gives rise to PNs in the LA and BA. The dorsal lateral ganglionic eminence (dLGE; in red) is a major source of the paracapsular ITCs and intercalated mass of the amygdala (IA) of the amygdala. The ventral lateral ganglionic eminence (vLGE, in purple) gives rise to projection neurons in the CeA. The MGE (in green) and likely CGE generate INs that reside in the LA, BA, and CeA. Stm, Striatum; P Ctx, pyriform cortex; BM, basomedial amygdala; R Th, reticular thalamus; EP, entopeduncular nucleus; GP, globus pallidus; MeA, medial amygdala. Adapted from Waclaw et al., 2010.

Another genetic fate map study of Nkx2.1+ neurons, which originate from the medial ganglionic eminence (MGE), revealed that these progenitors give rise to scattered neurons in the BLA and in the CeA (Xu et al., 2008). A subsequent study showed that Dlx5/6+ progenitors, which populate MGE, caudal ganglionic eminence (CGE) and LGE give rise to

neurons in the BLA (Waclaw et al., 2010). Additionally, the authors demonstrated that many of these cells expressed CB and CR. Since cortical GABAergic neurons expressing CB (e.g. PV+ and SOM+ cells) derive from the MGE, whereas many neurons expressing CR derive from the CGE (Wonders and Anderson, 2006), it is likely that CB+ and CR+ interneurons in the BLA share similar origins with their cortical counterpart. In line with this hypothesis, an embryonic transplantation study has shown that CGE progenitors also contribute to neurons of the BLA, BM and CeA (Nery et al., 2002).

Progenitors from the preoptic area, which form a relatively uniform population of GABAergic IN in neocortex (Gelman et al., 2009), might also contribute to BLA INs. Finally, examination of amygdala neurons in Sp8 knock-out mice (Sp8 is a transcription factor expressed in the dorsal LGE, dLGE) has revealed that ITCs originate from the dLGE (Waclaw et al., 2010).

1.5 Mechanisms of GABAergic transmission

GABAergic INs of the BLA fine-tune the activity of PNs via release of GABA, which is synthesised via two forms of glutamic acid decarboxylase (GAD): GAD67, expressed throughout the cytoplasm, and GAD65, more frequently localised in presynaptic terminals (Soghomonian and Martin, 1998). GABA is then packed into vesicles in the presynaptic terminals. This is achieved via activity of the vesicular GABA transporter (VGAT; McIntire et al., 1997), although other mechanisms might also come into play.

Voltage-gated P/Q-type ($Ca_v2.1$) and N-type ($Ca_v2.2$) Ca^{2+} channels open upon depolarization triggered by an action potential. This causes fusion of the vesicles containing glutamate with the plasma membrane, leading to GABA release from axon terminals (Südhof, 2004). Importantly, release of single vesicles occurs also in absence of presynaptic

depolarization (Fatt and Katz, 1952), leading to so-called miniature synaptic potentials (miniature EPSPs in the case of glutamate). GABA release from axon terminals activates postsynaptic ionotropic ($GABA_A$) GABA receptors and in some synapses also metabotropic ($GABA_B$) GABA receptors. At some synapses, $GABA_A$ and $GABA_B$ receptors are also located presynaptically.

1.5.1 $GABA_A$ receptors

$GABA_A$ receptors are pentameric assemblies of subunits that form an ion channel permeable to Cl^- (Connors et al., 1988) and bicarbonate (Kaila et al., 1993). Postsynaptic $GABA_A$ receptors can be both synaptic and extrasynaptic (Somogyi et al., 1989), thereby requiring different magnitudes of GABA release to be activated. Sixteen $GABA_A$ subunits have been cloned from the mammalian central nervous system: α1–6, β1–3, γ1–3, δ, ε, θ, π (Farrant and Nusser, 2005). However, the most common patterns of $GABA_A$ assembly involve α, β2 and γ2 subunits. Crucially, the composition of $GABA_A$ receptors by specific subunits varies depending on: (1) the cellular compartment that is innervated by the GABAergic terminal (e.g. Somogyi et al., 1989); (2) the synaptic or extrasynaptic location of the $GABA_A$ receptor (Nusser et al., 1998); (3) the kinetics and desensitization of the postsynaptic response (e.g. Bianchi and Macdonald, 2002; Labrakakis et al., 2014). In the BLA, inhibitory postsynaptic currents (IPSCs) onto PNs appear to be mediated by $GABA_A$ receptors carrying α1 and α2 subunits (Marowsky et al., 2004). In particular, α1 subunits, which confer slower kinetics to $GABA_A$ IPSCs compared to α2 subunits (Vicini et al., 2001), are expressed at synapses between CB1R+ INs (likely large CCK+ cells) and PNs (Marowsky et al., 2004)

One mode of GABAergic transmission via postsynaptic $GABA_A$ receptors is the "**phasic**" mode. This consists of high (0.3-1 mM) and brief (<0.5 ms) GABA transients

leading to postsynaptic $GABA_A$ receptor activation and opening of Cl^- conductances. At resting membrane potential (V_m), this generally causes a fast (≤20 ms) inhibitory postsynaptic potential (IPSP) because V_m is more positive than the equilibrium potential for Cl^-. In these conditions, the Cl^- flows inside the cell from the extracellular space, thereby causing fast membrane hyperpolarization. In some cases, however, GABAergic transmission can be depolarizing, thereby excitatory. This occurs when the equilibrium potential for Cl^- is more positive than resting V_m. An example of this phenomenon happens during development in the central nervous system, when the Na^+-K^+-$2Cl^-$ 1 (NKCC1) co-transporter that pumps Cl^- into the cell dominates on the K^+/Cl^- co-transporter 2 (KCC2) that pumps Cl^- out (Ben-Ari, 2002). Another example is represented by the synapses formed by cortical PV+ axo-axonic cells, which can cause depolarizing potential via GABA release since the axon initial segment of pyramidal cells lacks KCC2 (Szabadics et al., 2006).

Another mechanism through which $GABA_A$ transmission can inhibit the activity of the postsynaptic cell is via "shunting". The shunting effect consists in an increase in the postsynaptic membrane conductance that triggers a decrease in input resistance (R_{in}). In presence of shunting IPSPs, simultaneous excitatory postsynaptic potentials (EPSPs) are less able to change V_m, even when GABA is depolarizing (Staley and Mody, 1992). Notably, synaptic integration depends on the postsynaptic cellular compartment onto GABA is released. That is, when activation of postsynaptic $GABA_A$ receptors results in EPSPs, GABA release onto the soma can be shunting, and thus inhibitory, if it is coincident to a glutamatergic EPSP (Gulledge and Stuart, 2003). Conversely, GABA release onto the dendrites is always excitatory in these conditions (Gulledge and Stuart, 2003).

In contrast to phasic transmission, "**tonic**" activation of extrasynaptic $GABA_A$ receptors by 'ambient' GABA in the extracellular space regulates resting V_m and the integration of excitatory inputs in a longer timescale. Evidence suggests that ambient GABA arises from the

same vesicles that contribute to phasic transmission (Glykys and Mody, 2007), but other mechanisms of release might also come into play. Tonic $GABA_A$ currents provide constant membrane hyperpolarization (Kaneda et al., 1995) and constant decrease in R_{in}, so that current injections generate a higher firing rate when extrasynaptic $GABA_A$ receptors are blocked (Brickley et al., 1996). Furthermore, tonic $GABA_A$ activation decreases synaptic gain, because a higher frequency of EPSPs is necessary to trigger a given firing rate compared to when $GABA_A$ receptors are blocked (Mitchell and Silver, 2003). Finally, $GABA_A$ receptors are also expressed presynaptically. Evidence suggests that their activation leads to axon terminal depolarization and enhanced neurotransmitter release (Stell et al., 2007; Xiao et al., 2007; Ruiz et al., 2010).

Interestingly, an intermediate kinetic between tonic and phasic $GABA_A$ transmission exists. This has been termed $GABA_{A,slow}$ and it is mediated by volume transmission of GABA by neurogliaform cells (Szabadics et al., 2007; Manko et al., 2012), leading to activation of extrasynaptic $GABA_A$ receptors in postsynaptic PNs.

1.5.2 $GABA_B$ receptors

$GABA_B$ receptors are G-protein coupled receptors consisting of seven trans-membrane proteins. These receptors are therefore metabotropic and display a heterodimeric structure, being assembled with both $GABA_{B1}$ and $GABA_{B2}$ subunits (Bettler et al., 2004). The $GABA_{B1}$ subunit is the GABA-binding domain (Galvez et al., 2000), but both subunits are essential for correct receptor assembly and function (Jones et al., 1998). Similarly to $GABA_A$ receptors, $GABA_B$ receptors are expressed both postsynaptically and presynaptically (Figure 1.7). Most postsynaptic $GABA_B$ receptors are located extrasynaptically (Kulik et al., 2003), thereby requiring GABA spillover from the synaptic cleft to be activated (Scanziani, 2000). These receptors are primarily assembled with $GABA_{B1b}$ subunits, and only sporadically on

$GABA_{B1a}$ (Vigot et al., 2006). Their activation causes the downstream opening of G protein-coupled inwardly rectifying K^+ channels (GIRK), leading to slow membrane hyperpolarization (≥100 ms; Lüscher et al., 1997).

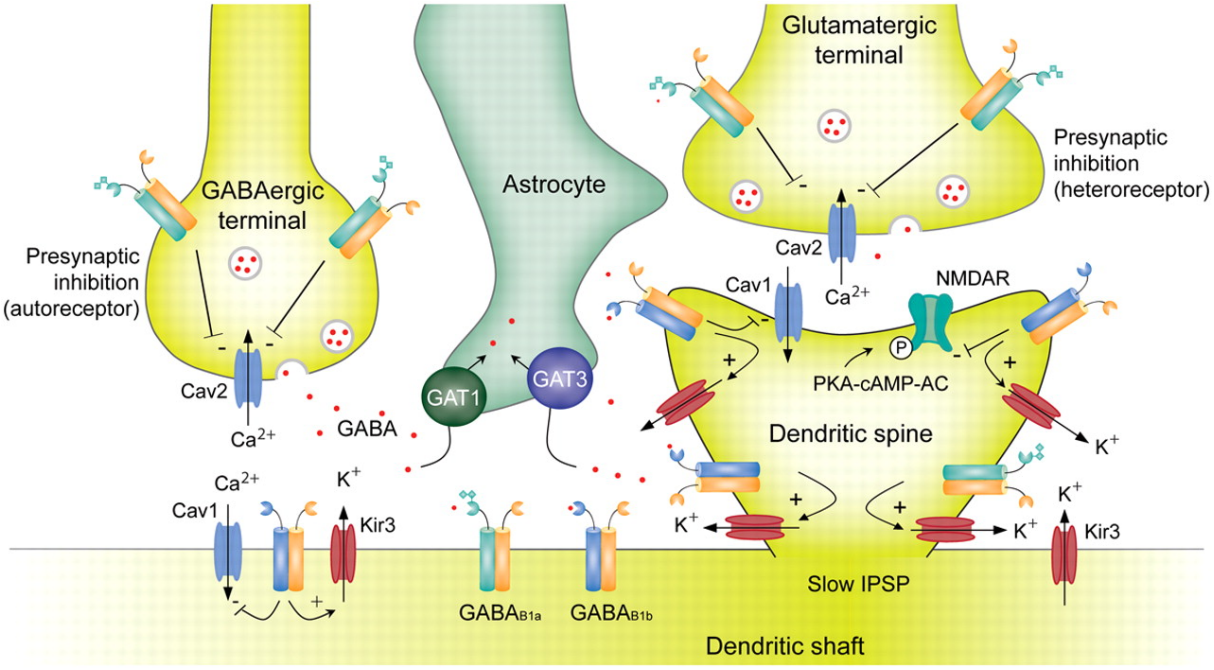

Figure 1.7. Subcellular localization and function of $GABA_B$ receptors.
$GABA_B$ receptors are located presynaptically, postsynaptically, and on extrasynaptic membranes. In general, the $GABA_{B1a}$ isoform is expressed in glutamatergic terminals, whereas both the $GABA_{B1a}$ and $GABA_{B1b}$ isoforms are present at GABAergic terminals. Postsynaptic $GABA_B$ receptors can be formed from either $GABA_{B1a}$ or $GABA_{B1b}$ subunits, depending on the cell type. Presynaptic $GABA_B$ receptors, via the Gβγ subunit of $G_{i/o}$, inhibit N-type ($Ca_v2.2$) or P/Q type ($Ca_v2.1$) Ca^{2+} channels, which results in inhibition of neurotransmitter release. Presynaptic $GABA_B$ receptors act as autoreceptors in GABAergic terminals and heteroreceptors in glutamatergic and other terminals. Postsynaptic $GABA_B$ receptors, also via the Gβγ subunit, trigger the opening of several K^+ channels, particularly inward rectifying K^+ channels (Kir3), which results in hyperpolarization and slow inhibitory postsynaptic potentials (IPSPs). $GABA_B$ receptors on dendritic spines counteract the excitatory synaptic currents elicited by glutamate; they promote voltage-sensitive block of NMDA receptor, inhibit protein kinase (PKA) activity that is necessary for phosphorylation and upregulation of NMDA receptors, and inhibit voltage-gated L-type (Ca_v1) Ca^{2+} channels. The extent of $GABA_B$ receptor signalling after GABA release may be determined by both GABA diffusivity and uptake via GABA transporters (GAT) expressed in astrocytes; GAT1 is expressed perisynaptically and GAT3 is also expressed in distal extrasynaptic regions. AC = adenylyl cyclase; cAMP = cyclic adenosine monophosphate. From Benarroch, 2012.

Presynaptic $GABA_B$ receptors are expressed extrasynaptically on glutamatergic terminals, but to a lesser extent also on GABAergic terminals (Kulik et al., 2003). These receptors are mainly assembled with the $GABA_{B1a}$ subunit (Vigot et al., 2006) and their activation leads to inhibition of P/Q- and/or N-type Ca^{2+} channels (Scholz and Miller, 1991; Mintz and Bean, 1993), thereby dampening neurotransmitter release. Similarly to $GABA_A$ receptors, also $GABA_B$ receptors can be activated tonically by ambient GABA, and this mode

of transmission can influence both membrane excitability and neurotransmitter release (Mapelli et al., 2009; Wang et al., 2015).

1.6 Afferent connectivity of the BLA

Most of the knowledge of the extrinsic connectivity of the BLA arises from tracer experiments in rats, although cats and monkeys have also been extensively studied. In all three species, these investigations have revealed that the BLA receives a wide variety of extrinsic inputs, which include sensory cortex and thalamus, medial temporal lobe structures involved in memory processes, the hypothalamus and subcortical neuromodulatory systems located in the midbrain and in the basal forebrain (Pitkänen, 2000; Sah et al., 2003). This suggests that the computation performed by BLA circuits to control defensive (and other emotional) responses is heavily influenced by a myriad of inputs conveying both sensory and cognitive information.

1.6.1 Sensory inputs

Afferent glutamatergic synapses on BLA neurons relay information from all sensory modalities: auditory, visual, olfactory, gustatory, somatosensory and visceral. Its major source are higher order association areas of the cerebral cortex (McDonald, 1998), but inputs from sensory thalamus are also prominent (Sah et al., 2003).

Olfactory inputs reach the BLA from the piriform cortex and the anterior olfactory nucleus (Luskin and Price, 1983). Auditory information is relayed from both the temporal association cortex (TeA; Shi and Cassell, 1997) and the medial geniculate nucleus of the thalamus (LeDoux et al., 1990a, 1991). Likewise, visual inputs arise from both higher order cortical visual areas and the thalamus (Shi and Davis, 2001), while gustatory and visceral afferents originate from the insular cortex (Shi and Cassell, 1998a). Crucially, all these

sensory pathways can convey information about a CS in a fear conditioning paradigm. However, cortical and thalamic auditory inputs have been object of intense investigation because of the wider use of an auditory CS for the study of conditioned fear.

Somatosensory innervation of the BLA emanates from the parietal insular cortex (Shi and Cassell, 1998b) and also from the thalamus (Linke et al., 2000). Hence, these pathways appear to be involved in the relay of the US during fear conditioning. Importantly, the afferent structures mentioned above project more densely to the LA than the BA. As a result, the LA is thought to be the nucleus in which prominent associative learning occurs via synaptic plasticity of CS and US pathways (Pitkänen et al., 1997; Duvarci and Paré, 2014), as it will be further described.

1.6.2 Inputs from areas involved in memory processing

In contrast to sensory inputs, innervation of the BLA by areas implicated in memory processing appears to follow the reverse pattern. Namely, perirhinal (Shi and Cassell, 1999) and entorhinal (McDonald and Mascagni, 1997) cortices, together with the ventral CA1 (vCA1) region of the HPC and the subiculum (Kishi et al., 2006) project more densely to the BA than to the LA. This is largely true also for the medial prefrontal cortex (mPFC), although its infralimbic part mainly targets the ventromedial part of the LA, with weaker projection to the BA (McDonald et al., 1996). Similarly to sensory inputs, these pathways are mostly glutamatergic. Interestingly, GABAergic projection neurons in the vCA1 have been shown to project to the BLA (Müller et al., 2012). However, the precise molecular identity, as well as their impact on the BLA microcircuit remains elusive. Collectively, these anatomical data suggest that LA and BA might perform different computations due to differential innervation by sensory and memory systems.

1.6.3 Subcortical neuromodulatory inputs

Besides being targeted by axons originating in the structures mentioned above, the BLA is under the tight control of several neuromodulatory pathways arising from subcortical nuclei. Specifically, cholinergic innervation of the BLA arises from the basal forebrain (Ben-Ari et al., 1977; Woolf and Butcher, 1982). In addition, monoaminergic pathways heavily innervate the BLA, namely axons releasing serotonin (5-hydroxytryptamine, 5-HT) from the dorsal raphe nucleus (DRN; Abrams et al., 2004; Muller et al., 2007b), dopaminergic terminals from the ventral tegmental area (Pinard et al., 2008; Muller et al., 2009), noradrenergic fibres from the locus coeruleus (Zhang et al., 2013) and histaminergic projections from the tuberomammillary nucleus (Köhler et al., 1985; Panula et al., 1989). Monoaminergic and cholinergic inputs, classically linked with arousal and memory functions (Robbins, 1997), appear to modulate fear memory via action on BLA circuits (McIntyre et al., 1998; Rosenkranz and Grace, 2002; LaLumiere et al., 2003; Tran et al., 2013). Like the inputs from the medial temporal lobe, most of these neuromodulatory pathways innervate the BA more densely than the LA (Woolf and Butcher, 1982; Muller et al., 2007b, 2009; Zhang et al., 2013).

1.7 Efferent connectivity of the BLA

1.7.1 Intra-amygdaloid outputs

BLA projections primarily run dorsoventrally, with LA PNs projecting to the BA, and both LA and BA PNs targeting, among other brain regions, the CeA (Figure 1.8; Krettek and Price, 1977a; Smith and Paré, 1994; Pitkänen et al., 1997).

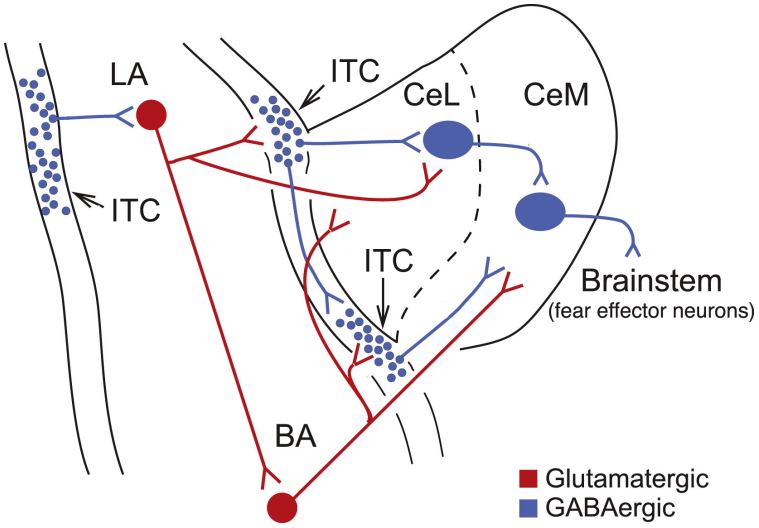

Figure 1.8 Basolateral amygdala and central amygdala connectivity
Dorsoventral information flow from the LA to CeM. LA PNs project to BA PNs and to CeL, but not to CeM. BA PNs project to both CeL and CeM but do not project back to the LA. Lateral ITCs mediate feedforward inhibition of BLA neurons for glutamatergic inputs from the external capsule, while medial ITCs provide feedforward inhibition to CeA neurons. Adapted from Duvarci and Pare, 2014.

The CeA contains mostly GABAergic neurons that innervate several brain stem nuclei to promote defensive responses (Veening et al., 1984; Ciocchi et al., 2010; Penzo et al., 2014). For example, CeA projections to the nucleus reticularis pontis caudalis mediate acoustic startle reflexes (Davis et al., 1982), whereas CeA projections to the periaqueductal grey region mediate freezing responses (LeDoux et al., 1988; Amorapanth et al., 1999; Penzo et al., 2014). More specifically, LA PNs appear to innervate the centrolateral nucleus (CeL) of the amygdala, but not the centromedial nucleus (CeM; Smith and Paré, 1994). In contrast, BA PNs project to both CeL and CeM (Savander et al., 1995). This is important because the majority of CeA neurons able to trigger defensive responses appear to reside in the CeM subdivision (Ciocchi et al., 2010; Duvarci and Paré, 2014).

1.7.2 Extra-amygdaloid outputs

Besides receiving a vast array of inputs relaying different modalities, BLA neurons (mainly glutamatergic PNs) target a multitude of brain areas. A detailed functional mapping of BLA extra-amygdaloid projections is critical, because different outputs appear to promote different behavioural responses (Felix-Ortiz et al., 2013; Senn et al., 2014; Namburi et al., 2015).

Several neocortical areas are targeted by the BLA (Pitkänen, 2000). Specifically, both LA and BA innervate lateral entorhinal, insular and perirhinal cortices, but the projections from LA PNs are more prominent (Krettek and Price, 1977a). The postrhinal area is instead targeted by the LA only, whereas both prelimbic and infralimbic regions of the medial prefrontal cortex (mPFC) are mainly innervated by BA PNs (Krettek and Price, 1977a).

In addition to neocortex, the BLA projects densely to the hippocampal formation (Pitkänen et al., 2000). In particular, the BA innervates vCA1 and subiculum, whereas the LA displays sparser projections (Krettek and Price, 1977b; Pikkarainen et al., 1999). However, both LA and BA target the parasubiculum (Pikkarainen et al., 1999). BLA output to the HPC appears to be important for aspects of emotionality because optogenetic manipulation of BLA PN axons synapsing onto ventral HPC (vHPC) neurons modulates anxiety-related behaviours (Felix-Ortiz et al., 2013).

Finally, BA PNs project to various subcortical areas, namely the mediodorsal thalamus (Krettek and Price, 1977a), the ventral caudate-putamen and the nucleus accumbens (McDonald, 1991), the bed nucleus of the stria terminalis and the substantia innominata (Krettek and Price, 1978). Among these, the innervation of the ventral striatum has recently become intriguing because of its involvement in reward learning (Bauer et al., 2007; Stuber et al., 2011; Namburi et al., 2015).

Thus, besides prominent innervation of CeA neurons, BLA PNs release glutamate onto neurons in several extra-amygdaloid regions. At least for some pathways, there appears to be remarkable functional segregation among BLA PNs, with target-specificity causally linked to elicited behavioural responses. For example, PNs targeting the prelimbic region of the mPFC are active during fear states, and their activity increases fear memory recall. In contrast, PNs innervating infralimbic area of the mPFC are active during fear extinction and their firing reduces fear memory recall (Senn et al., 2014). Furthermore, PNs projecting to the CeA

encode aversive stimuli, whereas PNs projecting to the nucleus accumbens encode palatable stimuli (Namburi et al., 2015; Beyeler et al., 2016).

1.8 BLA circuit dynamics underlying fear conditioning

A simple circuit model of fear learning (Sigurdsson et al., 2007) suggests that information about tone and shock is relayed, via glutamatergic fibres, from sensory areas of thalamus and cortex to PNs of the LA. Prior to fear conditioning these inputs are weak, but pairing the tone and shock together strengthens CS inputs to specific ensembles of PNs via LTP (Romanski et al., 1993; McKernan and Shinnick-Gallagher, 1997; Rogan et al., 1997; Collins and Paré, 2000; Goosens et al., 2003; Nabavi et al., 2014). Subsets of PNs of the BA are also excited by the CS, with stronger excitation following fear conditioning (Herry et al., 2008), and this could occur either by direct inputs from sensory and somatosensory cortex and thalamus, or via relay of CS and US by LA PNs. Thus, according to current views, subsequent presentations of the CS are able to drive freezing responses primarily due to stronger recruitment of LA PNs, presumably via their downstream action on BA and CeA neurons (Sigurdsson et al., 2007; Duvarci and Paré, 2014).

Different IN types control the inhibition of BLA PNs at different locations on the somato-dendritic tree (Figure 1.9; Muller et al., 2006, 2007a). As previously described, PV+ INs innervate the perisomatic region of PNs, heavily influencing PN spike timing (Muller et al., 2006; Woodruff and Sah, 2007b; Wolff et al., 2014), whereas SOM+ INs innervate the PN distal dendrites, controlling the integration of excitatory inputs (Muller et al., 2007a; Wolff et al., 2014). During US presentation, both PV+ INs and SOM+ INs are inhibited, leading to robust somatic and dendritic disinhibition of PNs (Wolff et al., 2014).

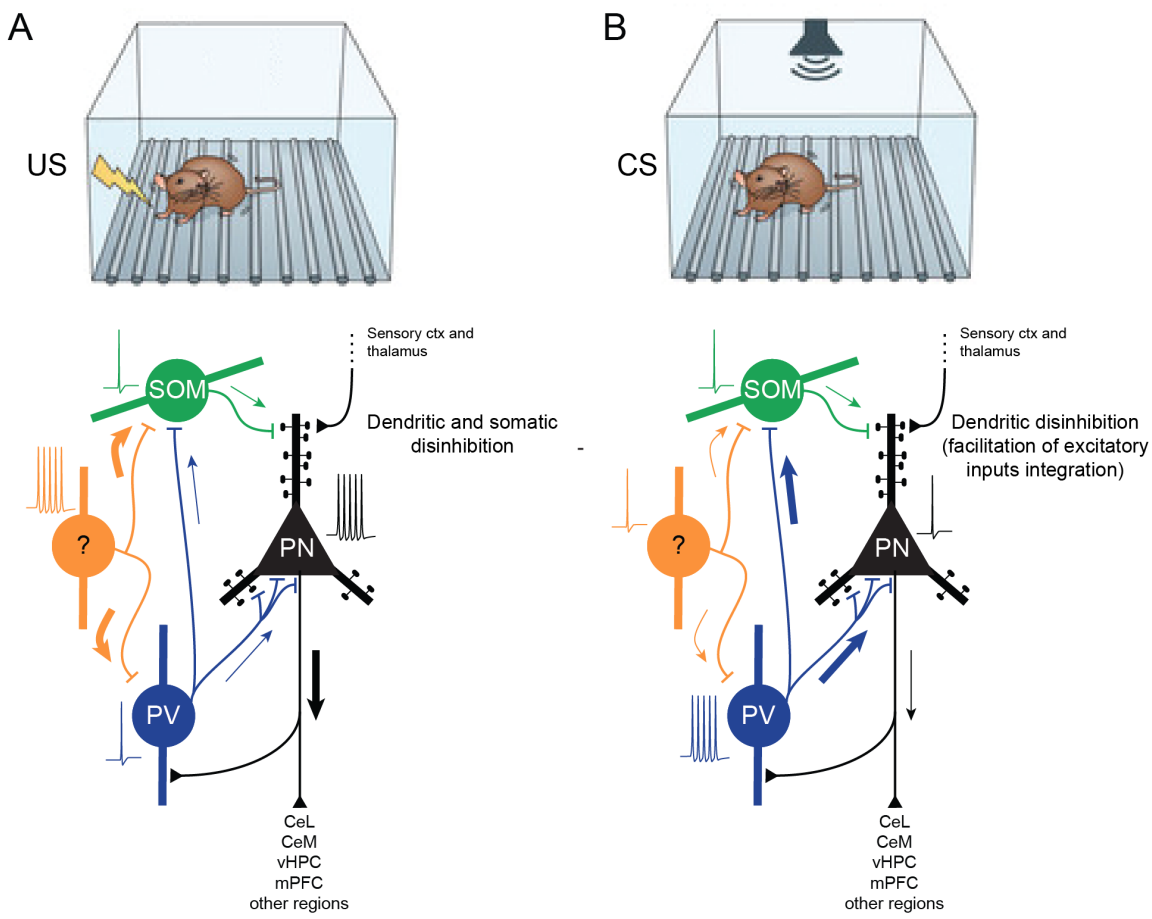

Figure 1.9. Activity of PV+ and SOM+ INs of the BLA during fear conditioning.
Model representing the activity of PV+ and SOM+ INs during fear conditioning according to opto-tagging data from Wolff *et al.*(Wolff et al., 2014). **A**, during US (footshock) presentation, the firing rates of PV+ and SOM+ INs reduce, presumably via the release of GABA from non-identified IN class(es). This produces disinhibition of both the perisomatic region and the distal dendrites of PNs and enhanced PN output. **B**, during CS (auditory tone) presentation, the firing rates of PV+ INs increase, leading to high GABA release onto SOM+ INs and PNs. This drives perisomatic inhibition but dendritic disinhibition of PNs, resulting in facilitation of excitatory inputs from thalamic axons. Single action potentials denote low excitability, bursts of action potentials depicts high excitability. The size of the arrows indicates the amount of neurotransmitter released onto the postsynaptic neuron. Top panels adapted from Tovote et al., 2015.

It is not clear whether a specific population of GABAergic neurons (e.g. VIP+ INs) mediate the concerted inhibition of PV+ and SOM+ INs.

In contrast, presentation of the CS produces excitation of PV+ INs, which in turn inhibit SOM+ INs, leading to disinhibition on PN dendrites, with a facilitation of excitatory inputs integration by PNs (Wolff et al., 2014). Large CCK+ INs, which are cannabinoid 1 receptor-positive (CB1R+), are also involved in fear conditioning. In fact, extinction of a fear memory increases the number of perisomatic appositions of CB1R+ and PV+ axons to BA PNs

originally activated by fear memory retrieval (Trouche et al., 2013). However CCK+ IN activity and their precise role in fear learning remains elusive.

While the cellular mechanisms of auditory fear conditioning appear to involve synaptic plasticity of glutamatergic pathways conveying CS and US to LA PNs, the neuronal dynamics underlying contextual fear learning might be very different. The HPC is necessary for the encoding of contextual fear (Selden et al., 1991; Kim and Fanselow, 1992; Phillips and LeDoux, 1992; Lovett-Barron et al., 2014) and severing the pathway from vHPC to BLA prevents the context-dependent renewal of an extinguished fear memory (Orsini et al., 2011). Thus, it has been hypothesised that synaptic plasticity of the vHPC input to the BLA could underlie contextual fear learning (LeDoux, 2000; Maren et al., 2013). However, no direct evidence supports the relay of contextual information from the vHPC to the BLA as yet, and a more complex interplay involving several medial temporal lobe regions might occur. For instance, optogenetic inhibition of the BLA projection to the entorhinal cortex during contextual fear memory acquisition impairs subsequent memory retrieval (Sparta et al., 2014).

1.9 Synaptic plasticity in BLA circuits

Mounting evidence suggests that long-term synaptic plasticity in the BLA underlies, at least in part, acquisition and consolidation of emotional memories (Pape and Paré, 2010). Thus, studying the cellular and molecular mechanisms of synaptic plasticity occurring in the BLA could be beneficial to understand how emotional memories are formed, stored, retrieved and extinguished. Additionally, altered synaptic plasticity in BLA circuits could contribute to pathological conditions such as PTSD.

1.9.1 General mechanisms of synaptic plasticity

Synaptic plasticity refers to changes in synaptic strength or efficacy. Namely synaptic transmission can be potentiated or depressed, and both these effects occur at multiple timescales, spanning from milliseconds to days (or perhaps even longer), depending on the molecular mechanisms involved.

1.9.1.1 Short-term synaptic plasticity

Short-term plasticity is thought to play a crucial role in the integration of sensory inputs and in transient changes in behavioural state. The simplest form of short-term plasticity occurs when two stimuli are delivered within a short interval, often leading to depression or facilitation of the response to the second stimulus. With inter-stimulus intervals ≤20 ms, this usually leads to depression of the second postsynaptic current (PSC). With inter-stimulus intervals ranging between 20 and 500 ms, the amplitude of the second PSC can be increased or decreased compared to the first PSC (phenomena termed paired-pulse facilitation and paired-pulse depression, respectively). Generally, synapses with a high initial probability of release (*p*) display paired-pulse depression, whereas synapses with a low initial *p* display paired-pulse facilitation (Dobrunz and Stevens, 1997; Zucker and Regehr, 2002). Paired-pulse facilitation is usually due to residual Ca^{2+} left over from the previous action potential. This residual Ca^{2+} enhances neurotransmitter release at the second action potential. In contrast, evidence suggests that inactivation of voltage-dependent Na^{+} or Ca^{2+} channels or a transient depletion of the release-ready pool of vesicles docked at the presynaptic terminal account for paired-pulse depression (Zucker and Regehr, 2002).

In addition to paired-pulse changes, trains of prolonged (200 ms – 5 s) high frequency stimulation (10-100 Hz) can lead to so-called post-tetanic potentiation (but also depression) that can last seconds or minutes. Potentiation can be caused by build-up of Ca^{2+} or

modifications of proteins in the presynaptic terminal (Magleby and Zengel, 1982; Zucker and Regehr, 2002). Conversely, depression can be caused by depletion of release-ready pool of neurotransmitter vesicles or desensitization of postsynaptic receptors (Betz, 1970; Zucker and Regehr, 2002).

Finally, enhancement or depression or neurotransmitter release can be triggered by activation of G-protein-coupled or ionotropic presynaptic receptors (Thompson et al., 1993). This could be a consequence of neurotransmitter spillover due to strong phasic release from the presynaptic cell (e.g. in the case of glutamate and GABA) or of retrograde messenger release from the postsynaptic cell (e.g. in the case of nitric oxide, brain-derived neurotrophic factor and endocannabinoids). For example, spillover of GABA on presynaptic $GABA_B$ receptors has been shown to depress transmitter release (Thompson and Gähwiler, 1989; Scholz and Miller, 1991; Mintz and Bean, 1993). Another compelling example is represented by depolarization-induced suppression of inhibition or excitation, which occurs when strong depolarization of the postsynaptic cell triggers retrograde release of endocannabinoids such as anandamide and 2-arachidonoylglycerol. This leads to activation of CB1 receptors on presynaptic terminals and subsequent inhibition of transmitter release (Kreitzer and Regehr, 2001; Ohno-Shosaku et al., 2001; Wilson and Nicoll, 2001).

The computational role of the different forms of short-term plasticity has not been fully understood yet. However, it has been proposed that synapses with a low *p* function as high-pass filters, whereas synapses with a high *p* would function as low-pass filters (Abbott and Regehr, 2004). In the BLA, these filtering properties could be crucial for the relay of sensory information. For example, cortical and thalamic glutamatergic synapses onto LA PNs generally display low *p* (Tsvetkov et al., 2004; Pan et al., 2009), and this could be a mechanism to give priority to emotionally-salient high frequency presynaptic activity.

1.9.1.2 Long-term synaptic plasticity

Long-term increases or decreases of synaptic strength lasting for hours, days and perhaps even longer periods of time have been reported in several brain areas, including the BLA (Citri and Malenka, 2008). Evidence suggests that LTP and long-term depression (LTD) represent a key molecular and cellular substrate of learning and memory (e.g. Whitlock et al., 2006; Nabavi et al., 2014).

1.9.1.3 LTP

LTP can display three important properties: cooperativity, associativity and input-specificity (Nicoll et al., 1988). Cooperativity means that the coincident activation of a certain number of synapses is necessary for LTP induction. Associativity occurs when a weak input is potentiated upon coincident activation with a stronger input. This property is thought to underlie the potentiation of the CS-relaying synapses onto LA PNs. Input specificity refers to the selective potentiation of the activated synapses, with no effect on adjacent, inactive synapses.

NMDA-dependent LTP: induction protocols

In many brain areas, including the BLA, induction of LTP at glutamatergic synapses requires a rise in postsynaptic Ca^{2+} concentration via activation of NMDA receptors (Malenka and Nicoll, 1993). Relief of the Mg^{2+} block via postsynaptic depolarization paired with synaptic activity is critical to activate NMDA receptors. For this reason, NMDA receptors are termed ‘coincident detectors’. Experimentally, NMDA-dependent LTP is induced in different ways. (1) High-frequency tetanic stimulation of the presynaptic axons. (2) Pairing postsynaptic depolarization with lower frequency synaptic activation. (3) Protocols inducing so-called ‘spike-timing-dependent plasticity (STDP; Caporale and Dan, 2008). STDP is induced by several pairings of presynaptic activity preceding a postsynaptic spike by an

interval <20 ms (Magee and Johnston, 1997; Markram et al., 1997). A critical cellular mechanism contributing to STDP is action potential backpropagation into the dendrites, which might help to relieve the Mg^{2+} block at dendritic excitatory synapses.

NMDA-dependent LTP: molecular cascade

Despite the intracellular cascade leading to LTP expression has not been fully dissected, evidence suggests that LTP induction relies on activation of defined protein kinases by strong rise in intracellular Ca^{2+} concentration. One of these kinases is calcium/calmodulin-dependent protein kinase II (CaMKII), which undergoes autophosphorylation upon LTP induction (Barria et al., 1997) and is necessary for LTP expression and learning (Silva et al., 1992). In addition, protein kinase A (PKA), the extracellular signal-regulated kinase (Erk)/mitogen-activated protein kinase (MAPK) pathway and protein kinase C (PKC), in particular its atypical isozyme, PKMζ, appear to be crucial for LTP induction (Citri and Malenka, 2008; Pape and Paré, 2010). The major mechanism of expression of LTP synapses involves incorporation of new AMPA receptors within the postsynaptic density (Figure 1.10; Malinow and Malenka, 2002). In addition, phosphorylation of AMPA receptor, leading to increased conductance, appears to play a role in LTP (Benke et al., 1998).

The 'late-phase of LTP' (i.e. potentiation following the first 1-2 h) appears to require transcription in the nucleus and dendritic protein synthesis (Thomas and Huganir, 2004; Sutton and Schuman, 2006). Activity in the nucleus seems to include activation of the transcription factors such as cAMP response element-binding protein (CREB) and immediate-early genes such as Zif268/Egr-1 and c-Fos (Thomas and Huganir, 2004). Protein synthesis could be at the root of structural changes such as growth of new dendritic spines, enlargement of pre-existing spines and their postsynaptic density (Abraham and Williams, 2003).

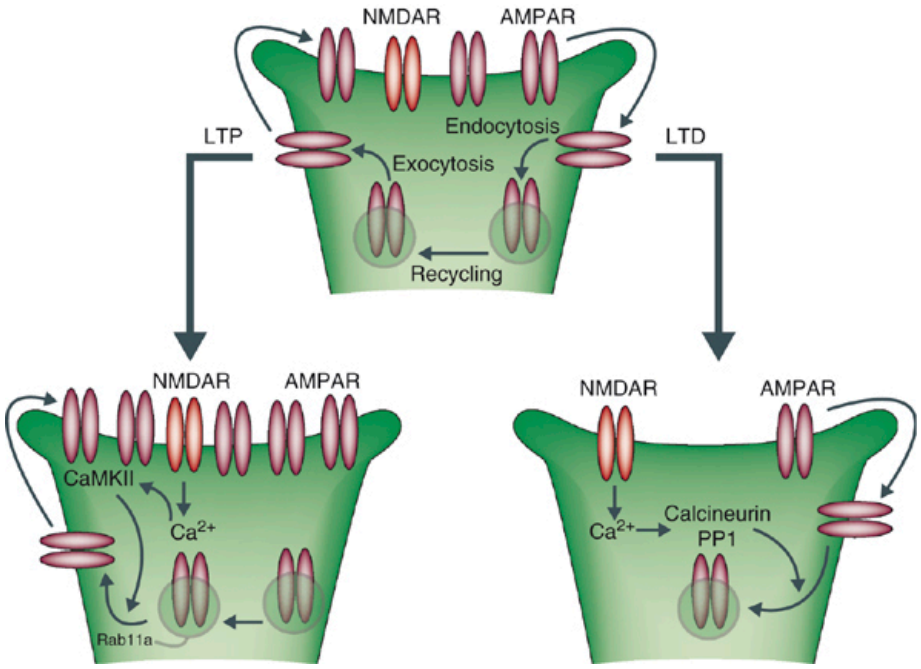

Figure 1.10. Model of AMPA trafficking during LTP and LTD
In the basal state (*top*), receptors cycle between the postsynaptic membrane and intracellular compartments. This is achieved through lateral mobility of the receptors out of the synapse into endocytic zones, where they are endocytosed into early endosomes in a clathrin- and dynamin-dependent manner. Normally, the receptors are transferred to recycling endosomes and returned to the plasma membrane by exocytosis. Following induction of LTP, there is enhanced receptor exocytosis and stabilization at the synapse through a calcium-driven process that involves CAMKII and fusion of recycling endosomes mediated by Rab11a. Following the induction of LTD, enhanced endocytosis at extrasynaptic sites occurs in a process that is calcium-dependent and involves protein phosphatases, primarily calcineurin and protein phosphatases 1 (PP1). While in the basal state endocytosis is presumably balanced by receptor recycling, following LTD receptors are retained within the cell, and perhaps degraded. From Citri and Malenka, 2008.

Presynaptic LTP

Alternatively or in addition to postsynaptic induction and expression mechanisms, LTP at certain synapses appear to induced and expressed via presynaptic mechanisms. Presynaptic LTP is triggered by high frequency tetanic stimulation, which causes a large increase in Ca^{2+} concentration in presynaptic axon terminals and involves presynaptic voltage-gated Ca^{2+} channels (Nicoll and Malenka, 1995). Importantly presynaptic LTP expression does not seem to involve increased Ca^{2+} entry in presynaptic terminals through voltage-gated Ca^{2+} channels (Kamiya et al., 2002). Rather, it may require a GTP-dependent interaction between two vesicle proteins, Rab3a and Rim1a, that are at the interface of synaptic vesicles and the active zone (Castillo et al., 1997, 2002).

1.9.1.4 LTD

While high frequency presynaptic stimulation is known to induce LTP, sustained (~15 min) presynaptic stimulation at low frequency (1 Hz) induces LTD at many synapses (Dudek and Bear, 1992; Mulkey and Malenka, 1992). Holding the postsynaptic neuron at ~-50 mV, thereby partially relieving the Mg^{2+} block of NMDA receptors, allows to reduce the duration and to change the frequency of the stimulation (Selig et al., 1995). This suggests that NMDA receptors and Ca^{2+} entry are necessary also for LTD induction. Indeed, blockade of NMDA receptors prevents LTD induction (Mulkey and Malenka, 1992).

In line with the lower frequency of stimulation required for LTD induction, LTD requires low Ca^{2+} concentrations, while LTP requires larger Ca^{2+} levels (Malenka and Nicoll, 1993; Cummings et al., 1996). Interestingly, LTD can also be input-specific (Mulkey and Malenka, 1992). Another protocol that is routinely used to induce NMDA-dependent LTD is an STDP protocol. In contrast to spike-timing-dependent LTP, spike-timing-dependent LTD requires several pairings of a postsynaptic spike followed by presynaptic activity (Markram et al., 1997; Bi and Poo, 1998).

LTD represents a mirror image of LTP at the molecular level. Specifically, LTD involves activation of a calcium-dependent protein phosphatase cascade consisting of the protein phosphatase 2B (also known as calcineurin), and protein phosphatase 1 (Lisman, 1989). The current leading theory for LTD expression is endocytosis of AMPA receptors in the postsynaptic cell (Figure 1.10; Carroll et al., 1999, 2001). However, dephosphorylation of the GluR1 subunit of AMPA receptors and subsequent decrease in AMPA receptor opening probability could also play an important role (Lee et al., 1998; Banke et al., 2000).

In addition to NMDA-associated mechanisms, LTD can be triggered at some synapses by the activation of type I metabotropic glutamate receptors (mGluR, see below) or by endocannabinoid release (Citri and Malenka, 2008). It is important to note that other forms of

synaptic plasticity, namely metaplasticity and homeostatic plasticity, have been described (Abraham, 2008; Turrigiano, 2012). However, their involvement in the encoding of emotional memories via amygdala circuits is still largely unclear.

1.9.2 Long-term synaptic plasticity in BLA circuits

Many mechanisms of long-term plasticity induction and expression that were originally discovered in the HPC have been found to also apply to the BLA (Pape and Paré, 2010). NMDA receptors are expressed in LA PNs at both cortical and thalamic synapses (Farb and LeDoux, 1997; Farb and Ledoux, 1999). In line with this, NMDA receptors antagonists block or reduce LTP at both cortical and thalamic synapses (Huang et al., 1998; Bauer et al., 2002; Shaban et al., 2006; Pan et al., 2009). NMDA-dependent LTP is thought to underlie CS-US associative learning, because infusion of NMDA receptor antagonists in the BLA disrupts acquisition but not expression of conditioned fear (Miserendino et al., 1990; Kim et al., 1991; Campeau et al., 1992). However, LTP appears to be induced also via Ca^{2+} influx via L-type Ca^{2+} channels (Bauer et al., 2002). Crucially, cortical and thalamic target different spines in LA PNs (Humeau et al., 2005) and LTP at these pathways is input-specific; however, LTP becomes heterosynaptic via glutamate spillover (Figure 1.11A; Tsvetkov et al., 2004).

Interestingly, an STDP protocol induces LTP at thalamic but not at cortical afferents, likely because thalamic axons target larger spines that display larger Ca^{2+} transients due to the presence of R-type Ca^{2+} channels (Figure 1.11B; Humeau et al., 2005). These results are consistent with prior *in vivo* findings showing greater LTP magnitude at thalamic connections (Doyère et al., 2003).

Besides postsynaptic NMDA-dependent LTP, presynaptic LTP at LA PN synapses has also been reported (Tsvetkov et al., 2002; Humeau et al., 2003). This form of LTP is associative, because it requires coincident activation of both cortical and thalamic pathways

(Humeau et al., 2003), and it is dependent on presynaptic NMDA receptor activation (Humeau et al., 2003) and presynaptic L-type Ca^{2+} channels (Figure 1.11A; Fourcaudot et al., 2009). Through this form of plasticity, heterosynaptic plasticity at weak cortical synapses can be triggered by coincident recruitment of stronger thalamic synapses. Furthermore, LTP at thalamic synapses as well as fear memory consolidation have been shown to be dependent on nitric oxide release (Schafe et al., 2005; Ota et al., 2008), in part by activating the Erk/MAPK signalling cascade via the cGMP-protein kinase G pathway (Ota et al., 2008).

LTD at excitatory synapses onto LA PNs has also been reported (Figure 1.11B). Interestingly, LTD can be induced at the thalamic, but not at the cortical, pathway via theta burst stimulation (TBS), and it is mediated by activation of group II mGluR (Heinbockel and Pape, 2000; Lin et al., 2000). A recent study reported that a more classic protocol (1 Hz stimulation for 15 min of both cortical and thalamic pathways) can also induce LTD of field EPSPs in the LA (Nabavi et al., 2014).

As the data presented above suggest, long-term synaptic plasticity in the BLA has been studied extensively at cortical and thalamic synapses on LA PNs. However, other studies suggest that excitatory synapses on BA PNs can also undergo potentiation. Excitatory synapses from axons in the EC on BA PNs undergo only short-term potentiation upon TBS of presynaptic terminals. However, activation of 5-HT_2 receptors enhances NMDA currents and allows induction of LTP (Chen et al., 2003). Additionally, activation of 5-HT_4 receptors promotes the induction of LTP at synapses between LA PNs and BA PNs (Huang and Kandel, 2007). This suggests that 5-HT is a crucial regulator of synaptic plasticity in the BA.

1.9.2.1 The role of GABAergic INs

GABAergic INs are involved in BLA long-term synaptic plasticity in two major ways. Firstly, GABA release orchestrates the induction of long-term plasticity at glutamatergic synapses on LA PNs. Secondly, long-term plasticity can be induced at thalamic and cortical synapses onto LA INs.

LTP in LA PNs can be induced via reduction of GABA release from INs by application of dopamine or noradrenaline, which hyperpolarize INs (Bissière et al., 2003; Tully et al., 2007), or by severing the slice to isolate LA PNs from dorsolateral ITCs (Morozov et al., 2011). Furthermore, TBS of cortical afferents does not induce LTP at cortical synapses onto LA PNs because of spillover of GABA onto presynaptic $GABA_B$ receptors at cortical synapses to PNs; blocking $GABA_B$ receptors allows LTP induction in PNs (Morozov et al., 2011).

Crucially, spillover of GABA onto presynaptic $GABA_B$ receptors does not seem to occur at cortical synapses with INs (Morozov et al., 2011). Finally, $GABA_B$ receptors at cortical afferents prevent, in basal conditions, the induction of homosynaptic LTP at cortical synapses. However, pharmacological blockade of $GABA_B$ receptors or genetic ablation of the $GABA_{B1a,2}$ subunits, which are expressed only presynaptically, allow the induction of this form of LTP (Shaban et al., 2006). Interestingly, $GABA_{B1a,2}$ knock-out mice display generalization of conditioned fear (Shaban et al., 2006), confirming the involvement of long-term synaptic plasticity in LA PNs in associative fear learning. Thus, these data suggest that INs and ITCs gate LTP induction at excitatory synapses onto LA PNs.

Notably, INs also receive prominent thalamic and cortical innervation (Szinyei et al., 2000) and LTP can be evoked at both pathways (Figure 1.11C; Sah and Mahanty, 1998; Szinyei et al., 2007).

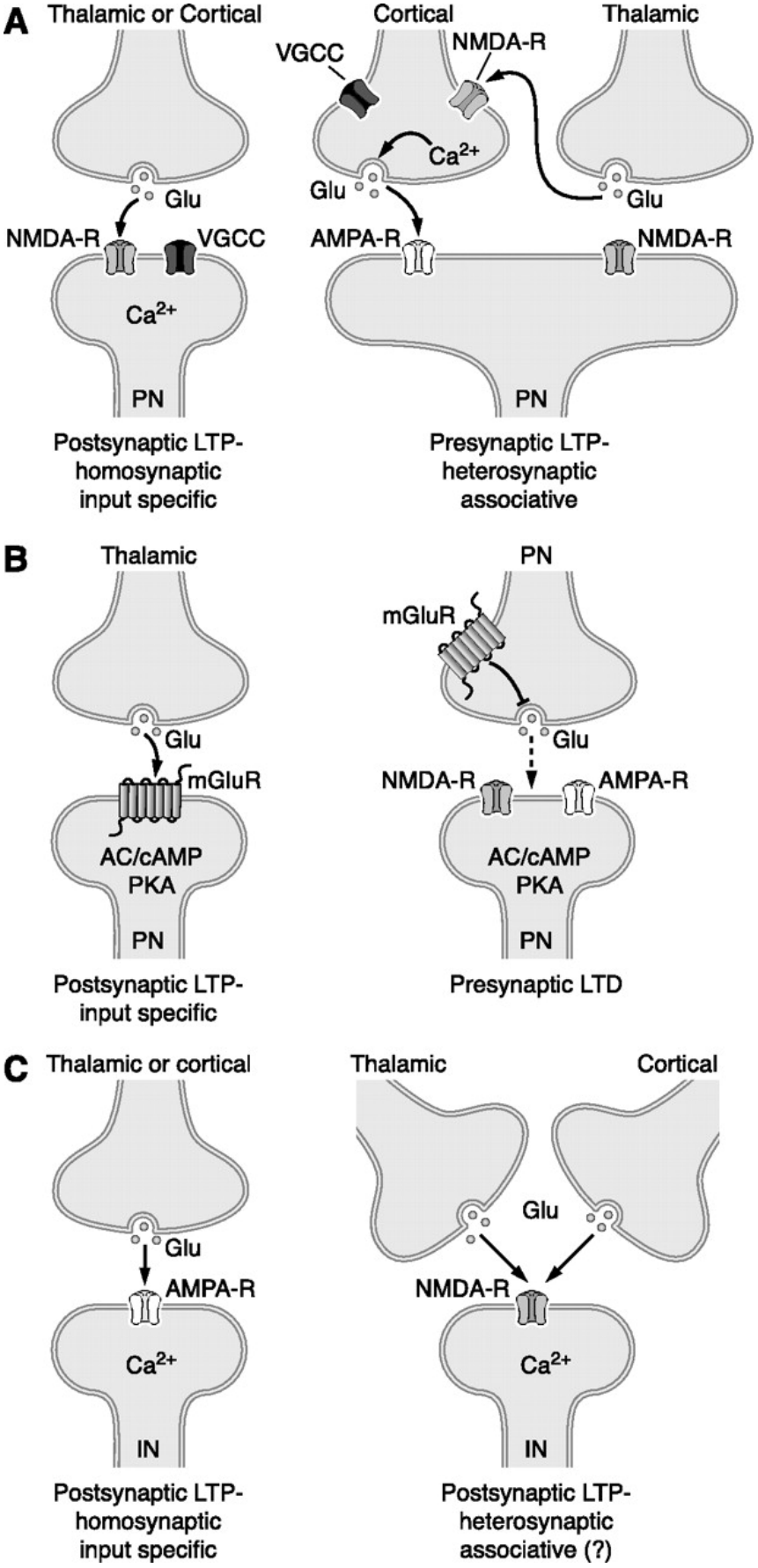

Figure 1.11. Long-term synaptic plasticity related to conditioned fear in the basolateral amygdaloid complex.
A, LTP in PNs. At thalamic or cortical inputs, LTP is mostly homosynaptic upon stimulation of postsynaptic NMDA receptors and/or voltage-gated Ca^{2+} channels (VGCC). At cortical inputs, a second form of LTP is heterosynaptic upon stimulation of presynaptic NMDA receptors through concurrent activation of thalamic inputs. **B**, LTD in PNs can be mediated via stimulation of postsynaptic metabotropic glutamate receptors (mGluRs) at thalamic inputs, or via presynaptic mGluRs at LA-BLA synaptic connections. **C**, LTP in local GABAergic IN at thalamic and cortical inputs can be homosynaptic upon stimulation of Ca^{2+}-permeable AMPA receptors, or heterosynaptic upon stimulation of NMDA receptors. From Pape and Paré, 2010.

Interestingly, since INs display much higher AMPA/NMDA ratio than PNs, LTP in the former cell type is mediated by Ca^{2+} permeable AMPA receptors, and not NMDA receptors (Sah and Mahanty, 1998).

1.10 Neuronal oscillations in BLA and interconnected structures

Accumulating evidence suggests that BLA circuits do not encode information only by net changes in firing rates of distinct neurons, but also by enhancement of neuronal synchrony, which can lead to facilitated synaptic plasticity (Pape and Paré, 2010). This indicates that probing the synchronous activity of large numbers of neurons may be a valuable approach to unravel the cellular mechanisms of emotional behaviour.

Synchronous activity can be monitored by local field potential (LFP) recordings, which reveal oscillatory patterns in different frequency bands occurring during specific brain states and behaviours (Buzsáki and Draguhn, 2004). These extracellular voltage signals arise predominantly from synaptic activity, but also from action potentials or sub-threshold membrane oscillations occurring synchronously in many neurons (Buzsáki et al., 2012). In the last decades, simultaneous multi-site LFP recordings have been employed to assess the involvement of BLA interplay with other structures involved in memory storage and retrieval in aversive or appetitive learning.

1.10.1 Theta oscillations

Oscillations in the theta frequency range (4-12 Hz) occur in the BLA *in vivo* (Paré and Collins, 2000). This rhythmic network activity likely originates in the synaptic inputs arising in areas interconnected with the BLA (such as the HPC or the mPFC; Pape and Paré, 2010) but also in intrinsic theta resonance of PN membranes (Paré et al., 1995; Pape and Driesang, 1998). In this regard, it is still unclear whether theta oscillations can be locally generated in

the BLA. *In vitro*, theta oscillations can be evoked by kainic acid application (Sinfield and Collins, 2006). PV+ INs could be a potential source of local theta generation (Amilhon et al., 2015; Karalis et al., 2016). In the BLA, PV+ INs are known to synchronise their activity via reciprocal gap junctions (Woodruff and Sah, 2007a) and pharmacological blockade of gap junctions abolishes kainic acid-evoked BLA theta oscillations *in vitro* (Sinfield and Collins, 2006). However, optogenetic activation of BLA PV+ INs *in vivo* does not evoke BLA theta oscillations; instead, optogenetic activation of mPFC PV+ INs does (Karalis et al., 2016).

Synchronised oscillations in the low theta band (~4 Hz) between BLA, mPFC and HPC increase during fear memory retrieval (Figure 1.12; Seidenbecher et al., 2003; Lesting et al., 2011; Likhtik et al., 2014; Karalis et al., 2016) and consolidation (Popa et al., 2010).

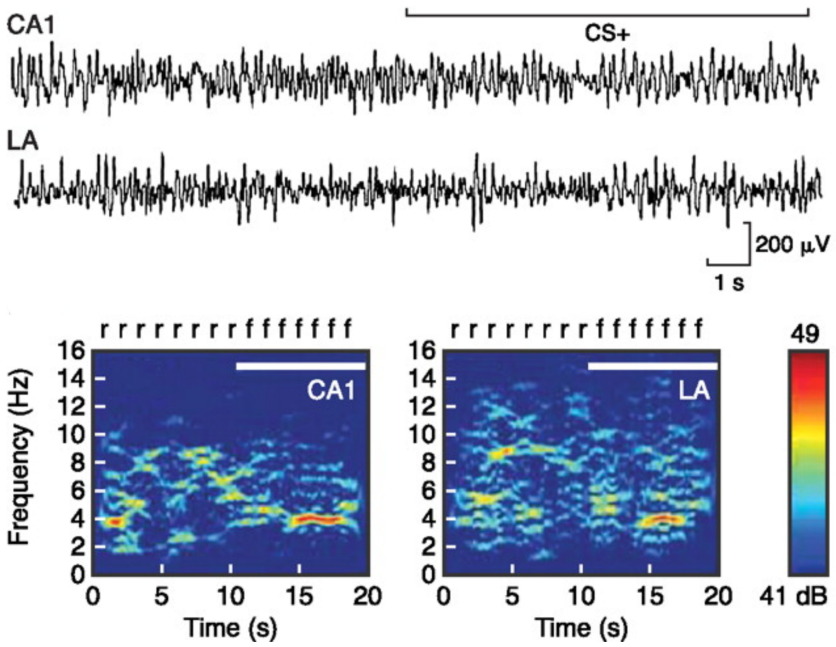

Figure 1.12 Increased theta oscillations in CA1 and LA of rats during fear memory retrieval
Top, example LFP traces from CA1 and LA during presentation of an auditory tone previously paired with a shock (CS+). *Bottom*, Colour-coded power spectra reveal increase in low theta (~4 Hz) power during freezing (f) compared to risk assessment (r) behaviour. From Narayanan et al., 2007.

Simultaneous LFP and unit recordings suggest that theta epochs reflect an enhanced theta rhythmicity of the firing of BLA neurons (Paré and Collins, 2000). This synchronised

firing is believed to facilitate communication between regions in response to aversive stimuli (Seidenbecher et al., 2003; Popa et al., 2010; Lesting et al., 2011; Likhtik et al., 2014; Karalis et al., 2016). In line with this, BLA neurons fire phase-locked with hippocampal (Bienvenu et al., 2012; Manko et al., 2012), entorhinal (Paré and Gaudreau, 1996) and mPFC theta oscillations (Likhtik et al., 2014; Karalis et al., 2016).

1.10.2 Gamma oscillations

In addition to theta oscillations, higher frequency oscillatory activity in the gamma band (35-120 Hz), has also been detected in the BLA and interconnected structures. As is the case of theta rhythms, gamma oscillations appear to be important for learning (Pape and Paré, 2010). The power and synchrony of low gamma oscillations (35-45 Hz) increases in BLA, rhinal cortices and striatum during appetitive learning (Popescu et al., 2009; Bauer, 2014). In addition, the power of fast gamma (70-120 Hz) decreases when an animal successfully discriminates an auditory cue predicting a footshock and increases when a cue not paired with the shock (thereby signalling safety) is presented (Stujenske et al., 2014). In this study, the authors additionally reported that power of BLA fast gamma oscillations can be modulated by the phase of mPFC theta oscillations, and this phase-amplitude coupling increases upon successful fear discrimination that leads to freezing.

Taken together, these findings suggest that oscillatory activity in theta and gamma bands occur in the BLA in relation to specific behaviours. These oscillations are believed to reflect enhanced neuronal synchrony at corresponding frequencies, both within the BLA itself and also between the BLA and interconnected areas such as the HPC, the mPFC and the ventral striatum. Increased neuronal synchrony across different structures is thought to facilitate spike timing-dependent plasticity and the selection of cell assemblies (Buzsáki and Draguhn, 2004), but direct experimental support for this view is still missing.

1.11 Aims of this thesis

Based on the evidence reviewed above, disentangling the functional organisation of extrinsic inputs to amygdala neurons is a necessary step to understand the brain circuits underlying emotional memories. In the research presented in this thesis, I focused on two prominent sources of BLA neuromodulation that, to date, have been poorly studied from a mechanistic viewpoint.

First, I examined the impact of the glutamatergic projection from pyramidal cells of the **CA1 region of the vHPC** (**Chapter 2**), a connection that has been suggested to be involved in learning and memory and may be altered in PTSD (Zhang et al., 2015; McDonald and Mott, 2016).

Second, I investigated the **modulation** of BLA circuits by 5-HT (**Chapter 3** and **4**). This input regulates emotionality (Asan et al., 2013) and bears clinical significance, because selective serotonin reuptake inhibitors (SSRIs), drugs that increase extracellular 5-HT levels, are a widely prescribed medication for PTSD and pathological anxiety (Nemeroff and Owens, 2002).

My central hypothesis is that GABAergic neurons of the BA are pivotal targets of these inputs, and their recruitment shapes the activity of PNs, the main output of the BA. In **Chapter 2**, I investigated **feedforward INs** targeted by CA1 pyramidal cells, while **Chapter 3** concentrates on the impact of 5-HT recruitment of **PV+ INs** on fear conditioning. Finally, to further characterise the GABAergic system in the BLA, I investigated a class of **inhibitory neurons expressing nNOS (Chapter 4**). These cells display an unusual 5-HT modulation that appears to be important for their activity across the sleep-wake cycle.

Chapter 2 Hippocampal modulation of basal amygdala circuits via feedforward interneurons

2.1 Introduction

A large body of evidence suggests that HPC-amygdala interactions influence acquisition and retrieval of emotional memories. The amygdala is thought to modulate hippocampal-dependent episodic memory by associating emotional valence (Anderson and Phelps, 2001; Phelps, 2004; Richardson et al., 2004). Conversely, the HPC is believed to modulate the amygdala by providing information about the episodic representation of an emotional memory (Phelps, 2004; Richardson et al., 2004; Fanselow, 2010). Dysfunctional HPC-amygdala interplay might be at the root of many psychiatric conditions (Spedding et al., 2005), including depression (Nestler et al., 2002) and PTSD (Elzinga and Bremner, 2002; Shin et al., 2006). Hence, a deep neurobiological understanding of how these two structures encode emotional memories could lead to improved therapies for these disorders.

Rodent studies have provided important knowledge on the critical role of the modulation of the amygdala by the HPC in emotion regulation. Namely, an extinguished auditory CS presented outside the extinction context renews fear responses and causes an increased c-Fos expression in vHPC neurons projecting to the BA (Orsini et al., 2011). Moreover, the disconnection of the vHPC to the BA prevents this fear renewal. This suggests that the vHPC might orchestrate fear responses by sending contextual information to the BA (Maren et al., 2013). Furthermore, optogenetic manipulation of the projections from the BLA

to the vHPC shows that these two structures are involved in anxiety-related behaviour (Felix-Ortiz et al., 2013).

Recordings from the BLA and the CA1 region of the HPC have shown that the LFPs of these two areas display high theta frequency synchronisation during fear memory retrieval (Seidenbecher et al., 2003; Popa et al., 2010). As BLA theta oscillations seem to originate, at least in part, from synaptic inputs from areas interconnected with the BLA (Pape and Paré, 2010), CA1-LA theta synchronisation could arise from rhythmic theta-frequency inputs from the CA1 that synchronise BLA neurons. In keeping with this, BLA neurons fire phase-locked to CA1 theta oscillations (Bienvenu et al., 2012). However, the mechanisms through which CA1 inputs recruit BLA neurons to drive network synchronisation remain unknown. Anatomical work has demonstrated reciprocal connections between vCA1 and BLA (Pitkänen et al., 2000). The BA and BM nuclei of the amygdala are the most densely innervated by the vCA1 (Kishi et al., 2006; Müller et al., 2012). These projections originate predominantly from vCA1 pyramidal neurons (Arszovszki et al., 2014; Ciocchi et al., 2015), and they are therefore excitatory. Interestingly, BLA-projecting vCA1 pyramidal cells are preferentially activated by fear renewal (Jin and Maren, 2015).

It is likely that vCA1 pyramidal neurons modulate the activity of BLA PNs because "fear neurons" have been shown to receive excitatory inputs from this area (Herry et al., 2008). Previous studies from our group have shown that specific BLA IN populations fire in phase with CA1 theta oscillations in anaesthetised rats (Bienvenu et al., 2012; Manko et al., 2012). Thus, we hypothesised that GABAergic INs of the BA could gate excitatory inputs from vCA1 to control the firing and synaptic plasticity of PNs. To test this hypothesis, we combined *in vivo* and *ex vivo* recordings from single neurons of the BA and optical stimulation of vCA1 pyramidal cell axons.

2.2 Materials and methods

2.2.1 Animals

CaMKIIα-Cre$^{+/+}$ (Jackson Laboratories, B6.Cg-Tg(Camk2a-cre)T29-1Stl/J, stock number 005359) and wild-type (WT) C57BL/6J mice (Charles River) were housed with their littermates with *ad libitum* access to food and water in a dedicated housing room with a 12/12-h light/dark cycle. All procedures involving experimental animals were performed in compliance with the European Convention for the Protection of Vertebrate Animals used for Experimental and Other Scientific Purposes (ETS no. 123), the European Communities Council Directive of 24 November 1986 (86/609/EEC), the Animals (Scientific Procedures) Act, 1986 (UK) and associated regulations, under approved project license by Home Office UK (30/2539), the Austrian Animal Experimentation Ethics Board (GZ66.011/28-BrGT/2009), and with Society for Neuroscience Policies on the Use of Animals in Neuroscience Research.

2.2.2 Expression of ChR2 in vCA1 pyramidal cells

CaMKIIα-Cre mice (postnatal day 20-25) were anaesthetised using 0.5-2% isoflurane in oxygen (2 L/min). Analgesia was also provided (buprenorphine, 0.1 mg/kg of body weight). In order to selectively express ChR2 in pyramidal neurons, the Cre-inducible recombinant viral vector AAV-EF1a-DIO-hChR2(E123T/T159C)-EYFP (UNC vector core, 0.3-0.4 μL volume) was delivered in the right vCA1 (3 mm posterior, +3.5 lateral from bregma and 3 mm ventral from the brain surface) through a glass pipette at a rate of 40-50 nL/min. At least 3 weeks were allowed for ChR2 expression before recording procedures. In preliminary experiments we also used AAV-EF1a-DIO-hChR2(H134R)-EYFP. However, this vector was not used in any subsequent experiment because of its slower kinetics (Figure 2.3D, E).

2.2.3 *In vivo* recordings

C57BL/6J or CaMKIIα-Cre mice (2-4 months old) were anaesthetised by intraperitoneal injections of urethane (1.5 g/kg body weight). For the duration of the surgery (~2 h), urethane anaesthesia was supplemented with 0.5% isoflurane in oxygen (2 L/min). Isoflurane was switched off at least 1 h before recordings. Supplemental injections of 10% the initial dose of urethane were administered when needed (approximately every 2 h). Body temperature was measured with a rectal probe, and maintained at 37 °C using a homoeothermic heating device (Harvard apparatus). Craniotomies were drilled above the right HPC and amygdala. To monitor the firing of amygdala neurons in relation to hippocampal SWA and theta oscillations, extracellular recordings were performed from the BA and the dorsal CA1 using separate glass pipettes filled with 3% Neurobiotin (Vector Laboratories) in 0.5 M NaCl (10–18 MΩ resistance *in situ*). Glass electrode signals were referenced against a wire implanted subcutaneously in the neck. To monitor oscillatory activity in the TeA, an electrocorticogram (ECoG) was recorded using a 1 mm diameter steel screw implanted at 4.2 mm posterior, 4.3 mm lateral from bregma. Glass electrode signals were amplified (ELC-01MX, NPI Electronic Instruments) and differentially filtered (DPA-2FS, NPI Electronic Instruments) to extract local field potentials (LFPs, 200× amplification, 0.3-5000 Hz filtering) and unit activities (10× amplification, 300-5000 Hz filtering). Raw ECoG signal was bandpass filtered (0.3–1500 Hz) and amplified (2000×). All signals were digitized online at 20 kHz using a Power 1401 analog-digital converter (Cambridge Electronic Design) and stored on a PC running Spike2 software (Cambridge Electronic Design). To photostimulate vCA1 pyramidal cell axons innervating the BA, a fibre optic cannula (200 µm core diameter, 0.39 numerical aperture (NA) Thorlabs) connected to a Luxx 488-200 diode laser (Omicron) was implanted 0.5-0.7 mm above the recording site (inserted 0.5 mm

posterior, 3 mm lateral from bregma, and advanced 4 mm at a 16° angle ventral from the brain surface). Light power at the fibre optic tip was measured using a PM100D power meter and photodiode sensor (Thorlabs). The TBS protocol consisted of 50 trains of 5 light pulses (3 ms duration, 19 ± 1.2 mW at fibre optic tip) delivered at 10 ms intervals (100 Hz), with 200 ms between trains. TBS was delivered every 20 s and was repeated for 8-15 trials for each neuron. After recordings, 14/27 PNs and 10/25 INs were filled with Neurobiotin by the juxtacellular method (Pinault, 1996). The position of neurons that could not be labelled after recording was calculated using a labelled reference neuron in the same brain. In order to verify the location of the hippocampal electrode, an extracellular Neurobiotin deposit was made in the dorsal CA1 (100 nA anodal current 1 s, 50% duty cycle for 20-30 min).

2.2.4 Analysis of *in vivo* recordings

All data were analysed off-line using Spike2 built-in functions and custom-made scripts (Tukker et al., 2007) and MATLAB (Mathworks, Inc.) custom-made scripts. Spike2 clustering function supervised manually was used to isolate single units. Before immunohistochemically determining whether labelled neurons were PNs or INs, putative PNs were separated from putative INs using *K-means* supervised clustering for 3 parameters: first positive peak of the spike to negative peak (P1-P2), negative peak to second positive peak (P2-P3) and the mean CV2, a measure of firing regularity (Figure 2.1). Theta epochs, occurring during activated cortical state, were isolated when the ratio of theta (3–6 Hz) to delta (2–3 Hz) power in 10 s windows of the dCA1 or TeA LFP was greater than 4 (Csicsvari et al., 1999; Klausberger et al., 2003). SWA epochs were defined as such when the theta/delta ratio was lower than 2. The mean firing rate of a given neuron was calculated by summing all spikes during theta or SWA epochs and dividing this by the sum of durations of the epochs. Only neurons that had stable spontaneous firing rates/patterns and stable spike widths, and did

not display any 'injury discharge' were included. To analyse responses to optogenetic TBS, peri-stimulus time histograms of firing rates (PSTHs, 50 ms bins) were generated for each trial (8-15 trials in total). PSTHs were normalised by dividing binned frequencies by the pre-TBS baseline mean (5 s). A neuron was considered optically modulated if the mean firing rate in the 50 ms bins during TBS light trains differed statistically from the mean baseline. To obtain population PSTHs, normalised PSTHs were generated from all trials from each neuron and averaged. The following rules were defined, based on histological verifications: (1) recorded neurons had to be located in the BA nucleus (either by observation of Neurobiotin filled neurons or by calculating the position of the recorded unlabelled neurons according to the position of a reference labelled neuron); (2) transfection with ChR2 had to be restricted to ventral/intermediate CA1; (3) the BA had to be innervated by a pattern of ChR2+ axons as shown in Figure 2.4B; (4) the fibre optic tip had to be located above the BA and ~500 μm above the recording site. If these criteria were not met, neurons were discarded and not analysed.

2.2.5 *Ex vivo* recordings and analysis

After allowing 3-4 weeks for ChR2 expression, mice (postnatal day 40-60) were decapitated under deep isoflurane anaesthesia (4% in O_2), and their brains were rapidly removed and placed in ice-cold sucrose-containing artificial cerebrospinal fluid (ACSF) cutting solution containing (in mM): 75 sucrose, 87 NaCl, 25 $NaHCO_3$, 2.5 KCl, 1.25 NaH_2PO_4, 0.5 $CaCl_2$, 7 $MgCl_2$, 25 glucose, saturated with 95% O_2, 5% CO_2, at pH 7.3-7.4. Slices (325 μm thickness) including amygdala were cut (Microm HM 650 V, Thermo Fisher Scientific Inc.) and transferred onto a nylon mesh where they were maintained in a chamber initially containing sucrose ACSF cutting solution at 37 °C for 30 min. During this period the

cutting solution was gradually substituted (5 mL/min) with normal ACSF consisting of (in mM): 130 NaCl, 24 $NaHCO_3$, 3.5 KCl, 1.25 NaH_2PO_4, 2 $CaCl_2$, 2 $MgCl_2$, 10 glucose, saturated with 95% O_2, 5% CO_2, at pH 7.3. Slices were then stored at room temperature (RT, 18-22 °C). Acute slices were secured under a nylon mesh, submerged and superfused with normal ACSF in a chamber mounted on the stage of an upright microscope (Axioskop, Zeiss). Slices were visualized with a 40×/0.1 NA water-immersion objective coupled with infrared and differential interference contrast (DIC) optics linked to a video camera (CCD Camera Orca R2, Hamamatsu). Somatic whole-cell patch clamp recordings (at ~33 °C) were made from visually identified cells using borosilicate glass capillaries (GC120F, 1.2 mm, Clarke Electromedical Instruments), pulled on a DMZ puller (Zeitz-instrumente GmbH) and filled with a filtered intracellular solution consisting of (in mM): 140 K-gluconate, 4 KCl, 4 ATP-Mg, 0.3 GTP-Na_2, 10 Na_2- phosphocreatine, 10 HEPES and 0.5% w/v biocytin, osmolarity 270–280 mOsmol/L without biocytin, pH 7.3 adjusted with KOH. A caesium-based intracellular solution was used in some experiments to block K^+ channels. This consisted of (in mM): 42 Cs-methansulfonate, 88 CsCl, 10 HEPES, 10 Na_2-phosphocreatine, 4 Mg-ATP, 0.3 Na-GTP and 0.5% w/v biocytin (all from Sigma-Aldrich), osmolarity 270–280 mOsmol/L without biocytin, pH 7.3 adjusted with CsOH. Resistance of the patch pipettes was 5-6 MΩ. Recordings were accepted only if the initial seal resistance was greater than 2 GΩ and series resistance did not change by more than 20% throughout the recording period. No correction was made for the junction potential (16 mV for the K-gluconate intracellular solution) between the pipette and the ACSF. For cell-attached recordings, glass electrodes were filled with 150 nM NaCl. Suction of the membrane was applied to achieve a loose-patch configuration (≤ 90 MΩ seal). For INs, recordings were performed in voltage clamp mode by setting the pipette potential to obtain 0 pA of membrane current (Alcami et al., 2012). As PNs were usually silent *ex vivo*, firing was induced by application of a positive pipette current (10-

1000 pA). For unlabelled neurons recorded in whole-cell mode, PNs were distinguished from INs according to the following parameters: 1) smaller fast after-hyperpolarization (fAHP) amplitude and prominent medium AHP in an instantaneous firing rate protocol; 2) adapting, <20 Hz maximum firing rates; 3) often lower R_{in}, < 150 MΩ); 4) often longer spike half-width (~1 ms). All electrophysiological signals were amplified (10 mV pA^{-1}, EPC9/2 amplifier HEKA Electronik, Lambrecht, Germany, PULSE software), low pass filtered at 2.9 kHz, digitized at 5 or 10 kHz. The amplifier was controlled with the PULSE data acquisition and analysis program (HEKA).

Optical stimulation of hippocampal ChR2-expressing afferents in the BA was performed using an optoLED system (Cairn Research), consisting of a 470 nm, 3.5 W LED mounted on a Zeiss Axioskop 2 FS microscope, to give 0.1 or 3 ms duration light pulses of ~5% of maximum output power. The steady-state light power at the tissue was measured using a PM100D power meter and photodiode sensor (Thorlabs). The illumination area corresponded to the area of the slice visualized using a 40×/0.8 NA water immersion objective. Optical TBS consisted of 10 trains of 5 light pulses (3 ms duration) delivered at 10 ms intervals (100 Hz), with 200 ms between trains. TBS was delivered every 20 s and was repeated at least 10 times.

Data were analysed with MATLAB (Mathworks, Inc.). The PSPs were defined as such if their amplitude was two standard deviations above or below the mean baseline. The EPSP peak was calculated throughout ten TBS trains using the pre-1st train V_m as baseline. The PSP amplitude was calculated from the pre-train V_m (baseline) to the peak of the PSP evoked by light pulses. To accurately determine PSP peak amplitude, only PSPs that did not lead to spike generation were analysed. The V_m for each train of the TBS was measured as the mean V_m across 20 ms preceding each train. To determine the reversal potential of the IPSC (E_{IPSC}),

I/V curves were constructed measuring the IPSC peak amplitude during the 1st and 2nd TBS trains for holding potentials ranging from -90 mV to +50 mV (5 mV steps). The peak of the disynaptic IPSC was detected at the 1st TBS train. For the 2nd train, the current was measured at the same time point where the peak of the IPSC was detected during the 1st train. Difference between this current value and the baseline holding current was considered as amplitude of the disynaptic IPSC during this train. Linear regression was used to calculate a best-fit line for the V_m/IPSC amplitude relationship. To calculate E_{IPSC} and slope conductance, the interpolated intercept of the linear fit with the abscissa and the slope of the linear fit were taken, respectively. Electrical stimulation was performed with a tungsten electrode. Evoked PSPs were recorded in whole-cell current clamp mode at -65 mV. Evoked IPSCs (Figure 2.14C) were recorded in voltage clamp mode at -50 mV. Electrical TBS consisted of trains of five stimuli (0.5 ms) at 10 ms intervals (100 Hz), with 200 ms between trains. The pairing-induced plasticity protocol consisted of pairing 50 optical TBS (ChR2+ vCA1 axons) trains with 50 electrical TBS (LA stimulation). The LA stimulation was set with delays of 10 ms or 100 ms from the optogenetic stimulation in order to evoke an EPSP from the LA input at the peak of the IPSP triggered by the vCA1 input, or when the IPSPs were virtually extinguished, respectively.

2.2.6 Histological processing

2.2.6.1 Processing of sections recorded *ex vivo*

Following intracellular recording *ex vivo*, slices were fixed overnight in 4% paraformaldehyde (PFA) and 15% saturated picric acid in 0.1 M phosphate buffer (PB; pH 7.4) at 4 °C. Sections were embedded in a block of 10% gelatine (Merck) in deionised water , postfixed in 4% PFA in 0.1 M PB including 1.25% glutaraldehyde (Polysciences Inc.) for 30 min, washed two times and then re-cut into 60 μm-thick consecutive sections on a vibratome (Leica VT 1000 S). The sections were collected in consecutive order in 0.1 M PB and stored at 6 °C until further usage. biocytin-labelled neurons were confirmed as PNs or INs according to their dendritic and axonal patterns: PNs displayed larger, pyramidal-shaped somata, thick spiny dendrites and projected outside the BLA. INs had usually smaller, ovoid somata, spine-sparse dendrites and their axons branched profusely within the BLA. Camera lucida reconstructions were performed using a drawing tube mounted onto a Zeiss Axioplan2 microscope with a 63× oil 1.4 NA objective.

2.2.6.2 Processing of whole brains

Mice were transcardially perfused with saline followed by 4% PFA with 15% saturated picric acid in 0.1 M PB. If the brain contained juxtacellularly labelled neuron(s), perfusion took place one to four h after cell labelling. Brains were sectioned using a vibratome (Leica VT 1000 S) into 60 μm thick slices. Sections were stored in 0.1 M PB containing 0.05% sodium azide until further processing.

2.2.6.3 Immunohistochemistry

The expression of yellow fluorescent protein (YFP) in hippocampal fibres was visualized by incubating sections in 1:1000 chicken anti-green fluorescent protein (GFP, Aves

Labs) in tris-buffered saline (T-BS) containing 0.1% Triton X-100 and 1% normal donkey serum (NDS) overnight at 4°C followed by anti-chicken Alexa488-conjugated secondary antibody raised in donkey (1:500, Jackson Immunoresearch) in T-BS containing 0.1% Triton X-100 for 2 h at RT. To facilitate anatomical characterisation, the sections were incubated for 30 min with 1:200 Nissl-Cy5 stain (Neurotrace, Invitrogen). For visualisation of neurons labelled *ex vivo*, free-floating sections were washed in T-BS and then blocked in 20% NGS in T-BS containing 0.1% Triton X-100 for 2 h at RT. To visualise the biocytin, the sections were incubated in Cy3-conjugated streptavidin (1:1000; Vector Laboratories), for 72 h at 6 °C in a solution consisting of T-BS containing 2% NGS and 0.1% Triton X-100. For visualisation of neurons labelled *in vivo*, sections were incubated in Cy3-conjugated streptavidin (1:1000-3000) diluted in a solution of phosphate-buffered saline (PBS) containing 0.3% Triton X-100 for 3 h at RT. After washing with T-BS/PBS the sections were mounted on glass slides and coverslipped with Vectashield (Vector Laboratories) as embedding medium. The exposure to light was kept at minimum for the whole procedure. To assess immunoreactivity of the neurons labelled *in vivo*, sections were blocked in 10% NDS in PBS containing 0.3% Triton X-100 and then incubated with one of the following primary antibodies: anti-CaMKIIα raised in goat (1:200, Santa Cruz, cat. no. sc-5391) or anti-VGAT raised in guinea pig (1:500, Synaptic systems, cat. no. 131004) antibodies. Following washes in PBS, sections were incubated with an Alexa647-conjugated secondary antibody raised in donkey (1:250, Jackson Immunoresearch) in a solution of PBS containing 0.3% Triton X-100. The boundary between LA and BA nuclei was determined by either light microscopy or a VGluT3 staining (anti-VGluT3 antibody raised in guinea pig, 1:250, Chemicon, cat. no. AB5421, and AMCA- or Alexa647-conjugated secondary antibodies raised in donkey, Jackson Immunoresearch).

2.2.6.4 Electron microscopy

Pre-embedding immunocytochemistry experiments were carried out according to previously published procedures with minor modifications (Sreepathi and Ferraguti, 2012). Briefly, cryoprotected free-floating sections were freeze-thawed twice to allow antibody penetration. After blocking unspecific binding sites with 20% normal goat serum in T-BS for 2 h at RT, sections were incubated for ~72 h at 6 °C with an anti-GFP antibody raised in rabbit (1:1000, Molecular Probes, cat no. A-11122) made up in a solution containing 2% normal goat serum in T-BS, and then overnight at 6 °C with an anti-rabbit biotinylated secondary antibody raised in goat (diluted 1:100, Vector Laboratories). Antigen-antibody complexes were visualised by a horseradish peroxidase-based reaction. Sections were contrast enhanced with 2% OsO_4 in 0.1 M PB for 40 min at RT and 1% uranyl-acetate in 50% ethanol for 30 min at RT, making sure they were protected from light. After dehydration with graded ethanol and propylene oxide, sections were embedded in epoxy resin (Durcupan ACM-Fluka, Sigma). Serial ultrathin sections (70 nm) were cut using a diamond knife (Diatome) on an ultramicrotome (EM UC7, Leica), collected on copper slot grids coated with pioloform (Agar) and analysed with a transmission electron microscope (TEM, Philips CM120) equipped with a Morada CCD camera (Soft Imaging Systems). Images were level adjusted and cropped in Photoshop (Adobe).

Sodium dodecyl sulphate (SDS)-digested freeze-fracture replica immunolabelling (SDS-FRIL) was performed according to previously published procedures with minor modifications (Kasugai et al., 2010). The brains of adult C57BL/6J mice were perfusion-fixed with PB (0.1 M, pH 7.4) containing 1% formaldehyde, and 15% of a saturated solution of picric acid. Blocks containing the amygdala were cut into 140 μm coronal sections by a Leica VT1000S vibratome and the BA was dissected out under a stereomicroscope. BA tissue

blocks were cryoprotected with 30% glycerol in 0.1 M PB overnight at 4 °C, high-pressure frozen (HPM 010, Bal-Tec), fractured and replicated in a freeze-etching device (BAF 060, Bal-Tec). Fractured faces were replicated by rotary deposition of carbon (5 nm) evaporated with an electron beam gun positioned at a 90° angle, shadowed unidirectionally by platinum-carbon (2 nm) with the gun positioned at a 60° angle, followed by an additional carbon layer (15 nm) applied from a 90° angle. Tissue was solubilised in a solution containing 2.5% SDS and 20% sucrose made up in 15 mM Tris buffer, pH 8.3, at 80 °C on a shaking platform for 18 h. Replicas were kept in the same solution at RT until further processing. On the day of immunolabelling, replicas were washed in 25 mM T-BS containing 0.05% bovine serum albumin (BSA) and incubated in a blocking solution containing 5% BSA in 25 mM T-BS for 1 h. Subsequently, the replicas were sequentially incubated in primary antibodies: anti-$GABA_B$ raised in rabbit, 1:200, kindly donated by Prof. R. Shigemoto, followed by anti-VGAT raised in rat, 1:300, Synaptic Systems, cat no. 131044). After several washes, the replicas were sequentially reacted overnight at RT with gold-coupled secondary antibodies (anti-rabbit 5 nm followed by anti-guinea pig 10 nm, both raised in goat, 1:30, British Biocell International) made up in 25 mM T-BS and 5% BSA. Replicas were then washed, picked up on 100-line copper grids and analysed using the same TEM imaging system (CM120 TEM, Morada CCD camera) described before. To test for cross-reactivity of gold-conjugated secondary antibodies in co-localisation studies, control replicas were reacted with one of the primary antibodies and a mixture of secondary antibodies conjugated to different sizes of gold and directed against different species. No non-specific cross-reactivity of gold-conjugated secondary antibodies was observed.

2.2.6.5 Confocal microscopy

The sections were analysed with a confocal microscope (TCS SP5 confocal, Leica) using the LAS-AF software (Leica) for acquisition. Confocal images were deconvoluted with the Huygens software (Scientific Volume Imaging), and analysed with Imaris 7.1 (Bitplane). In 3D images, ChR2-YFP positive boutons were observed to form appositions with dendrites of filled neurons. The identification of putative synapses was based on the finding that YFP labelled boutons were always in close proximity to a labelled dendrite/spine when viewed from different perspectives. The length of the observed dendrites was also measured with Imaris.

2.2.7 Statistical analyses

Data are presented as means ± SEM. For electrophysiological data, distributions passing Shapiro-Wilk test for normality were compared using Student's t-tests. Non-normal distributions were compared using non-parametric tests (Mann Whitney U test, Wilcoxon signed rank test). Comparisons of individual T-BS trains were performed with ANOVAs and Bonferroni *post hoc* corrections. Differences were considered significant at $p < 0.05$. For anatomical data, distributions were compared with Mann-Whitney U test. Differences were considered significant at $p < 0.001$.

2.2.8 Drugs

All drugs were obtained from Tocris Biosciences or Sigma-Aldrich.

2.3 Results

2.3.1 Differential firing of BA PNs and INs during theta oscillations *in vivo*

First, we set out to investigate the activity of PNs and GABAergic INs of the BA during theta oscillations in areas interconnected with the amygdala. We recorded the firing of single neurons of the BA and the LFP in CA1 and/or TeA, two structures projecting to the BLA, in urethane-anaesthetised mice. In the BA, PNs (n = 27) and INs (n = 25) could be separated on the basis of their spike waveforms and firing regularity (Figure 2.1, see section 2.2.4 Analysis of *in vivo* recordings for details), in agreement with previous observations (Bienvenu et al., 2012).

Immunoreactivity for CaMKIIα (14/14) and VGAT (10/10) was confirmed for a subset of PNs and INs juxtacellularly labelled after their recording (Figure 2.2B and E, respectively). The firing rates of the recorded neurons were cell-type specific and brain state dependent, consistent with previous data obtained in awake cats (Paré and Gaudreau, 1996). Specifically, BA PNs fired at higher frequencies during cortical and hippocampal SWA (0.52 ± 0.08 Hz) and at significantly lower frequencies during theta oscillations (0.04 ± 0.02 Hz, $p < 0.0001$, n = 16; Figure 2.2A, C). In contrast, INs fired at lower rates during cortical and hippocampal SWA (5.42 ± 1.35 Hz) and at significantly higher rates during theta oscillations (8.35 ± 1.48 Hz, $p < 0.05$, n = 20; Figure 2.2D, F). Although most of the INs (16/20) increased their firing rates during theta episodes, a few (4/20) showed a reduction. These results suggest that the firing of BA PNs might be more tightly controlled by GABAergic INs during theta epochs compared to slow wave states.

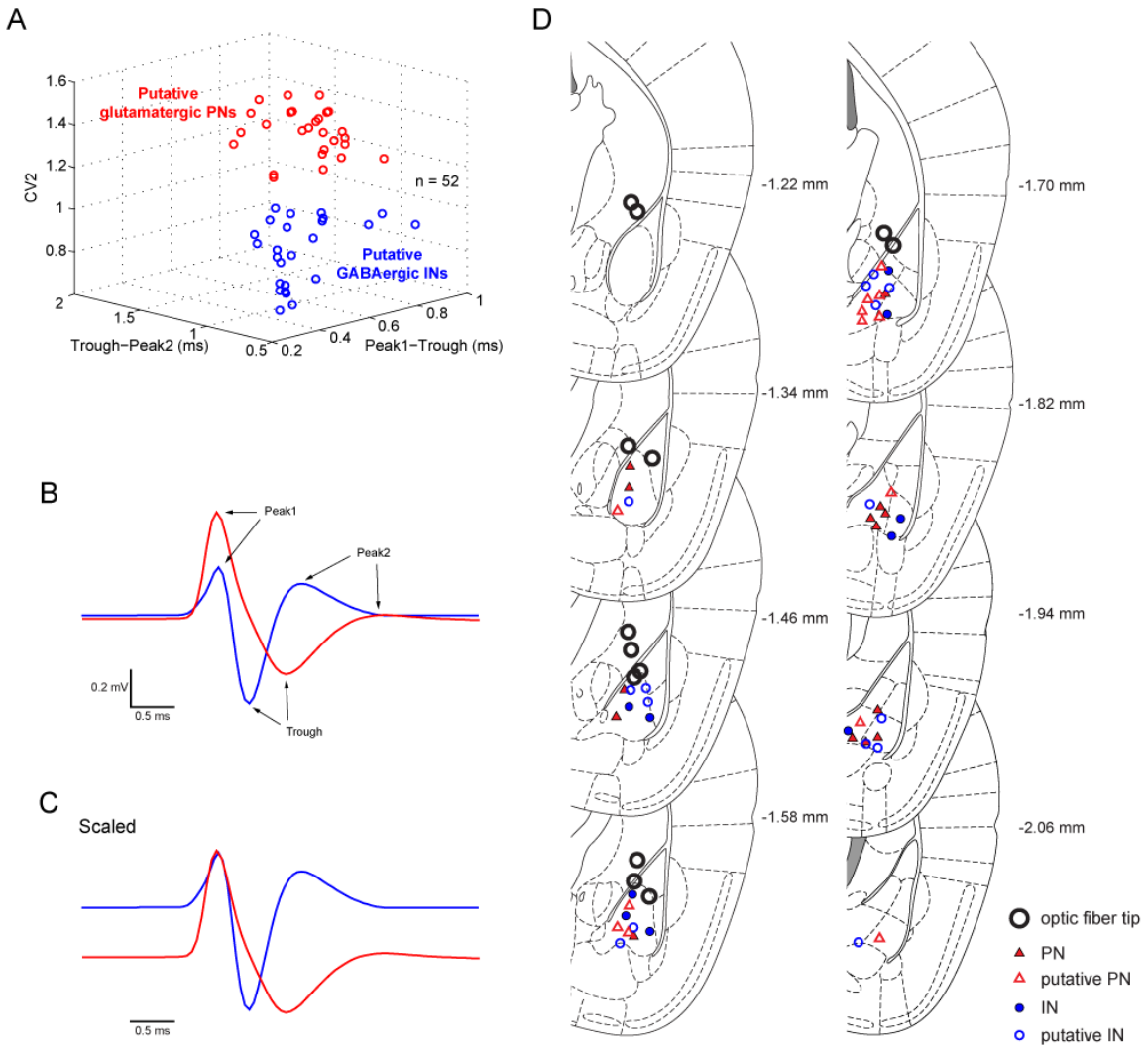

Figure 2.1. Clustering of PNs and INs and histologically verified positions of fibre optic tip and recorded neurons. **A**, recorded neurons (n = 52) could be separated into putative PNs (n = 27) and INs (n = 25) using K-means clustering on the basis of three parameters: mean CV2 of the interspike interval (an index of regularity), time between first action potential peak and trough, time between action potential trough and second peak. **B**, averages of 100 spikes of a putative PN (red) and a putative IN (blue) illustrating the methodology used for quantification. **C,** scaled averages of the action potential in B. **D**, histologically verified positions of the tip of fiber optic cannulas (black empty circles, each one represents a separate experiment, n = 13) and *in vivo* recorded neurons. Juxtacellularly labelled and immunohistochemically verified neurons are represented with filled red (PNs) and blue (INs) shapes. Approximate positions of unlabelled (putative) neurons (empty red and blue shapes) were calculated using a labelled reference neuron in the same brain. The fibre optic cannula was implanted from the front with a 16° angle (see 2.2.3 *In vivo* recordings for details).

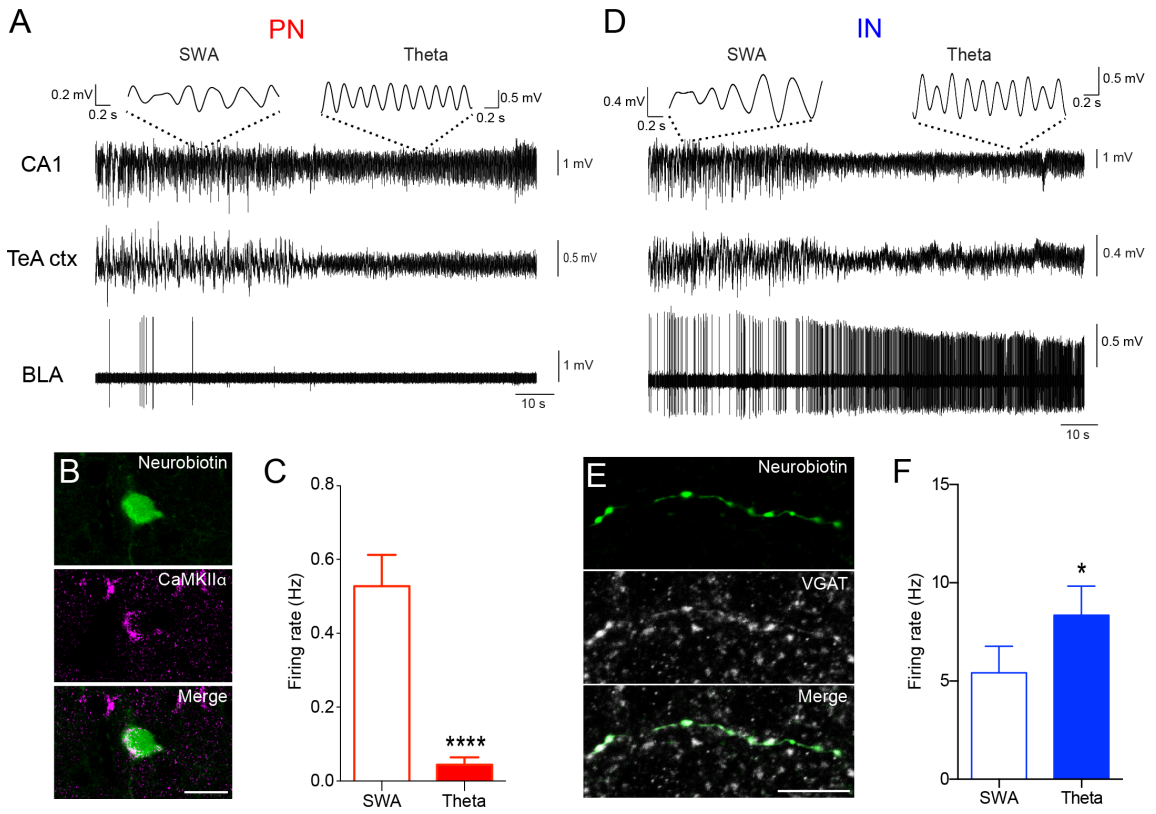

Figure 2.2. Differential firing frequencies of PNs and INs during theta epochs.
A, *in vivo* single unit recording from a representative PN of the BA during SWA and theta oscillations recorded from CA1 HPC and TeA cortex (ctx). This cell became silent at the onset of theta oscillations. Insets show 2 s of CA1 LFP trace bandpass filtered between 2 and 3 Hz (SWA, left) and 3 and 6 Hz (theta oscillations, right). **B**, juxtacellularly labeled PN displaying immunoreactivity for CaMKIIα. **C**, PNs fired at higher frequencies during cortical and hippocampal SWA (0.52 ± 0.08 Hz) and at significantly lower frequencies during theta oscillations (0.04 ± 0.02 Hz, **** $p < 0.0001$ n = 16). **D**, *in vivo* single unit recording from an IN of the BA during SWA and theta oscillations recorded from CA1 HPC and TeA. The firing frequency increased during theta oscillations. *Insets*: 2 s of CA1 LFP trace bandpass filtered between 2 and 3 Hz (SWA, *left*) and 3 and 6 Hz (theta oscillations, *right*). **E**, juxtacellularly labelled GABAergic IN displaying axonal immunoreactivity for VGAT. **F**, INs fired at lower frequencies during cortical and hippocampal SWA (5.42 ± 1.35 Hz) and at significantly higher frequencies during theta oscillations (8.35 ± 1.48 Hz, * $p < 0.05$, n = 20). Scale bars: B, 20 µm; E, 10 µm. Data are presented as means ± SEM.

2.3.2 Theta stimulation of vCA1 pyramidal cell axons inhibits BA PNs and activates INs *in vivo*

We then sought to understand the influence of a theta frequency input from vCA1 pyramidal cells on the firing of BA neurons. To this end, we transfected pyramidal cells of vCA1 with the ultrafast (E123T/T159C) Channelrhodopsin-2 (ChR2, Figure 2.3A-C), which more efficiently evokes action potentials at high frequency stimulation compared to the H134R variant (Berndt et al., 2011). In line with this, light pulses evoked action potentials in vCA1 pyramidal cells with both ChR2 variants, but the E123T/T159C type ensured faster kinetics, especially when 100 Hz burst stimulation was delivered (Figure 2.3D, E). In light of these results, only E123T/T159C was used in subsequent experiments.

Three-four weeks after viral injection, ChR2/YFP+ axons densely innervated the BA and BM, together with the external and intermediate capsules surrounding the BLA, whereas only sparse fibres were observed in the LA (Fig. 2B). This pattern of innervation was consistent with previous tracing studies in rodents (Kishi et al., 2006; Müller et al., 2012). To optically stimulate ChR2+ vCA1 pyramidal cell axons while recording from single neurons of the BA *in vivo*, we implanted a fibre optic above the BA (Figure 2.1D and Figure 2.4C). During navigation CA1 pyramidal cells can fire high frequency bursts of action potential organised by the theta rhythm (O'Keefe and Dostrovsky, 1971; O'Keefe, 1976; Harvey et al., 2009; Epsztein et al., 2011). To mimic a theta-rhythmic input from CA1 pyramidal cells, we delivered an optical TBS during spontaneous non-theta epochs (Luo et al., 2011). Optical TBS of vCA1 axons inhibited the firing of BA PNs (n = 10; 2 additional cells were not responsive) during light trains (baseline 0.5 ± 0.05 Hz, light trains 0.1 ± 0.03 Hz, $p < 0.0001$, n = 10, Fig. 2D, E), suggesting that the hippocampal input may disynaptically inhibit BA PNs via recruitment of GABAergic INs.

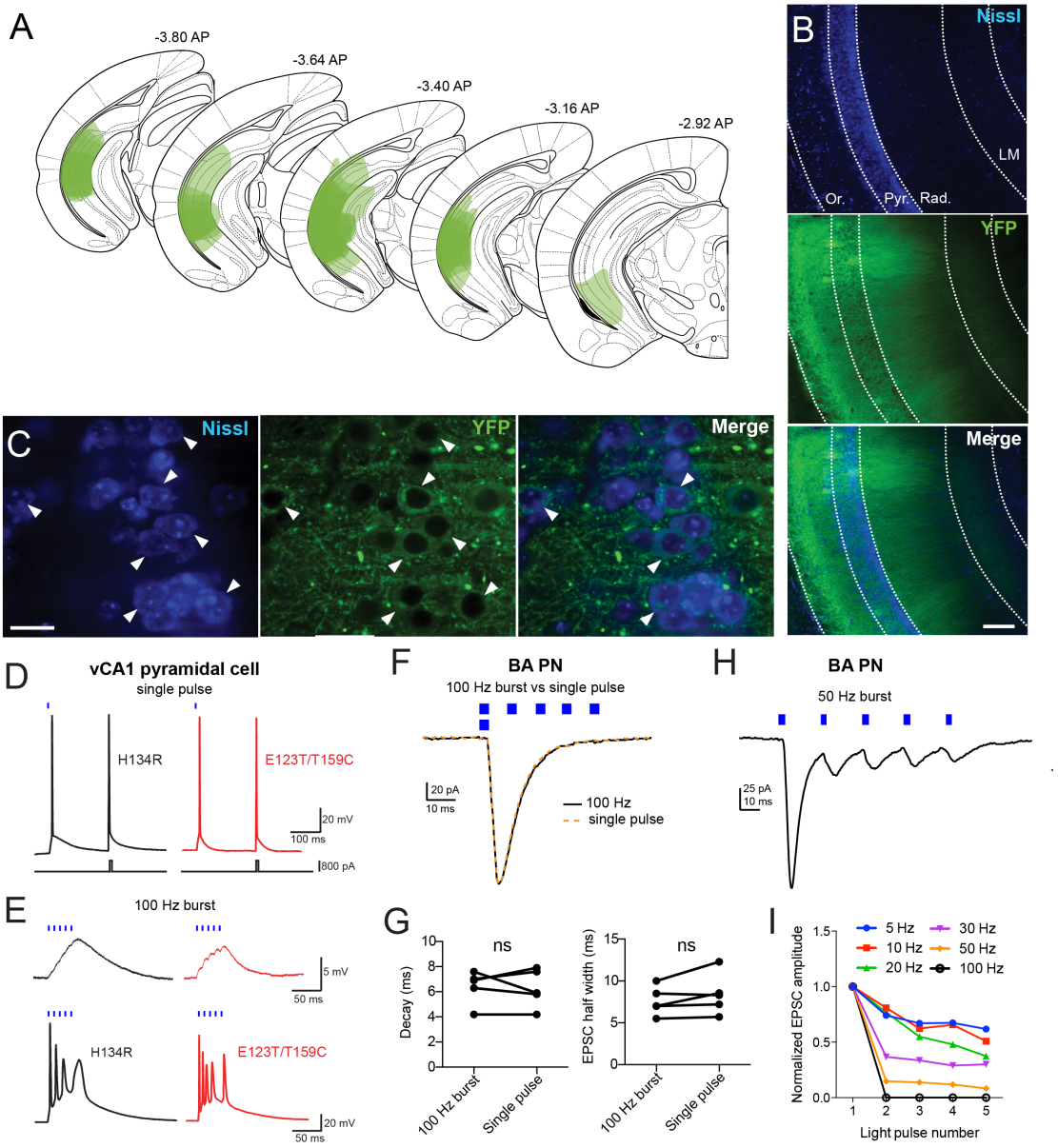

Figure 2.3. Responses to high frequency stimulation of vCA1 pyramidal cell soma or axons expressing ultrafast ChR2/YFP.

A, localisation of 32 injection sites restricted to the ventral/intermediate CA1 areas. Colour intensity reflects the frequency of overlapping injection sites. **B**, Nissl staining of the vCA1 pyramidal cell layer and YFP-ChR2 staining labelling vCA1 pyramidal cells. **C**, high magnification showing expression of YFP-ChR2 in the membrane of individual pyramidal cell somata (arrowheads). Scale bar: 20 mm. **D**, Action potentials elicited by a single light pulse (470 nm, 0.1 ms, left) and by a current step (+800 pA, 0.9 ms) in vCA1 pyramidal cells infected either with H134R (black traces) or E123T/T159C-ChR2 (red traces). After-depolarizations recorded in neurons transfected with E123T/T159C-ChR2 showed faster decay with a similar kinetics that the one induced by a short current pulse. **E**, 100 Hz burst stimulation (5 light pulses, 1 ms duration), as used in TBS, produces a depolarization with faster kinetic and a more reliable induction of action potentials in vCA1 pyramidal cells when the E123T/T159C-ChR2 is used (compare red with black traces, n = 3). *Top*, sub-threshold response (low light intensity). *Bottom*, supra-threshold response (higher light intensity). **F**, representative superimposed EPSCs recorded in voltage clamp from a BA PN (-75 mV) evoked either by 100 Hz burst stimulation (5 light pulses, 3 ms duration, 2 mW/mm^2) or by a single light pulse (3 ms duration, 2 mW/mm^2). **G**, decay and half-width of burst-evoked and single pulse-evoked EPSCs are similar (both $p > 0.05$, n = 5). **H**, representative EPSCs recorded from a BA PN (-75 mV) evoked by a 50 Hz burst stimulation. **I**, EPSCs amplitude (normalised to the 1st EPSC) evoked by 5-100 Hz stimulation in the neuron shown in H. Note the frequency-dependent depression of the EPSCs. Abbreviations: Ctx, cortex; LM, stratum lacunosum moleculare; Or., stratum oriens; Pyr., stratum pyramidale; Rad., stratum radiatum.

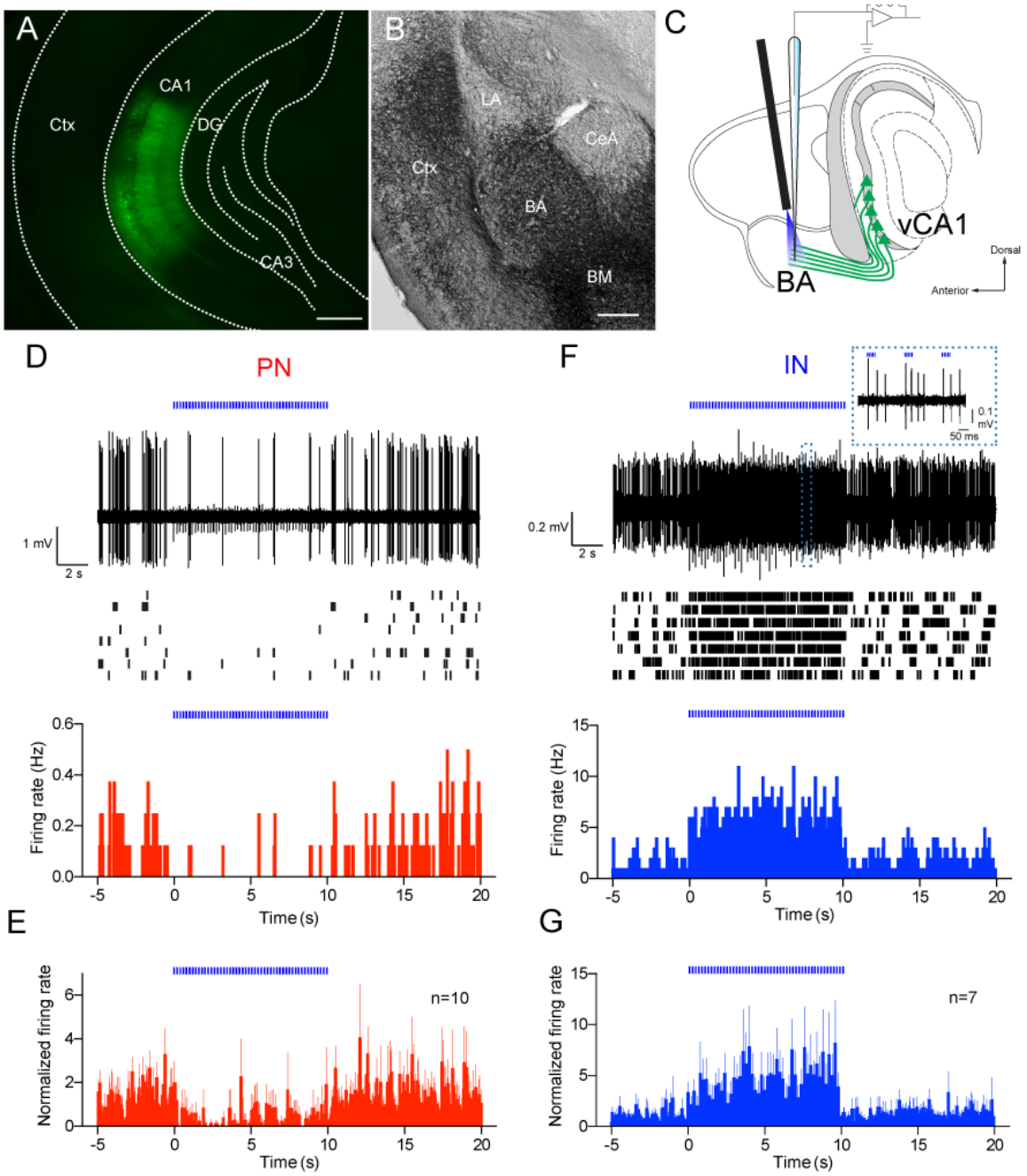

Figure 2.4 Optical TBS of hippocampal axons inhibits PNs and triggers firing in INs of the BA *in vivo*.
A, expression of ChR2/YFP in ventral/intermediate CA1. **B**, light micrograph showing ChR2/YFP-positive axons in the amygdaloid complex. BA and BM nuclei showed densest innervation, whereas only few fibres were detectable in the LA and CeA. **C**, scheme showing experimental configuration: single unit recordings and juxtacellular labelling from neurons of the BA and photostimulation of vCA1 pyramidal cells axons through a fibre optic implanted above the BA. **D**, representative PN was inhibited by optical TBS. Superimposed traces (n = 8, *top*), singularly represented in rasterplot (*middle*), peri-stimulus time histogram (PSTH, 50 ms bins, *bottom*). Note spikelet-like events during TBS are stimulation artefacts. **E**, normalised firing rates (50 ms bins) of BA PNs in response to optical TBS of hippocampal axons (baseline *versus* TBS, $p < 0.01$, n = 10). **F**, representative IN was activated by optical TBS. Superimposed traces (n = 8, *top*), singularly represented in rasterplot (*middle*), PSTH (50 ms bins, *bottom*). *Inset*: TBS evokes action potentials primarily following the first pulse of each train. **G**, normalised firing rates (50 ms bins) of BA INs in response to optical TBS of hippocampal axons (baseline *versus* TBS, $p < 0.05$, n = 7). Scale bars: A, 350 µm; B, 250 µm. Data are presented as means ± SEM.

Consistent with this hypothesis, the same optogenetic stimulation evoked firing in INs (n = 7; 4 additional cells were not responsive; baseline 1.2 ± 0.2 Hz, light trains 3.4 ± 1 Hz, $p < 0.05$, Figure 2.4F, G).

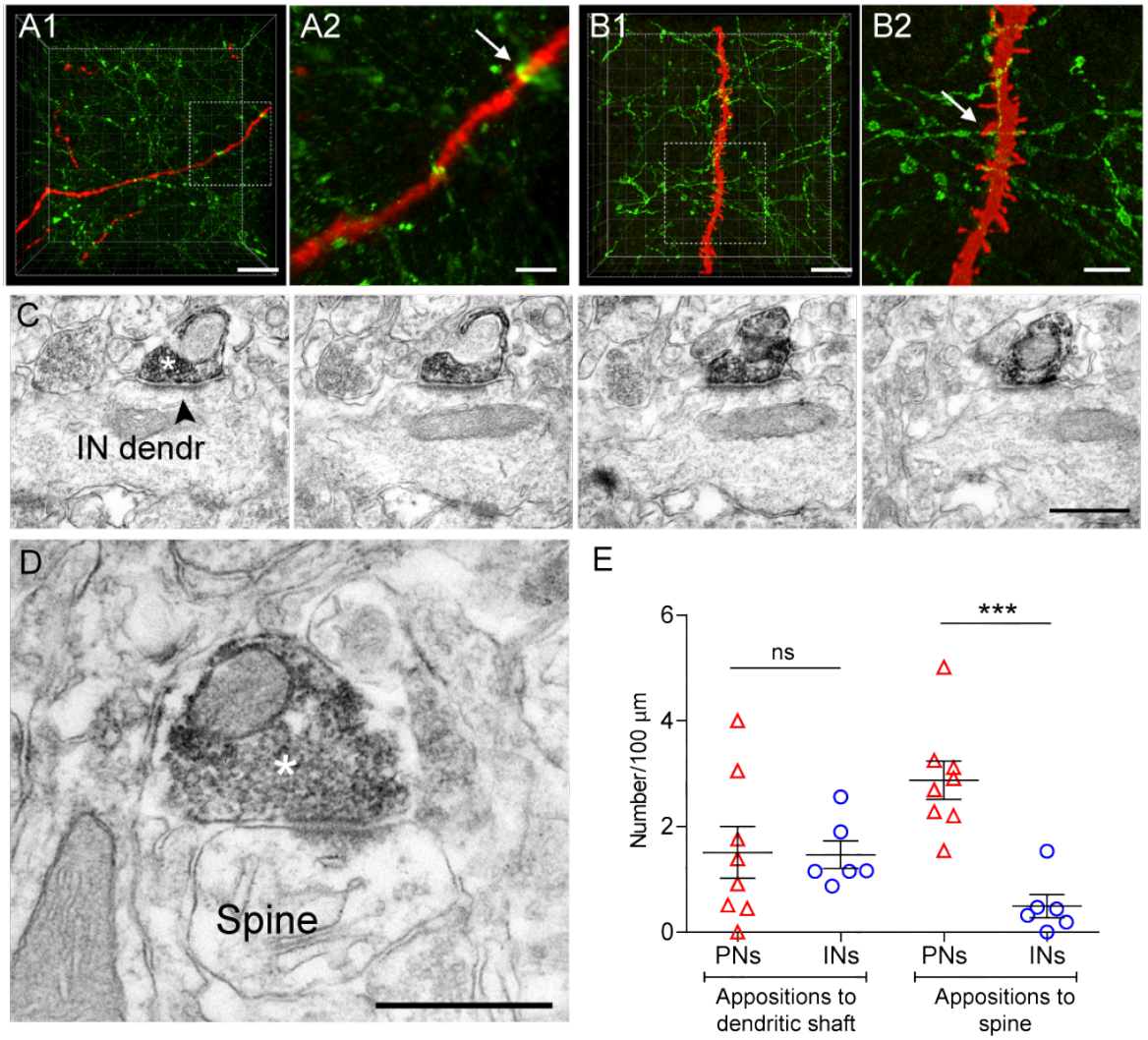

Figure 2.5. CA1 pyramidal cells axons form asymmetric synapses onto both INs and PNs of the BA.
A, low and high magnification micrographs of a Huygens-deconvoluted confocal stack (z-stack: 24 µm; step size: 0.4 µm) of a representative aspiny dendrite of a recorded and biocytin-filled IN (shown in red). The fluorescence of the YFP (shown in green) reveals CA1 hippocampal axons and terminals. The arrow indicates an apposition to the dendritic shaft. **B**, low and high magnification micrographs of a Huygens-deconvoluted confocal stack (z-stack: 14 µm) of a representative spiny dendrite of a recorded and biocytin-filled PN (shown in red). The arrow indicates an apposition of a hippocampal bouton to a spine of the PN. **C**, serial electron micrographs of a GFP-immunolabelled hippocampal axon terminal forming a Type I (asymmetric) synaptic contact (arrowhead) with the dendritic shaft of a putative IN (IN dendr). Asterisk, note the diffuse electron-dense labelling that fills the entire bouton. **D**, GFP-immunolabelled hippocampal axon terminal (asterisk) forming a Type I (asymmetric) synaptic contact with a PN spine. **E**, density of appositions of CA1 hippocampal axons to IN (n = 6) and PN (n = 8) dendritic shafts and spines (per 100 µm). INs and PNs did not show any significant difference ($p > 0.5$) in the density of appositions to dendritic shafts. Conversely, PNs had a significantly higher density of appositions to spines compared to INs (*** $p < 0.001$). Scale bars: A1 10 µm; A2 3 µm; B1 10 µm; B2, 3 µm; C-D, 500 nm. Data are presented as means ± SEM.

To test whether vCA1 axons directly target BA neurons, confocal microscopy of recorded and biocytin-filled BA PNs and INs was used to detect ChR2-YFP positive boutons apposed to their dendrites (Figure 2.5A, B). Hippocampal axons were found to preferentially innervate PNs by targeting dendritic spines, whereas INs were primarily, but not exclusively, contacted on dendritic shafts (Figure 2.5E). Further electron microscopy data confirmed that axons of vCA1 pyramidal cells formed excitatory synapses with PNs and INs dendrites (Figure 2.5C, D). Thus, vCA1 pyramidal cell axons monosynaptically contact PNs and INs of the BA. However, their theta frequency activation evoked opposite responses on PNs and INs recorded *in vivo*. These effects resembled the contrasting firing rates between PNs and INs observed during theta oscillations.

2.3.3 Theta stimulation of vCA1 axons drives feedforward inhibition in BA PNs

Because vCA1 pyramidal cells are glutamatergic, we hypothesised that the inhibition of PNs was due to the disynaptic inhibition triggered by activation of feedforward INs, while the monosynaptic excitation of PNs would remain sub-threshold. To test this hypothesis, we optogenetically dissected the BA circuit activated by vCA1 HPC *ex vivo*. We prepared acute brain slices 3-4 weeks after the ChR2 injection and recorded single BA neurons in cell-attached mode. This configuration did not alter the intracellular milieu of the recorded cell and mimicked our extracellular *in vivo* conditions. PNs and INs could be distinguished by their soma size (diameter $\geq$ 20 μm for PNs, < 15 μm for INs). After cell-attached recordings, 8/40 PNs and 6/18 INs were re-patched in whole-cell mode to confirm their identity. Optical stimulations were delivered through the microscope objective to excite vCA1 axons within an area of ~200 μm diameter around the soma of the recorded neurons. We observed that the power of single light pulse stimulation had to be significantly higher ($p < 0.0001$) to trigger

one action potential in PNs (9.5 ± 0.3 mW/mm^2, n = 33) compared to INs (2.5 ± 0.2 mW/mm^2, n = 11, Figure 2.6G). This suggests that the synchronous activation of a larger number of vCA1 pyramidal cell axons is required to make PNs fire, compared to INs.

To investigate how synaptic excitation and inhibition evoked by activation of vCA1 fibres influence the firing of BA neurons, we recorded neurons in whole-cell mode. Intracellularly-recorded neurons were classified as PNs or INs according to both electrophysiological and anatomical parameters (see 2.2.5 *Ex vivo* recordings and analysis for details). Single light pulse stimulation triggered a monosynaptic EPSP followed by an early-fast and late-slow IPSPs in 66% of PNs (n = 80/122, Figure 2.7A), and EPSP followed by early IPSP in 15% of PNs (n = 18/122, Figure 2.7B).

When we recorded from BA INs (n = 31) or intercalated neurons (ITCs, n = 13, Figure 2.8; pooled in the experiments presented below) the same stimulation evoked an EPSP in 61% of the neurons (n = 27/44, Figure 2.6F). All types of synaptic responses observed in PNs or INs are summarised in Figure 2.7. Notably, 11/13 recorded ITCs were histologically verified, and their cell bodies found either in the external capsule (n = 4), intermediate capsule (n = 4) or main intercalated nucleus (n = 3). The IPSPs were disynaptic because they were abolished by the application of the glutamate receptor antagonists NBQX (10 μM) and APV (100 μM; Figure 2.6H, n = 5).

In PNs the early and late IPSPs were mediated by $GABA_A$ and $GABA_B$ receptors because they were abolished by SR95531 (10 μM, Figure 2.6I, J, n = 5) and CGP54626 (5 μM, Figure 2.6J, n = 26), respectively. We further confirmed that the optogenetic stimulation activated presynaptic Na^+ channels by blocking PSPs with 1 μM tetrodotoxin (n = 3, data not shown).

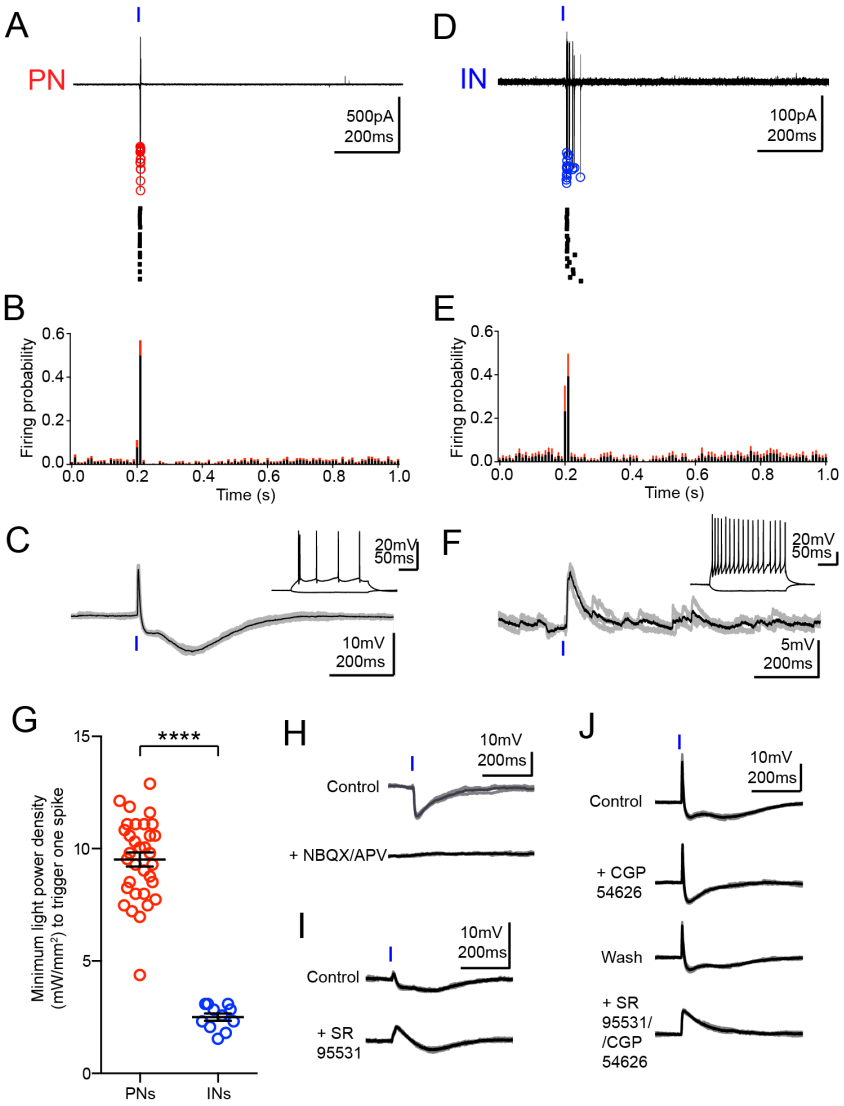

Figure 2.6 Activation of hippocampal inputs provides feedforward inhibition of BA principal neurons.
A, *ex vivo* cell-attached recording from a representative PN in response to single light pulses (20 superimposed sweeps, top, singularly represented in rasterplot, bottom). Red circles denote spike negative peak. **B**, mean probability of firing of PNs (bins=10 ms, black: mean, red: SEM; n = 24). **C**, whole-cell recording of the same cell as in A showing that the light pulse induced a PSP composed of an EPSP followed by a biphasic IPSP. On average, the peak amplitudes of the EPSP, early IPSP and late IPSP were 8.9 ± 1 mV, 4.1 ± 0.8 mV and 2.7 ± 0.6 mV (n = 24), respectively. *Inset*: Response to hyperpolarizing and depolarizing current injections showing stereotypic PN firing. **D**, cell-attached recording from a representative IN in response to a single light pulse (20 superimposed sweeps, top, singularly represented in rasterplot, bottom). Blue circles denote spike negative peak. **E**, mean probability of firing of INs (bin = 10 ms, black: mean, red: SEM; n = 11). **F**, whole-cell recording of the same cell as in D showing that the light stimulation evoked a monophasic EPSP. On average, the peak amplitude of the EPSP was 8.1 ± 0.7 mV (n = 24). *Inset*: Response to hyperpolarizing and depolarizing current injections displaying stereotypic IN firing. **G**, minimum light power density (mW/mm^2) necessary to trigger one spike in PNs (n = 33) and INs (n = 11). Significantly higher power was necessary to reach spike threshold in PNs (**** $p < 0.0001$). **H**, the IPSP induced by a single light pulse was blocked by glutamatergic antagonists NBQX (10 µm)/APV (100 µm) suggesting it was mediated by feedforward inhibition due to activation of BA INs (n = 5). I, the early IPSP was blocked by the GABAA receptor antagonist SR95531 (10 µm, n = 5). **J**, the late IPSP was blocked by the $GABA_B$ receptor antagonist CGP54626 (5 µm, n = 26). Co-application of SR95531 and CGP54626 abolished IPSPs and increased the duration of the EPSP. All data from whole-cell recordings shown are three superimposed (grey) and average traces (black). Data are presented as means ± SEM.

Blockade of $GABA_A$ receptors alone or together with blockade of $GABA_B$ receptors increased the duration of the EPSPs (Figure 2.6I, J and Figure 2.7C), consistent with previous demonstrations that feedforward inhibition narrows the time window for the integration of synaptic excitation (Pouille and Scanziani, 2001; Gabernet et al., 2005).

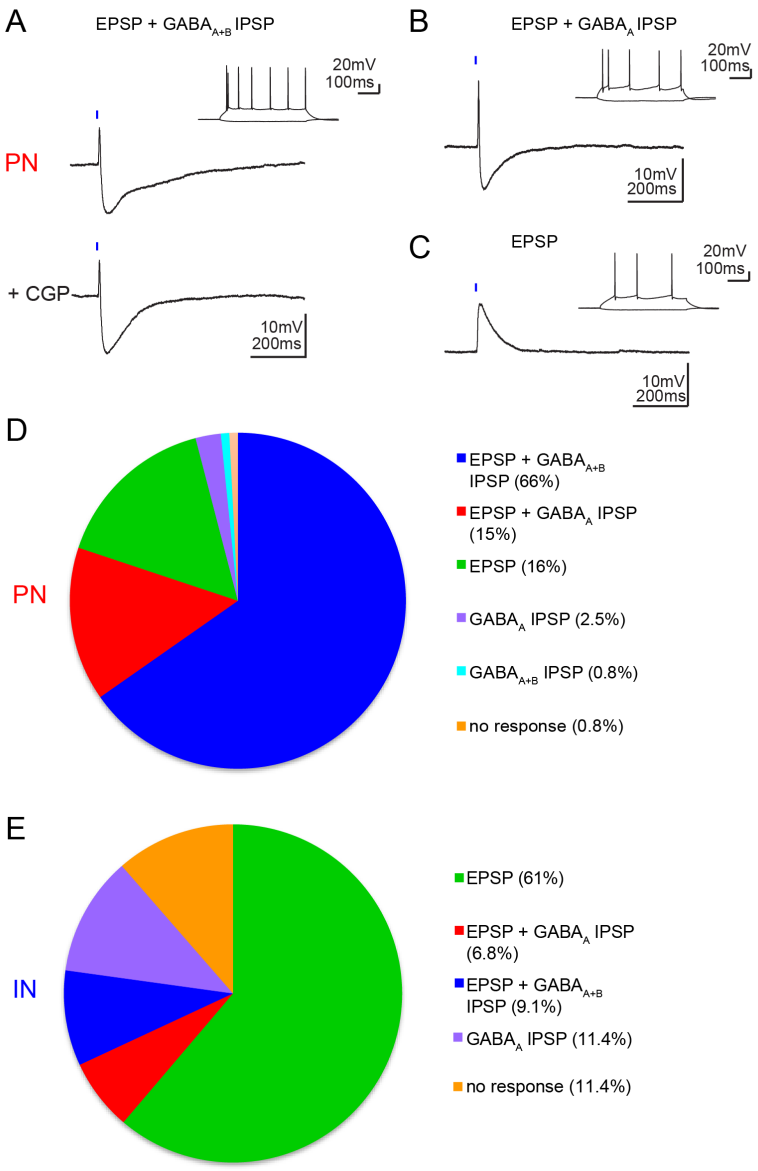

Figure 2.7 Optogenetic stimulation of vCA1 axons evokes heterogeneous responses in BA PNs. **A**, representative EPSP + $GABA_{A+B}$ IPSP response in a BA PN. The late $GABA_B$ IPSP is blocked by 5 µM CGP54626. **B**, representative EPSP + $GABA_A$ IPSP response in a BA PN. **C**, representative EPSP only response in a BA PN. **D**, summary of all responses obtained by a single light pulse in BA PNs. An EPSP + $GABA_{A+B}$ was evoked in 80/122 cells, an EPSP + $GABA_A$ IPSP was obtained in 18/122 cells and an EPSP only was recorded in 19/122 cells. Furthermore, a few PNs (3/122) displayed only $GABA_A$ IPSP, one PN showed a $GABA_{A+B}$ IPSP, and another PN did not show any detectable response. **E**, summary of all responses obtained by a single light pulse in BA INs. An EPSP only was evoked in the majority of them (27/44). We also observed: EPSP + $GABA_A$ IPSP (3/44); EPSP + $GABA_{A+B}$ IPSP (4/44); $GABA_A$ IPSP only (5/44); no response (5/44).

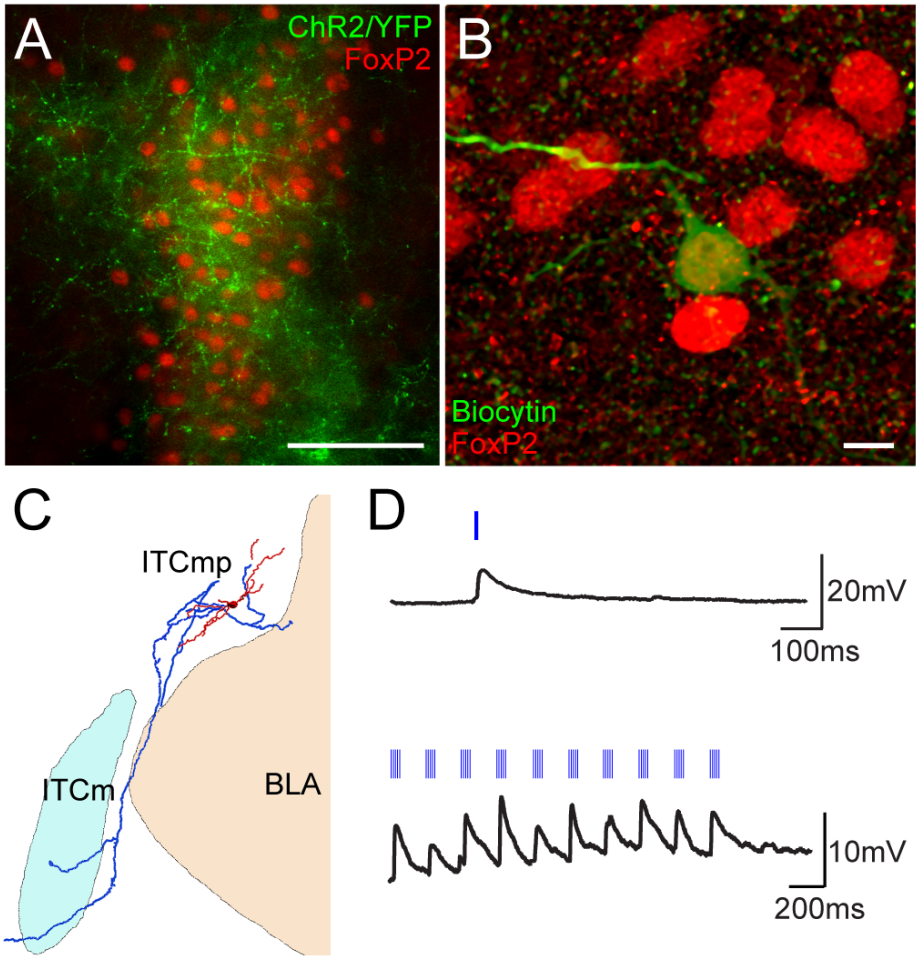

Figure 2.8. ITCs receive excitatory inputs from vCA1 pyramidal cells.
A, immunofluorescence micrograph of vCA1 hippocampal axons expressing ChR2-YFP (shown in green) coursing through the dorso-medial cluster of ITCs identified for their nuclear expression of the transcription factor FoxP2 (shown in red). **B**, high magnification micrograph of a Huygens-deconvoluted confocal stack (z-stack: 26 µm; the z-step size was 0.46 µm) of the soma of a representative recorded and biocytin-filled medium spiny ITC (shown in green) identified by its FoxP2 immunolabelling (shown in red). Fluorescence of the YFP tag of ChR2 in vCA1 hippocampal axons and terminals is visualized here also in the green channel.
C, collapsed image of a 3D Neurolucida reconstruction of a recorded and biocytin-filled medium spiny ITC revealing axonal branches running along the intermediate capsule. Soma and dendrites are shown in red, axon in blue. **D**, optogenetic activation of vCA1 axons evoked EPSPs in a representative ITC. Top, single light pulse (3 ms). Bottom, Theta burst stimulation (3 ms light pulses). Scale bars: A, 50 µm; B, 5 µm. Abbreviations: BLA, basolateral amygdala; ITCmp, medial paracapsular ITC nucleus; ITCm, main ITC nucleus.

Next, we wished to test whether TBS-evoked inhibition of PN spontaneous firing occurred in a slice preparation. In these conditions, long-range projections to the BA are cut, ruling out that their stimulation would in turn trigger activation of other regions projecting to the BA. First, we optically activated vCA1 fibres at theta frequency while recording from BA neurons in cell-attached mode, using light intensities sufficient to evoke an action potential in

INs but not in PNs (range: 2-3 mW/mm^2). Optogenetic TBS transiently inhibited the firing of PNs (Figure 2.9A-C, 2nd train *versus* baseline $p < 0.0001$, $n = 7$). In contrast, TBS triggered action potentials synchronised to each light train in INs (Figure 2.9D-F, 2nd train *versus* baseline $p < 0.01$, $n = 7$).

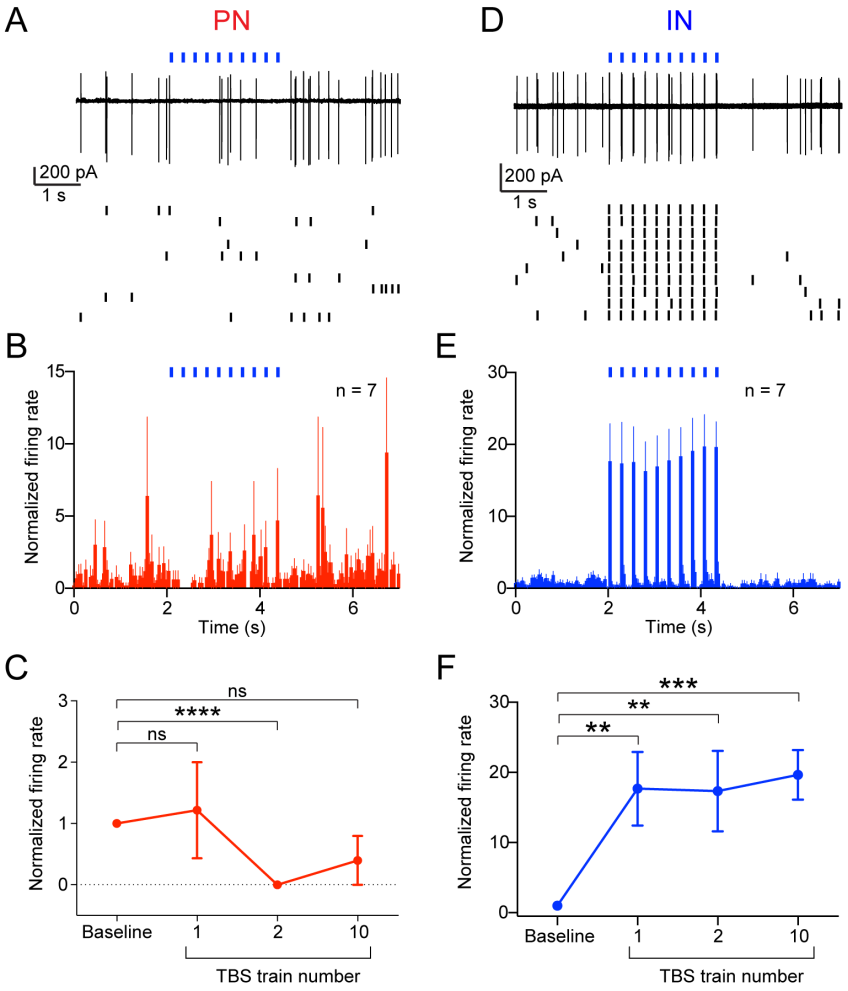

Figure 2.9. Optical TBS of hippocampal axons transiently inhibits PNs and triggers firing in INs ex vivo. **A,** *ex vivo* cell-attached recording from a representative BA PN inhibited by TBS of vCA1 axons (10 superimposed sweeps, top, singularly represented in rasterplot, bottom). **B**, pooled data showing PNs firing rates over time during TBS (bin = 50 ms, n = 7). **C**, firing rates of PNs compared between baseline, 1st, 2nd and 10th trains of the TBS. Firing is significantly reduced during the 2nd train and partially recovers at 10th train. **D**, ex vivo cell-attached recording from a representative BA IN. TBS of vCA1 axons triggers action potentials (10 superimposed sweeps, top, singularly represented in rasterplot, bottom). **E**, pooled data showing INs firing rates over time during TBS (bin = 50 ms, n = 7). **F**, firing rates of INs compared between baseline, 1st, 2nd and 10th trains of the TBS. Firing is significantly increased during TBS trains. ** $p < 0.01$; *** $p < 0.001$; **** $p < 0.0001$. Data are presented as means ± SEM.

We also used higher light intensities, sufficient to evoke action potentials in PNs (> 10 mW/mm^2) to examine the impact of TBS on evoked firing. In this case, optogenetic TBS transiently depressed the evoked spike probability in BA PNs (Figure 2.10A, B, 2nd *versus* 1st TBS trains $p < 0.001$, $n = 22$) via activation of $GABA_B$ receptors (Figure 2.10E, F, 2nd *versus* 1st train $p > 0.05$, $n = 9$).

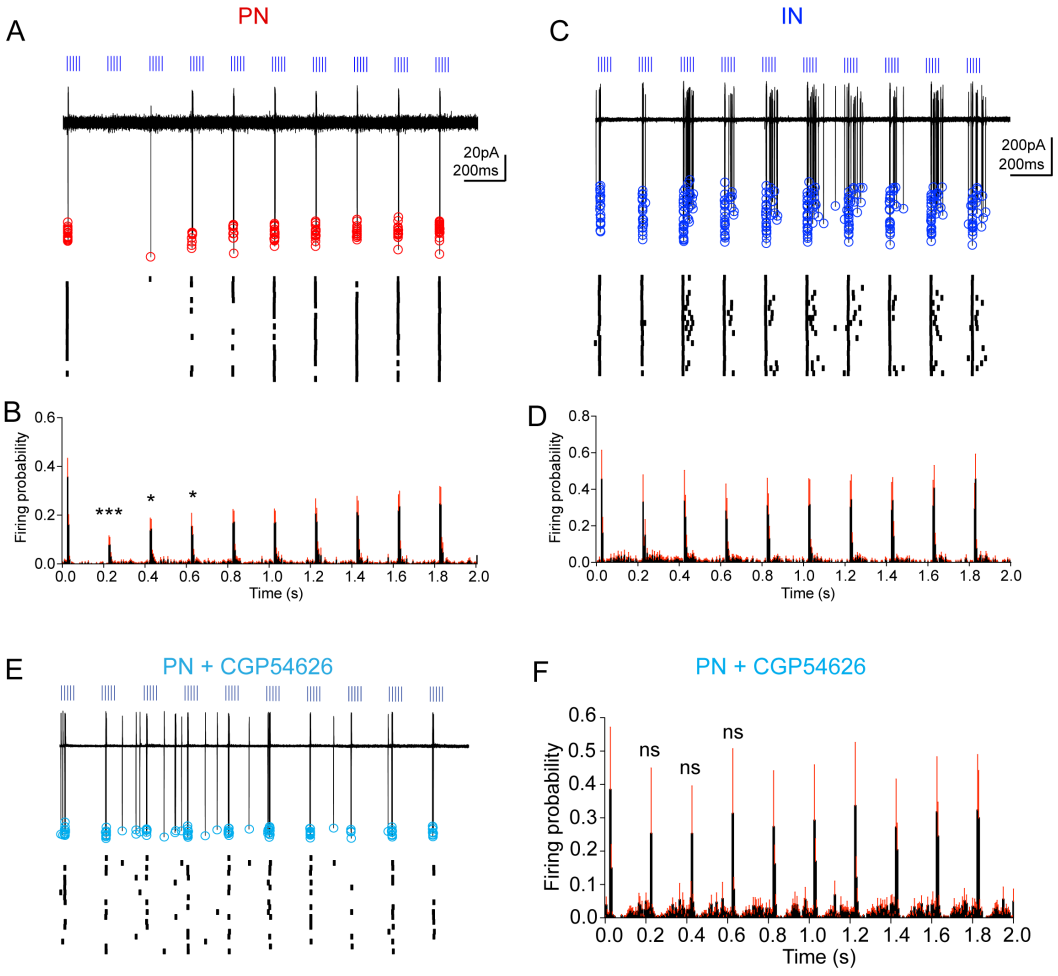

Figure 2.10. High intensity TBS of vCA1 axons transiently depresses the firing of PNs in a $GABA_B$ receptor manner, and reliably activates INs *ex vivo*.
A, representative *ex vivo* cell-attached recording from a PN during TBS (20 superimposed sweeps, top, singularly represented in rasterplot, bottom). The first train of light pulses (> 10 mW/mm^2) reliably evoked spikes, while the firing probability was reduced in the following 3 trains. Red circles denote spike negative peak. **B**, pooled data showing firing probability over time during TBS (bin = 5 ms, black: mean, red: SEM; n = 22, * $p < 0.05$, *** $p < 0.001$). **C**, representative cell-attached recording from an IN during TBS (20 superimposed sweeps, top, singularly represented in rasterplot, bottom). TBS (> 10 mW/mm^2) reliably evoked spikes throughout all the 10 TBS trains. Blue circles denote spike negative peak. **D**, pooled data showing firing probability over time during TBS (bin = 5 ms, black: mean, red: SEM; n = 9, $p > 0.05$). **E**, representative cell-attached recording from a PN during TBS applied at high intensity (> 10 mW/mm^2) in presence of CGP54626 (top, 20 superimposed sweeps; bottom, rasterplot). Blockade of $GABA_B$ receptors prevents the reduction in firing probability. **F**, mean firing probability over time during TBS in the presence of CGP54626 (bin = 5 ms, black: mean, red: SEM; $p > 0.05$, $n = 10$). Data are presented as means ± SEM.

In contrast, TBS did not reduce the spike probability of INs (Figure 2.10C, D, 2nd *versus* 1st TBS trains $p > 0.05$, $n = 10$). These results suggest that the activation of hippocampal fibres by TBS preferentially recruits GABAergic INs of the BA, inhibiting the spontaneous firing of PNs or sculpting their hippocampal-driven firing via feedforward inhibition.

2.3.4 Cellular dynamics evoked by theta stimulation of vCA1 axons

Next, we investigated synaptic and membrane excitability dynamics that are likely to cause modulation of firing by TBS in PNs. To this end, we performed whole-cell recordings of PNs and INs in the BA during optical TBS. First, TBS elicited a transient membrane hyperpolarization (Figure 2.11A, B, 2nd train *versus* 1st train $p < 0.0001$, $n = 34$), that resulted in EPSP peak transiently lowered to more hyperpolarized potentials (Figure 2.11A, C, 2nd train *versus* 1st train $p < 0.001$, $n = 34$). Both effects were mediated by $GABA_B$ receptors since they were blocked by CGP54626 (5 μM; Figure 2.11A-C, 2nd train *versus* 1st train $p > 0.05$, $n = 17$). Second, TBS caused a depression of the IPSP amplitude (Figure 2.11A, D, 2nd train *versus* 1st train $p < 0.0001$, $n = 34$). This led to a significant increase of the EPSP area (Figure 2.11A, E, 2nd train *versus* 1st train $p < 0.05$, $n = 30$), consistent with feedforward inhibition constraining the duration of excitatory inputs. These effects were also dependent on $GABA_B$ receptor activation because they were blocked by 5 μM CGP54626 (Figure 2.11A, D, E, 2nd train *versus* 1st train $p > 0.05$, $n = 17$). Furthermore, when light stimulation elicited only an EPSP followed by $GABA_A$-IPSP, as observed in a few PNs, the membrane hyperpolarization and the depression of IPSP amplitude were greatly reduced (Figure 2.12, $p > 0.05$, $n = 9$), consistent with the $GABA_B$-receptor dependency of these effects. In these cases, the GAT-1 blocker SKF89976A (25 μM) produced a transient hyperpolarization and depression of the IPSP amplitude (Figure 2.12, $p < 0.05$, $n = 6$). most likely through GABA spillover and

activation of extrasynaptic $GABA_B$ receptors (presynaptic $GABA_B$ receptors mediating IPSP depression, postsynaptic $GABA_B$ receptors mediating hyperpolarization).

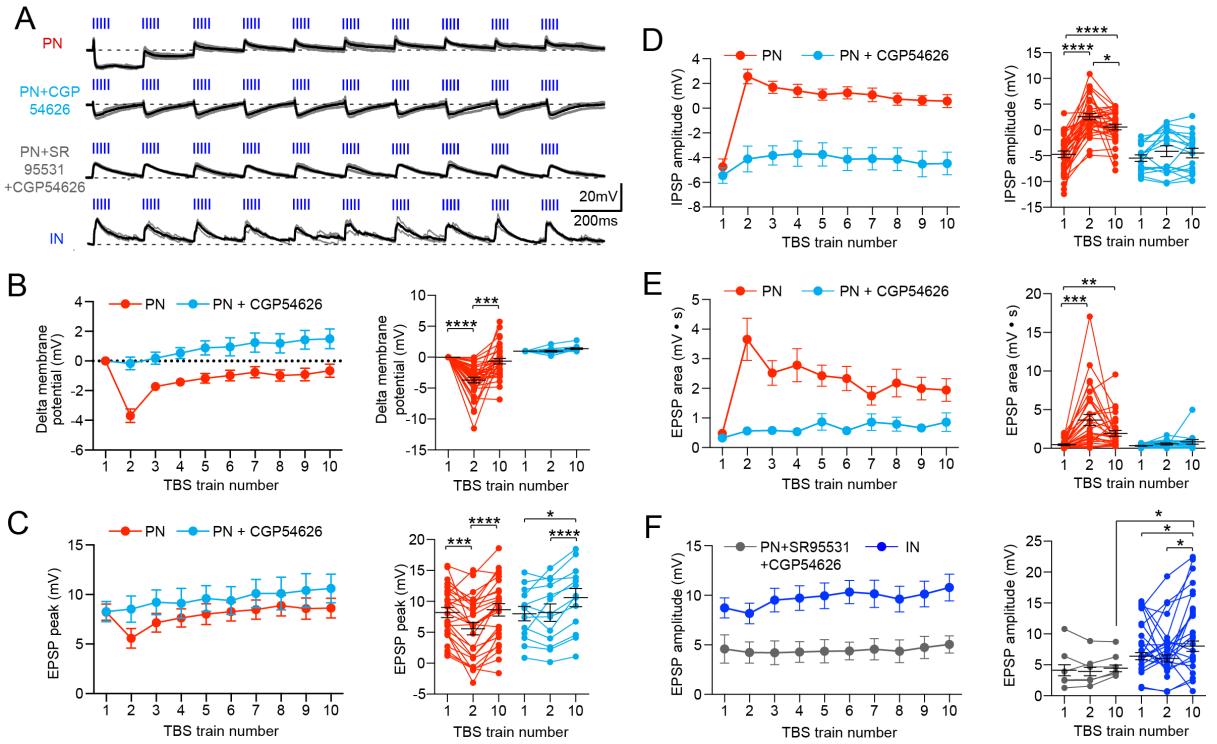

Figure 2.11. Synaptic dynamics evoked by TBS in BA PNs and INs.
A, synaptic potentials (3 superimposed sweeps, grey traces; average, black trace) evoked by TBS in representative PNs and in a representative IN in control and in presence of the $GABA_A$ (SR95531, 10 µM) and $GABA_B$ receptor (CGP54626, 5 µM) antagonists. **B**, **C**, *left*, peak of EPSP and V_m recorded from PNs for each TBS train in control (n = 34) and in the presence of CGP54626 (n = 17). *Right*, V_m and EPSP peak compared between the 1st, 2nd and 10th trains of the TBS. Hyperpolarization and depression of the EPSP peak were blocked by CGP54626. In control, the V_m change from baseline was -3.7 ± 0.5 mV at the 2nd train and -0.7 ± 0.5 mV at the 10th train. In the presence of CGP54626, these values were -0.2 ± 0.4 mV and +1.5 ± 0.7 mV. In control, the EPSP peak change from the 1st train was -2.6 ± 0.6 mV at the 2nd train and +0.4 ± 0.5 mV at the 10th train. In the presence of CGP54626, these values were +0.2 ± 0.7 mV and +2.6 ± 0.8 mV. **D**, *left*, IPSP amplitude recorded from PNs for each TBS train in control (n = 34) and in presence of CGP54626 (n = 17). Note that the control IPSP that starts as hyperpolarizing (negative potential value), becomes depolarizing in response to the following stimuli during TBS (positive potential values). *Right*, IPSP amplitude is compared between the 1st, 2nd and 10th trains of the TBS. IPSP depression was blocked by CGP54626. In control, the IPSP amplitude change from the 1st train was +7.3 ± 0.8 mV at the 2nd train and +5.3 ± 0.5 mV at the 10th train. In the presence of CGP54626, these values were +1.3 ± 0.6 mV and +1 ± 0.6 mV. **E**, *left*, EPSP area recorded from PNs for each TBS train in control (n = 30) and in the presence of CGP54626 (n = 15). *Right*, broadening of EPSP area with the 2nd TBS train. Broadening still persisted at the 10th train and was blocked by CGP54626. In control, the EPSP area change from the 1st train was +3.2 ± 0.7 mV at the 2nd train and +1.5 ± 0.4 mV at the 10th train, In the presence of CGP54626, these values were +0.2 ± 0.1 mV and +0.5 ± 0.3 mV. **F**, *left*, EPSP amplitude for each train of the TBS in presence of SR95531 and CGP54626 in PNs (n = 6) and in INs (n = 23). *Right*, the EPSP amplitude was stable in PNs in presence of SR95531 and CGP54626. In INs the EPSP amplitude significantly increased at the 10th TBS train. At the 10th train, EPSP amplitude was significantly more depolarized in INs than PNs. In control, the EPSP amplitude change from the 1st train was -0.6 ± 1 mV at the 2nd train and +2.6 ± 1 mV at the 10th train. In the presence of CGP54626, these values were -0.3 ± 0.5 mV and +0.5 ± 0.8 mV. * $p < 0.05$; ** $p < 0.01$; *** $p < 0.001$; **** $p < 0.0001$. Data are presented as means ± SEM.

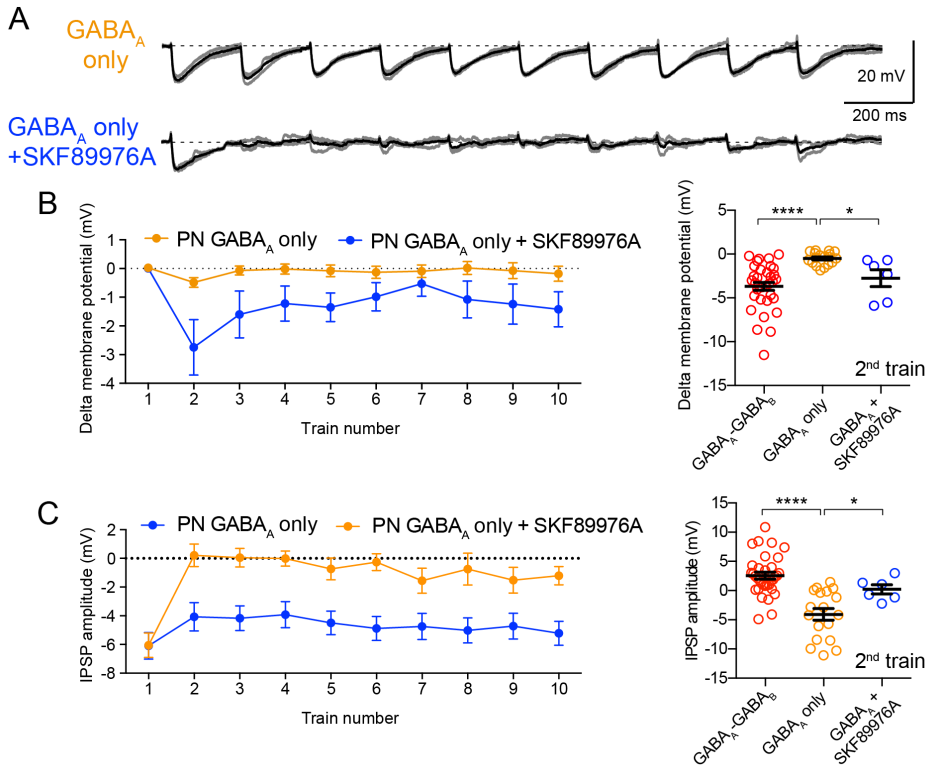

Figure 2.12. Blockade of GABA reuptake evokes depression of feedforward inhibition in PNs with vCA1-evoked GABA$_A$ receptor only IPSPs.
A, representative synaptic potentials (3 superimposed sweeps, grey traces; average, black trace) evoked by TBS in a PN were a GABA$_A$ only IPSP was induced by single light pulses (*top*). Same protocol delivered in presence of the GAT-1 blocker SKF89976A (25 µM, *bottom*). **B**, *left*, V_m recorded from PNs for each TBS train in control (n = 34) and in the presence of SKF89976A (n = 18). *Right*, V_m was significantly more depolarized during the 2nd train in PNs where TBS evoked GABA$_A$ and GABA$_B$ IPSPs than in PNs where a GABA$_A$ IPSPs only were evoked. SKF89976A significantly increased membrane hyperpolarization in PNs where a GABA$_A$ IPSPs only were evoked (n = 6). **C**, *left*, IPSP amplitude recorded from PNs for each TBS train in control (n = 9) and in the presence of SKF89976A (n = 6). *Right*, IPSP amplitude was significantly reduced during the 2nd train in PNs where TBS evoked GABA$_A$ and GABA$_B$ IPSPs, compared to PNs where a GABA$_A$ IPSPs only were evoked. However, TBS depressed GABA$_A$ IPSP only recorded in PNs in the presence of SKF89976A (n = 6). * $p < 0.05$; **** $p < 0.0001$. Data are presented as means ± SEM.

To verify whether the depression of feedforward inhibition occurs during a physiological, non-rhythmic input from vCA1 pyramidal cells, we used as optical stimulation a spike train that was recorded during open field exploration from a vCA1 place cell projecting to the BLA by Prof. Thomas Klausberger's group (Ciocchi et al., 2015). This stimulation elicited responses in BA PNs highly similar to TBS, namely a transient membrane hyperpolarization (2nd light pulse *versus* 1st light pulse $p < 0.001$, n = 8) and a dynamic depression of feedforward inhibition (2nd light pulse *versus* 1st light pulse $p < 0.0001$, n = 8; Figure 2.13A-E).

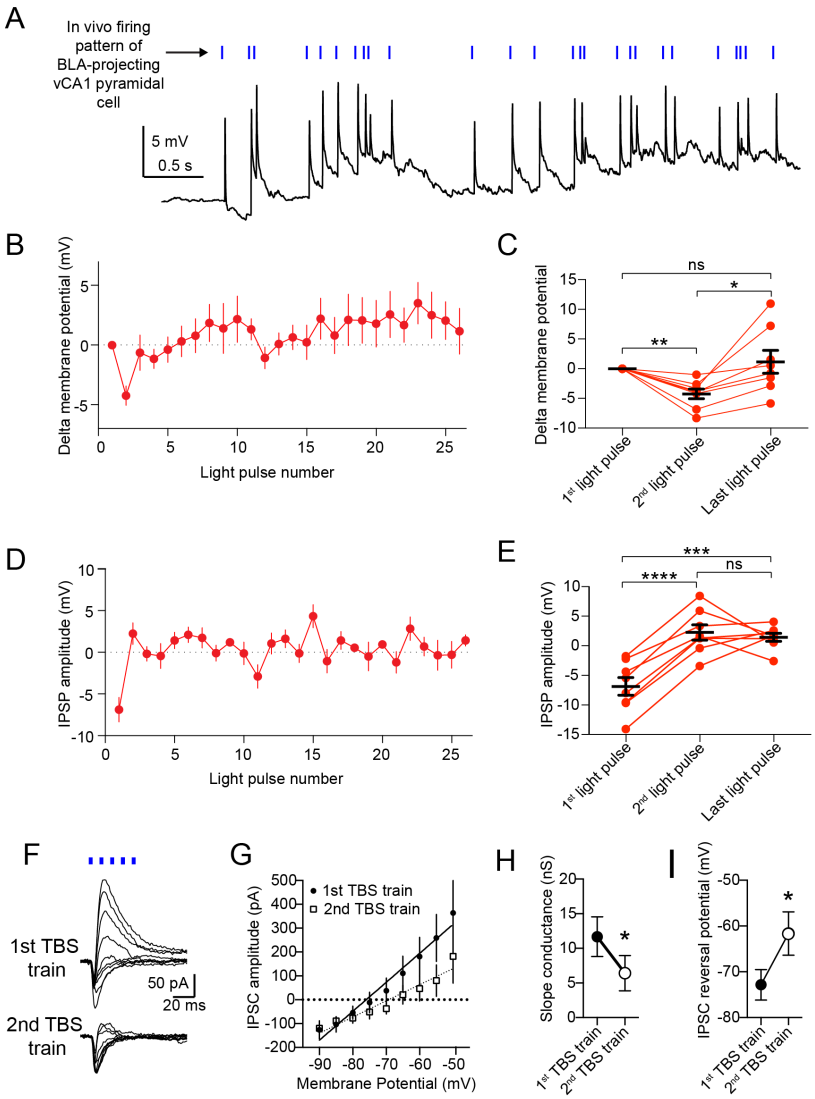

Figure 2.13. Optical stimulation of vCA1 axons with firing pattern of a vCA1 pyramidal cell recapitulates synaptic dynamics evoked by TBS. **A**, synaptic potentials evoked by optical stimulation of vCA1 axons with firing pattern of a BLA-projecting vCA1 pyramidal cell recorded during exploratory behaviour. **B**, PNs V_m preceding each light pulse (n = 8). **C**, V_m compared between 1st, 2nd and last light pulses. Hyperpolarization occurs at the 2nd light pulse, but is recovered by the last light pulse. Delta V_m (compared to V_m before the 1st light pulse) was -4.2 ± 0.8 mV (2nd light pulse) and +1.2 ± 1.9 mV (last light pulse). **D**, IPSP amplitude plotted for each light pulse (n = 8). **E**, IPSP amplitude compared between 1st, 2nd and last light pulses. IPSP depresses at the 2nd light pulse and remains significantly reduced until the last light pulse. The change of the IPSP amplitude (compared to IPSP amplitude following 1st light pulse) was +9.1 ± 0.8 mV (2nd IPSP) and +8.3 ± 1.7 mV (last IPSP). **F**, representative voltage clamp trace from PN showing TBS-evoked EPSPs and IPSPs at the 1st and 2nd TBS trains at different holding potentials (from -90 mV to -50 mV, 5 mV steps). **G**, IPSC amplitude plotted for each holding potential for 1st and 2nd TBS trains (n = 6). **H**, the 2nd TBS train causes a significant decrease in $GABA_A$ synaptic conductance. I, the 2nd TBS train causes a significant shift of the IPSC reversal potential (E_{IPSC}) towards more depolarized Vms. * $p < 0.05$; ** $p < 0.01$; *** $p < 0.001$; **** $p < 0.0001$. Data are presented as means ± SEM.

Furthermore, we tested whether the depression of the IPSP was caused by a reduction in $GABA_A$ conductance. We recorded PNs in voltage clamp mode, applying optical TBS at different holding potentials to plot the peak current of the 1st and 2nd IPSC *versus* the holding potential. The slope of this I/V relationship was reduced for the 2nd IPSC (from 11.7 ± 2.9 nS to 6.4 ± 2.6 nS, $p < 0.05$, $n = 6$), suggesting that the $GABA_A$ conductance was indeed decreased. We also observed that the E_{IPSC} shifted from -72.8 ± 3.3 mV for the 1st IPSC to -

61.6 ± 4.7 mV for 2nd IPSC ($p < 0.05$, $n = 6$, Figure 2.13F-H). The E_{IPSC} shift suggests that a reduction in the driving force for Cl^- may contribute to the depression of feedforward inhibition during TBS, consistent with the residual IPSP depression still present with CGP54626 and previous reports (Segal and Barker, 1984; Huguenard and Alger, 1986). Thus, $GABA_B$-dependent reduction of $GABA_A$ conductance, and perhaps also the shift in the E_{IPSC} account for the synaptic dynamics observed.

The $GABA_B$ receptor-mediated effects could be due to the depression of either glutamatergic synapses from vCA1 fibres onto BA INs, and/or GABAergic synapses from BA INs onto PNs. We distinguished between these two possibilities by recording directly from GABAergic INs with the soma in the BA and ITCs. The EPSPs recorded in these cells displayed a gradual increase in amplitude through the TBS (Figure 2.11A, F, 10th *versus* 1st train $p < 0.05$, $n = 23$). Hence, vCA1-BA INs excitatory synapses could not be responsible for the transient depression of the IPSPs recorded from PNs. Furthermore, the amplitude of the EPSPs recorded from PNs was stable in presence of antagonists for GABA receptors (Figure 2.11A, F, 10th *versus* 1st train $p > 0.05$, $n = 6$), indicating that vCA1-BA PNs excitatory synapses do not undergo depression during TBS.

Next, we tested whether presynaptic mechanisms contribute to the depression of the IPSP amplitude. Monosynaptic IPSPs were triggered in PNs through local electrical stimulation in the presence of NBQX (10 μM) and APV (100 μM). The application of the $GABA_B$ receptor agonist baclofen (10 μM) abolished the monosynaptic IPSPs (Figure 2.14A, B, $n = 5$, $p < 0.01$).

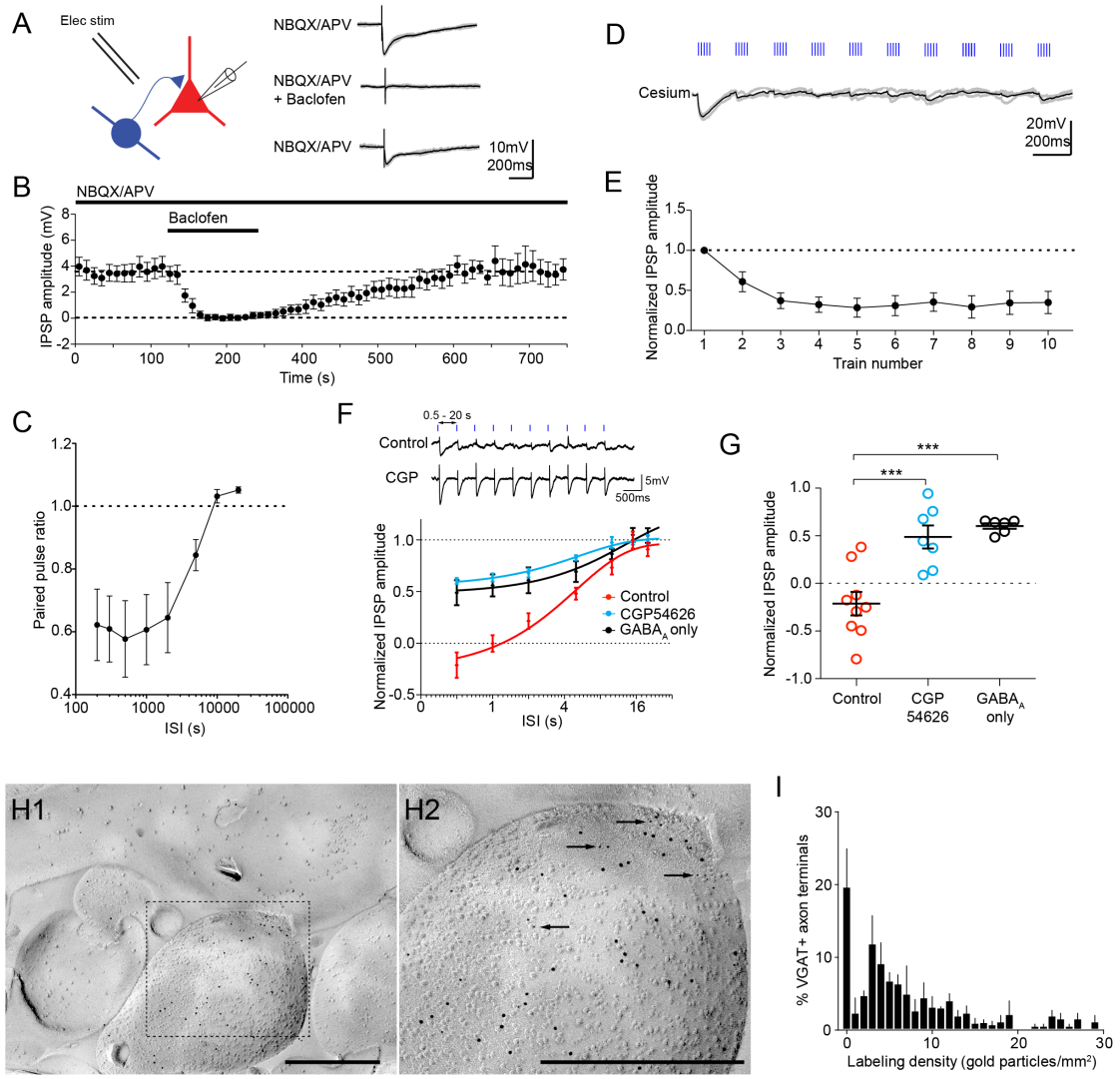

Figure 2.14. Presynaptic GABA$_B$ receptors at BA IN-PN synapses mediate depression of feedforward inhibition
A, *left*, schematic of the experimental configuration. Local electrical stimulation is applied while recording from PNs. *Right*, representative current clamp recording (–65 mV) showing monosynaptic IPSP induced by local electrical stimulation in presence of NBQX/APV. The IPSP was abolished by the GABA$_B$ receptor agonist baclofen (10 µM). During baclofen application, neurons hyperpolarized but were held at –65 mV to avoid changes in driving force for Cl^-. **B**, pooled data, (n = 6). **C**, paired-pulse ratio of IPSCs recorded in PNs and evoked by local electrical stimulation. Paired-pulse ratio reduced with shorter inter-stimulus intervals (ISIs). **D**, the depression of IPSPs during TBS occurred in a PN recorded at 0 mV with caesium-containing intracellular solution. **E**, pooled data (n = 7). **F**, trains of ten single pulses were delivered with variable ISIs (0.5, 1, 2, 5, 10, 15, and 20 s) while recording from PNs. *Top*, representative trace during which light pulses were delivered at 0.5-s intervals. Depression of the IPSP was largely blocked by CGP54626. *Bottom*, average of the last three IPSPs evoked for each ISI normalised to the first IPSP. The IPSP amplitude became smaller with shorter ISIs. This depression was reduced when stimulation evoked only GABA$_A$ receptor IPSPs or in presence of CGP54626 (5 µM). **G**, mean amplitudes of last three IPSPs elicited with a train of ten single pulses delivered every 0.5 s: IPSP amplitude in control conditions (n = 9) was significantly lower than in presence of CGP54626 ($p < 0.001$ *versus* control, n = 7) or in PNs where only a GABA$_A$ IPSP was evoked ($p < 0.001$ *versus* control, n = 6). **H1**, electron micrograph of a GABAergic terminal in the BA as obtained with the SDS-digested FRIL method. Scale bar: 500 nm. **H2**, enlarged view of the area within the dashed lines in (H1). Larger gold particles (10 nm) reveal VGAT, whereas smaller gold particles (5 nm; arrowheads) identify GABA$_B$ receptors. Scale bar: 500 nm. **I**, Frequency distribution of VGAT+ axon terminals with different density of GABA$_B$ receptor labelling (n = 179 synapses obtained from three mice). Data are presented as means ± SEM.

The magnitude of this effect suggests that activation of presynaptic $GABA_B$ receptors and an increase in postsynaptic membrane conductance induced by baclofen accounted for this effect. To further corroborate the involvement of presynaptic $GABA_B$ receptors in the depression of the IPSP amplitude, additional experiments were carried out. First, electrical stimulation was delivered while recording postsynaptic neurons in voltage clamp mode. The paired-pulse ratio of electrically-evoked IPSCs, a parameter critically dependent on presynaptic $GABA_B$ receptors (Davies et al., 1990), became smaller with shorter inter-stimulus intervals (Figure 2.14C, n = 5). Second, we observed depression of IPSPs during optical TBS using a caesium-based intracellular solution to block postsynaptic K^+ channels linked to $GABA_B$ receptors (Figure 2.14D, E, n = 7; Gähwiler and Brown, 1985). Third, we delivered trains of 10 single light pulses with varying inter-stimulus intervals; the IPSP amplitude was inversely related to the inter-stimulus interval (Figure 2.14F). In the presence of CGP54626, such use-dependent depression of the IPSPs was significantly reduced (5 μM, $p < 0.001$ *versus* control, Figure 2.14F-G). Likewise, TBS-induced depression of the IPSPs was attenuated in PNs in which $GABA_A$-only IPSPs were evoked ($p < 0.001$ *versus* control, Figure 2.14F, G). This suggests that when spillover of GABA onto extrasynaptic $GABA_B$ receptors at postsynaptic site is weak or absent, resulting in $GABA_A$ only IPSP, spillover of GABA on presynaptic $GABA_B$ receptor (López-Bendito et al., 2004) is also less likely to occur, ensuing more stable IPSPs. Fourth, we detected $GABA_B$ receptors at the axon terminals of INs using the SDS FRIL method (Figure 2.14H, I). Taken together, these data demonstrate that vCA1-driven feedforward inhibition on BA PNs is dynamically modulated by $GABA_B$ receptors located on the axon terminals of GABAergic INs. What could be the consequences of feedforward inhibition dynamics for synaptic integration and plasticity in PNs?

2.3.5 Theta stimulation of vCA1 axons gates heterosynaptic plasticity in BA PNs

The PNs, which are the major output of the BA, represent the downstream target not only of vCA1 axons but also of LA neurons that may convey information from somatosensory areas (Pitkänen et al., 1997). Since the depression of the IPSPs affects the temporal window for synaptic integration, we reasoned that this phenomenon might gate synaptic plasticity of quasi-coincidental excitatory inputs from other sources. To test this idea, we electrically stimulated the LA while recording from BA PNs (Figure 2.15A). First, we observed that the monosynaptic EPSP induced by LA stimulation was not significantly different following electrical TBS of the LA (Figure 2.15B–D, last 5 min *versus* baseline $p > 0.05$, $n = 6$) even in the presence of the $GABA_A$ receptor antagonist picrotoxin (100 μM, last 5 min *versus* baseline $p > 0.05$, $n = 5$, Figure 2.16A, B), ruling out LA-driven feedforward inhibition as gatekeeper of LA-BA plasticity. Additionally, optical TBS of vCA1 axons did not induce LTP at synapses between vCA1 pyramidal cells and BA PNs (Figure 2.16C, D), but only short-term potentiation, in line with previous reports (Maren and Fanselow, 1995). Hence, depression of feedforward inhibition evoked by vCA1 input does not seem to produce homosynaptic long-term plasticity. Thus, we asked whether it could promote heterosynaptic long-term plasticity of a parallel excitatory pathway, namely the glutamatergic connection between LA PNs and BA PNs. To test this, we paired TBS of the LA with optical TBS of vCA1 axons. LA electrical stimuli were delayed by 10 ms from the optical stimuli so that LA inputs occurred near the peak of the IPSP, which depresses during optical TBS. Strikingly, vCA1-LA pairing induced LTP at excitatory synapses between LA PNs and BA PNs (Figure 2.15B–D, last 5 min *versus* baseline $p < 0.05$, $n = 7$). In contrast, when LA electrical stimuli were delayed by 100 ms from the optical stimuli, thus occurring when vCA1 EPSPs had completely decayed, vCA1-LA pairing did not elicit LTP (Figure 2.15B–D, last 5 min *versus*

baseline $p > 0.05$, $n = 7$). Finally, the application of 5 µM CGP54626 blocked the pairing-induced LTP (Figure 2.15B–D, last 5 min *versus* baseline $p > 0.05$, $n = 5$).

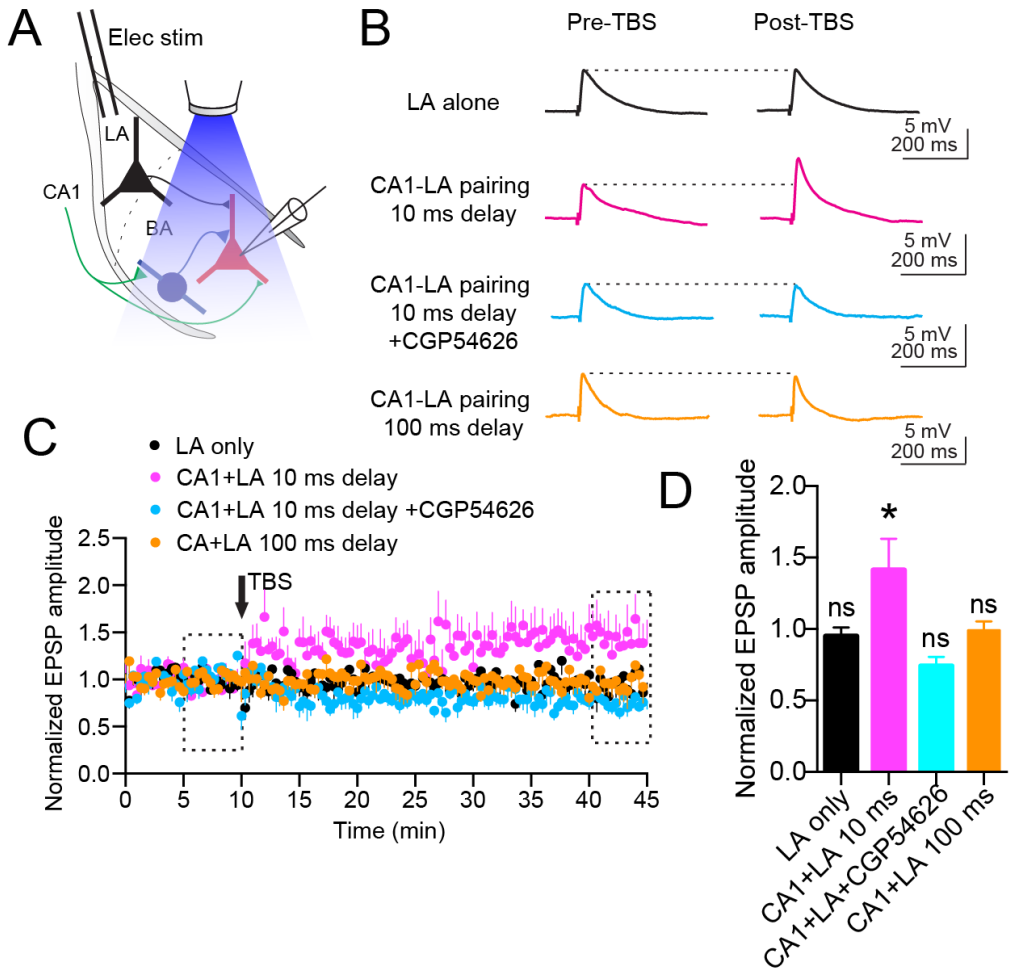

Figure 2.15. TBS of hippocampal inputs gates LTP of LA-BA synapses.
A, schematic of the experimental configuration: optical stimulation of vCA1 axons in the BA was paired with electrical stimulation of the LA while recording from PNs. **B**, representative traces (average of ten sweeps) showing EPSPs evoked by electrical stimulation of the LA before and after TBS (50 trains). TBS was applied to the LA only (*top*), to the LA 10 ms after optical TBS of vCA1 axons without (*upper middle*) or with CGP54626 (5 µM, *lower middle*), or to the LA 100 ms after optical TBS of vCA1 axons (*bottom*). Stimulation artefacts are truncated. **C**, the EPSP amplitude plotted over time (stimulation occurs every 10 s). Dashed rectangles represent intervals used for statistical comparisons in (D). Pairing of LA-vCA1 TBS ($n = 7$) induced LTP, which did not occur with TBS of the LA only ($n = 6$), but also in the presence of CGP54626 ($n = 5$) or when TBS of the LA was evoked 100 ms after TBS of the vCA1 axons ($n = 7$). **D**, quantification of the intervals in (C). Each condition is compared with its own baseline. The EPSP amplitude was significantly increased ($*p < 0.05$) after LA-vCA1 pairing with 10-ms delay. Data are presented as means ± SEM.

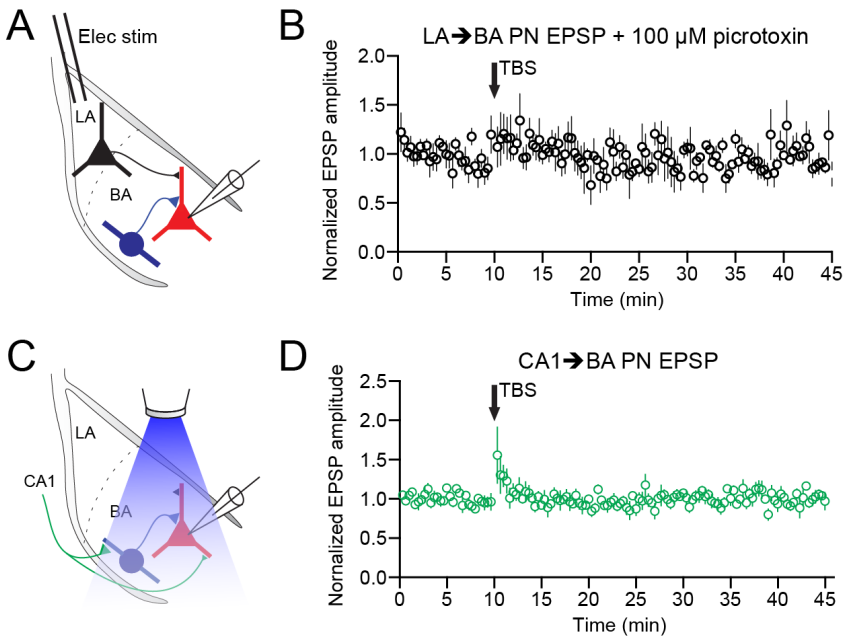

Figure 2.16. Blockade of $GABA_A$ receptors does not unmask LA-BA PN LTP, and TBS of vCA1 axons does not evoke vCA1-BA PN LTP.
A, schematic of the experimental configuration: the LA was stimulated electrically while recording from BA PNs. **B**, LA-BA PN EPSP amplitude plotted over time (stimulation occurs every 10 s). Electrical TBS of the LA did not evoke LTP at LA-BA PN synapses in presence of the $GABA_A$ receptor antagonist picrotoxin (100 µM, n = 5). **C**, schematic of the experimental configuration: vCA1 axons were stimulated optically while recording from BA PNs. **D**, vCA1-BA PN EPSP amplitude plotted over time (stimulation occurs every 10 s). Optical TBS of vCA1 axons evoked a short-term facilitation of the vCA1-BA PN EPSP, but no LTP (n = 5). Data are presented as means ± SEM.

Taken together, these data suggest that the vCA1 HPC gates the induction of LTP of excitatory connections between LA PNs and BA PNs in a delay-dependent manner by depressing feedforward inhibition from local INs via presynaptic $GABA_B$ receptors (Figure 2.17).

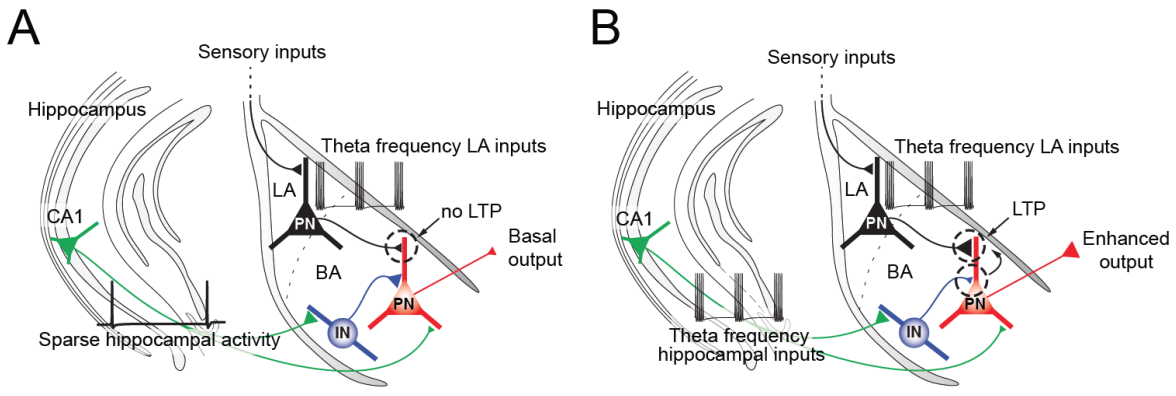

Figure 2.17 Model of the vCA1-BA circuit.
A, during sparse firing of CA1 pyramidal neurons projecting to the BA, strong vCA1 input to BA INs drives feedforward inhibition onto BA PNs. This results in brief vCA1-mediated excitation and hyperpolarization of PNs via $GABA_B$ receptors. Theta frequency stimulation of the LA alone does not elicit LTP. **B**, during theta frequency inputs driven by vCA1 pyramidal cells to BA neurons, a $GABA_B$ receptor-dependent depression of GABA release from INs occurs. This results in broadening of the temporal window for the integration of excitation in PNs. This mechanism allows the induction of heterosynaptic LTP at LA-BA synapses when LA is simultaneously stimulated at theta frequency. Coloured triangles depict presynaptic terminals and their size indicates synaptic strength.

2.4 Discussion

This study provides learning-relevant cellular mechanisms for hippocampal gating of amygdala information processing. We found that theta frequency firing of vCA1 pyramidal cells caused inhibition of BA PN firing by driving local INs. Inhibition of PNs was accompanied by a reduction of GABA release from feedforward INs onto PNs via the activation of presynaptic $GABA_B$ receptors and potentially by changing postsynaptic $GABA_A$-receptor-mediated Cl^- driving force. This depression of feedforward inhibition reduced the hyperpolarization; broadened the temporal window for integration of excitatory stimuli; and, when occurring together with a synchronous input from the LA, gated the induction of LTP at LA-BA synapses.

We found an opposite pattern of activity of BA PNs and INs *in vivo* following transitions from SWA to theta oscillations in afferent structures (CA1 and TeA). This is consistent with the increase in BLA PNs firing rate during slow wave sleep (Paré and Gaudreau, 1996). Our data suggest that theta frequency input from vCA1 to the BA may account for this brain state-dependent firing, as photostimulation of vCA1 axons inhibited BA PNs firing via activation of feedforward INs and $GABA_B$ receptors.

One way in which theta frequency activation of afferent vCA1 hippocampal fibres might lead to decreased PN firing is by membrane hyperpolarization. We demonstrate that this was mediated by excitation of feedforward INs and activation of postsynaptic $GABA_B$ receptors in PNs. This hyperpolarization implies that sparse excitatory inputs are less effective because they are less likely to reach threshold for spike generation. An explanation of the stronger inhibitory effect of hippocampal theta input on PNs firing observed *in vivo* might reside in lower PNs firing rates during urethane anaesthesia, greater GABA release in an intact brain, and stimulation-driven EPSPs remaining sub-threshold. Indeed, higher

stimulation intensities were needed to evoke supra-threshold responses in PNs compared to INs *ex vivo*, consistent with previous reports in the cortex (Gabernet et al., 2005). As the number of appositions and, therefore, of putative synaptic contacts made by hippocampal afferents was higher on PNs than on INs, the higher excitability of INs could be explained by greater synaptic strength of vCA1-INs synapses and/or R_{in}, which is usually higher in INs than PNs.

Our observations challenge the simple prediction that excitatory inputs from vCA1 would lead to sustained excitation and increase in firing of PNs of the BA. We show that feedforward inhibition rapidly and powerfully overrides excitation, dampening the spike output of BA PNs. Our data are consistent with prominent feedforward inhibition triggered by recruitment of INs after the stimulation of excitatory CA1 fibres in the BA (Hübner et al., 2014; Zhang et al., 2015). Moreover, electrical stimulation of the BLA inhibits pyramidal cells and excites INs of the mPFC in anaesthetized rats (Dilgen et al., 2013), suggesting that vHPC, BLA, and mPFC are wired through similar cellular patterns. Hence, it is appealing to speculate that the effect of reduction in firing of putative BLA PNs by directional theta input from the mPFC recently reported (Likhtik et al., 2014) is also mediated by recruitment of local INs.

It is a general principle that feedforward inhibition shapes synaptic integration in PNs of various brain areas (Pouille and Scanziani, 2001; Gabernet et al., 2005; Mittmann et al., 2005). In our experiments, activation of vCA1 fibres led to a use- and time-dependent attenuation of feedforward inhibition of the BA via presynaptic $GABA_B$ receptors and by postsynaptic reduction of the IPSC driving force. This triggered a dynamic increase of the temporal window for the integration of coincident EPSPs. As a result, pairing TBS of the LA input with TBS of the vCA1 HPC elicited LTP at LA-BA excitatory synapses onto PNs. Such

temporal mechanism of coincidence detection acts in synergy with reduced likelihood to reach the action potential threshold for sparse excitatory inputs caused by V_m hyperpolarization. The use-dependent suppression of feedforward inhibition could also provide a cellular mechanism for the short-lasting facilitation of the EPSP or the field potential evoked in the BLA by optical or electrical high-frequency stimulation of HPC fibres to the BLA (present results and previously reported data: Maren and Fanselow, 1995).

A transient shift in the E_{Cl} due to frequent activation of $GABA_A$ receptors is consistent with previous report (Segal and Barker, 1984; Huguenard and Alger, 1986). However, it is important to note that the contribution of the shift of the E_{Cl-} to the depression of feedforward inhibition could have been overestimated, because an increase in the duration of the monosynaptic EPSC might have contaminated the measurement (see 2.2.5 *Ex vivo* recordings and analysis for details). To avoid this contamination, we performed the voltage clamp experiment shown in Figure 2.13F-I in presence of picrotoxin, reasoning that subtraction of the picrotoxin voltage clamp traces from the control traces would have revealed the pure disynaptic IPSC component (without the monosynaptic EPSC). Unfortunately, blockade of $GABA_A$ receptors with picrotoxin resulted in bursts of polysynaptic EPSCs (not shown) that prevented a reliable subtraction. As a result, activation of presynaptic $GABA_B$ receptors could in fact account for the majority of the IPSP depression. Future experiments examining a monosynaptic IPSC in BA PNs triggered by stimulation of BA INs could clarify whether a shift in E_{Cl} plays a role in this effect.

Our data are likely to predict cellular dynamics that underlie physiological interactions between vCA1 and BA during behaviour. However, because our data were collected *in vivo* under anaesthesia or *ex vivo*, it is possible that differences exist in awake, behaving animals. Interestingly, we observed similar effects, namely transient membrane hyperpolarization and

short-term IPSP plasticity, when a spike train occurring during open field exploration of a vCA1 place cell projecting to the BLA (Ciocchi et al., 2015) was used as optical stimulation.

We cannot exclude that other mechanisms, in addition to the depression of feedforward inhibition, could be involved in the heterosynaptic plasticity observed. The activation of PV+ INs by vCA1 input could in turn inhibit SOM+ INs, leading to disinhibition of the dendrites of PNs (Wolff et al., 2014). In this regard, a recent report suggests the activation of several types of BA INs, including fast-spiking and non-fast-spiking PV+ cells, as well as PV-negative INs by CA1 fibres in the mouse (Hübner et al., 2014).

Furthermore, we report here that ITCs show excitatory responses to the optogenetic stimulation of vCA1 axon in the BA. This result is consistent with anatomical data obtained with classical tracing methods in the rat (Kishi et al., 2006). In addition to ITCs of the external capsule (Marowsky et al., 2005), it is likely that some ITCs with the soma in the intermediate capsule also mediate feedforward inhibition of BA PNs (Asede et al., 2015; Bienvenu et al., 2015).

Apart from ITCs, this study did not clarify which IN types are recruited by the vCA1 to drive feedforward inhibition onto PNs. Future experiments could reveal which IN types receive a monosynaptic EPSP from vCA1 pyramidal cells. This could be achieved by anatomical analysis of the recorded cells, including their neurochemical content and their postsynaptic targets. This analysis could be facilitated by the use of transgenic mice in which PV+, SOM+, CCK+ or VIP+ cells are fluorescently labelled. An AAV driving the expression of ChR2 under the control of the CaMKIIα promoter could still allow selective targeting of vCA1 pyramidal cells. Additionally, it is important to understand which IN types express presynaptic $GABA_B$ receptors and mediate the depression of feedforward inhibition. A

previous study from our laboratory suggests that neurogliaform cells might be a candidate (Manko et al., 2012).

Our data were obtained using optogenetic, synchronous TBS of several vCA1 hippocampal fibres. The exposure to a single behavioural context consistently activates an elevated number of CA1 cells in the mouse (Liu et al., 2014), as it occurs in the TBS protocol where several CA1 fibres are activated by the optogenetic stimulation. It is important to keep in mind, however, that CA1 pyramidal cells usually do not fire simultaneously (Pastalkova et al., 2008) and that the number of active place cells is lower in vHPC than in dorsal HPC (Kjelstrup et al., 2008; Royer et al., 2010). Furthermore, the stimulation of vCA1 fibres would activate not only the feed-forward circuit defined here, but also other parallel circuits. These could include (1) activation of feedback INs that would in turn inhibit PNs, (2) disynaptic excitation of PNs by axon collaterals of nearby PNs, and (3) antidromic activation of vCA1 pyramidal cells leading to release of glutamate in other brain areas, such as mPFC, in turn projecting to the BA. Regarding the latter, individual vCA1 neurons can project to both the mPFC and the amygdala (Ciocchi et al., 2015), as well as to other brain structures (Arszovszki et al., 2014; Ciocchi et al., 2015). However, we observed modulation of firing patterns by TBS of vCA1 fibres in neurons recorded *in vitro*. In these conditions, changes in the excitability exerted by other extra-amygdaloid inputs, such as those from the mPFC should be negligible.

Our data further suggest that activation of $GABA_B$ receptors plays a crucial role in the induction of long-term plasticity at BA synapses. Specifically, we propose that vCA1 theta inputs gate LTP at synapses between LA and BA PNs by depressing feedforward inhibition from local INs via $GABA_B$ receptors located at their axon terminals. This mechanism occurring in BA neurons mirrors the suppression of feedforward inhibition by dopamine, which gates the induction of LTP in the LA (Bissière et al., 2003). While $GABA_B$ receptors at

excitatory fibres suppress TBS-induced LTP in LA PNs (Pan et al., 2009), our data demonstrate that $GABA_B$ receptors at inhibitory axon terminals promote TBS-induced LTP in BA PNs.

Notably, the present study has not investigated in detail the mechanisms of LTP induction at synapses between LA PNs and BA PNs via activity of vCA1 axons. One possibility is that repetitive vCA1 pyramidal cell firing, by broadening the EPSP integration window, can decrease the synchrony at which LA and vCA1 neurons need to fire to lead to EPSP summation and action potential generation in BA PNs (implying postsynaptic induction of NMDA-dependent STDP). Alternatively, postsynaptic induction of LTP via Ca^{2+} influx through NMDA receptors could rely on net depolarization (thus independently from postsynaptic spike generation). Blocking postsynaptic action potential with QX-314 could distinguish between these two possibilities. However, the associative nature of this LTP suggests that induction mechanisms could also imply activation of presynaptic NMDA receptors on LA PN terminals via glutamate spillover from vCA1 terminals (similarly to Humeau et al., 2003). In the last two scenarios, even irregular firing of vCA1 pyramidal cells (such as the *in vivo* firing pattern replayed and shown in Figure 2.13) could have higher chances to promote LTP at synapses between LA PNs and BA PNs, compared to the first scenario (STDP), which would require higher firing rhythmicity in both LA PNs and vCA1 pyramidal cells.

In any case, vCA1 pyramidal cell repetitive firing seems to increase the likelihood of LA-BA synapses strengthening during behaviour, which might be important for associative learning. For example, during fear conditioning somatosensory information is thought to reach the BA primarily via the LA (Pitkänen et al., 1997). Thus, hippocampal feedforward inhibition could be critical to gate LA information in the BA. This could imply stronger BA

excitatory output, which might have repercussions on CeA neurons and extra-amygdaloid areas targeted by BA PNs to modulate fear responses. Future studies could clarify whether an optogenetic hippocampal theta input to the BA can alter fear learning. Facilitation of LTP at synapses between LA and BA PNs suggests that a theta frequency vCA1 input to the BA could strengthen fear memory acquisition. This hypothesis is appealing because "fear neurons" receive prominent inputs from vHPC (Herry et al., 2008), but further experimental evidence is necessary to validate it.

In summary, our findings provide critical cellular and molecular mechanisms mediating HPC-amygdala interactions. Dissection of this circuit is essential not only to decode fear memory formation, but also to unravel the cellular basis of psychiatric disorders whereby HPC-amygdala changes have been reported.

Chapter 3 Impact of serotonin transporter overexpression on fear and basal amygdala parvalbumin interneurons

3.1 Introduction

3.1.1 5-HT innervation of BLA neurons

5-HT projections to the BLA arise predominantly from midbrain DRN (Abrams et al., 2004), with only very sparse innervation from the median raphe nuclei (Vertes et al., 1999).

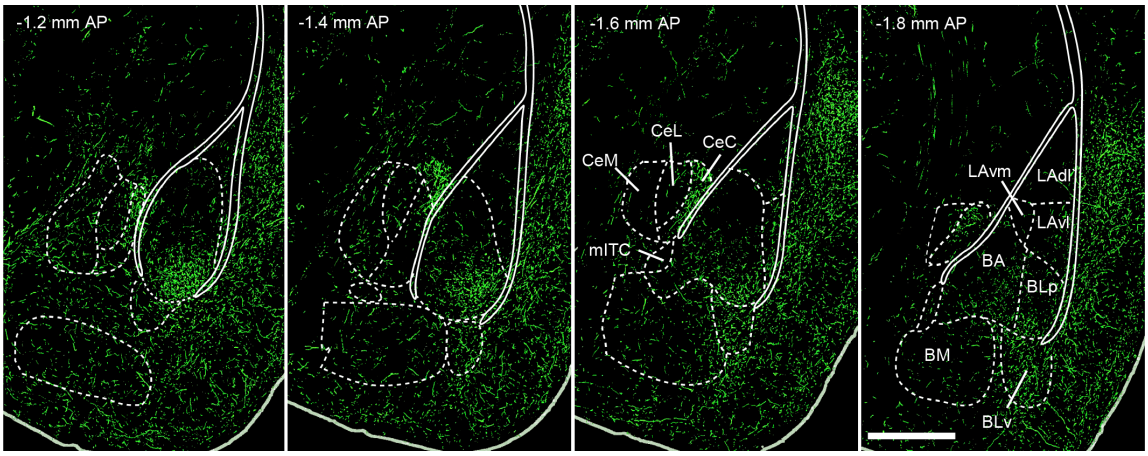

Figure 3.1. 5-HT innervation of the mouse amygdala.
GFP expressed in 5-HTT+ DRN neurons via injection of the Cre-dependent anterograde tracer rAAV2/1.hSynapsin.EGFP.WPRE.bGH in the DRN of SLC6A4-Cre (5-HTT-Cre) mice. This produces a pattern of innervation of the amygdaloid complex that is similar to the one previously described using antibodies for 5-HT or the 5-HTT. The densest innervation occurs in BA and BLp nuclei. Weaker innervation is observed in LA, BM and CeA, with the exception of CeC.
BA: basal amygdala; BLp: basolateral amygdala posterior portion; BLv: basolateral amygdala ventral portion; BM: basomedial amygdala; CeC: centrocentral amygdala; CeL: centrolateral amygdala; CeM: centromedial amygdala; LAdl: lateral amygdala dorsolater portion; Lavl: lateral amygdala ventrolateral portion; Lavm: lateral amygdala ventromedial portion; mITC: main intercalated cell cluster nucleus; AP: antero-posterior (distance from bregma); scale bar: 500 µm.
Adapted from: Allen Mouse Brain Connectivity Atlas(Oh et al., 2014), experiment 114155190. Website: © 2015 Allen Institute for Brain Science. Available from: http://connectivity.brain-map.org.

5-HT projections to the amygdaloid complex have been described in several ways, including the use of immunohistochemical labelling of either 5-HT (Steinbusch, 1981; Muller

et al., 2007b) or the 5-HTT (Sur et al., 1996a). Both approaches reveal similar innervation patterns in the amygdala of rodents. Typically, 5-HT-containing axons project strongly to the BA, moderately to LA, BM and CeM nuclei and only weakly to the CeL (Figure 3.1; Steinbusch, 1981; Sur et al., 1996b; Muller et al., 2007b). In the BLA, they innervate both PNs and INs (Muller et al., 2007b).

3.1.1.1 5-HT innervation of BLA PNs

McDonald and colleagues found that 5-HT terminals form synaptic contacts with the distal dendrites of PNs (Muller et al., 2007b). In the LA, both autoradiographic and *in situ* hybridization studies indicate high expression of 5-HT_{2C} receptors (Li et al., 2003; Greenwood et al., 2012). Because more than 80% of LA neurons are PNs, this is consistent with the 5-HT_{2C}-mediated depolarizing effect of exogenous 5-HT found in LA PNs (Yamamoto et al., 2014). In contrast, in the BA McDonald and Mascagni reported labelling of PN dendrites obtained with two out of three 5-HT_{2A} antibodies, while another antibody stained only PNs of the dorsolateral division of the LA (McDonald and Mascagni, 2007). However, BA PNs are not depolarized by 5-HT_2 agonists (Yamamoto et al., 2014). Thus, 5-HT_{2A} receptors may not alter the membrane excitability in PNs at the level of the soma, but rather modulate the integration of dendritic inputs. Consistent with this idea, Chen and colleagues (Chen et al., 2003) found that 5-HT_2 activation enhanced NMDA receptor-mediated synaptic plasticity in putative PNs. In addition, a minority of PNs appears to be directly hyperpolarized by 5-HT (Rainnie, 1999). This hyperpolarization could occur via activation of 5-HT_{1A} receptors, which have been shown to be densely expressed in the BLA (Saha et al., 2010).

3.1.1.2 5-HT innervation of BLA INs

5-HT fibres target various IN classes in the BLA (Figure 3.2; Muller et al., 2007b; Bonn et al., 2013). Although PNs appear to be oppositely modulated by 5-HT in LA and BA, it is not clear yet whether IN populations express the same 5-HT receptor(s) in both nuclei or whether differences exist. The PV+ INs are innervated by 5-HT axons in the perisomatic region. This innervation is both synaptic and non-synaptic (Muller et al., 2007b). In both LA and BA, PV+ INs express 5-HT_{2A} receptors (McDonald and Mascagni, 2007; Jiang et al., 2009), which mediate membrane depolarization (Table 3.1).

The SOM+ INs, thought to contribute to fear learning via their dendritic inhibition of PNs (Wolff et al., 2014), are also targeted by 5-HT fibres (Muller et al., 2007b). McDonald and Mascagni (2007) obtained labelling of ~30% of SOM+ INs using one of three 5-HT_{2A} antibodies. Thus, a minority of these neurons might also be depolarized via 5-HT_{2A} signalling, but this has not been tested so far. Approximately 30% of SOM+ neurons co-express neuropeptide Y (NPY; McDonald, 1989). These NPY neurons receive dense 5-HT innervation (Bonn et al., 2013). Around 50-60% of NPY INs express 5-HT_{1A}, suggesting they might be inhibited by 5-HT, while 30-40% express 5-HT_{2C}, indicating they could be depolarized (Table 3.1; Bonn et al., 2013). Modulation of these neurons by 5-HT could be important for emotional aspects, because the activity of NPY cells has been proposed to be anxiolytic (Truitt et al., 2009). However, their involvement in fear memory processing is unclear.

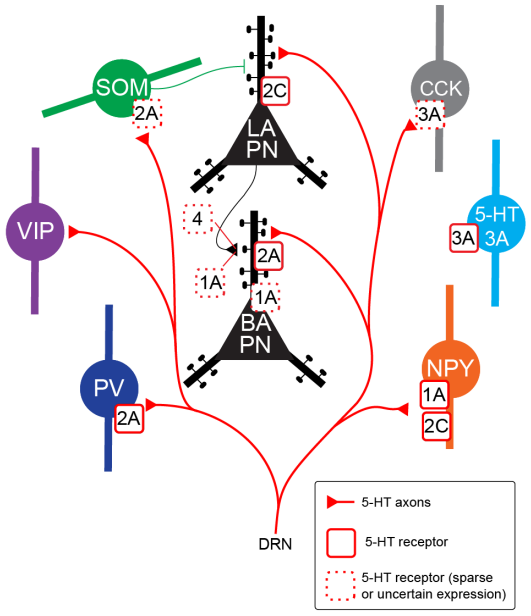

Figure 3.2. 5-HT innervation and 5-HT receptor expression of BLA neurons.
All the IN populations illustrated have been shown to receive somatic and/or dendritic 5-HT innervation (apart from CCK-negative 5-HT_{3A}+ INs). PV+ INs express excitatory, metabotropic 5-HT_{2A} receptors. 30% of SOM+ INs also seem to express 5-HT_{2A}. Ionotropic, excitatory 5-HT_{3A} receptors are expressed by a small proportion of CCK+ INs and a population of INs not expressing any other known marker. NPY+ INs express either inhibitory, metabotropic 5-HT_{1A} receptors or excitatory, metabotropic 5-HT_{2C} receptors. In some cases, both receptors could be localised on the same neuron. It is not clear what 5-HT receptor may be expressed by VIP+ INs. In the whole BLA, PNs are innervated by 5-HT axons only on dendrites, often on spines. In the LA, they appear to express excitatory 5-HT_{2C} receptors mediating membrane depolarization. Axon terminals of LA PNs innervating BA PNs might express 5-HT_{1A} and/or 5-HT_4 receptors. In the BA, PNs seem to express 5-HT_{2A} receptors on their distal dendrites. These receptors do not lead to depolarization, they might rather favour synaptic plasticity of excitatory inputs. A proportion of BA PNs might also express inhibitory 5-HT_{1A} receptors, mediating membrane hyperpolarization. DRN: dorsal raphe nuclei. For a schematic diagram representing the connectivity of BLA neurons see Figure 1.5.

Vasoactive intestinal peptide (VIP)-expressing INs are innervated synaptically and non-synaptically by 5-HT axons (Muller et al., 2007b), but it is not clear yet which 5-HT receptors they express. In neocortex, VIP+ INs are depolarized by 5-HT by an action at ionotropic 5-HT_3 receptors (Férézou et al., 2002), but virtually no VIP+ IN appears to express 5-HT_3 receptors in the BLA (Mascagni and McDonald, 2007). In the HPC, CCK+ INs are a key target for 5-HT input and they express ionotropic 5-HT_3 receptors (Morales and Bloom, 1997), which mediate fast synaptic depolarization (Férézou et al., 2002; Varga et al., 2009). This seems to be the case in the BLA as well, but only a minority of large CCK+ INs were labelled with a 5-HT_{3A} antibody (Mascagni and McDonald, 2007). Surprisingly, the majority of 5-HT_{3A}+ neurons do not belong to any previously characterized GABAergic population (Mascagni and McDonald, 2007). As well as postsynaptic innervation, axon terminals expressing 5-HT form appositions with 5-HT-negative axon terminals in the BLA (Muller et al., 2007b). This suggests that 5-HT not only modulates BLA neuron excitability

postsynaptically, but also the release of other neurotransmitters presynaptically. In agreement with this, pharmacological experiments performed in acute brain slices show that 5-HT can modulate glutamate release in the BLA (Cheng et al., 1998; Huang and Kandel, 2007), suggesting glutamatergic axon terminals might express 5-HT receptors. Taken together, these observations demonstrate that DRN 5-HT neurons innervate both BLA PNs and various types of GABAergic IN populations synaptically and non-synaptically, and that 5-HT acts on both excitatory and inhibitory 5-HT receptors.

Table 3.1. 5-HT receptor types expressed in the BLA and their function
a.t.: axon terminals; d.d.: distal dendrites; s.d.: somatodendritic; AC: adenylyl cyclase; PLC: phospholipase C

5-HT receptor	Class	Molecular cascade	Downstream effect	Functional effects	Localization in the BLA
5-HT_{1A}	metabotropic	$G_{i/o}$ AC↓	• Opening of GIRK (s.d.); • Inhibition of P/Q- and N-type Ca^{2+} channels (a.t.)	• slow membrane hyperpolarization (s.d.) • inhibition of neurotransmitter release (a.t.)	PNs (s.d., BA only)? NPY+ INs (s.d.) LA PNs to BA PNs a.t.?
5-HT_{1B}	metabotropic	$G_{i/o}$ AC↓	unknown	• slow membrane hyperpolarization (s.d); • inhibition of neurotransmitter release (a.t.)	PNs (s.d., BA only)? DRN a.t.?
5-HT_{2A}	metabotropic	$G_{q/11}$ PLC↑	Inhibition of leak K^+ conductance (not precisely identified)	• slow membrane depolarization (s.d.); • facilitation of neurotransmitter release (a.t.)	PNs (d.d.) PV+ INs (s.d.) SOM+ INs (s.d.)?
5-HT_{2C}	metabotropic	$G_{q/11}$ PLC↑	• Decrease of resting K^+ conductance (not precisely identified) • Activation of Na^+/Ca^{2+} exchanger	• slow membrane depolarization (s.d.); • facilitation of neurotransmitter release (a.t.)	PNs (s.d.?, LA only) NPY+ INs (s.d.)
5-HT_{3}	ionotropic	Cation channel opening	• Opening of mixed $Na^+/K^+/Ca^{2+}$ with higher permeability to Na^+ (s.d.) • Opening of mixed $Na^+/K^+/Ca^{2+}$ with high permeability to Ca^{2+} (a.t.)	• fast membrane depolarization • Facilitation of neurotransmitter release (a.t.)	CCK+ (s.d.) unknown IN class (s.d.)
5-HT_{4}	metabotropic	G_s AC↑	• Increase in I_h (s.d.) • Activation of PKA (a.t.)	Facilitation of neurotransmitter release (a.t.)	LA PNs to BA PNs a.t.?

3.1.2 Impact of genetic variations of the 5-HT transporter on the BLA and fear learning

5-HT transmission is tightly regulated by the 5-HTT, a transmembrane protein that clears 5-HT from the extracellular space and therefore controls the duration and extent of 5-HT transmission (Blakely et al., 1994; Torres and Amara, 2007). In humans, a 44 base pair insertion/deletion polymorphism in the 5-HTT gene promoter region (5-HTT-linked polymorphic region, *5-HTTLPR*) gives rise to long (*L*) and short (*S*) allele variants. The S allele is associated with reduced transcriptional efficacy, and hence lower transporter expression, leading to reduced 5-HT reuptake and high extracellular 5-HT levels (Greenberg et al., 1999). This variation has been associated with greater risk for anxiety-related traits (Lesch et al., 1996) and post-traumatic stress disorder (Lee et al., 2005). Furthermore, *S* carriers show heightened fear learning (Garpenstrand et al., 2001; Brocke et al., 2006; Lonsdorf et al., 2009) and increased depression/anxiety susceptibility (Lesch et al., 1996), particularly when combined with adverse environmental factors (Caspi et al., 2003; Uher and McGuffin, 2010). Notably, the *5-HTTLPR* is also associated with functional alterations in amygdala activity. Specifically, compared to *LL* homozygotes, *S* carriers exhibit greater amygdala activation to fearful faces (Hariri et al., 2002, 2005) and reduced amygdala-medial prefrontal cortex (mPFC) functional connectivity (Canli et al., 2005; Pezawas et al., 2005). However, the association between *5-HTTLPR* genotype and amygdala reactivity in humans remains controversial and the effect size is small (Murphy et al., 2013).

Mice with genetically modified 5-HTT expression offer a more controllable model to investigate the impact of 5-HTT variation on fear learning and amygdala function. 5-HTT knock-out (5-HTTKO) mice display higher extracellular 5-HT levels (Mathews et al., 2004; Jennings et al., 2010) and impaired recall of fear extinction compared to WT littermate

controls (Wellman et al., 2007). Furthermore, 5-HTTKO mice exhibit abnormal dendritic spine density of BLA PNs (Wellman et al., 2007). Conversely, 5-HTTOE mice have lower extracellular 5-HT levels than WT littermate controls (Jennings et al., 2006, 2010) and exhibit impaired fear learning (Figure 3.3A; Barkus et al., 2014; Line et al., 2014; McHugh et al., 2015). Additionally, recordings from the BLA of 5-HTTOE mice have revealed attenuated fear-evoked theta oscillations (Figure 3.3B; Barkus et al., 2014). Collectively, these findings suggest that alterations in 5-HTT gene expression impact on the microcircuitry of the BLA, however the mechanisms are unknown.

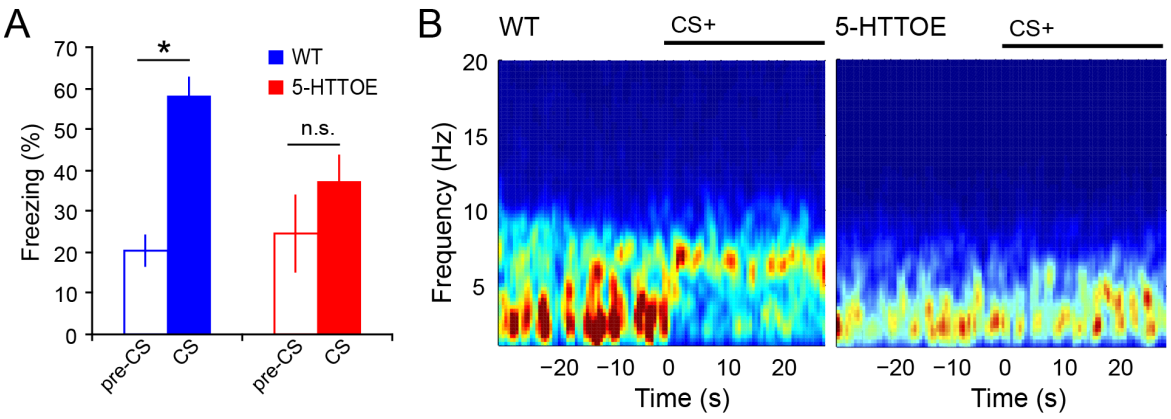

Figure 3.3. Reduced fear-evoked BLA theta oscillations in 5-HTTOE mice.
A, wild-type mice (WT) exhibit significantly increased freezing during conditioned auditory tone (CS), whereas 5-HTTOE mice do not. **B**, representative spectrograms showing auditory cue-evoked oscillations in the BLA of a WT and a 5-HTTOE mouse. CS+ presentation evokes a higher increase in oscillations in the theta band (5-12 Hz) in the BLA of the WT compared to the 5-HTTOE mouse. Adapted from Barkus et al., 2014.

Timed inhibition from GABAergic INs, in particular PV+ INs, to PNs is thought to be involved in the control of theta oscillations (Klausberger et al., 2003; Courtin et al., 2014; Amilhon et al., 2015). Hence, we hypothesised that reduced theta power in response to aversive cues in the BLA of 5-HTTOE mice could be a sign of dysfunctional inhibitory inputs from PV+ INs to PNs. To test this hypothesis, we examined whether BA PV+ INs of 5-HTTOE mice would display differential recruitment during fear memory retrieval combined with altered sensitivity to 5-HT.

3.2 Materials and methods

3.2.1 Animals

We used female 5-HTTOE mice and littermate WT controls (C57BL/6J × CBA background, 4-6 months age for electrophysiology, 8-11 months age for behaviour). A detailed description of how 5-HTTOE mice were generated can be found in Jennings et al., 2006. Mice were housed 2-6 per cage on a 12 h light/dark cycle and at a temperature of 19-22 °C with free access to food and water. Testing took place during the light cycle. Mice were handled in the two days before fear conditioning began. The experiments were conducted in accordance with the United Kingdom Animals Scientific Procedures Act (1986) under project licenses PPL 30/3061 and 30/3068 and were approved by local ethical review at the University of Oxford.

3.2.2 Fear conditioning

Mice underwent cued fear conditioning training over two days (day 1: training, day 2: test). At the start of the training session, mice were placed into an operant chamber and allowed to explore the environment for 180 s. Mice were then presented with five auditory cues (2900 Hz pure tone; 30 s duration; 80 dB), with a mean inter-stimulus interval of 120 s (range: 90-150 s; standard deviation: 24.5 s). For mice in the paired condition, the tone always co-terminated with a footshock (0.3 mA, 0.5 s). Mice in the tone-alone condition received presentations of the auditory cues but no footshocks at any point. The total session duration was 840 s. After the training session, mice were taken in individual cages to a darkened room and left for 2 h to habituate them to the procedure that would follow after the testing session.

For the testing session (24 h later), mice were placed into a novel context: an operant chamber with the same dimensions as the training context but with distinct flooring, visual

pattern on the walls, and odour. At the start of the testing session mice were allowed to explore the environment for 180 s before stimulus presentation. Then, mice from all training groups were presented with a single tone (2900 Hz, 60 s duration, 80 dB) and they remained in the chamber for 180 s after tone offset. No shocks were delivered to any of the mice during the testing session and the total session duration was 420 s. After the testing session, mice were taken in individual cages to a darkened room and left for 2 h before perfusion.

3.2.2.1 Fear conditioning apparatus

Fear conditioning was conducted in one of two operant chambers (ENV-307A, Med Associates Inc.), each with distinct visual and olfactory cues. The floor was made of stainless steel metal bars through which the shocks were delivered (Med Associates shock generator). Fear testing was conducted in a novel context (i.e. a mouse trained in context A would be tested in context B). A plastic insert was placed on top of the bars on the testing day to provide an additional cue to signal the shift in context compared to the training session. Training and testing contexts were counterbalanced across conditions and genotypes. Stimulus delivery was controlled by software written in the Med Associates programming language (MED-PC). All sessions were recorded using a video camera mounted in the ceiling of the chamber and stored on a digital video recorder.

3.2.3 Fear conditioning data analysis

Freezing behaviour was measured using a script in NIH Image (Barkus et al., 2014), which analysed consecutive video frames (1 Hz sampling) for pixel changes and assigned a freezing score if the % pixel change was below a set threshold calibrated for an absence of movement except for breathing. This automated system has over 80% concordance with human ratings of freezing behaviour and gives an unbiased measure of immobility, as

described elsewhere (Richmond et al., 1998). We calculated a 'freezing difference score' by subtracting freezing during the pre-CS period from freezing during CS presentation. Positive freezing difference scores therefore indicate increased freezing compared to the pre-CS period, whereas negative difference scores indicate decreased freezing compared to the pre-CS period.

3.2.4 *Ex vivo* recordings

Naïve WT and 5-HTTOE mice were decapitated under deep isoflurane anaesthesia (4% in O_2). The brain was removed and the slicing procedure, cutting solution and incubation were the same as described in Chapter 2, section 2.2.5 *Ex vivo* recordings and analysis. Slices were transferred to a submerged recording chamber and continuously perfused with oxygenated ACSF at a rate of ~5 mL/min at 34 ± 1 °C. Neurons were visualized with an upright Axioskop microscope (Zeiss) using phase contrast microscopy under a LUMPlanFI 60× immersion objective (Olympus). Somatic whole-cell patch clamp recordings were performed from visually identified neurons in the BA, because in this nucleus the density of PV+ INs (McDonald and Mascagni, 2001a) and 5-HT axons (Asan et al., 2013) is higher than the LA. Glass electrodes, intracellular K-gluconate-based solution, biocytin and patch clamp recording procedures were the same as described in Chapter 2, section 2.2.5 *Ex vivo* recordings and analysis. Recordings were performed blind to genotypes.

The IPSCs were recorded by voltage clamping the neurons at -50 mV. V_m during 5-HT application was monitored while holding PNs at -60 ± 1 mV and INs at -70 ± 1 mV. Hyperpolarizing (-50 pA) and depolarizing (range from +10 to +120 pA) current steps were injected every 10 s to monitor R_{in} and firing, respectively. Sinusoidal current injections (6 Hz frequency, 1.7 s duration) were injected every 10 s in PNs current clamped at -60 ± 1 mV.

Current amplitude was set to evoke firing in ~50% of the oscillation peaks in baseline conditions (baseline firing rates: 3.3 ± 0.6 Hz in WT and 3.6 ± 0.9 Hz in 5-HTTOE, $p > 0.5$). Slices containing biocytin-filled neurons were fixed and re-sectioned as described in Chapter 2, section 2.2.5 *Ex vivo* recordings and analysis.

3.2.5 Analysis of *ex vivo* recordings

Analysis of synaptic currents and intrinsic membrane properties were performed using Igor Pro (Wavemetrics, Inc.) and MATLAB (Mathworks, Inc.). IPSCs were detected using TaroTools toolbox for Igor Pro (https://sites.google.com/site/tarotoolsregister/). Frequency of sIPSCs and V_m were normalised by subtracting the average baseline values (respectively 3 and 4 min preceding drug application) for each neuron. The R_{in} was calculated from the slope of steady-state voltage responses to a series of 8-10 sub-threshold current injections (from -30 to +60 pA, 10 pA steps) lasting 400 ms. The fAHP (mV) was determined from the first spike in response to a positive current injection just above threshold. The half-width of the action potential was measured at half action potential amplitude, between the threshold potential and the peak of the action potential, which was evoked by a strong (800-1000 pA) and short (2-5 ms) depolarizing current pulse. The membrane time constant τ was estimated from the monoexponential curve fitting of voltage responses to a -30 pA hyperpolarizing pulse. The rheobase (pA) was determined as the 50 ms current injection able to generate a spike in 50% of the cases out of 10 trials. The instantaneous firing rate (Hz) was defined as the number of action potentials evoked during a 1 s depolarizing current pulse of twice the amplitude of the rheobase current. The membrane capacitance was calculated as the ratio between the time constant and the R_{in}. The adaptation index (range: 0-1) was defined as the ratio between the first and last inter-spike intervals (ISI, ms) elicited by the same pulse used to measure the

instantaneous firing rate. PNs were distinguished from INs as explained in Chapter 2, section 2.2.5 *Ex vivo* recordings and analysis.

3.2.6 Immunohistochemistry

Sections from fear conditioned mice were blocked with 10% NDS for 1 h at RT, followed by overnight incubation at 4 °C with the following primary antibodies: anti-PV raised in guinea pig (1:2000, Synaptic Systems, cat. no. 195-004) and anti-c-Fos raised in rabbit (1:500, Abcam, cat. no. ab7963), with 1% NDS. Following washing with PBS, sections were incubated overnight at 4 °C in AMCA-conjugated anti-guinea pig (1:250) and Cy3-conjugated anti-rabbit (1:500) secondary antibodies (both raised in donkey, from Jackson Immunoresearch).

Sections containing recorded and biocytin-filled neurons were incubated overnight at 4 °C in 1:1000/3000 Cy3-conjugated (Life Technologies) or Alexa488-conjugated Streptavidin (Invitrogen). Sections containing the soma of the recorded neurons were blocked with 10% NDS for 1 h at RT, and then incubated overnight at 4 °C with the same anti-PV primary antibody described above or an anti-PV primary antibody raised in goat (1:500, Abcam, cat. no. ab32895). To reveal PV immunoreactivity, Alexa647-conjugated secondary antibodies (1:250, Jackson Immunoresearch) were used. All reagents were diluted in PBS containing 0.3% Triton X-100. Immunoreactivity of the recorded neurons was visualised using an epifluorescence microscope (AxioImager M2, Zeiss) or a laser-scanning confocal microscope (LSM 710, Zeiss).

3.2.7 Quantification of c-Fos+ and PV+ neurons

Coronal sections containing the BA from fear conditioned mice were imaged with the epifluorescence microscope mentioned above and StereoInvestigator software (MBF Bioscience). A region of interest delineating the BA was defined using a 5× 0.16 NA objective lens. Stereological sampling was carried out in both hemispheres from one out of four coronal sections in the range from -1.4 to -2 mm from bregma. Series of tiled stacked images were acquired using a 40× 1.3 NA oil-immersion objective and 1 μm steps at depth of 2 to 22 μm ('optical sections') from the upper surface of each section. In order to minimise artefacts arising from surface irregularities, the first 2 μm from the upper surface were defined as 'guard zone' and not scanned. Counting was performed offline in StereoInvestigator. A neuron was counted only if its immunopositive nucleus came into focus in the optical section. Nuclei already in focus at the top optical section were not counted (West, 1999)**.** Counting was performed blind to genotype and behavioural testing conditions. Data were exported to Excel (Microsoft) and pooled for further analysis.

3.2.8 Statistical analyses

Data are presented as means ± SEM values. Distributions passing the Shapiro-Wilk test for normality were compared using Student's t-tests and ANOVAs with Bonferroni *post hoc* correction. Non-normal distributions were compared using Mann Whitney U test and Kruskall-Wallis test with Dunn's multiple comparisons correction. Cumulative distributions of inter-IPSCs intervals were compared using Kolmogorov-Smirnov test. Statistical analysis was performed with Graphpad Prism and $p < 0.05$ was considered statistically significant.

3.2.9 Drugs

Serotonin hydrochloride, MDL 72,222, RS 102221, MDL 100,907, SR95531, CGP54626 hydrochloride and citalopram hydrobromide were purchased from Tocris Bioscience. Picrotoxin, kynurenic acid and α-methylserotonin maleate salt were purchased from Sigma-Aldrich.

3.3 Results

3.3.1 5-HTT overexpression leads to impaired PV+ IN activation by fear memory

In the BLA, PV+ INs are excited by the conditioned stimulus (CS) during fear conditioning (Wolff et al., 2014). Since PV+ INs are also strongly involved in the generation of local theta oscillations, we postulated that abnormal CS-evoked theta activity in 5-HTTOE mice (Barkus et al., 2014) might reflect reduced recruitment of PV+ INs.

To test this, we subjected 5-HTTOE and littermate WT mice to an auditory fear conditioning paradigm. During the fear memory test session, the onset of the tone CS evoked a large increase in freezing in mice in the paired condition, with a slight increase in freezing in mice in the unpaired condition, and either no increase (WT) or a slight decrease in freezing (5-HTTOE) in mice in the tone-alone condition (Figure 3.4).

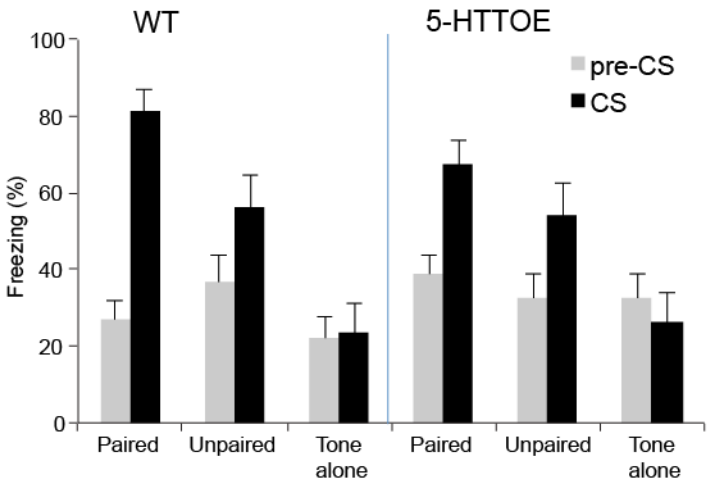

Figure 3.4. WT and 5-HTTOE mice freezing levels during fear memory retrieval.
Percentage of time spent freezing before and during CS presentation in the test session. The time spent freezing during CS presentation in the paired condition does not differ significantly between WT and 5-HTTOE. However, WT mice display a larger CS – pre-CS freezing difference compared to 5-HTTOE (see Figure 3.5).

Statistical analysis confirmed these observations. Mice in the paired condition showed a significantly larger increase in freezing with cue onset than mice in the tone-alone and unpaired conditions (phase(pre-tone *versus* tone) × training condition interaction:

$F(1,38)=20.4$; $p < 0.001$). These differences were present only during tone presentation (paired *versus* unpaired: $p < 0.05$; paired *versus* tone-alone: $p < 0.001$) with no differences in freezing during the pre-tone periods (all $p > 0.5$). Although the three-way interaction between genotype, training condition, and phase did not reach significance ($F(2,50)=2.0$, $p > 0.05$), we performed separate ANOVAs (with factors of genotype and phase) for each training condition. In the paired condition, there was a genotype × phase interaction ($F(1,24)=7.2$, $p < 0.05$) reflecting the larger increase in freezing from the pre-CS to CS period in WT compared to 5-HTTOE mice. Performing a t-test on the freezing 'difference score' (CS freezing – pre-CS freezing) confirmed that the change in freezing evoked by the CS was greater in WTs than 5-HTTOEs ($t(24)=2.7$, $p < 0.05$; Figure 3.5A). For the ANOVAs performed on the unpaired and tone-alone condition, there was no effect of genotype or interaction between phase and genotype, with WTs and 5-HTTOEs showing similar responses in these training conditions (Figure 3.5A). Thus, in the paired condition, cue-evoked freezing was lower in 5-HTTOE mice, consistent with previous reports (Barkus et al., 2014; Line et al., 2014).

Two h after the fear memory test session, mice were perfused and sections containing the BA were immunostained for both c-Fos, a marker of neuronal activation, and PV to probe the activation of PV+ INs during fear memory retrieval. Somatic c-Fos immunoreactivity was detected in the BA of both WT and 5-HTTOE mice (Figure 3.5B). We observed a significant effect of condition in the amount of c-Fos+ neurons ($F(2, 24)=5.412$, $p < 0.05$). Mice in the paired condition displayed a greater number of c-Fos+ cells compared to mice in the unpaired and tone alone condition (both $p < 0.05$). These results suggest that fear memory retrieval reliably recruited BA neurons in both WT and 5-HTTOE mice.

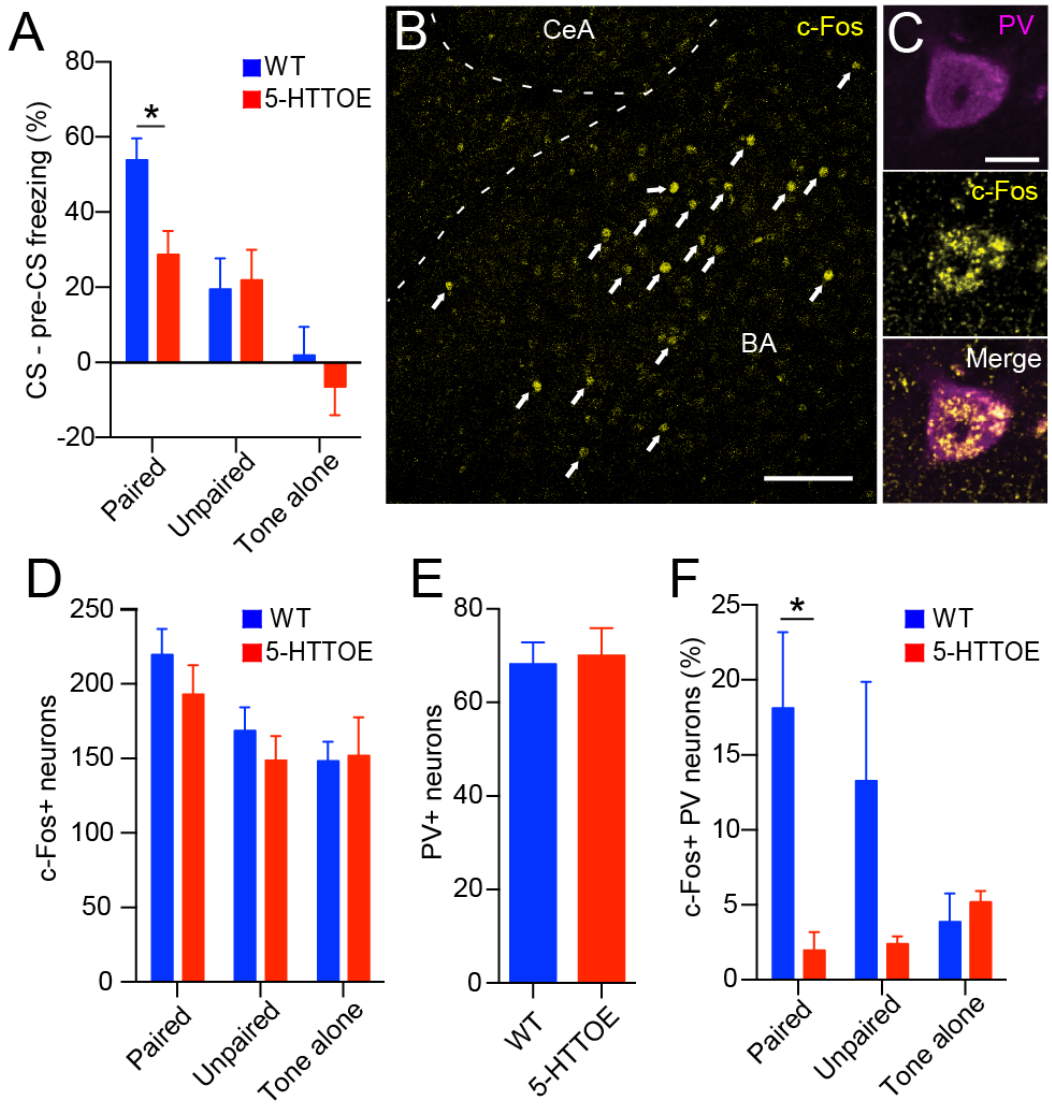

Figure 3.5. Increased 5-HTT expression leads to reduced fear recruitment of PV+ INs of the BLA.
A, reduced freezing responses in 5-HTTOE mice in the paired condition during fear testing session (paired: WT n = 14, 5-HTTOE n = 12; unpaired: WT n = 8, 5-HTTOE n = 8; tone alone: WT n = 8, 5-HTTOE n = 8. **B**, Representative c-Fos expression in the BLA following the fear testing session. Arrows indicate c-Fos+ neurons. Scale bar: 100 µm. **C**, immunoreactivity of a representative neuron for PV and c-Fos. Scale bar: 10 µm. **D**, Overall numbers of c-Fos+ neurons of the BLA do not differ between WT and 5-HTTOE mice following the fear testing session (n = 5 per genotype and condition). **E**, Overall numbers of PV+ neurons of the BA do not differ between WT and 5-HTTOE mice following the fear testing session (n = 5 per genotype). **F**, Reduced numbers of c-Fos+/PV+ in the BA of 5-HTTOE in the paired condition. No significant difference between WT and 5-HTTOE in the unpaired and tone alone condition (n = 5 per genotype and condition). * $p < 0.05$. Data are presented as means ± SEM.

Although WT and 5-HTTOE mice displayed similar numbers of c-Fos+ cells (main effect of genotype $F(1, 24)=0.9100$, $p > 0.1$; Figure 3.5D), c-Fos+/PV+ co-labelled cells (Figure 3.5C) were far more numerous in WT compared to 5-HTTOE mice following fear memory recall (Figure 3.5F; main effect of genotype: $F(1, 24)=8.767$, $p < 0.01$). *Post hoc* comparisons revealed that WT mice had a greater proportion of c-Fos+/PV+ cells than 5-HTTOE mice ($p < 0.05$) in the paired condition, while there was no significant difference in the unpaired ($p > 0.1$) or tone alone ($p > 0.9$) conditions. This difference was not driven by a significantly reduced number of c-Fos+ (Figure 3.5D) or PV+ cells (Figure 3.5E) in 5-HTTOE mice, arguing that 5-HTTOE mice displayed a cell type, behaviour-specific deficit in activation of PV+ INs of the BA evoked by fear memory retrieval.

3.3.2 5-HTT overexpression leads to impaired 5-HT excitation of PV+ INs

Next, we asked whether reduced fear activation of PV+ INs in the BA of 5-HTTOE mice was accompanied by alterations at the physiological level. As 5-HTT manipulations result in altered synaptic 5-HT levels, and fear conditioning causes release of 5-HT in the BLA (Zanoveli et al., 2009), we investigated the 5-HT sensitivity of PV+ INs in 5-HTTOE and WT mice. Acute coronal brain slices were prepared and INs recorded in the BA in whole-cell mode (Figure 3.6A). Neurons were filled with biocytin (Figure 3.6B) to allow *post hoc* immunohistochemical identification of PV+ INs (Figure 3.6C). Notably, we found no significant difference of PV+ INs membrane properties between WT and 5-HTTOE mice (Table 3.2), suggesting that we sampled from two relatively uniform populations.

Table 3.2. Electrophysiological membrane properties of PV+ INs recorded from WT and 5-HTTOE mice.
Inter-genotypes comparisons of intrinsic membrane properties of PV+ INs (unpaired t-tests). No significant genotypic difference in membrane properties was detected. WT PV+ INs n = 7 from 6 animals; 5-HTTOE PV+ INs n = 5 from 5 animals. R_{in}: input resistance; C_m: membrane capacitance; fAHP: fast after-hyperpolarization; AP: action potential; resting V_m: resting membrane potential.

	WT PV+ INs (n = 7)	5-HTTOE PV+ INs (n = 5)
R_{in} (MΩ)	486.9 ± 34.4	458.1 ± 139.9
Membrane τ (ms)	20.8 ± 2.5	14.8 ± 1.9 (p = 0.1101)
C_m (pF)	44 ± 5	45 ± 11
Rheobase (pA)	58 ± 14	74 ± 22
Instantaneous firing rate (Hz)	39.3 ± 7.2	38.7 ± 5.6
Adaptation index	0.576 ± 0.123	0.381 ± 0.077
fAHP (mV)	22.1 ± 2.7	16.7 ± 1.7
AP half width (ms)	0.46 ± 0.03	0.46 ± 0.09
Resting V_m (mV)	-68.7 ± 2.3	-68.9 ± 2

Table 3.3. Electrophysiological differences between BA PNs and PV+ INs.
Comparison of intrinsic membrane responses between BA PNs and PV+ INs of WT mice (unpaired t-tests). WT PNs n = 11 from 6 animals; WT PV+ INs n = 7 from 6 animals; R_{in} input resistance; C_m: membrane capacitance; fAHP: fast after-hyperpolarization; AP: action potential; resting V_m.: resting membrane potential ** p < 0.01; *** p < 0.001; **** p < 0.0001

	PNs (n = 11)	PV+ INs (n = 7)
R_{in} (MΩ)	145 ± 11.3	486.9 ± 34.4 ***
Membrane τ (ms)	32 ± 4.8	20.8 ± 2.5 (p = 0.0974)
C_m (pF)	224 ± 31	44 ± 5 ***
Rheobase (pA)	121 ± 13	58 ± 14 **
Instantaneous firing rate (Hz)	11.6 ± 1.4	39.3 ± 7.2 ***
Adaptation index	0.148 ± 0.03	0.576 ± 0.123 ***
fAHP (mV)	14.8 ± 3.1	22.1 ± 2.7
AP half width (ms)	0.99 ± 0.07	0.46 ± 0.03 ****
Resting V_m (mV)	-67.6 ± 1.7	-68.7 ± 2.3

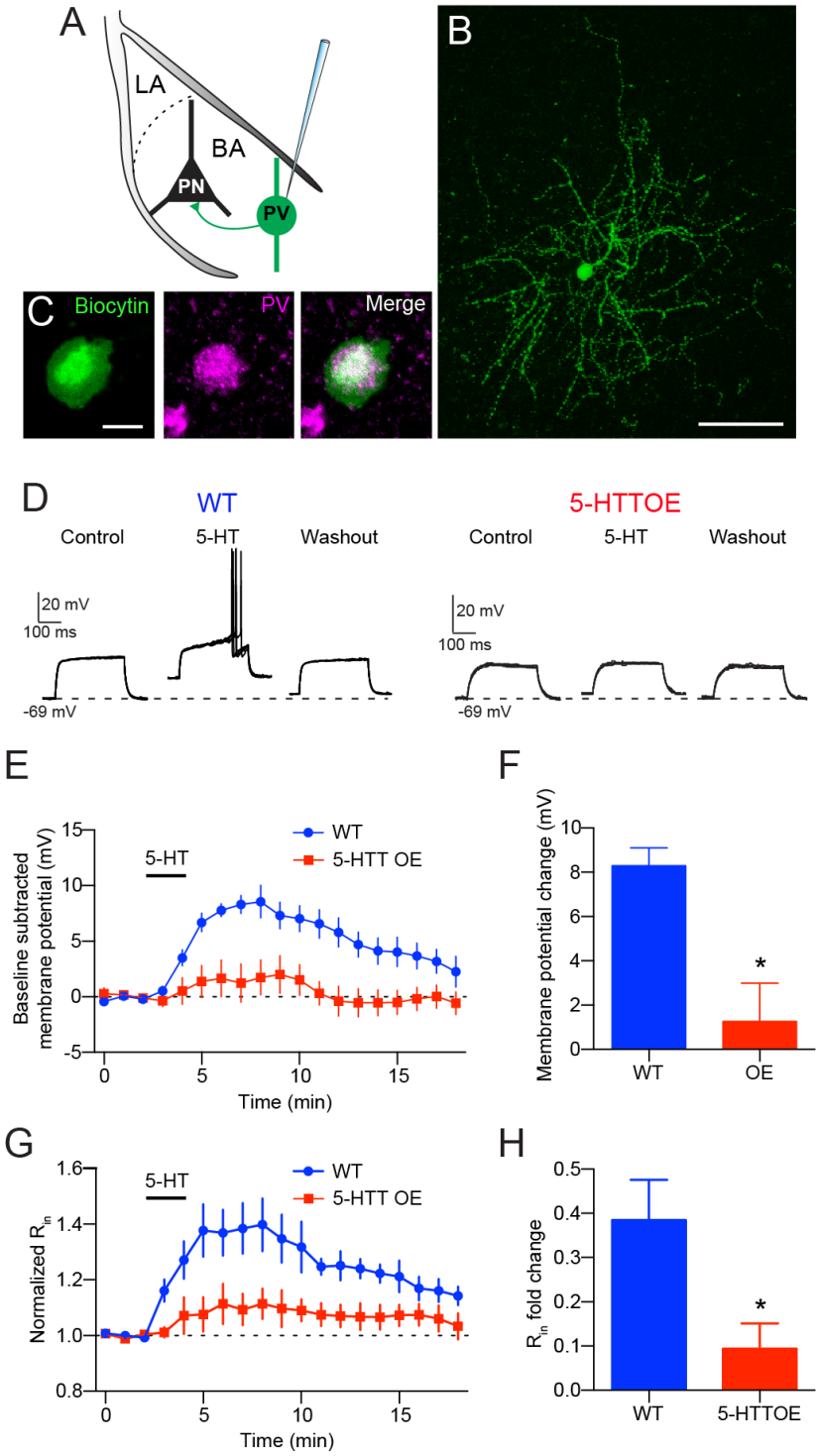

Figure 3.6. 5-HT-evoked depolarization of PV+ INs of the BA is impaired in 5-HTTOE mice.
A, recording configuration and schematic connectivity between PV+ INs and PNs. **B**, Representative PV+ IN filled with Neurobiotin during recording. Scale bar: 50 µm. **C**, representative immunoreactivity for PV+ of a biocytin-filled neuron (same neuron as in B). **D**, five superimposed voltage responses to depolarizing current injections of representative PV+ INs from a WT (160 pA, 300 ms left) and 5-HTTOE mouse (120 pA, 300 ms, right) during control, bath application of 5-HT (50 µM) and washout. In control, the current intensities used were set just below action potential threshold. **E**, Time course of the effect of 5-HT on the V_m of WT and 5-HTTOE PV+ INs. **F**, 5-HTTOE PV+ INs (n = 5 from 5 animals) are significantly less depolarized by 5-HT than WT PV IN (n = 7 from 6 animals). **G**, Time course of the effect of 5-HT on the R_{in} of WT and 5-HTTOE PV+ INs. **H**, 5-HT causes a significantly weaker increase in R_{in} in 5-HTTOE compared to WT PV+ INs. * $p < 0.05$. Data are presented as means ± SEM.

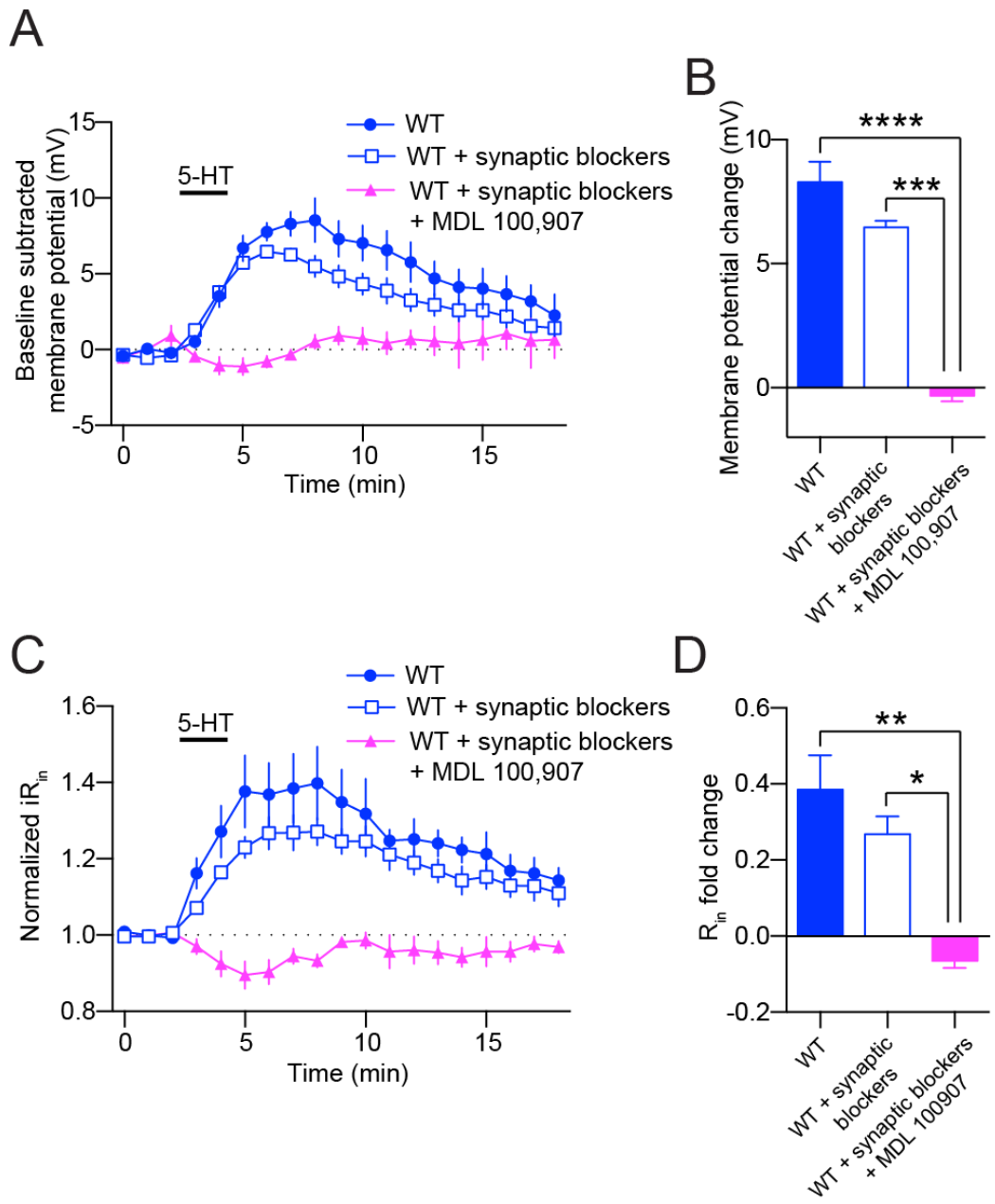

Figure 3.7. Direct 5-HT depolarization of PV+ INs via 5-HT$_{2A}$ receptors
A, time course of the effect of bath application of 5-HT (50 µM) on BA PV+ INs V_m with and without pre-incubation with MDL 100,907 (150 nM) and/or kynurenic acid (3 mM), SR95531 (10 µM) and CGP54626 (5 µM). **B**, membrane depolarization occurs when glutamatergic and GABAergic transmissions are blocked (n = 5 from 3 animals), demonstrating direct effect. Further blockade of 5-HT$_{2A}$ receptors with MDL 100,907 abolishes membrane depolarization (n = 5 from 4 animals). **C**, time course of the effect of bath application of 5-HT on BA PV+ INs R_{in} with and without pre-incubation with MDL 100,907 (150 nM) and/or kynurenic acid (3 mM), SR95531 (10 µM) and CGP54626 (5 µM). **D**, increase in R_{in} occurs when glutamatergic and GABAergic transmissions are blocked (n = 5 from 3 animals), demonstrating direct effect. Further blockade of 5-HT$_{2A}$ receptor with MDL 100,907 abolishes increase in R_{in} (n = 5 from 4 animals). **** $p < 0.0001$; *** $p < 0.001$; ** $p < 0.01$; * $p < 0.05$. Data are presented as means ± SEM.

All PV+ INs recorded from the BA of WT mice depolarized in response to bath application of 5-HT (50 μM, n = 7 from 6 animals, Figure 3.6D-F) and displayed an increase in R_{in} (Figure 3.6G, H), in line with the report of inhibition of a leak K^+ conductance triggered by activation of 5-HT_{2A} receptors (Andrade and Nicoll, 1987). Depolarization and change in R_{in} were blocked by the 5-HT_{2A} receptor selective antagonist MDL 100,907 (150 nM, $p < 0.0001$ and $p < 0.01$, respectively, n = 5 from 4 animals, Figure 3.7), consistent with previous studies reporting the localization of 5-HT_{2A} receptors on this IN type (McDonald and Mascagni, 2007; Jiang et al., 2009). These effects were due to a direct effect of 5-HT on PV+ INs because they were detected also in presence of synaptic blockers (3 mM kynurenic acid, 10 μM SR95531, and 5 μM CGP54626, Figure 3.7). In contrast, BA PV+ INs of 5-HTTOE mice (n = 5 from 5 animals) displayed significantly reduced depolarization and change in R_{in} in response to 5-HT compared to PV+ INs of WT mice ($p < 0.05$, Figure 3.6D-H). These results suggest a link between the impaired recruitment of PV+ INs of the BA in 5-HTTOE mice during fear memory retrieval and a specific deficit in sensitivity to 5-HT in the same neuron type.

3.3.3 5-HTT overexpression causes reduced 5-HT-evoked inhibitory drive onto PNs

As PV+ INs form the major IN population in the BLA and are the source of a significant inhibitory input to PNs (Woodruff and Sah, 2007b), we postulated that reduced 5-HT excitation of PV+ INs could impact on the 5-HT-mediated inhibition of PNs. To test this, we performed whole-cell patch clamp recordings from PNs of the BA of both WT and 5-HTTOE mice (Figure 3.8A, B). PNs were identified according to defined electrophysiological parameters (see 2.2.5 *Ex vivo* recordings and analysis).

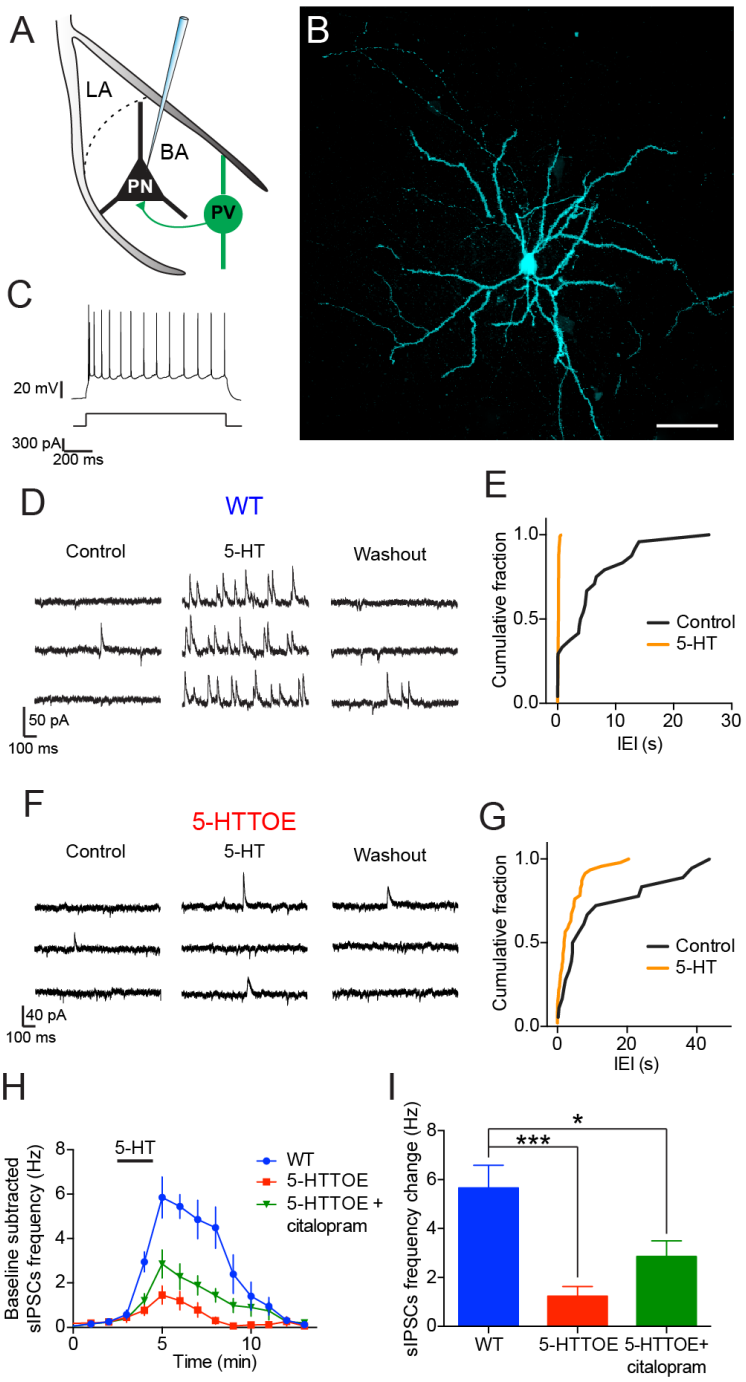

Figure 3.8. Indirect 5-HT inhibition of PNs is impaired in 5-HTTOE mice.
A, recording configuration and schematic connectivity between PV+ INs and PNs. **B**, representative PN filled with Neurobiotin during recording. Scale bar: 100 µm. **C**, adapting firing pattern of the neuron shown in B in response to prolonged (1 s) current injection (300 pA). **D**, representative voltage clamp (-50 mV) trace from a WT PNs during control, 5-HT (50 µM) application and washout. **E**, cumulative probability distributions of the inter-event intervals (IEI) for the sIPSCs of the neuron in D during control and in presence of 5-HT. 5-HT significantly increases the sIPSCs frequency ($p < 0.0001$, Kolmogorov-Smirnov test).
F, representative voltage clamp (-50 mV) trace from a 5-HTTOE PNs during control, 5-HT application and washout. **G**, cumulative probability distributions of the inter-event intervals (IEI) for the sIPSCs of the neuron in F during control and in presence of 5-HT. 5-HT does not significantly increase sIPSCs frequency ($p > 0.05$, Kolmogorov-Smirnov test). **H**, time course of the effect of 5-HT on sIPSCs frequency in WT and 5-HTTOE PNs. **I**, 5-HT evokes a significantly lower sIPSCs frequency in 5-HTTOE (n = 9 from 7 animals), compared to WT (n = 9 from 8 animals) PNs. Acute citalopram (1 µM, n = 8 from 4 animals) application does not fully rescue 5-HTTOE deficit (. *** $p < 0.001$; * $p < 0.05$. Data are presented as means ± SEM

Table 3.4. Overexpression of the 5-HTT does not alter electrophysiological membrane properties of BA PNs
Inter-genotypes comparisons of intrinsic membrane properties of PNs (unpaired t-tests). No significant genotypic difference in membrane properties was detected. WT PNs n = 11 from 6 animals; 5-HTTOE PNs n = 10 from 7 animals; R_{in}: input resistance; C_m: membrane capacitance; fAHP: fast after-hyperpolarization; AP: action potential; resting V_m: resting membrane potential

	WT PN (n = 11)	5-HTTOE PN (n = 10)
R_{in} (MΩ)	145 ± 11.3	171.9 ± 18.3
Membrane τ (ms)	32 ± 4.8	34.7 ± 4.6
C_m (pF)	224 ± 31	226 ± 4
Rheobase (pA)	121 ± 13	128 ± 18
Instantaneous firing rate (Hz)	11.6 ± 1.4	15.5 ± 0.8
Adaptation index	0.148 ± 0.03	0.183 ± 0.047
fAHP (mV)	14.8 ± 3.1	21.2 ± 2.4
AP half width (ms)	0.99 ± 0.07	0.98 ± 0.09
Resting V_m (mV)	-67.6 ± 1.7	-65.9 ± 1.3

We recorded spontaneous IPSCs (sIPSCs), a read-out of the activity of local GABAergic INs. These currents were blocked by application of the $GABA_A$ antagonist picrotoxin (100 μM, n = 3, data not shown), confirming the GABAergic nature of these inputs. Consistent with previous reports (Rainnie, 1999; Jiang et al., 2009), 5-HT (50 μM) markedly enhanced the frequency of sIPSCs in all PNs recorded from WT mice (n = 9 from 7 animals, Figure 3.8D, E). In agreement with earlier observations (Jiang et al., 2009), this effect of 5-HT appeared to be mediated primarily by 5-HT_{2A} receptors, as the selective antagonist MDL 100,907 (150 nM, n = 5 from 4 animals) significantly reduced the 5-HT facilitation of sIPSCs (increase in sIPSCs frequency in WT *versus* WT+MDL 100,907 $p < 0.05$, Figure 3.9). Additional blockade of 5-HT_{2C} and 5-HT_3 receptors (using 1 μM RS 102221 and 20 μM MDL 72,222, respectively, n = 4 from 4 animals) completely prevented

the increase in sIPSC frequency induced by 5-HT ($p < 0.01$ *versus* WT, Figure 3.9), in line with evidence for the presence of these receptors on non-PV+ IN types in the BLA (Mascagni and McDonald, 2007; Bonn et al., 2013).

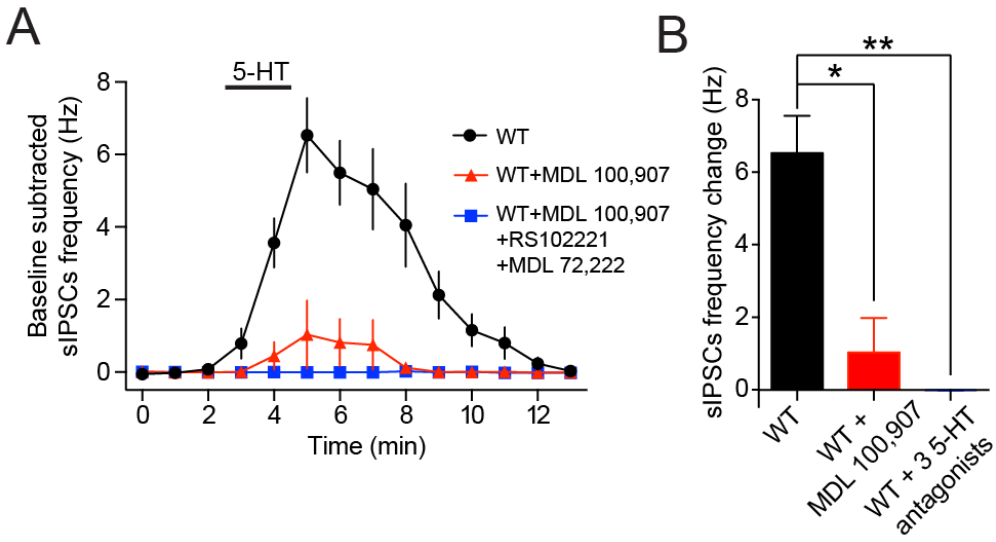

Figure 3.9. 5-HT promotes indirect inhibition of BA PNs of the primarily through 5-HT$_{2A}$ receptors. **A**, time course of the effect of bath application of 5-HT (50 µM) on sIPSCs recorded from PNs of the BA in control conditions and in presence of MDL 100,907 (150 nM), RS 102221 (5-HT$_{2C}$ antagonist, 1 µM) and MDL 72,222 (5-HT$_3$ antagonist, 20 µM). **B**, blocking 5-HT$_{2A}$ receptors with MDL 100,907 blocks 79.2±17.3 % of the 5-HT-mediated sIPSCs frequency increase (n = 5 from 4 animals). Additional antagonism of 5-HT$_{2C}$ and 5-HT$_3$ receptors with RS 102221 and MDL 72,222 completely blocks the effect of 5-HT (n = 4 from 4 animals). * $p < 0.05$; ** $p < 0.01$. Data are presented as means ± SEM.

In 5-HTTOE mice (n = 9 neurons from 8 animals), 5-HT produced a smaller increase in the frequency of sIPSCs compared to WT mice ($p < 0.001$, Figure 3.8F-I). Overall, these data suggest that the 5-HT facilitation of GABA release onto PNs of the BA is impaired in 5-HTTOE mice. Consequently, 5-HT led to a significant membrane hyperpolarization in PNs from WTs (baseline *versus* 5-HT $p < 0.01$, n = 8) but not from 5-HTTOEs ($p > 0.5$, n = 10, Figure 3.10A, B, D). A minority of PNs showed a direct hyperpolarization to 5-HT, but this effect appeared unaffected by 5-HTT overexpression (Figure 3.10C-D). Notably, pre-incubation of the slices with the SSRI citalopram (1 µM, n = 8 from 4 animals) ameliorated, but did not completely rescue, the deficit in 5-HT-evoked sIPSCs observed in PNs recorded in 5-HTTOE mice (increase in sIPSCs frequency in 5-HTTOE *versus* 5-HTTOE+citalopram, p

> 0.05, Figure 3.8H, I). These data suggest that 5-HTTOE mice display a deficit in 5-HT-induced inhibition of PNs of the BA by GABAergic INs. This deficit is likely to be mediated, at least in part, by impaired 5-HT-mediated depolarization of PV+ INs. This loss of sensitivity to 5-HT in the 5-HTTOE mice is not entirely explained by an on-going increase in reuptake of 5-HT, as it could not be substantially rescued by pharmacological blockade of the 5-HTT.

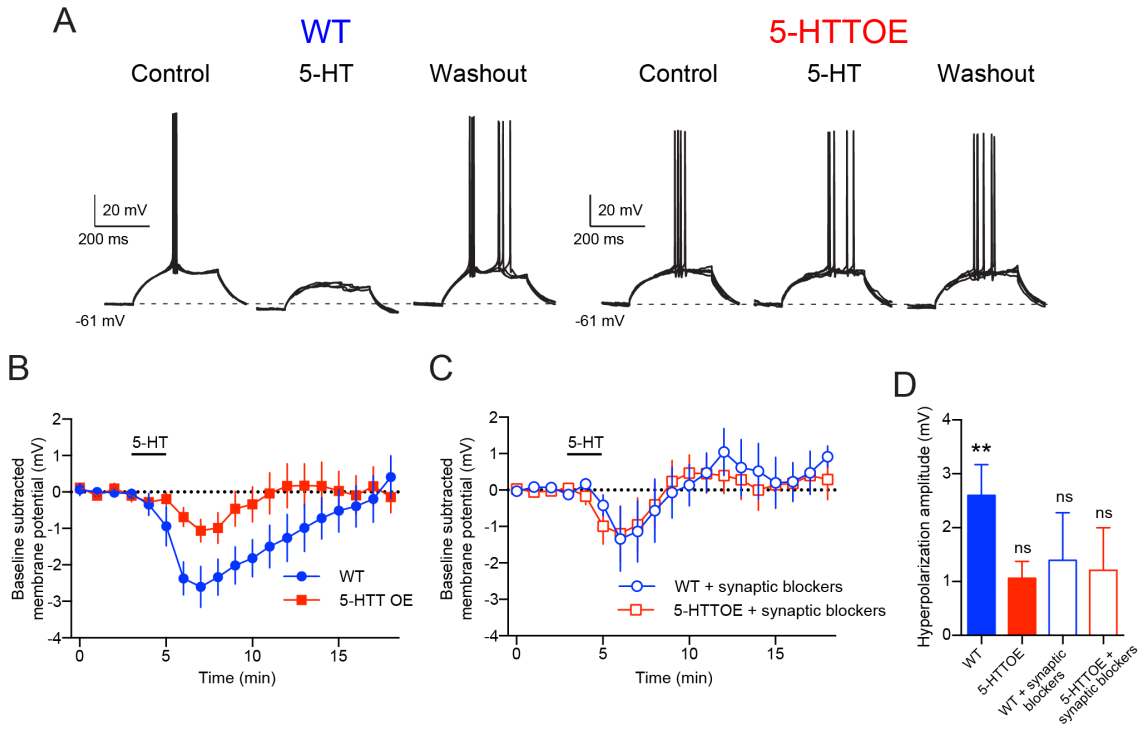

Figure 3.10. Impairment of 5-HT facilitation of GABA release leads to reduced hyperpolarization of PNs. **A**, five superimposed voltage responses to depolarizing current injections of representative PNs from a WT (100 pA, 300 ms , left) and 5-HTTOE mouse (70 pA, 300 ms, right) during control, bath application of 5-HT (50 µM) and washout. In control, the current intensities used were set just above threshold to evoke an action potential. **B**, time course of the effect of 5-HT on the V_m of WT and 5-HTTOE PNs. 5-HT evokes stronger hyperpolarization in WT compared to 5-HTTOE PNs **C**, time course of the effect of 5-HT on the V_m of WT and 5-HTTOE PNs in presence of kynurenic acid (3 mM), SR95531 (10 µM) and CGP54626 (5 µM). 4/9 WT and 2/6 5-HTTOE PNs hyperpolarized following 5-HT application, suggesting a direct response. Direct inhibitory responses are similar in WT and 5-HTTOE. **D**, 5-HT evoked hyperpolarization amplitude compared to control. 5-HT produces a significant membrane hyperpolarization only in WT PNs (n = 8 from 5 animals). V_m is not significantly hyperpolarized in 5-HTTOE (n = 10 from 7 animals) PNs or in WT and 5-HTTOE PNs in which glutamatergic and GABAergic transmissions are blocked (n = 9 from 6 animals and n = 6 from 2 animals, respectively). Data are presented as means ± SEM.

3.3.4 Impaired 5-HT_{2A} function underlies deficit in 5-HT-evoked inhibition of PNs

We reasoned that the reduced 5-HT-evoked excitation of PV+ INs observed in the 5-HTTOE mice could be caused by a loss of function at the level of 5-HT_{2A} receptors. Crucially, the 5-HT_{2A} receptor is the main mediator of the excitatory effect of 5-HT on BLA INs, and this receptor is located primarily on PV+ INs (McDonald and Mascagni, 2007; Jiang et al., 2009). Thus, we asked whether reduced 5-HT_{2A} receptor function could account for impaired 5-HT-induced excitation of PV+ INs in 5-HTTOE mice.

The direct acting 5-HT_2 agonist, α-methyl-5-HT, was applied while recording sIPSCs on PNs. In WT mice, bath application of α-methyl-5-HT (30 μM, n = 13 from 4 animals) increased the frequency of sIPSCs (Figure 3.11A, B). This effect was almost entirely abolished by MDL 100,907 (150 nM, n = 5; increase in sIPSCs frequency WT *versus* WT+MDL 100,907 $p < 0.01$, Figure 3.11C, D, G, H), indicating that α-methyl-5-HT acts on 5-HT_{2A} receptors to facilitate GABA release, presumably by depolarization of PV+ INs (Jiang et al., 2009). In comparison to WT mice, in 5-HTTOE mice application of α-methyl-5-HT produced a much smaller increase in sIPSC frequency in PNs ($p < 0.01$, n = 13 from 3 animals, Figure 3.11E-H). Taken together these data demonstrate that, in the BA, increased 5-HTT expression is associated with impaired 5-HT_{2A} receptor-mediated activation of INs innervating PNs. As PV+ INs are the main IN type expressing 5-HT_{2A} receptors in the BA, this deficit likely arises from dysfunctional PV+ INs.

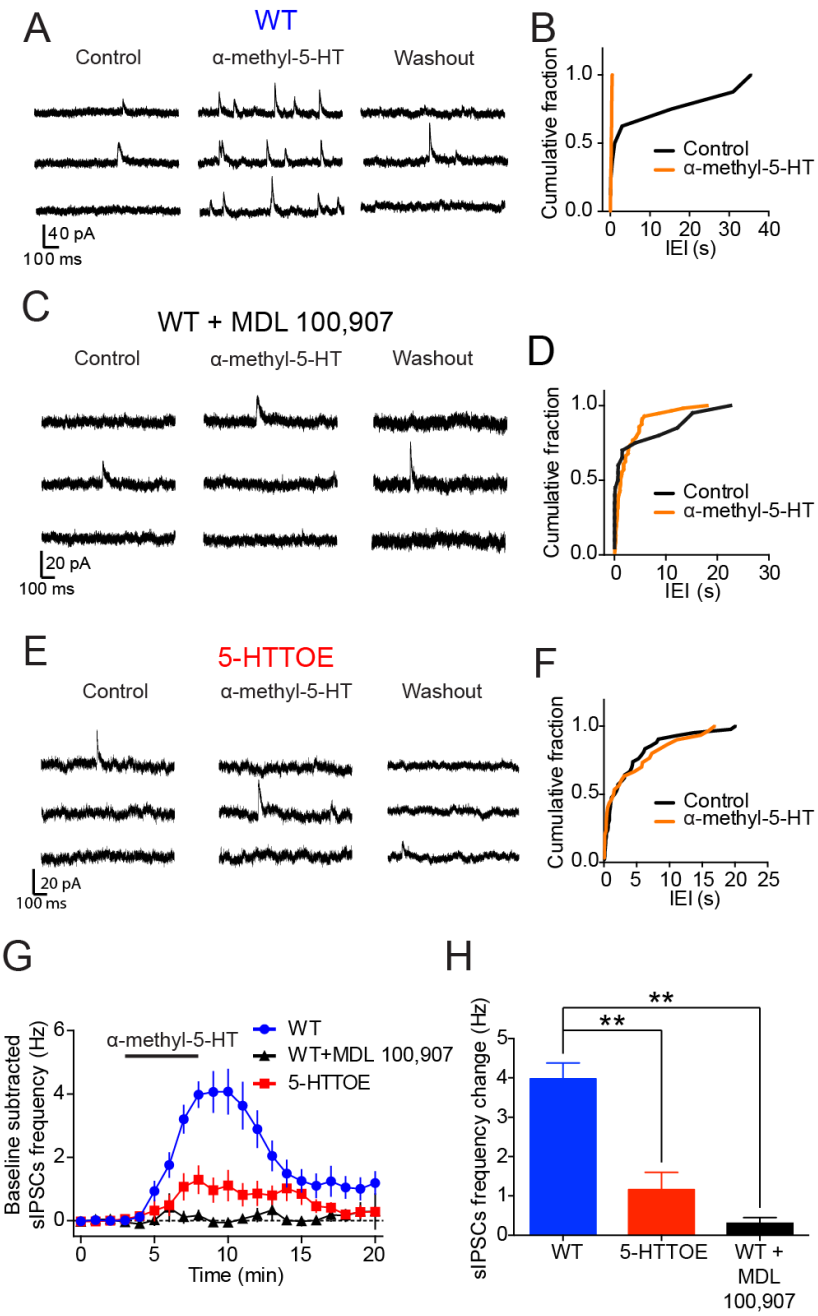

Figure 3.11. 5-HT$_{2A}$-mediated inhibition of PNs is impaired in 5-HTTOE mice.
A, representative voltage clamp (-50 mV) trace from a WT PNs during control, α-methyl-5-HT (30 μM) application and washout. **B**, Cumulative probability distributions of the inter-event intervals (IEI) for the sIPSCs of the neuron in D during control and in presence of α-methyl-5-HT. α-methyl-5-HT significantly increases the sIPSCs frequency ($p < 0.0001$, Kolmogorov-Smirnov test). **C**, representative voltage clamp (-50 mV) trace from a WT PNs in presence of the 5-HT$_{2A}$ antagonist MDL 100,907 (150 nM) during control, α-methyl-5-HT application and washout. **D**, cumulative probability distributions of the inter-event intervals (IEI) for the sIPSCs of the neuron in D during control and in presence of α-methyl-5-HT. α-methyl-5-HT does not significantly increase the sIPSCs frequency ($p > 0.05$, Kolmogorov-Smirnov test). **E**, representative voltage clamp (-50 mV) trace from 5-HTTOE PNs during control, α-methyl-5-HT application and washout. **F**, Cumulative probability distributions of the inter-event intervals (IEI) for the sIPSCs of the neuron in F during control and in presence of α-methyl-5-HT. α-methyl-5-HT does not significantly increase sIPSCs frequency ($p > 0.05$, Kolmogorov-Smirnov test). **G**, time course of the effect of α-methyl-5-HT on sIPSCs frequency in WT (with and without 5-HT$_{2A}$ antagonist MDL 100,907) and 5-HTTOE PNs. **H**, α-methyl-5-HT evokes a significantly higher sIPSCs frequency in WT (n = 13 from 4 animals) compared to 5-HTTOE (n = 13 from 3 animals) PNs. MDL 100,907 blocks the effect of α-methyl-5-HT (n = 5 from 2 animals). ** $p < 0.01$. Data are presented as means ± SEM

3.3.5 5-HTT overexpression causes deficient 5-HT modulation of PN firing

Finally, to understand the functional consequences of reduced 5-HT-driven inhibition of PNs, we examined 5-HT modulation of PN firing in the two genotypes. We injected theta frequency sinusoidal currents that evoked firing in ~50% of the oscillation peaks.

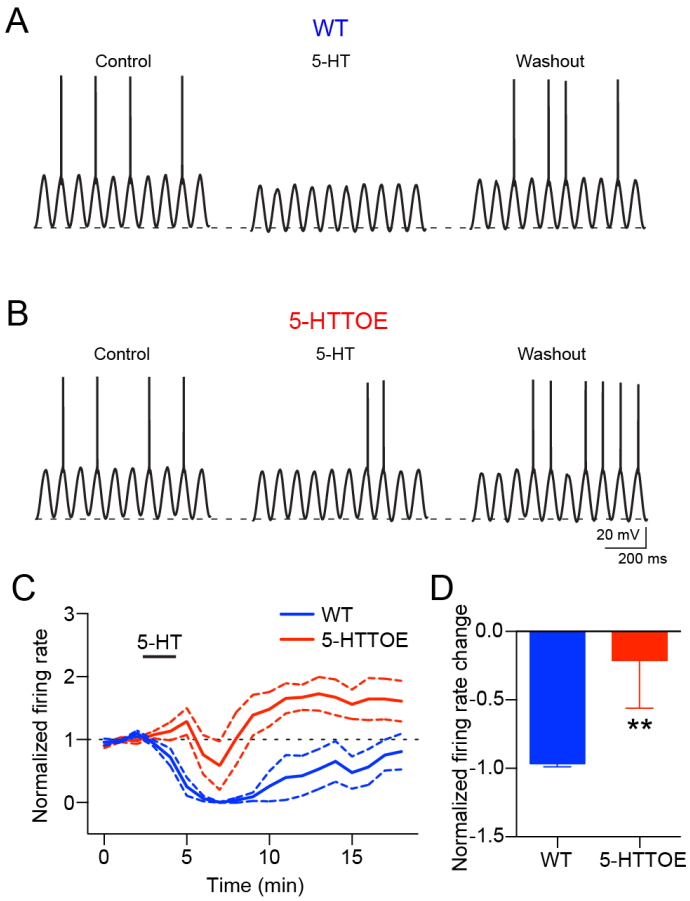

Figure 3.12. Increased 5-HTT expression alters the output of BA PNs. **A**, sinusoidal current (+160 pA intensity) injected at theta frequency (6 Hz) in a representative WT PN current clamped at -60 mV. Application of 5-HT (50 μM) causes hyperpolarization and suppression of firing. **B**, sinusoidal current injection (+190 pA) at theta frequency (6 Hz) in a representative 5-HTTOE PN current clamped at -60 mV. Application of 5-HT produces a weaker hyperpolarization and fails to suppress firing. **C**, time course of the effect of 5-HT on the firing rate of WT and 5-HTTOE PNs (sinusoidal current injections shown in A and B delivered every 10 s). **D**, 5-HT evokes a significantly stronger depression of firing rate in WT (n = 6 from 3 animals) compared to 5-HTTOE (n = 5 from 2 animals) PNs. ** $p < 0.01$. Data are presented as means ± SEM

Application of 50 μM 5-HT reliably suppressed the firing of PNs from WT mice (n = 6 from 3 animals, Figure 3.12A, C). In contrast, the reduction in firing rate evoked by 5-HT was significantly weaker in PNs from 5-HTTOE mice ($p < 0.01$, n = 5 from 2 animals, Figure 3.12B-D). Thus, 5-HTT overexpression can radically modify BA excitatory output.

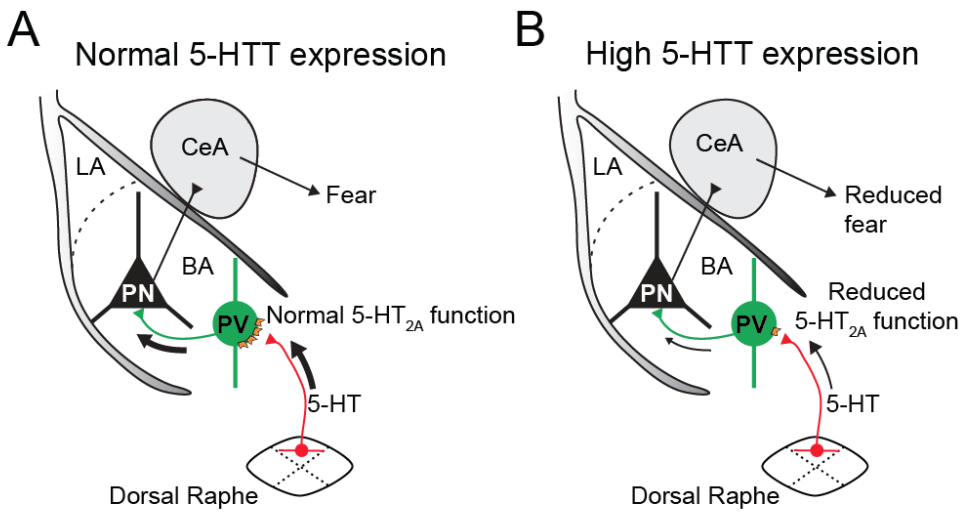

Figure 3.13. Model of amygdala circuit alterations in 5-HTTOE mice.
A, DRN firing, leading to release of 5-HT in the BA, excites PV+ INs through 5-HT_{2A} receptors, leading to indirect perisomatic inhibition of PNs. **B**, increased 5-HTT expression, characterized by lower 5-HT tone due to more efficient 5-HT reuptake, causes reduced 5-HT_{2A} receptor function on PV+ INs, leading to failure of DRN activity to recruit PV+ INs. This could affect the encoding of sensory stimuli (CS and US) by the PNs, dampening fear responses. CeA: central amygdala.

3.4 Discussion

This study presents two novel findings on how variation in 5-HTT expression has an impact upon the microcircuitry of the BA. First, our c-Fos data show that increased 5-HTT expression results in reduced recruitment of BA PV+ INs during fear memory retrieval. Second, our electrophysiological results reveal a selective impairment in 5-HT-evoked excitation of PV+ INs, leading to reduced inhibition of PNs. Thus, increased 5-HTT expression leads to a loss of 5-HT control over PV+ INs and therefore over PNs firing, likely affecting BA output to the central amygdala and the processing of fear (see model in Figure 3.13A, B). These findings provide the first evidence of changes in the function of neurochemically-defined neuron types due to genetic alterations in 5-HTT expression.

PV+ INs of the BLA increase their firing rates in response to CS presentation during fear conditioning (Wolff et al., 2014). Our data are consistent with this finding because

presentation of a tone predicting a footshock significantly increased c-Fos expression in BA PV+ INs in WT mice. PV+ INs target the perisomatic region of PNs (Bienvenu et al., 2012), inhibiting and synchronising their firing (Woodruff and Sah, 2007b; Popescu and Paré, 2011; Ryan et al., 2012) and disinhibiting their dendrites (Wolff et al., 2014). Hence, they tightly control the BLA output to the CeA, orchestrating fear responses. Crucially, inhibiting PV+ INs during the CS weakens fear learning (Wolff et al., 2014). Thus, reduced freezing responses to the CS observed in 5-HTTOE mice (Barkus et al., 2014; Line et al., 2014) could be directly linked with disrupted excitation of PV+ INs during the CS. Although the present study does not demonstrate a causal relationship between reduced PV+ IN activation and reduced fear in 5-HTTOE mice, a defective encoding of the CS by PV+ INs could (1) fail to disinhibit PN dendrites, by lack of direct inhibition of SOM+ INs neurons, which are also inhibited by PV+ INs (Wolff et al., 2014); (2) contribute to recently reported weaker theta oscillations (Barkus et al., 2014); and (3) lead to reduced fear (current study and previous reports (Barkus et al., 2014; Line et al., 2014; McHugh et al., 2015)). However, we cannot exclude that other mechanisms contribute to the altered fear behaviour of 5-HTTOE mice. Furthermore, we cannot fully resolve whether PV+ INs activation arises from fear memory recall, sensitization by footshock or fear generalization to the tone or the testing context. This is because CS-evoked freezing and PV+ INs activation were weaker but not absent in the unpaired condition. Future experiments could test whether manipulation of PV+ INs of the BA is sufficient to rescue the fear deficits in 5-HTTOE mice.

The present study also provides a putative mechanism underpinning the reduced excitation of PV+ INs of the BA in 5-HTTOE mice, namely reduced sensitivity to 5-HT. This was evident in electrophysiological experiments showing that both 5-HT-evoked depolarization of PV+ INs, associated with the closure of a membrane conductance, and 5-

HT-evoked IPSCs in PNs were reduced in 5-HTTOE mice. These deficits are likely caused by reduced functionality of 5-HT_{2A} receptors, since sensitivity to the direct acting 5-HT_{2A} receptor agonist, α-methyl-5-HT, was also impaired. Reduced 5-HT_{2A} function, likely leading to reduced inhibition of a leak K^+ conductance in PV+ INs (Andrade and Nicoll, 1987), could arise from either downregulation or dysfunctional receptor-effector coupling (Béïque et al., 2004). Surprisingly, 5-HTT blockade failed to rescue fully the loss of sensitivity to 5-HT in the 5-HTTOE mice. Therefore, the 5-HT deficit in the BA associated with increased 5-HTT expression appears to be dependent more on 5-HT_{2A} receptor function than on reduced 5-HT extracellular levels mediated by greater reuptake in 5-HTTOE mice.

The impaired sensitivity of PV+ INs in 5-HTTOE mice to 5-HT could be responsible for reduced c-Fos/PV co-expression evoked by fear memory retrieval. This view is appealing because fear activates 5-HT neurons in the midbrain (Spannuth et al., 2011) and triggers the release of 5-HT in the BLA (Zanoveli et al., 2009). Additionally, midbrain 5-HT neurons can fire phase-locked to limbic theta oscillations (Kocsis and Vertes, 1992), thus their temporally precise excitation of PV+ INs could contribute to the generation of theta rhythms in the BLA which are reduced in 5-HTTOE mice (Barkus et al., 2014). However, other circuits could also contribute to the weaker activation of PV+ INs during fear memory retrieval. For instance, 5-HTT overexpression might alter the function of other areas such as the mPFC and the HPC, which are also targeted by 5-HT fibres and project to the BLA (Hensler, 2006). Unlike PV+ INs, we did not detect genotypic differences in the overall amount of c-Fos in the paired condition, despite our *in vitro* finding that PNs receive reduced inhibition in 5-HTTOE mice. Although these activated neurons likely represent a majority of PNs, it is important to keep in mind that other IN population might be included. Similar numbers of activated PNs could be due to 5-HTTOE mice learning CS-US association, although displaying lower freezing levels

compared to WTs. Furthermore, impaired PV+ INs output could result in a different temporal distribution of action potentials in PNs rather than a long-lasting reduction in their firing rates, with c-Fos protein expression lacking the temporal resolution to reveal such changes.

Our data provide compelling evidence linking increased expression of the 5-HTT with abnormal PN function. The 5-HT_{2A} receptor, which depolarizes PV+ INs, appears to play a key role in this relationship. We cannot fully rule out that other IN types also contribute to the deficient 5-HT-driven inhibitory inputs to PNs, because 5-HT depolarizes many INs and other INs might express 5-HT_{2A}. In this study, we could not reliably compare PV-negative INs of WT and 5-HTTOE mice because we cannot exclude that lack of PV immunoreactivity is due to washout of the protein from the cytoplasm by the whole cell recording. Thus, future studies could examine other IN populations (e.g. SOM+ or CCK+ INs) in 5-HTTOE mice, potentially crossing these mice with transgenic lines to fluorescently tag these cells and facilitate recordings.

In any case, PV+ INs are the major GABAergic cell type expressing 5-HT_{2A} receptors in the BLA, in addition to a small number of SOM+ INs (McDonald and Mascagni, 2007). Adaptive changes in 5-HT_{2A} receptor function due to pharmacological or genetic manipulation of the 5-HTT are consistent with previous studies (Li et al., 2003; Marek et al., 2005; Jennings et al., 2008; Sarkar et al., 2014). Importantly, putative 5-HT_{1A}-mediated inhibition of PNs was unaffected in 5-HTTOE. Altered 5-HT levels during development due to higher 5-HT reuptake may be responsible for loss of 5-HT_{2A} function from PV+ INs. In contrast, 5-HT_{1A} receptors have been shown to develop later in cortical pyramidal cells (Béïque et al., 2004), thus their later expression on BA PNs might prevent receptor exposure during a sensitive developmental period (Gross et al., 2002). Further experiments examining PV+ INs function during development are necessary to corroborate this hypothesis.

In summary, our results suggest a novel mechanism through which increased expression of the 5-HTT gene can alter the microcircuitry of the amygdala, namely by changing the function of PV+ INs. Probing the effects of genetic variation in the 5-HTT or SSRI treatment on neural circuits in limbic areas may open new horizons for the understanding of the biological basis of emotional behaviour.

Chapter 4 Bidirectional modulation of paracapsular nitric oxide synthase expressing neurons by sleep and serotonin

4.1 Introduction

Besides classic IN populations such as those expressing PV and SOM, many other types of GABAergic neuron have been detected in the BLA of rodents (Spampanato et al., 2011). These cells express a variety of molecular markers, such as CB (McDonald and Mascagni, 2001a; Bienvenu et al., 2012), CR (McDonald and Mascagni, 2001a), VIP (Mascagni and McDonald, 2003), CCK (Mascagni and McDonald, 2003; Jasnow et al., 2009), neurokinin-1 receptors (NK1; Sreepathi and Ferraguti, 2012), NPY (McDonald, 1989; Manko et al., 2012), and nNOS (McDonald et al., 1993; Usunoff et al., 2006).

Neurons of the BLA expressing nNOS represent a particularly intriguing cell population(s) for several reasons. First, in areas with IN diversity similar to the BLA, such as HPC or neocortex, nNOS+ neurons are as abundant, or even more abundant, than PV+ or SOM+ cells (Fuentealba et al., 2008; Tricoire and Vitalis, 2012), suggesting a prominent impact on both networks. Second, they are able to modulate neurons through a variety of mechanisms, including slow inhibition (Capogna and Pearce, 2011), retrograde release of nitric oxide (Li et al., 2014), and potentially via other neuropeptides (Fuentealba et al., 2008; Tricoire and Vitalis, 2012), suggesting they may fulfil a different function from other classes of INs. Third, neocortical nNOS+ neurons co-expressing SOM and NPY are thought to be atypical long-range GABAergic projection neurons (Tomioka et al., 2005; Tamamaki and

Tomioka, 2010), and this might apply also to the BLA (McDonald et al., 2012; McDonald and Zaric, 2015). Interestingly, this neocortical cell type has been shown to be activated during sleep in three different mammalian species and it is suggested to be a component of the homeostatic sleep/wake regulation system (Gerashchenko et al., 2008; Morairty et al., 2013). It is important to keep in mind, however, that not all nNOS+ neurons are GABAergic. Indeed, in the lateral amygdala (LA), some of them appear to be glutamatergic PNs (Lange et al., 2012).

In spite of their prominence, the intrinsic physiology of GABAergic nNOS+ neurons of the BLA, as well as their modulation by neuromodulators (including 5-HT) and behavioural states remain elusive. As previously described, the most commonly established effect of 5-HT in the BLA is the depolarization of the majority of GABAergic cells (Rainnie, 1999). However, recent *in situ* hybridization data have shown that BLA NPY+ cells, some of which are thought to be nNOS+ (McDonald et al., 1993), can also express inhibitory 5-HT_{1A} receptors (Bonn et al., 2013). Thus, it is important to verify whether the modulation of nNOS+ neurons of the BLA by 5-HT is in line with the effect of this neuromodulator on the majority of INs (i.e. membrane depolarization), or rather implies different effects (e.g. membrane hyperpolarization).

In Chapter 3, 5-HT transmission in the BLA was described in relation to fear conditioning. However, 5-HT signalling is also involved in the sleep-wake cycle (Portas et al., 2000; Gao et al., 2002). Specifically, extracellular forebrain 5-HT levels are low during sleep and high during wake (Portas et al., 1998; Bjorvatn et al., 2002). These findings are in agreement with unit recordings showing that DRN 5-HT neurons fire at higher rates during wakefulness, with a dramatic reduction during slow wave sleep and a complete cessation during rapid eye movement (REM) sleep (Sakai, 2011). Since the activity of BLA neurons

also follows the sleep-wake cycle (Paré and Gaudreau, 1996), this could occur, at least in part, via 5-HT release.

Thus, defining the diversity of 5-HT actions on BLA neuron types could advance the knowledge of the cellular dynamics occurring in the BLA across different brain states. These dynamics could also be important for emotional learning, because oscillatory activity in the BLA during REM sleep that follows fear conditioning predicts the degree of fear memory consolidation (Popa et al., 2010). Furthermore, REM sleep deprivation delays fear memory extinction (Silvestri, 2005), whereas general sleep deprivation impairs fear memory consolidation (Graves et al., 2003; Kumar and Jha, 2012).

In this study, we aimed to functionally characterise nNOS+ neurons of the mouse BLA and to shed light on their modulation by 5-HT. Additionally we asked whether nNOS+ neuron activity *in vivo* is consistent with their regulation by 5-HT.

4.2 Materials and methods

4.2.1 Animals

Since nNOS is broadly expressed during development (Bredt and Snyder, 1994), but its expression is more restricted to particular cells following postnatal day 15 (Kubota et al., 2011; Taniguchi et al., 2011), an inducible Cre driver line (nNOS-Cre^{ER}, Jackson Laboratories, B6;129S-*Nos1*$^{tm1.1(cre/ERT2)Zjh}$/J, stock number 014541) was used to induce Cre recombination post-natally. nNOS-Cre$^{ER+/-}$ mice were crossed with Ai9$^{+/+}$ reporter mice (Jackson Laboratories, B6.Cg-*Gt(ROSA)26Sor*$^{tm9(CAG-tdTomato)Hze}$*/J*, stock number 007909) to generate nNOS-Cre;Ai9 offspring. To quantify the overlap of neurochemical markers, WT C57BL/6J mice (Charles River) were used. Mice were housed with their littermates with *ad*

libitum access to food and water in a dedicated housing room with a 12/12 h light/dark cycle. To induce Cre recombinase and label nNOS+ neurons with tdTomato, nNOS-Cre;Ai9 mice (postnatal day 20-45) received 1-3 intraperitoneal injections of tamoxifen (10 mg/ml in corn oil, 10 µl/g body weight per day). For patch clamp and anatomical experiments, mice (postnatal day 27-60 age) were used at least one week after the first tamoxifen injection.

For sleep experiments, adult male C57BL/6J mice (15 weeks age) were individually housed in custom-made clear plexiglass cages (20.3 x 32 x 35 cm) with free access to a running wheel and *ad libitum* food and water. Cages were located in ventilated, sound-attenuated Faraday chambers (Campden Instruments, two cages per chamber) under a standard 12/12 h light-dark cycle (lights on 0800, ZT0, light levels ~120-180 lux). RT and humidity were maintained at 22 ± 1°C and 50 ± 20%, respectively. Mice were habituated to both the cage and recording cables for a minimum of 16 days prior to recording.

All procedures involving experimental animals were performed in compliance with the Animals (Scientific Procedures) Act, 1986 (UK) and associated regulations, under approved project licenses by Home Office UK (30/3061 and 70/7483) and with Society for Neuroscience Policies on the Use of Animals in Neuroscience Research.

4.2.2 *Ex vivo* recordings

nNOS-Cre;Ai9 mice (postnatal day 27-60) were decapitated under deep isoflurane anaesthesia (4% in O_2). Slice preparation, extracellular solutions and microscopy were the same as described in Chapter 3, section 3.2.4 *Ex vivo* recordings. A mercury vapour short-arc lamp (100W, N HBC 103, Zeiss) was connected to an epifluorescence system to visualize the tdTomato+ neurons. Somatic whole-cell patch clamp recordings were performed from visually identified tdTomato+ neurons. Intracellular solutions and whole-cell patch clamp recording procedures were the same as in Chapter 3, section 3.2.4 *Ex vivo* recordings. Cell-

attached recordings were performed as in Chapter 2, section 2.2.5 *Ex vivo* recordings and analysis.

V_m during 5-HT application was monitored while holding neurons at -60 ± 2 mV. Hyperpolarizing and depolarizing current steps were injected every 10 s to monitor R_{in} and firing, respectively. At the end of the recording, some slices containing biocytin-filled cells were fixed overnight at 4 °C in 4% PFA and 15% saturated picric acid in 0.1 M PB. After 24 h, slices were embedded in gelatin and re-sectioned into 60-70 µm thick sections with a VT-1000 vibrating microtome (Leica).

4.2.3 Analysis of *ex vivo* recordings

Analysis of *ex vivo* recordings was performed using Igor Pro (Wavemetrics, Inc.) and MATLAB (Mathworks, Inc.). Analysis of intrinsic membrane properties was the same as reported in Chapter 3, section Analysis of *ex vivo* recordings. Neurons were defined as 'bursting' during 5-HT application if the peak of ISI histogram (in Log scale) was <100 ms.

4.2.4 EEG Recordings and Sleep deprivation

4.2.4.1 Surgical procedures and electrode implantation

Surgical procedures were carried out using aseptic techniques under isoflurane anaesthesia (3-5% induction, 1-2% maintenance) and Metacam (1-2 mg/kg, subcutaneous injection, Boehringer Ingelheim Ltd.) was administered preoperatively. During surgery, animals were head-fixed using a stereotaxic frame (David Kopf Instruments) and liquid gel (Viscotears, Alcon Laboratories Ltd.) was applied to protect the eyes. In all animals, electroencephalogram (EEG) screws were placed in the frontal (motor area, AP +2 mm, ML 2 mm) and occipital (visual area, V1, AP -3.5/-4 mm, ML 2.5 mm) cortical regions using

procedures previously described (Cui et al., 2014). A reference screw electrode was placed above the cerebellum and an additional anchor screw was placed in the left parietal hemisphere to ensure implant stability. EEG screws were soldered (prior to implantation) to custom-made headmounts (Pinnacle Technology) and all screws and wires were secured to the skull using dental acrylic. Two single stranded, stainless steel wires were inserted either side of the nuchal muscle to record electromyography (EMG). Saline (0.1 mL/20 g body weight, subcutaneous injection) was administered post-operatively and animals were provided thermal support throughout and following surgery. Metacam (1-2 mg/kg) was orally administered for at least three days after surgery. A minimum two week recovery period was permitted prior to cabling the animals.

4.2.4.2 Experimental design

On the experimental day, following a stable 24 h baseline recording, mice were divided into two groups: sleep deprivation (SD, n = 4) and SD+recovery sleep (RS, n = 4). RS was defined as the sleep opportunity occurring immediately following SD, and was limited to 1.5-2 h (Morairty et al., 2013). In both groups, SD was performed in the animal's home cage for a continuous 4 h period starting at light onset. During this time, animals were spontaneously awake and their behaviour as well as their EEG/EMG recordings were under constant visual observation. Sleep was prevented by regularly providing the animals with novel objects, an effective method that mimics natural conditions of wakefulness, is ethologically relevant, and does not appear to stress the animals (Palchykova et al., 2006; Vyazovskiy et al., 2007). All mice were well habituated to the experimenter and to the exposure to novel objects prior to the experiment. Novel objects included nesting and bedding material from other cages, wooden blocks, paper boxes and tubes of different shape and colour. SD was successful with 97.9 ± 2.5% of time spent awake during the 4 h procedure. After completion of the SD,

animals in the SD-group were intraperitoneally injected with an overdose of Euthanal (pentobarbitone sodium, 200 mg/mL, 0.3 ml) and upon loss of a response to toe pinch were perfused transcardially with 30 ml of 0.9% PBS followed by 50 mL of 4% PFA in 0.1 M PB (pH 7.4). All mice were perfused within approximately 30 min after the end of 4 h SD, and were kept awake continuously until the moment of injection with Euthanal. The SD+RS group were allowed to sleep undisturbed for a period of 1.5-2 h (an average of 1.81 ± 0.15 h spent in NREM and REM sleep) and then perfused according to the same procedure. Special care was taken to ensure that the animals in SD+RS group were not awake for longer than a few min prior to the injection of Euthanal. Brains were removed, post-fixed in 4% PFA (in 0.1 M PB) overnight at 4 °C, then thoroughly washed in PBS and left in 0.1 M PB + 0.05% sodium azide until further processing for c-Fos/nNOS immunohistochemical analysis (see below).

4.2.4.3 EEG recordings and power spectra analysis

Data acquisition was performed using the Multichannel Neurophysiology Recording System (TDT). Cortical EEG was recorded from frontal and occipital derivations. EEG/EMG data were filtered between 0.1-100 Hz, amplified (PZ5 NeuroDigitizer pre-amplifier, TDT) and stored on a local computer at a sampling rate of 256.9 Hz. EEG/EMG data were resampled offline at a sampling rate of 256 Hz. Signal conversion was performed using custom-written MATLAB scripts and was then transformed into European Data Format (EDF) using open source Neurotraces software (www.neurotraces.com). For each recording, EEG power spectra were computed by a Fast Fourier Transform (FFT) routine for 4 s epochs (using a Hanning window), with a 0.25 Hz resolution (SleepSign Kissei Comtec Co.). Vigilance states were scored offline through manual visual inspection of consecutive 4 s epochs (SleepSign, Kissei Comtec Co.). Two EEG channels (frontal and occipital) and EMG

were displayed simultaneously to aid vigilance state scoring. Vigilance states were classified as waking (low voltage, high frequency EEG with a high level or phasic EMG activity), NREM sleep (presence of slow waves, EEG signal of a high amplitude and low frequency) or REM sleep (low voltage, high frequency EEG with a low level of EMG activity). Great care was taken to eliminate epochs contaminated by eating, drinking or gross movements resulting in artefacts in at least one of the two EEG derivations.

4.3 Histological procedures

4.3.1 Immunohistochemistry

For quantification of the overlap between neurochemical markers, mice were transcardially perfused with saline followed by 4% PFA, 15% saturated picric acid, in 0.1 M PB. Brains were sectioned using a vibratome (Leica VT 1000 S) into 60 µm-thick slices. Sections were stored in 0.1 M PB containing 0.05% sodium azide until further usage. Sections containing recorded and biocytin-filled neurons were incubated overnight at 4 °C in 1:2000 Alexa488-conjugated Streptavidin (Invitrogen). Following blocking with 10% NDS for 1 h at RT, sections were incubated overnight at 4 ºC with different combinations of the following primary antibodies. Anti-c-Fos raised in rabbit (1:500, Abcam, cat. no. ab7963), anti-nNOS raised in goat (1:500, Abcam, cat. no. ab1376), anti-NK1 (substance P receptor) raised in rabbit (1:1000, Chemicon, AB5060), anti-NPY raised in rabbit (1:5000, Immunostar, cat no. 22940), anti-SOM raised in rat (1:250, Chemicon, cat. no. MAB354), anti-VGAT raised in guinea pig (1:500, Synaptic systems, cat. no. 131004). Following 3× washes in PBS, immunoreactivity was revealed with Alexa488- (1:500), Cy3- (1:500) or Alexa647-conjugated (1:250) secondary antibodies (all raised in donkey, Jackson Immunoresearch). For negative controls, the primary antibody was routinely omitted from the staining procedure; in

these cases no positive fluorescence signal was detected. In some cases, each secondary antibody was omitted in turn to confirm its specificity. Nissl staining was obtained via incubation in NeuroTrace® 640/660 Deep-Red Fluorescent Nissl Stain (1:200, Thermo Fisher, cat. no. N-21483).

All reagents were diluted in PBS containing 0.3% Triton X-100. Immunoreactivity was visualised using an epifluorescence microscope (AxioImager M2, Zeiss) or a laser-scanning confocal microscope (LSM 510, Zeiss). For representation of axonal and dendritic arborisation of nNOS neurons, tiled stacked images (1 μm step size) of biocytin-filled cells were acquired with the confocal microscope mentioned above under a 40× objective. Stacks were collapsed with a standard deviation Z-projection function in ImageJ. Tiled images were stitched and axon and dendrites colour-coded in Photoshop (Adobe). The boundaries between nuclei were determined with brightfield microscopy or Nissl stainings.

4.3.2 Quantification of overlap between neurochemical markers

Sections containing the BLA of SD and SD+RS mice were imaged with the epifluorescence microscope mentioned above and StereoInvestigator software (MBF Bioscience). A region of interest delineating either the BLA or the external capsule (EC) next to the LA was defined using and brightfield microscopy under a 5× 0.16 NA objective lens. For quantification of neurochemical markers expressed by nNOS cells, stereological sampling was carried out in both hemispheres from one out of three double or triple immunolabelled sections in the range -0.8 to -2.2 mm from bregma. Series of tiled stacked images were acquired using a 40× 1.3 NA oil-immersion objective and 1 μm steps at depth of 2 to 22 μm (‘optical sections’) from the upper surface of each section. In order to minimise artefacts arising from surface irregularities, the first 2 μm from the upper surface were defined as

'guard zone' and not scanned. Markers expressed by nNOS+ or Nissl-stained neurons were counted offline in StereoInvestigator and blind to behavioural testing conditions. A neuron was counted only if its immunopositive nucleus came into focus in the optical section. Nuclei already in focus at the top optical section were not counted (West, 1999)**.** For quantification of overall percentage of activated cells, stereological counting was performed by sampling three evenly spaced sections in the range -0.8 to -2.2 mm from bregma. Data were exported to Excel (Microsoft) and pooled for further analysis.

4.3.3 Drugs

Serotonin hydrochloride, WAY 100635 maleate, NBQX, D-APV, SR95531 and ZD7288 were purchased from Tocris Bioscience. Tamoxifen was purchased from Sigma-Aldrich.

4.3.4 Statistical analyses

Data are presented as means ± SEM values. Distributions were compared using Student's t-tests and one-way ANOVAs with Bonferroni *post hoc* correction. Statistical analysis was performed with Graphpad Prism and $p < 0.05$ was considered statistically significant.

4.4 Results

4.4.1 Neurochemical profile of nNOS+ type I neurons of the BLA

We aimed to uncover the anatomical and physiological features of GABAergic nNOS+ neurons of the BLA. First, I immunolabelled mouse coronal brain sections containing the amygdala for nNOS. I detected neurons with strong nNOS expression (type I) and others with light immunoreactivity (type II; Figure 4.1A), suggesting that nNOS+ neurons of the BLA can be classified according to the intensity of nNOS expression, as is the case of the neocortex (Smiley et al., 2000; Lee and Jeon, 2005). Type I nNOS+ cells displayed large ovoid somata and bitufted dendrites whereas type II neurons had more heterogeneous soma size and dendritic emissions.

To further characterise their neurochemical content, I quantified the proportion of nNOS+ cells co-expressing other markers often accompanying nNOS in other brain areas, namely SOM, NPY and NK1. I found that 93 ± 4% of nNOS+ type I cells co-expressed SOM (n = 3 brains), 95 ± 2% co-expressed NPY (n = 6 brains) and 85 ± 2% co-expressed NK1 (n = 3 brains, Figure 4.1A-C). In contrast, nNOS+ type II cells were mostly devoid of these neurochemical markers, with 2 ± 2% overlap with SOM (n = 3 brains), 9 ± 3% with NPY (n = 6 brains) and no cell expressing NK1 (n = 3 brains; data not shown). Thus, intense nNOS labelling identifies a neurochemically homogeneous population of BLA neurons. Since type II cells are likely to be more heterogeneous and comprise several cell types (Tricoire and Vitalis, 2012), further investigations were focused on nNOS+ type I neurons.

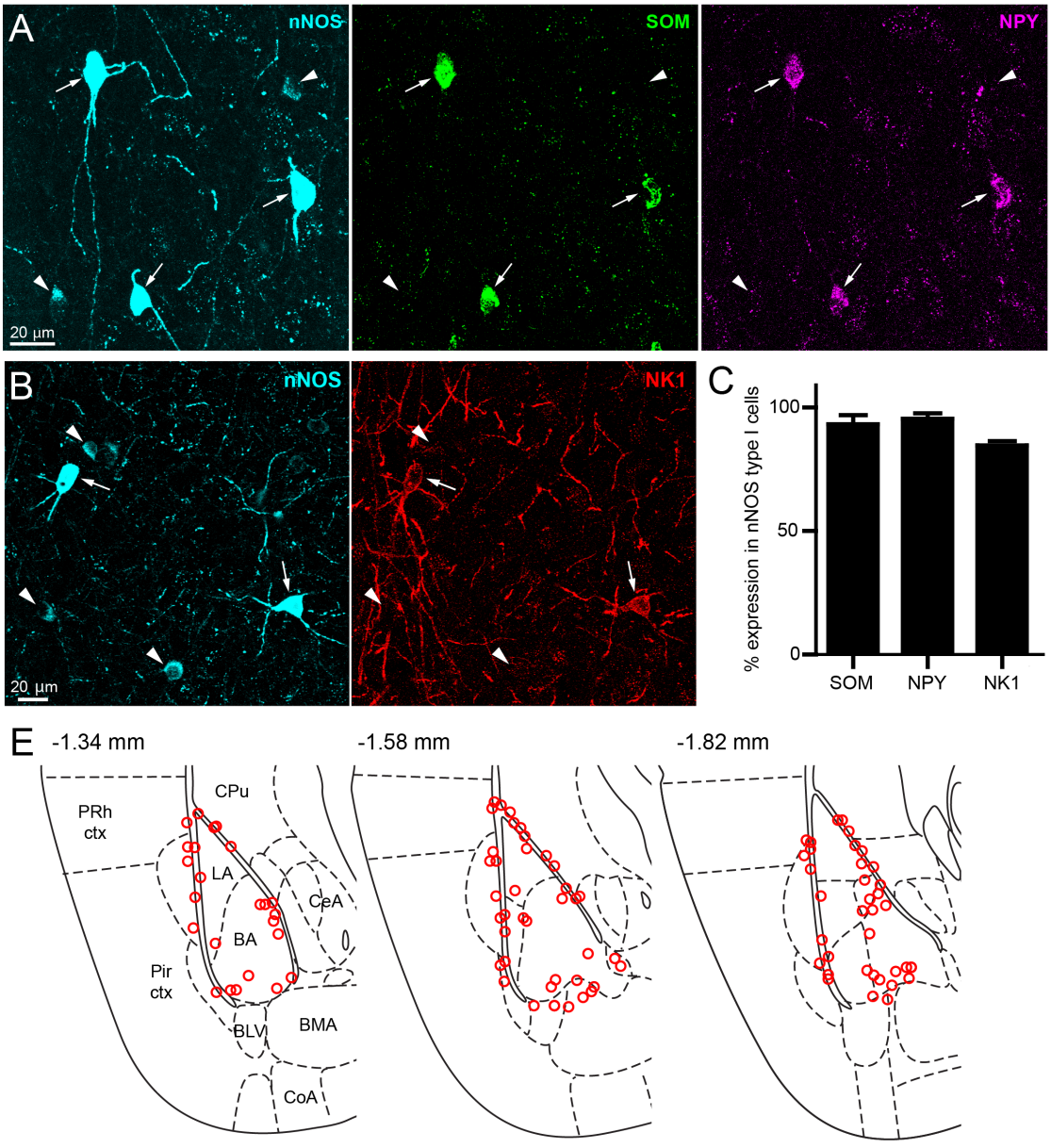

Figure 4.1. Neurochemical profile and localisation of nNOS+ type I neurons of the BLA.
A, co-localization of SOM and NPY in BLA neurons with strong nNOS expression (nNOS+ type I, arrows) and no SOM and NPY immunoreactivity in neurons with weak nNOS expression (nNOS+ type II, arrowheads). **B**, co-localization of NK1 in BLA nNOS+ type I neurons (arrows) and no NK1 immunoreactivity nNOS+ type II neurons (arrowheads). **C**, 93.2 ± 6.5% of nNOS+ type I neurons co-expressed SOM (n =3 brains), 95.4 ± 5.4% co-expressed NPY (n = 6 brains) and 84.6 ± 3.1 co-expressed NK1 (n = 3 brains). **D**, Three coronal sections illustrating the distribution of BLA nNOS+ type I neurons at different rostrocaudal positions. nNOS+ type I cells plotted at each level were mapped by collapsing three neighboring 60 µm-thick sections. Data are presented as means ± SEM.

Interestingly, these cells were localized primarily along BLA borders, namely adjacent to the EC, intermediate capsule and the border between basal (BA) and basomedial nuclei (Figure 4.1E), in line with previous reports of nNOS+ 'border cells' (McDonald et al., 1993;

Usunoff et al., 2006). Hence, the specific localisation of nNOS+ type I cells of the BLA suggests they could be ideally suited to receive inputs from fibres within the EC and intermediate capsule, for instance glutamatergic axons from cortical and thalamic regions.

4.4.2 Anatomical and electrophysiological features of paracapsular nNOS+ type I neurons

Although the neurochemical content of nNOS+ type I neurons of the BLA suggests they might be GABAergic cells, we wished to uncover their inhibitory nature and their anatomical hallmarks. I took advantage of a nNOS-Cre;Ai9 mouse line (Taniguchi et al., 2011) that labels nNOS+ neurons with high specificity (Figure 4.2A, B). To selectively target nNOS+ type I neurons, I prepared acute coronal brain slices and performed whole-cell patch clamp recordings from tdTomato+ cells located along the EC that separates the LA from the endopiriform claustrum/piriform cortex (in the following named as paracapsular nNOS+, pc-nNOS+, neurons). In this region, type I cells constitute 80 ± 3% (n = 3 brains) of nNOS+ neurons and are easily distinguishable from type II cells due to their significantly larger ovoid somata (128 ± 5 *versus* 88 ± 2 μm^2, $p < 0.0001$, n = 25 cells from 6 brains).

Filling of intracellularly recorded pc-nNOS+ cells with biocytin (Figure 4.2C) revealed mostly bitufted dendrites, which were largely aspiny and ran in parallel to the EC (Figure 4.2D). The projection pattern of pc-nNOS+ neurons was examined in 13 cells in which the axon was labelled with biocytin. The majority of pc-nNOS+ cells (77%) innervated the BLA complex, with 54% projecting only to the LA and 23% to both LA and BA.

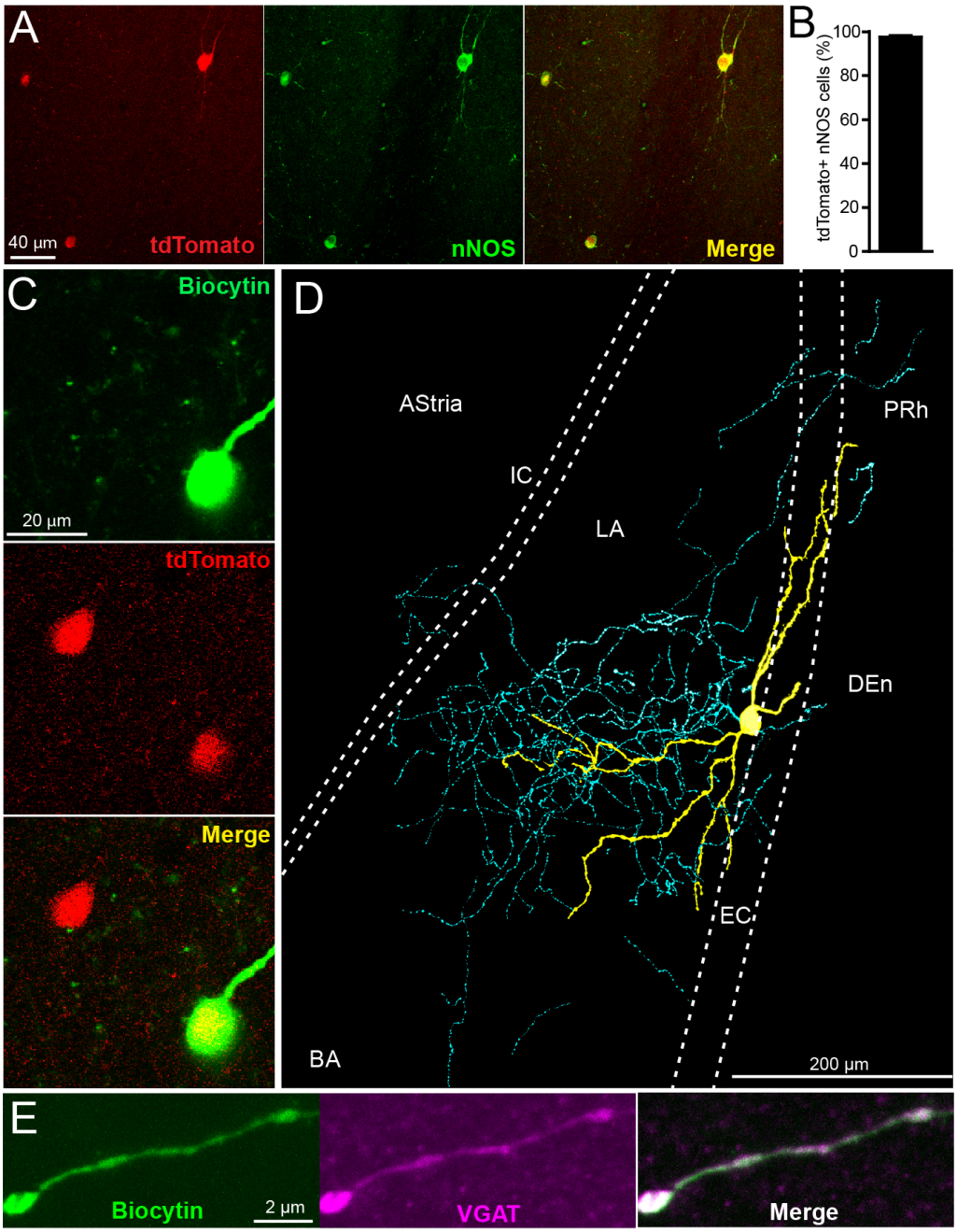

Figure 4.2. Anatomical features of pc-nNOS+ neurons
A, co-localisation of tdTomato and nNOS in paracapsular BLA neurons from a nNOS-Cre;Ai9 mouse. **B**, expression of tdTomato is restricted to nNOS+ neurons (97.9 ± 0.7% nNOS/tdTomato overlap, n = 3 brains). **C**, biocytin-labelled pc-nNOS+ neuron co-expressing tdTomato. **D**, a biocytin-filled pc-nNOS+ neuron projecting predominantly within the LA, but some projections can also be seen outside the BLA. Soma and dendrites are labelled in yellow and the axon is labeled in cyan. Abbreviations: AStria: amygdalo-striatal transition area; BA: basal amygdala; DEn: dorsal endopiriform claustrum; EC: external capsule; IC: intermediate capsule; LA: lateral amygdala; PRh: perirhinal cortex. **E**, representative biocytin-filled pc-nNOS+ neuron axon displaying VGAT immunoreactivity. Data are presented as means ± SEM.

Frequently (61%), pc-nNOS+ also sent axonal branches outside the BLA, specifically to the endopiriform claustrum (54%), perirhinal (46%) and piriform (31%) cortices.

Additionally, one cell innervated the ectorhinal cortex and TeA, one the amygdalo-striatal transition area and one the caudate putamen. A subset of cells (n = 5) was tested for axonal VGAT immunoreactivity, and all of them exhibited VGAT immunopositivity (Figure 4.2E), thereby demonstrating their GABAergic identity. Thus, pc-nNOS+ neurons likely modulate BLA and extra-amygdaloid neurons via release of GABA and, potentially, via slower functional actions mediated by SOM and NPY (Meis et al., 2005; Sosulina et al., 2008).

Next, I examined the intrinsic membrane responses displayed by pc-nNOS+ neurons in brain slices (Figure 4.3 and Table 4.1, n = 10 neurons). These cells were characterized by high R_{in} (852.8 ± 51.8 MΩ), high membrane time constant (τ, 27.2 ± 2.0 ms) and high excitability (rheobase current 28.3 ± 4.0 pA), with even small positive current injections leading to sustained firing. Consistent with the general physiology of BLA SOM+ neurons (Wolff et al., 2014), pc-nNOS+ neurons were not fast-spiking (instantaneous firing rate 23.2 ± 1.8 Hz) and showed relatively broad spikes (half-width 0.75 ± 0.04 ms, Figure 4.3C, E). Additionally, pc-nNOS+ cells exhibited very depolarized resting V_m (-39.7 ± 2.4 mV), resulting in spontaneous firing (Figure 4.3D). Finally, when hyperpolarizing currents were injected, pc-nNOS neurons displayed a depolarizing sag and rebound depolarization. Both responses were mediated by the hyperpolarization-activated cationic current, I_h, because they were abolished by the I_h blocker ZD7288 (30 μM, n = 5, Figure 4.3F).

Collectively, these data show that pc-nNOS+ neurons represent a distinctive GABAergic neuron type, because they appear different both electrophysiologically and anatomically from IN types studied so far, namely PV+ (see Rainnie et al., 2006 and Table 3.2), CCK+ (see Jasnow et al., 2009) and other NPY+ INs (see Manko et al., 2012).

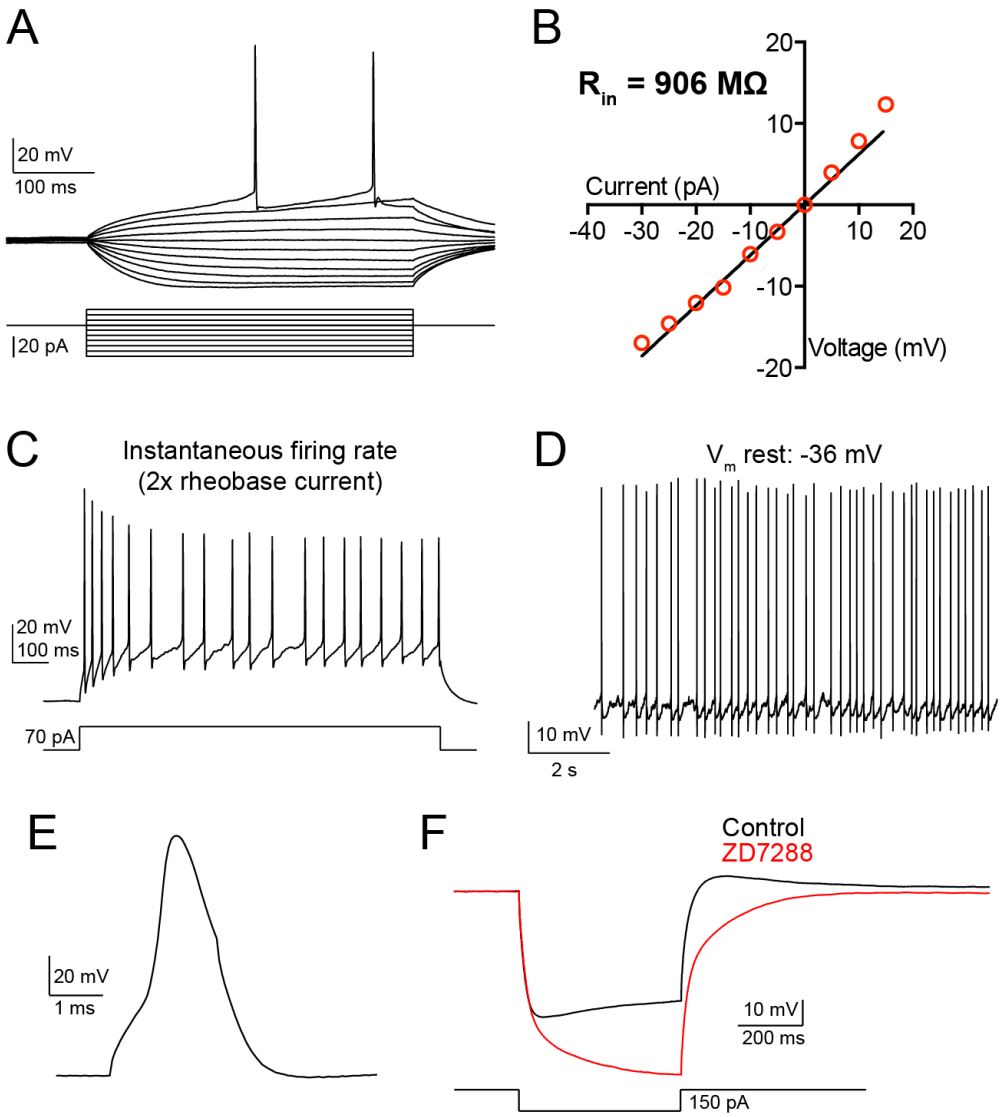

Figure 4.3. Electrophysiological features of pc-nNOS+ neurons
A, voltage responses to hyperpolarizing-depolarizing current pulses (range: –30/+15 pA, 5 pA steps, 400 ms) used to construct the I–V plot shown in **B** and to determine the value of R_{in}. **C**, adapting instantaneous firing, obtained by injecting twice the rheobase current for 1 s. **D**, spontaneous firing at resting V_m. **E**, action potential evoked by a short depolarizing current (3 ms, +800 pA). **F**, voltage sag and rebound depolarization generated by hyperpolarizing current injection (500 ms, -150 pA) and blocked by I_h blocker ZD7288 (30 μM).

Table 4.1. Electrophysiological parameters of pc-nNOS+ neurons
Abbreviations: R_{in}: input resistance; CV ISI: coefficient of variation of the interspike interval (calculated on the instantaneous firing rate); fAHP: fast after-hyperpolarization; resting V_m: resting membrane potential.

Electrophysiological parameter	Mean ± SEM (n = 10)
R_{in} (MΩ)	852.8 ± 51.8
Membrane τ (ms)	27.2 ± 2.0
Membrane capacitance (pF)	32.8 ± 3.1
Rheobase current (pA)	28.3 ± 4.0
Instantaneous firing rate (Hz)	23.2 ± 1.8
Adaptation index	0.623 ± 0.045
CV ISI	0.429 ± 0.071
Rebound depolarization amplitude (mV)	9.6 ± 1.4
Rebound depolarization area (mV×s)	36.5 ± 0.8
Sag ratio	0.915 ± 0.010
Spike half width (ms)	0.75 ± 0.04
Spike amplitude (mV)	80.6 ± 1.6
fAHP (mV)	16.5 ± 1.2
Threshold potential (mV)	-31.6 ± 0.8
resting V_m (mV)	-39.7 ± 2.4

4.4.3 Sleep activates pc-nNOS+ neurons

What could be a behavioural role for the pc-nNOS+ neurons of the BLA? In the neocortex, nNOS+ neurons have been shown to be inactive after a period of wakefulness, but active after a period of spontaneous sleep or sleep following SD (Gerashchenko et al., 2008; Morairty et al., 2013). Notably, SD prior to sleep appears to be crucial for their activation (Dittrich et al., 2014). Since SD is associated with emotional imbalance (Baglioni et al., 2010) and heightened amygdala responsiveness to salient stimuli (Yoo et al., 2007), a similar pattern

of pc-nNOS+ activation could mean that these neurons track the emotional component of sleep homeostasis.

To investigate whether the activity of pc-nNOS+ neurons is associated with vigilance state, we performed chronic sleep EEG recordings in 8 mice. As expected, during baseline the animals slept predominantly during the light period, and both the typical declining trend of EEG SWA and characteristic vigilance state-dependent differences in EEG spectra were apparent (Figure 4.4A-B; Huber et al., 2000). To determine the activity of pc-nNOS+ neurons in relation to sleep-wake state mice were subjected to a 4 h SD beginning at light onset. The SD was successful, with on average 97.98 ± 2.51% of time spent awake during the four hour period. While one group was sacrificed immediately after SD (SD, n = 4 mice), ensuring animals were continuously awake until the moment of perfusion, a second group of mice (SD+RS group, n = 4 mice) were allowed a 1.5-2 h sleep opportunity (group average: 1.81 ± 0.15 h) before perfusion. During this interval, the animals were awake for only 5.86 ± 4.13 % of the total recording time, while 94.14 ± 4.13 % of the interval was spent asleep (89.07 ± 4.78 and 12.48 ± 0.97 min of NREM and REM sleep respectively). As typical for early sleep after sleep deprivation, NREM EEG spectral power in slow frequencies during RS interval were consistently above corresponding baseline values, with the maximal increase observed below 4 Hz (Figure 4.4D).

To determine the activation of pc-nNOS+ neurons, we performed dual nNOS and c-Fos staining in both groups (SD and SD+RS) of mice (Figure 4.4E). Strikingly, we detected no c-Fos+ pc-nNOS+ in mice sacrificed immediately after SD. In contrast, the percentage of c-Fos+ pc-nNOS+ neurons was significantly higher in SD+RS mice ($p < 0.01$, n = 4 per condition, Figure 4.4F).

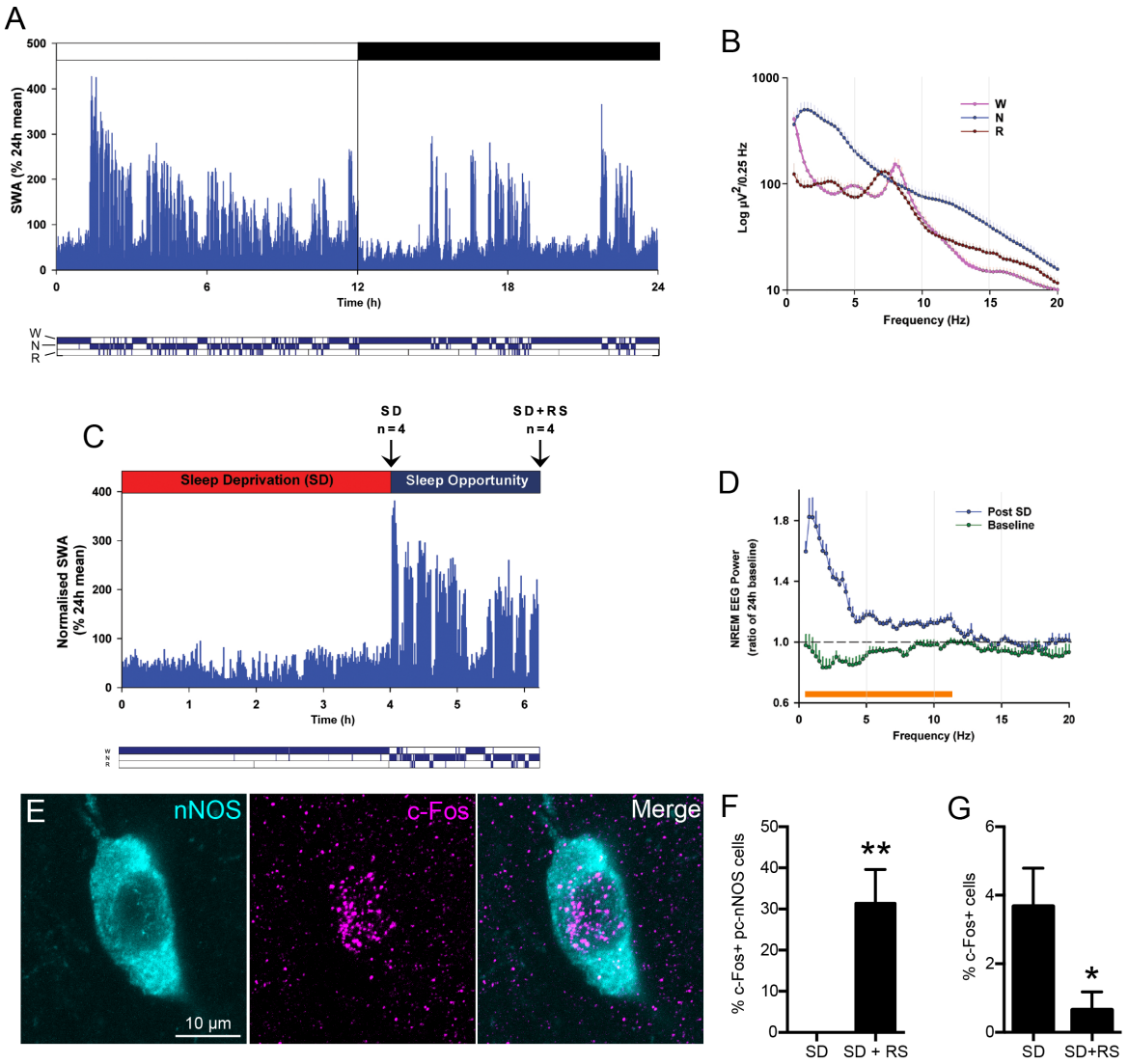

Figure 4.4. pc-nNOS+ neurons are activated during sleep
A, 24 h profile of EEG slow wave activity (SWA, EEG power between 0.5-4.0 Hz, displayed as % of mean 24 h baseline; white bar: 12 h light period; dark bar: 12 h dark period) recorded in the frontal cortex and below the distribution of sleep-wake stages (W= wakefulness, N= NREM sleep, R= REM sleep) from a representative mouse. Note, as expected, sleep predominates and SWA shows a typical decline during the 12 h light period. **B**, EEG power spectral density during waking, NREM sleep and REM sleep shown for the frontal EEG (n = 7). Note the state dependent differences in cortical activity. **C**, *top*, representative profile of SWA during the 4h sleep deprivation (SD) and subsequent sleep opportunity/recovery sleep (RS) in one individual mouse. *Bottom*, the distribution of sleep-wake stages. Mice in the SD Group were sacrificed at the end of SD at ZT4 (n = 4) while the remaining mice in the SD+RS Group (n = 4) were scarified after the sleep opportunity. **D**, EEG spectral density in NREM sleep (displayed as a ratio of the mean 24 h baseline) during the sleep opportunity after SD (n = 4). Note the typical increase in SWA relative to the corresponding baseline interval after a period of prolonged waking. Significant differences between NREM EEG power during baseline and post SD are depicted by the orange bar (significant repeated measures two-way ANOVA and Bonferroni *post hoc* test). **E**, c-Fos expression in a representative pc-nNOS+ neuron following SD+RS. **F**, Quantification of c-Fos expression in pc-nNOS+ neurons. No pc-nNOS+ neuron expressed c-Fos following SD, whereas 31.4 ± 16.4% were c-Fos+ after subsequent RS (n = 4 per condition). **G**, Quantification of c-Fos expression in paracapsular Nissl-stained cells. Overall, c-Fos+ neurons were more abundant following SD (3.7 ± 1.1%) than subsequent RS (0.6 ± 0.5%, n = 4 per group) ** $p < 0.01$. * $p < 0.05$. Data are presented as means ± SEM.

Notably, the effect of SD and RS was highly specific for pc-nNOS+ neurons, because the proportion of c-Fos+ neurons (regardless of their neurochemical identity) in the paracapsular region was higher after SD and lower after RS ($p < 0.05$, Figure 4.4G), in line with previous reports (Cirelli et al., 1995; Semba et al., 2001). These results define a relationship between a GABAergic neuron type of the amygdala, namely nNOS+ neurons adjacent to the EC, and vigilance state.

4.4.4 5-HT inhibits pc-nNOS+ neurons

It has been proposed that the brain state-dependent activity of cortical nNOS+ type I cells is powerfully controlled by inhibition exerted by neuromodulators released in arousal states, such as 5-HT, acetylcholine, noradrenaline and histamine (Kilduff et al., 2001). Conversely, sleep-promoting peptides and hormones have been suggested to promote the recruitment of cortical nNOS+ type I cells (Kilduff et al., 2011). Indeed, the release of 5-HT from midbrain raphe neurons is highly dependent on the sleep-wake cycle (Portas et al., 2000). Specifically, the firing of raphe neurons and, as a consequence, extracellular forebrain 5-HT levels are low during sleep and high during wakefulness (Portas et al., 1998; Sakai, 2011). Furthermore, forebrain 5-HT levels are higher during SD than during sleep (Bjorvatn et al., 2002). Therefore, we asked whether the action of 5-HT on pc-nNOS+ might be inhibitory, and not excitatory, as found for all the other BLA GABAergic neuron populations examined so far (Rainnie, 1999; Jiang et al., 2009; Chapter 3)

To test this hypothesis, I recorded pc-nNOS+ neurons in cell-attached configuration ($n = 18$). As reported above, pc-nNOS+ neurons fired spontaneously in control conditions. Bath application of 50 μM 5-HT produced a dramatic reduction in firing rate (from 3.6 ± 1.6 Hz to 1.6 ± 0.4 Hz, $p < 0.0001$, Figure 4.5A, B), suggesting an inhibitory effect of 5-HT. Furthermore, 5-HT enhanced pc-nNOS+ cell firing irregularity (CV ISI: 0.5 ± 0.06 in control

and 2.9 ± 0.4 in presence of 5-HT, $p < 0.0001$, Figure 4.5C) and, in a minority of cells (n = 7), caused a switch from tonic to burst firing (intra-burst ISI: 25-70 ms range, Fig. 5A, D, E).

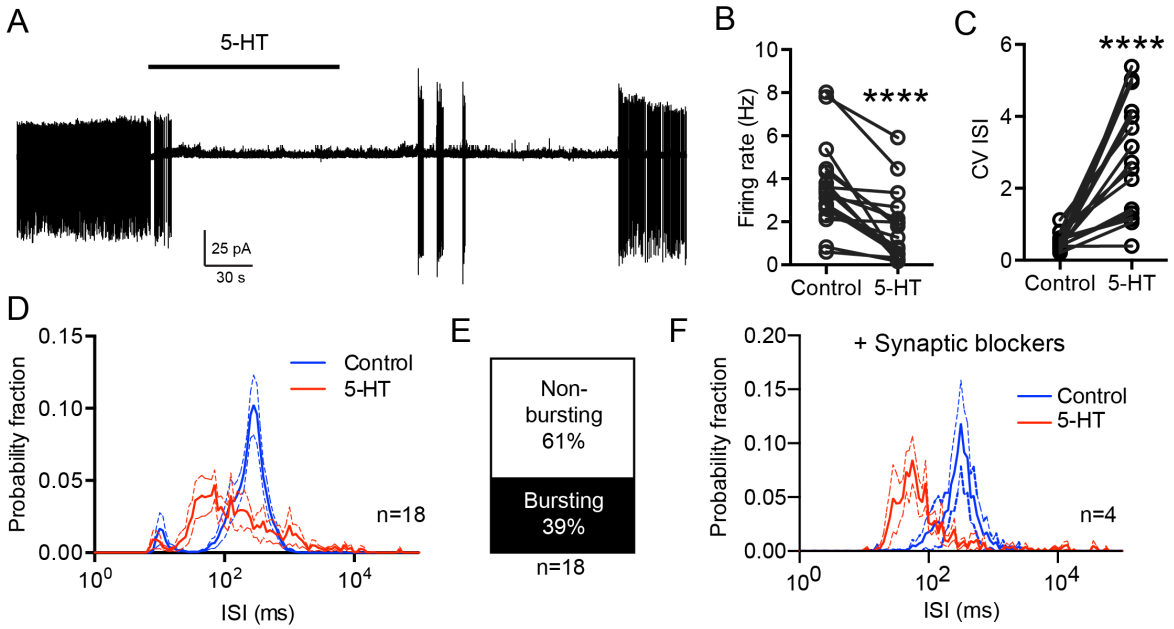

Figure 4.5. 5-HT inhibits pc-nNOS+ neurons.
A, representative cell-attached recording from pc-nNOS+ neuron (voltage clamp mode) showing inhibition of spontaneous firing by 5-HT. In this cell, 5-HT also elicited burst firing. **B**, significant decrease in firing rate promoted by 5-HT (from 3.6 ± 1.6 Hz to 1.6 ± 0.4 Hz, $p < 0.0001$, paired t-test, n = 18). **C**, significant increase in firing irregularity (measured by the CV of the ISI: from 0.5 ± 0.06 to 2.9 ± 0.4, $p < 0.0001$, paired t-test, n = 18) caused by 5-HT. **D**, 5-HT application enhances the burstiness of pc-nNOS+ neurons: the peak of the ISI histogram (in Log scale) shifts to the left (n = 18). **E**, 5-HT triggered spike bursts only in 7/18 pc-nNOS+ neurons. The remaining neurons displayed only a reduction in firing rate (or complete silencing) upon 5-HT application. **F**, In 4 cells displaying bursts upon 5-HT application, 5-HT was re-applied in presence of synaptic blockers (10 µM NBQX, 50 µM AP-V and 10 µM SR95531). In these conditions 5-HT still triggered bursting (the peak of the Log ISI histogram shifted to the left), suggesting synaptic inputs are not necessary for bursting activity. **** $p < 0.0001$. Data are presented as means ± SEM.

To study the mechanisms through which 5-HT inhibits pc-nNOS+ neurons firing, I performed whole-cell patch clamp recordings from these neurons in current clamp mode. Application of 50 µM 5-HT elicited membrane hyperpolarization (from -59.3 ± 0.2 mV to -64 ± 0.7 mV, $p < 0.001$, n = 10, Figure 4.6A, B, D), together with a reduction of the R_{in} (by 11.3 ± 1.9%, $p < 0.001$, n = 10, Figure 4.6C, E). Both effects were blocked by prior incubation with the 5-HT_{1A} antagonist WAY100635 (10 µM; V_m control: -60.3 ± 0.4 mV, V_m 5-HT: -60.8 ± 0.2, $p > 0.1$; R_{in} reduction: 3.6 ± 1.8%, $p > 0.3$, n = 5, Figure 4.6F, G). Thus, pc-

nNOS+ cells are hyperpolarized by 5-HT via 5-HT$_{1A}$ receptors, in line with the expression of 5-HT$_{1A}$ mRNA in NPY+ BLA neurons (Bonn et al., 2013).

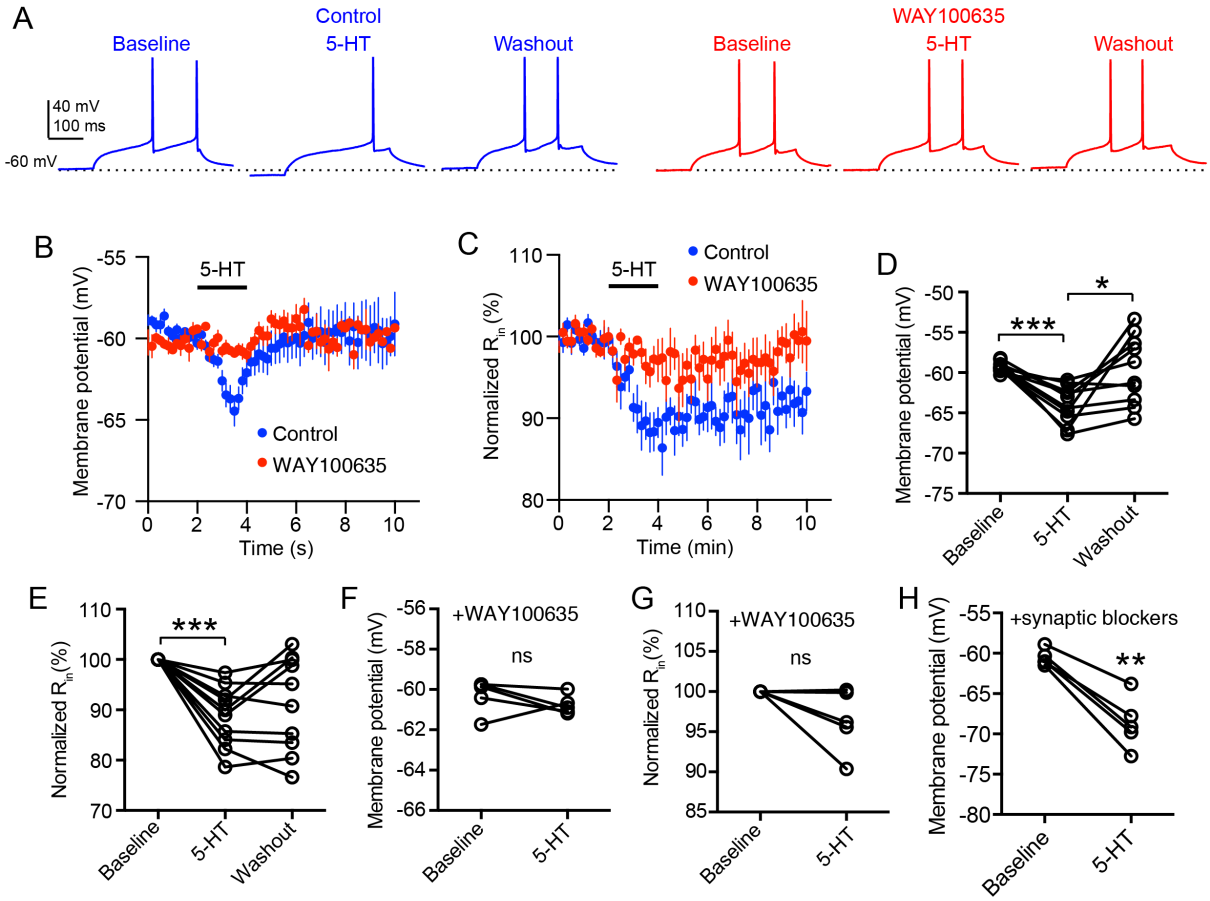

Figure 4.6. Direct hyperpolarization of pc-nNOS+ neurons by 5-HT via 5-HT$_{1A}$ receptors
A, effect of 5-HT on voltage responses to depolarizing current injection of representative pc-nNOS+ neuron (20 pA, 300 ms) in control conditions (*left*) and in presence of 5-HT$_{1A}$ antagonist WAY100635 (10 µM, *right*). **B**, time course of the effect of 5-HT on the V_m of pc-nNOS+ neurons (n = 10). **C**, time course of the effect of 5-HT on the R_{in} of pc-nNOS+ neurons (n = 10). **D**, 5-HT significantly hyperpolarizes pc-nNOS+ cells (from -59.3 ± 0.2 mV to -64 ± 0.7 mV, $p < 0.001$, n = 10). **E**, 5-HT significantly reduced the R_{in} of pc-nNOS+ cells (by 11.3 ± 1.9%, $p < 0.001$, n = 10). **F-G**, 5-HT-evoked hyperpolarization and R_{in} reduction is blocked by 10 µM WAY100635 ($p > 0.1$ and $p > 0.3$, respectively, n = 5). **H**, 5-HT significantly hyperpolarizes pc-nNOS+ cells even in presence of synaptic blockers (10 µM NBQX, 50 µM AP-V and 10 µM SR95531; n = 5), suggesting a direct effect. **** $p < 0.0001$. *** $p < 0.001$. ** $p < 0.01$. * $p < 0.05$. Data are presented as means ± SEM.

Finally, I confirmed that 5-HT$_{1A}$-mediated hyperpolarization occurred by a direct effect on pc-nNOS+ neurons, and was not an indirect network action, because it persisted in presence of synaptic blockers (10 µM NBQX, 50 µM AP-V, 10 µM SR95531, $p < 0.01$, n = 5, Figure 4.6H).

Together, these data indicate that pc-nNOS+ neurons are distinct from other BLA neurons in that they are hyperpolarized and not depolarized by 5-HT. This hyperpolarization leads to a reduction in firing rate and, in a few cases to a switch in firing mode. Such 5-HT inhibition could mediate, at least in part, the sleep-wake cycle dependent modulation of pc-nNOS+ activity, because extracellular forebrain 5-HT levels are lower during sleep than during wake and SD (Portas et al., 1998; Bjorvatn et al., 2002).

4.5 Discussion

This study provides critical data about the neurochemical homogeneity, intrinsic membrane responses, activity throughout sleep and wakefulness and 5-HT modulation of BLA nNOS+ type I neurons. We discovered that nNOS+ type I neurons are distributed along the boundaries of the BLA and express SOM, NPY and NK1. We observed that pc-nNOS+ neurons are GABAergic, display distinct membrane features, and project both inside and outside the BLA nucleus. The activity of pc-nNOS+ (measured by their c-Fos expression) is low during SD and high during subsequent sleep. As a putative cellular mechanism of pc-nNOS+ cell inhibition during SD (and more generally wake), 5-HT, known to depolarize GABAergic cells in the BLA, instead hyperpolarizes pc-nNOS+ cells. Although previous groups reported the presence of putative GABAergic nNOS+ neurons of the BLA (McDonald et al., 1993; Usunoff et al., 2006), their physiology and role in behaviour was unexplored.

The discovery that nNOS+ type I neurons immunoreactive for SOM, NPY and NK1, initially described in neocortex (Kubota et al., 2011), inhabit the mouse BLA (mostly its margins) corroborate the notion that this amygdaloid nucleus exhibits cortex-like GABAergic neuron diversity patterns (Spampanato and Sah, 2011; Capogna, 2014). Interestingly, BLA nNOS+ type I neurons are preferentially located around the BLA, namely along the EC,

intermediate capsule and border between BA and BM nucleus. The functional reason of this specific localisation remains enigmatic. Since EC and intermediate capsule are fibre bundles containing axons that originate from several external structures and pc-nNOS+ neuron dendrites appear to run in parallel to the EC, this distribution might be important for the excitatory inputs received by these cells.

Interestingly, SOM+ and NPY+ neurons located in the EC next to the BLA have been shown to be long-range projection neurons sending their axons to entorhinal cortex (McDonald and Zaric, 2015) and basal forebrain (McDonald et al., 2012). Our study did not demonstrate unequivocally whether pc-nNOS+ cells are indeed long-range projection neurons, mainly because pc-nNOS+ axons are likely severed in brain slices. Nevertheless, the observation that their axons often innervate extra-amygdaloid regions such as the endopiriform clastrum, the piriform and perirhinal cortices suggests, together with their SOM and NPY expression, that these might be the same cells described by McDonald and colleagues.

The stereotypical membrane properties of pc-nNOS+ neurons, including high R_{in}, depolarized resting V_m and non-fast-spiking phenotype, are consistent with the physiology of GABAergic 'hub' cells of the HPC (Picardo et al., 2011), which are known to mediate powerful network synchronisation. Collectively, pc-nNOS+ specific localisation along the EC, their ability to be easily activated, even by small excitatory inputs, and their projections within and outside the BLA suggest that these GABAergic cells are ideally suited to synchronise amygdaloid and extra-amygdaloid regions. *In vivo* labelling of pc-nNOS+ neurons with biotin or tracers is necessary to corroborate this hypothesis. In addition, these techniques could be advantageous to delineate pc-nNOS+ neurons postsynaptic targets in both the BLA and extra-amygdaloid regions. In the BLA, SOM+ neurons target distal dendrites of

PNs, as well as dendrites and cell bodies of INs, but it is not clear whether pc-nNOS+ neurons synapse on the same subcellular domains.

Besides GABA, pc-nNOS+ cells boast a vast assortment of neurochemicals, including nNOS, NPY and SOM. Thus, pc-nNOS+ cells could modulate neuronal activity through these molecules as well. For example, nitric oxide signalling has been shown to promote long-term potentiation at inhibitory synapses in the LA (Lange et al., 2012), while SOM and NPY appear to hyperpolarize LA PNs via GIRK activation (Meis et al., 2005; Sosulina et al., 2008).

Given their dichotomous c-Fos expression, pc-nNOS+ neurons are likely to release high quantities of these neurotransmitters during sleep (at least when RS follows SD) and lower amounts during wakefulness. Thus, selective sleep activation of nNOS+ type I neurons appears to be more widespread and not only restricted to the cortex (Gerashchenko et al., 2008; Morairty et al., 2013; Dittrich et al., 2014), with pc-nNOS+ cells displaying a similar pattern of activation. Our results represent the first demonstration of a specific neuron type of the amygdala that dichotomously changes its activity as a function of vigilance state. Given the crucial involvement of the BLA in conditioned fear and anxiety (Tovote et al., 2015), this discovery is particularly compelling because SD has been shown to impact both emotional phenomena (Graves et al., 2003; Silva et al., 2004).

Notably, the present study demonstrates that 5-HT hyperpolarizes pc-nNOS+ cells via 5-HT_{1A} receptors. As this hyperpolarization was associated with a decrease in R_{in}, it likely arises from the opening of a GIRK conductance, as described in hippocampal neurons (Andrade and Nicoll, 1987). Interestingly, striatal nNOS INs are also inhibited by 5-HT, but this effect is mediated by another class of serotonin receptors (5-HT_{2C}; Cains et al., 2012). Furthermore, in a minority of cells 5-HT also altered the pc-nNOS+ neurons' firing mode

from tonic to phasic. Such intrinsic electrophysiological responses resemble those observed in striatal low-threshold spike INs (Beatty et al., 2012), which also express nNOS and NPY (Kawaguchi, 1993; Ibáñez-Sandoval et al., 2011). However, this seems to originate from different conductances because pc-nNOS+ neurons did not display a low threshold spiking phenotype in our experiments. The effect exerted by 5-HT provides a putative cellular mechanism that could explain, at least in part, the activity of pc-nNOS+ neurons across sleep and wakefulness. Their 5-HT-mediated inhibition, an effect previously proposed by Kilduff et al. (2011), could be prominent during SD, when 5-HT release from DRN is high, compared to NREM and REM sleep, when 5-HT release is lower (Portas et al., 1998). Intriguingly, this effect might not only apply to pc-nNOS+ neurons, but potentially to all cortical nNOS+ type I cells. However, further studies are needed to confirm this postulate.

It is unlikely that 5-HT is the only neurotransmitter released during wake and arousal that suppresses pc-nNOS+ neuron activity. For example, paracapsular SOM+ and NPY+ neurons co-express the muscarinic type 2 acetylcholine receptor (McDonald and Mascagni, 2011) and project to extra-amygdaloid regions (McDonald and Zaric, 2015). Thus, acetylcholine, 5-HT and potentially other neurotransmitters, might exert a concerted inhibitory action on pc-nNOS+ neurons. Future studies should establish whether pc-nNOS+ neuron activity is high during sleep due to intrinsic membrane properties or also by stronger excitatory inputs from afferent neurons. These inputs could include peptides and hormones released during sleep such as adenosine, as recently proposed (Kilduff et al., 2011). Furthermore, pc-nNOS+ neurons are mostly aligned to the EC, which contains glutamatergic axons from several cortical areas (McDonald, 1998). Thus, in addition to slow neuromodulators, cortical afferents could contribute to the excitation of pc-nNOS+ neurons, and this input might be important for their recruitment during sleep, but this hypothesis requires validation with experimental data.

Since pc-nNOS+ neurons express NK1 receptors, another putative source of excitatory drive on these cells is the NK1 agonist, substance P. This neurotransmitter has been implicated in stress and anxiety (Ebner and Singewald, 2006), suggesting that the activity of pc-nNOS+ neurons might not only follow sleep-wake states, but also could be involved in emotional behaviour. Consistent with this idea, one study suggests that activation of NK1+ neurons of the BLA could be anxiolytic (Truitt et al., 2009). Although this perspective is intriguing because SD appears to be causally linked with anxiety (Silva et al., 2004), it should be tested directly, particularly since other BLA INs express NK1 (Sreepathi and Ferraguti, 2012).

Our work turns the spotlight on the relationship between BLA circuits and sleep-wake history. In agreement with previous findings (Semba et al., 2001), we show that the overall neuronal activation in the paracapsular area is higher after SD than RS, i.e. a pattern of activation that is opposite to the one of pc-nNOS+ neurons. This observation suggests cell type-specific, and not broad, sleep activation in the BLA. Importantly, it is not clear whether all nNOS+ type I neurons along or inside BLA boundaries are equally inhibited by 5-HT and activated by RS following SD. In this study, the quantification was limited to pc-nNOS+ neurons adjacent to the EC to match the location of the patch clamp recordings. In the future, intersectional genetic approaches will likely allow selective tagging of nNOS+ type I neurons, for instance by taking advantage of their SOM, NPY or NK1 expression. In addition to facilitating their targeting for electrophysiological recordings, these strategies could also permit specific manipulation of BLA nNOS+ type I cells during behaviour, which could probe their precise role in sleep and emotion regulation.

Chapter 5 General discussion and future directions

5.1 Main findings and implications

The results presented in this thesis shed light on cellular mechanisms underlying the extrinsic modulation of BLA circuits by the hippocampal formation and by 5-HT inputs. Synaptic interplay between HPC and amygdala is thought to be dysregulated in psychiatric disorders such as depression, anxiety and PTSD (Spedding et al., 2005; Shin and Liberzon, 2010). In addition, SSRIs, which increase extracellular 5-HT levels and are widely prescribed antidepressants and anxiolytics (Nemeroff and Owens, 2002), alter amygdala reactivity to salient stimuli (Bigos et al., 2008; Murphy et al., 2009). Furthermore, susceptibility to anxiety and depression, together with amygdala responsiveness, appear to be modified in genetic variations of the 5-HTT (Munafò et al., 2008). Despite this evidence from human data, the neurobiological mechanisms orchestrating the influence of the HPC and 5-HT on amygdala circuits remain largely unexplored.

This thesis highlights the importance of GABAergic cells of the BLA for the relay of the information carried by hippocampal and 5-HT inputs. My data (Chapter 2) demonstrate that BA INs recruited by vCA1 dynamically inhibit PNs. Indeed, the frequency of IN activation can shift the circuit from strong feedforward inhibition, and thus hyperpolarization of BA PNs (at low frequency) to a depression of feedforward inhibition via $GABA_B$ receptors located on IN axon terminals (at higher frequencies). This dynamic feedforward inhibition gates the induction of heterosynaptic LTP at glutamatergic synapses between LA PNs and BA

PNs. Hence, feedforward INs are likely to sculpt the time window in which synchronous inputs from extrinsic areas have to occur to induce synaptic plasticity in the BA.

Previous reports demonstrated that GABAergic INs can gate synaptic plasticity of cortical and thalamic afferents onto LA PNs via activation of presynaptic $GABA_B$ receptors (Shaban et al., 2006; Pan et al., 2009). My results of Chapter 2 expand the ways through which GABAergic cells can regulate the integration of excitatory inputs of PNs, namely via spillover of GABA not only onto presynaptic glutamatergic axons, but also onto GABAergic terminals. Activation of $GABA_B$ receptor located on presynaptic cortical and thalamic terminals could occur primarily in the LA, with $GABA_B$-dependent depression of feedforward inhibition mostly restricted to the BA. Alternatively, both mechanisms could co-exist in both nuclei.

It remains to be seen whether depression of feedforward inhibition occurs specifically via the hippocampal input to the BA. For example, vCA1 could specifically recruit GABAergic INs expressing $GABA_B$ receptors on their axon terminals, for example neurogliaform cells. Indeed, previous work from our lab has shown that the unitary IPSCs produced by a presynaptic BLA neurogliaform cell onto a postsynaptic PN decrease in amplitude above a certain frequency due to presynaptic $GABA_B$ receptor activation (Manko et al., 2012). However, the depression of feedforward inhibition, could also be evoked by several other inputs, for instance the mPFC, the entorhinal cortex or neuromodulators such as 5-HT, and by $GABA_B$ receptors located in the axon terminals of other IN types. In the HPC, the IPSCs from PV+ INs onto pyramidal cells depress upon presynaptic $GABA_B$ receptor activation (Booker et al., 2013). In the BLA, PV+ INs have been shown to receive glutamatergic inputs from vHPC (Hübner et al., 2014), but it is not known whether these cells express $GABA_B$ receptor on their presynaptic terminals.

In Chapter 3, I showed that PV+ INs are crucial hotspots for 5-HT modulation in the BA, as they are powerfully depolarized by 5-HT via 5-HT_{2A} receptors. My data also demonstrate that genetically altered 5-HTT expression (and 5-HT levels) lead to dysregulation of the recruitment of PV+ cells by 5-HT and fear. Importantly, these data do not fully resolve whether the deficient 5-HT depolarization underlies PV+ IN reduced activation during fear memory retrieval. Nonetheless, reduced 5-HT_{2A} function and greater 5-HT reuptake are likely to contribute to PV+ IN reduced fear-excitation because 5-HT is highly released in the BLA following fear memory recall (Zanoveli et al., 2009).

These results turn the spotlight on PV+ INs of the BA not only for 5-HT_{2A} receptor altered function in genetic variations of the 5-HTT, but also regarding SSRI treatment, one of the major therapeutic options for depression, anxiety and PTSD (Nemeroff and Owens, 2002). Indeed, chronic SSRI treatment is known to alter 5-HT_{2A} receptor binding (Massou et al., 1997; Syvälahti et al., 2006) and might therefore affect PV+ INs of the BA. Thus, examining the action of 5-HT and SSRI from a neural circuit viewpoint is critical. Specifically, understanding on which cell types and subcellular compartments 5-HT receptors are expressed and what are their physiological functions could reveal the mechanisms through which SSRI work. Furthermore, it could help design novel, more selective treatments for mood disorders.

In Chapter 4, I reported that a previously unknown population of GABAergic cells, namely pc-nNOS+ neurons, which are SOM+ and NPY+, are hyperpolarized, and not depolarized, by 5-HT via 5-HT_{1A} receptors. These data expand our knowledge on the action of 5-HT on BLA circuits, because GABAergic cells were hitherto believed to be either excited or unaffected by 5-HT (Rainnie, 1999). Notably, the unusual effect of 5-HT on pc-nNOS+ cells matches their unconventional anatomical features, because, unlike PV+ INs,

they are likely to be long-range projection cells (McDonald et al., 2012; McDonald and Zaric, 2015). My experiments have not examined whether pc-nNOS+ neurons release GABA onto BLA PNs. If that is the case, 5-HT release could trigger disinhibition of BLA PN dendrites, since SOM+ cells target this subcellular compartment (Wolff et al., 2014).

This 5-HT_{1A}-mediated inhibition could underlie the suppression of pc-nNOS+ cell activity during sleep deprivation and their activation during sleep, which were demonstrated by their c-Fos immunoreactivity. Thus, these data represent the first report of an amygdala cell type that is preferentially recruited during sleep. Pc-nNOS cells could be important for emotional memory storage, because sleep deprivation appears to impair the consolidation of fear memories (Graves et al., 2003; Kumar and Jha, 2012). Although pc-nNOS+ neuron physiology during fear conditioning is still unknown, one could predict them to be inactive during fear memory retrieval, when 5-HT release is typically high (Zanoveli et al., 2009).

My experiments have not clarified to what extent the GABAergic cells recruited by vCA1 and the ones depolarized by 5-HT overlap. The question of whether these two pathways influence a similar circuit or operate independently is intriguing, because these two scenarios could imply radically different computations. Likely, some degree of overlap exists, because PV+ INs have been shown to receive inputs from vHPC (Hübner et al., 2014).

Given the excitation of PV+ cells (Chapter 3) and presumably other INs (Rainnie, 1999) by 5-HT, pc-nNOS+ cells are likely to operate differently from classic GABAergic populations of the BLA. Data in Chapter 2 are in line with this result because the majority of BA INs fire at higher rates during theta oscillations (occurring during lighter anaesthesia and cortical de-synchronisation, a condition more similar to wakefulness) compared to SWA (a brain state similar to slow wave sleep). Besides recruitment of IN by inputs such as the vHPC or cortex, their higher firing rates during theta could be driven by greater release of neuromodulators such as acetylcholine and 5-HT. Nonetheless, *in vivo* recordings from

identified PV+ INs and pc-nNOS+ cells during anaesthesia, but especially during the sleep-wake cycle, are necessary to delineate their brain state-dependent physiology. In addition, it should be clarified whether pc-nNOS+ cells are recruited by vCA1 pyramidal cells, and, if so, whether they drive feedforward inhibition onto PNs. Our data suggest that vCA1 pyramidal cell axons are bundled in the EC, suggesting they overlap with pc-nNOS+ cell dendrites, and may therefore innervate these cells.

5.2 Technical limitations and future directions

The majority of the electrophysiological experiments described in this thesis were performed in 325 μm-thick coronal brain slices. This approach is widely used to dissect synaptic mechanisms in the BLA. Inevitably, this strategy does not consider the BLA in a three-dimensional fashion, because it neglects many rostrocaudal synaptic connections among BLA neurons that are severed by the slicing procedure. Two studies by Paré's group have shown that the majority of inhibitory connections from INs to PNs occur in the coronal plane, while the horizontal plane includes a larger amount of excitatory contacts among PNs (Samson et al., 2003; Samson and Paré, 2006).

In principle, functional dissections of long-range inputs to the BLA should be performed *in vivo*. However, current technical limitations render *ex vivo* recordings in brain slices the most viable option to study BLA circuits from a mechanistic viewpoint. Among those, whole-cell patch clamp recordings with low access resistance are still extremely challenging in deep brain regions. Furthermore, light activation of ChR2+ projections is still much more accurate with illumination of brain slices through a microscope objective than with an implanted optic fibre *in vivo*. Coronal slices appear to be most suitable to study BLA inhibitory circuits *ex vivo*: firstly because amygdaloid nuclei can be more accurately identified

than in horizontal or sagittal sections, and secondly because more inhibitory connections are preserved.

5.2.1 Achieving more physiological stimulations of afferent pathways of the BLA

It is crucial to keep in mind that in the experiments described in Chapter 3 and 4 I investigated the effect of 5-HT on BLA circuits by exogenous application of the 5-HT. In the future, more physiological approaches should be employed to confirm these findings and further disentangle the complex effects of 5-HT. Our group has recently taken this largely unexplored path via expression of ChR2 in DRN 5-HT neurons (Sengupta *et al.*, in preparation) and optical activation of 5-HT axons in the BLA in brain slices. Unpublished results confirm both excitatory 5-HT_{2A}-mediated and inhibitory 5-HT_{1A} actions on BLA GABAergic neurons. However, they also demonstrate that DRN 5-HT+ neurons recruit BLA GABAergic cells not only by the release of 5-HT but also by glutamate co-transmission. In contrast, PNs never receive glutamate from DRN 5-HT+ axons, but they are inhibited both indirectly (via depolarization of INs) and directly (via 5-HT_{1A} receptors).

To better understand the behavioural implications of the mechanisms of extrinsic modulation of amygdala circuits described in the present thesis, expression of light-activated ion channels in vCA1 pyramidal cells and DRN 5-HT neurons could be employed in the future to manipulate these pathways in behaving mice. This would allow selective stimulation/inhibition of these inputs with millisecond-timescale precision during different phases of fear conditioning. Recently, Baratta et al., (2015) have shown that optical inhibition of DRN 5-HT axon terminals in the BLA during CS-US pairings (or unpaired USs) during the acquisition phase impaired fear memory retrieval. Interestingly, this deficit occurred only when mice were subjected to two days of stress prior to fear conditioning, but not in unstressed mice. Assessment of c-Fos immunoreactivity following optical inhibition of 5-HT

axons in the BLA during the expression phase could reveal whether 5-HT contributes to the recruitment of PV+ INs during fear memory recall.

The optogenetic dissection of the vCA1 input to the BA described in the present thesis involved synchronous activation of several pyramidal cell axons. It is important to note that the synchrony of CA1 pyramidal cells in behaving mice is usually low, at least during spatial navigation (Pastalkova et al., 2008). Additionally, the number of active place cells is lower in vHPC than in dorsal HPC (Kjelstrup et al., 2008; Royer et al., 2010). As a result, it should be established whether one or few vCA1 pyramidal cells are able to drive prominent BA IN activation, leading to high GABA release and activation of both postsynaptic and presynaptic $GABA_B$ receptors. Preliminary data from our laboratory suggest that even optical activation of vCA1 axons using small illumination areas (10-50 μm) can drive postsynaptic $GABA_B$ IPSPs in PNs, and depression of feedforward inhibition at theta frequency.

Recent technological developments enable all-optical interrogation of neural circuits (Emiliani et al., 2015). Specifically, 2-photon microscopy can be employed to both image the Ca^{2+} transients of genetically-defined neurons *in vivo* and at the same time activate ChR2+ cells (Packer et al., 2014). In the future, patterns of activity of vCA1 pyramidal cells could be imaged during behaviour, and subsequently replayed with restricted illumination in the BLA, reading out the activity of PNs. This could allow a more physiological investigation of the vCA1 glutamatergic input to the BLA network. Given the challenge of imaging neurons in deep brain regions with sufficient detail, this experimental scenario is still remote. Nonetheless, some groups have recently started to image BLA neurons with integrated microscopes equipped with a microendoscopes (Ghosh et al., 2011), and the imaging quality of these microscopes is rapidly progressing.

5.2.2 Achieving temporally-precise read-out of BLA neuronal activity

Together with the need of higher spatial resolution to study inputs to the BLA circuits, the data presented in this thesis could be integrated with further investigations using temporally-precise recordings of identified BLA neurons *in vivo*. For example, c-Fos immunoreactivity lacks the temporal detail to reveal the precise activity of PV+ INs and PNs of the BA in 5-HTTOE mice. Likewise, c-Fos expression did not uncover what firing rates and firing modes nNOS+ type I neurons display during wakefulness and sleep. The identification of genetically-defined neurons in behaving mice has now reached a reasonable yield through 'optogenetic tagging' (Kvitsiani et al., 2013; Roux et al., 2014). In this approach, light-sensitive opsins are expressed in a specific neuronal population; subsequently, extracellular recordings and local photostimulation are performed using an optrode. This strategy enables to infer that light-responsive neurons belong to the population of interest, allowing read-out of their activity during behaviour.

Hence, optogenetic tagging could clarify whether encoding of the CS, or also of the US, is altered in PV+ INs of 5-HTTOE mice. Additionally, it could reveal whether deficient recruitment of PV+ INs in 5-HTTOE mice during the CS results in altered temporal coding of PNs, as I hypothesised in Chapter 3. Specifically, in 5-HTTOE mice the synchrony of PNs could be reduced, and PN firing might be less accurately phase-locked to local theta oscillations.

Optogenetic tagging could also be employed to record the activity of nNOS+ type I neurons of the BLA across the sleep-wake cycle. This experiment would elucidate: (1) the firing rates and firing modes of nNOS+ type I cells across the sleep-wake cycle, potentially high and tonic during sleep, while low and bursting during wake, when 5-HT release is high; (2) whether their firing is phase-locked with theta oscillations from areas involved in memory processing, namely the HPC and the entorhinal cortex. These experiments could give insights on the rate coding and temporal coding properties of nNOS+ type I cells, and could

potentially resolve whether these neurons coordinate network oscillations between different areas. Critically, tagging of nNOS+ type I neurons requires an intersectional genetic approach, since currently available nNOS-Cre^{ER} mice indiscriminately tag nNOS+ type I and type II cells. For instance, expression of Cre could be limited to neurons expressing both nNOS and SOM (e.g. nNOS-Cre^{ER};SOM-Flp mice).

5.2.3 Achieving temporally-precise manipulation of BLA neuronal activity

In addition to recordings from given neuronal populations, temporally-precise optical manipulations of genetically-defined GABAergic neurons *in vivo* could provide unprecedented information about their sufficiency and necessity for network activity and particular behaviours. For instance, light activation of PV+ INs of 5-HTTOE mice during fear memory retrieval could demonstrate whether reduced recruitment of these cells by the CS and 5-HT drives the fear memory deficits of this mouse line. Together with the investigation of BA PV+ INs activity following SSRI treatment, this experiment could identify PV+ INs as promising therapeutic targets for anxiety and fear disorders for which SSRIs are currently prescribed.

Furthermore, optical manipulation of nNOS+ type I cells of the BLA combined with extracellular recordings *in vivo* could demonstrate whether these cells are necessary and sufficient for synchronisation of BLA network activity with extra-amygdaloid regions, for example with the entorhinal cortex, a brain region which these cells are likely to innervate (McDonald and Zaric, 2015). Light activation/inhibition of nNOS+ type I neurons in freely moving mice can also elucidate whether these cells are causatively involved in: (1) control of vigilance states, namely facilitation of NREM sleep; (2) fear memory retrieval, which is

known to be associated with network synchronisation between the BLA and other regions (Seidenbecher et al., 2003; Karalis et al., 2016).

5.2.4 Probing the interplay between hippocampal and 5-HT inputs to the BLA

Both CA1 pyramidal cells and DRN 5-HT neurons increase their firing rates upon presentation of aversive stimuli (Schweimer and Ungless, 2010; Lovett-Barron et al., 2014; Cohen et al., 2015), suggesting their modulation of BLA circuits could occur coincidentally. Hence, apart from examining hippocampal and serotonergic BLA afferents independently, it is also critical to explore the interaction between these inputs. First, it would be important to test whether excitation of PV+ INs by vCA1 is altered in 5-HTTOE mice. In fact, 5-HT exerts a similar control on PNs and INs also in the HPC (Puig and Gener, 2015), namely depolarization of several IN classes via 5-HT_{2A} receptors and a biphasic hyperpolarization-depolarization of PNs via 5-HT_{1A} and 5-HT_{2A} receptors, respectively (Andrade and Nicoll, 1987; Shen and Andrade, 1998; Puig and Gener, 2015). Additionally, CCK+ INs are depolarized via ionotropic 5-HT_3 receptors (Varga et al., 2009). Hence, 5-HTT overexpression could also cause rearrangements in HPC circuits and alter the hippocampal input to the BLA.

More generally, it is not known whether 5-HT release can alter the integration of vCA1 inputs in BA PNs. For instance, another subcortical neuromodulator, dopamine, controls the weight of glutamatergic pathways to CA1 pyramidal cells via feedforward PV+ INs (Rosen et al., 2015), and 5-HT could operate in a similar fashion in the BA. Furthermore, it could be valuable to test whether 5-HT modulates synaptic plasticity at vCA1 terminals onto BA PNs, since 5-HT application allows the induction of LTP at synapses between axons in the EC (some of which arise from vCA1) and PNs (Chen et al., 2003). For example, optical stimulation of vCA1 pyramidal cells axons could be performed while recording from BA PNs

in the presence of bath applied 5-HT. This could reveal whether 5-HT modulates EPSCs from vCA1 pyramidal cells to BA PNs, as well as feedforward inhibition. Additionally, optical TBS of vCA1 fibres in presence of 5-HT could reveal whether 5-HT facilitates LTP of this pathway via activation of 5-HT_{2A} receptors located on PN dendrites.

5.3 Conclusion

In summary the data presented in this thesis add novel pieces to the puzzle of BLA circuits and their control by external structures. Given the myriad of inputs, and therefore of multi-modal information, processed by the amygdala, unravelling the cellular dynamics governing its modulation by extrinsic sources can be key to gain a mechanistic understanding of emotion regulation in health and disease. This work emphasises the pivotal role of GABAergic neurons of the BLA in relaying external information to PNs and, as a result, shape BLA output to other areas. Hence, it stresses the need to study the impact of specific pathways on distinct cell types.

My data on pc-nNOS+ cells of the BLA fuel recent interests in long-range GABAergic projection neurons (Caputi et al., 2013). It is becoming increasingly evident that recruitment of BLA GABAergic cells does not simply impact BLA PN activity, but might also directly influence distant brain regions (McDonald et al., 2012; Bienvenu et al., 2015; McDonald and Zaric, 2015). These findings broaden the picture of neuronal circuits controlling emotional behaviour, prompting further investigation on the BLA GABAergic output. A thorough investigation of the extrinsic modulation of amygdala inhibitory circuits could pave the way for more selective and effective treatments for psychiatric conditions impacting amygdala networks.

References

Abbott LF, Regehr WG (2004) Synaptic computation. Nature 431:796–803.

Abraham WC (2008) Metaplasticity: tuning synapses and networks for plasticity. Nat Rev Neurosci 9:387.

Abraham WC, Williams JM (2003) Properties and mechanisms of LTP maintenance. Neuroscientist 9:463–474.

Abrams JK, Johnson PL, Hollis JH, Lowry CA (2004) Anatomic and functional topography of the dorsal raphe nucleus. Ann N Y Acad Sci 1018:46–57.

Adolphs R, Tranel D, Damasio H, Damasio AR (1995) Fear and the human amygdala. J Neurosci 15:5879–5891.

Adolphs R, Tranel D, Hamann S, Young AW, Calder AJ, Phelps EA, Anderson A, Lee GP, Damasio AR (1999) Recognition of facial emotion in nine individuals with bilateral amygdala damage. Neuropsychologia 37:1111–1117.

Alcami P, Franconville R, Llano I, Marty A (2012) Measuring the firing Rate of high-resistance neurons with cell-attached recording. J Neurosci 32:3118–3130.

Amilhon B, Huh CYL, Manseau F, Ducharme G, Nichol H, Adamantidis A, Williams S (2015) Parvalbumin interneurons of hippocampus tune population activity at theta frequency. Neuron 86:1277–1289.

Amorapanth P, Nader K, LeDoux J (1999) Lesions of periaqueductal gray dissociate-conditioned freezing from conditioned suppression behavior in rats. Learn Mem 6:491–499.

Anderson AK, Phelps EA (2001) Lesions of the human amygdala impair enhanced perception of emotionally salient events. Nature 411:305–309.

Andrade R, Nicoll RA (1987) Pharmacologically distinct actions of serotonin on single

pyramidal neurones of the rat hippocampus recorded in vitro. J Physiol 394:99–124.

Arszovszki A, Borhegyi Z, Klausberger T (2014) Three axonal projection routes of individual pyramidal cells in the ventral CA1 hippocampus. Front Neuroanat 8:53.

Asan E, Steinke M, Lesch K (2013) Serotonergic innervation of the amygdala: targets, receptors, and implications for stress and anxiety. Histochem Cell Biol 139:785–813.

Ascoli GA et al. (2008) Petilla terminology: nomenclature of features of GABAergic interneurons of the cerebral cortex. Nat Rev Neurosci 9:557–568.

Asede D, Bosch D, Lüthi A, Ferraguti F, Ehrlich I (2015) Sensory inputs to intercalated cells provide fear-learning modulated inhibition to the basolateral amygdala. Neuron:541–554.

Baglioni C, Spiegelhalder K, Lombardo C, Riemann D (2010) Sleep and emotions: a focus on insomnia. Sleep Med Rev 14:227–238.

Banke TG, Bowie D, Lee H, Huganir RL, Schousboe A, Traynelis SF (2000) Control of GluR1 AMPA receptor function by cAMP-dependent protein kinase. J Neurosci 20:89–102.

Baratta M V, Kodandaramaiah SB, Monahan PE, Yao J, Weber MD, Lin PA, Gisabella B, Petrossian N, Amat J, Kim K, Yang A, Forest CR, Boyden ES, Goosens KA (2015) Stress Enables Reinforcement-Elicited Serotonergic Consolidation of Fear Memory. Biol Psychiatry.

Barkus C, Line SJ, Huber A, Capitao L, Lima J, Jennings K, Lowry J, Sharp T, Bannerman DM, McHugh SB (2014) Variation in serotonin transporter expression modulates fear-evoked hemodynamic responses and theta-frequency neuronal oscillations in the amygdala. Biol Psychiatry 75:901–908.

Barria A, Muller D, Derkach V, Griffith LC, Soderling TR (1997) Regulatory phosphorylation of AMPA-type glutamate receptors by CaM-KII during long-term

potentiation. Science 276:2042–2045.

Bauer EP (2014) Serotonin in fear conditioning processes. Behav Brain Res 277:68–77.

Bauer EP, Paz R, Paré D (2007) Gamma oscillations coordinate amygdalo-rhinal interactions during learning. J Neurosci 27:9369–9379.

Bauer EP, Schafe GE, LeDoux JE (2002) NMDA receptors and L-type voltage-gated calcium channels contribute to long-term potentiation and different components of fear memory formation in the lateral amygdala. J Neurosci 22:5239–5249.

Beatty J a, Sullivan M a, Morikawa H, Wilson CJ (2012) Complex autonomous firing patterns of striatal low-threshold spike interneurons. J Neurophysiol 108:771–781.

Bechara A, Tranel D, Damasio H, Adolphs R, Rockland C, Damasio AR (1995) Double dissociation of conditioning and declarative knowledge relative to the amygdala and hippocampus in humans. Science 269:1115–1118.

Béïque J-C, Campbell B, Perring P, Hamblin MW, Walker P, Mladenovic L, Andrade R (2004) Serotonergic regulation of membrane potential in developing rat prefrontal cortex: coordinated expression of 5-hydroxytryptamine (5-HT)1A, 5-HT2A, and 5-HT7 receptors. J Neurosci 24:4807–4817.

Ben-Ari Y (2002) Excitatory actions of gaba during development: the nature of the nurture. Nat Rev Neurosci 3:728–739.

Ben-Ari Y, Zigmond RE, Shute CC, Lewis PR (1977) Regional distribution of choline acetyltransferase and acetylcholinesterase within the amygdaloid complex and stria terminalis system. Brain Res 120:435–444.

Benarroch EE (2012) GABAB receptors: Structure, functions, and clinical implications. Neurology 78:578–584.

Benke TA, Lüthi A, Isaac JT, Collingridge GL (1998) Modulation of AMPA receptor unitary

conductance by synaptic activity. Nature 393:793–797.

Bergado JA, Lucas M, Richter-Levin G (2011) Emotional tagging--a simple hypothesis in a complex reality. Prog Neurobiol 94:64–76.

Berndt A, Schoenenberger P, Mattis J, Tye KM, Deisseroth K, Hegemann P, Oertner TG (2011) High-efficiency channelrhodopsins for fast neuronal stimulation at low light levels. Proc Natl Acad Sci U S A 108:7595–7600.

Bettler B, Kaupmann K, Mosbacher J, Gassmann M (2004) Molecular structure and physiological functions of GABA(B) receptors. Physiol Rev 84:835–867.

Betz WJ (1970) Depression of transmitter release at the neuromuscular junction of the frog. J Physiol 206:629–644.

Beyeler A, Namburi P, Glober GF, Simonnet C, Calhoon GG, Conyers GF, Luck R, Wildes CP, Tye KM (2016) Divergent routing of positive and negative information from the amygdala during memory retrieval. Neuron.

Bi GQ, Poo MM (1998) Synaptic modifications in cultured hippocampal neurons: dependence on spike timing, synaptic strength, and postsynaptic cell type. J Neurosci 18:10464–10472.

Bianchi MT, Macdonald RL (2002) Slow phases of GABA(A) receptor desensitization: structural determinants and possible relevance for synaptic function. J Physiol 544:3–18.

Bielle F, Griveau A, Narboux-Nême N, Vigneau S, Sigrist M, Arber S, Wassef M, Pierani A (2005) Multiple origins of Cajal-Retzius cells at the borders of the developing pallium. Nat Neurosci 8:1002–1012.

Bienvenu TCM, Busti D, Magill PJ, Ferraguti F, Capogna M (2012) Cell-type-specific recruitment of amygdala interneurons to hippocampal theta rhythm and noxious stimuli in vivo. Neuron 74:1059–1074.

Bienvenu TCM, Busti D, Micklem BR, Mansouri M, Magill PJ, Ferraguti F, Capogna M

(2015) Large intercalated neurons of amygdala relay noxious sensory information. J Neurosci 35:2044–2057.

Bigos KL, Pollock BG, Aizenstein HJ, Fisher PM, Bies RR, Hariri AR (2008) Acute 5-HT reuptake blockade potentiates human amygdala reactivity. Neuropsychopharmacology 33:3221–3225.

Bissière S, Humeau Y, Lüthi A (2003) Dopamine gates LTP induction in lateral amygdala by suppressing feedforward inhibition. Nat Neurosci 6:587–592.

Bjorvatn B, Grønli J, Hamre F, Sørensen E, Fiske E, Bjørkum AA, Portas CM, Ursin R (2002) Effects of sleep deprivation on extracellular serotonin in hippocampus and frontal cortex of the rat. Neuroscience 113:323–330.

Blakely RD, De Felice LJ, Hartzell HC (1994) Molecular physiology of norepinephrine and serotonin transporters. J Exp Biol 196:263–281.

Bolles RC (1970) Species-specific defence reactions and avoidance learning. Psychol Rev vol. 77:pp. 32–48.

Bonn M, Schmitt A, Lesch KP, Van Bockstaele EJ, Asan E (2013) Serotonergic innervation and serotonin receptor expression of NPY-producing neurons in the rat lateral and basolateral amygdaloid nuclei. Brain Struct Funct 218:421–435.

Booker SA, Gross A, Althof D, Shigemoto R, Bettler B, Frotscher M, Hearing M, Wickman K, Watanabe M, Kulik Á, Vida I (2013) Differential GABAB-receptor-mediated effects in perisomatic- and dendrite-targeting parvalbumin interneurons. J Neurosci 33:7961–7974.

Bredt DS, Snyder SH (1994) Transient nitric oxide synthase neurons in embryonic cerebral cortical plate, sensory ganglia, and olfactory epithelium. Neuron 13:301–313.

Brickley SG, Cull-Candy SG, Farrant M (1996) Development of a tonic form of synaptic

inhibition in rat cerebellar granule cells resulting from persistent activation of GABAA receptors. J Physiol 497:753–759.

Brocke B, Armbruster D, Muller J, Hensch T, Jacob CP, Lesch K-P, Kirschbaum C, Strobel A (2006) Serotonin transporter gene variation impacts innate fear processing: Acoustic startle response and emotional startle. Mol Psychiatry 11:1106–1112.

Büchel C, Dolan RJ, Armony JL, Friston KJ (1999) Amygdala-hippocampal involvement in human aversive trace conditioning revealed through event-related functional magnetic resonance imaging. J Neurosci 19:10869–10876.

Buzsáki G, Anastassiou CA, Koch C (2012) The origin of extracellular fields and currents--EEG, ECoG, LFP and spikes. Nat Rev Neurosci 13:407–420.

Buzsáki G, Draguhn A (2004) Neuronal oscillations in cortical networks. Science 304:1926–1929.

Cains S, Blomeley CP, Bracci E (2012) Serotonin inhibits low-threshold spike interneurons in the striatum. J Physiol 590:2241–2252.

Campeau S, Davis M (1995) Involvement of the central nucleus and basolateral complex of the amygdala in fear conditioning measured with fear-potentiated startle in rats trained concurrently with auditory and visual conditioned stimuli. J Neurosci 15:2301–2311.

Campeau S, Miserendino MJ, Davis M (1992) Intra-amygdala infusion of the N-methyl-D-aspartate receptor antagonist AP5 blocks acquisition but not expression of fear-potentiated startle to an auditory conditioned stimulus. Behav Neurosci 106:569–574.

Canli T, Omura K, Haas BW, Fallgatter A, Constable RT, Lesch KP (2005) Beyond affect: a role for genetic variation of the serotonin transporter in neural activation during a cognitive attention task. Proc Natl Acad Sci U S A 102:12224–12229.

Capogna M (2014) GABAergic cell type diversity in the basolateral amygdala. Curr Opin Neurobiol 26C:110–116.

Caporale N, Dan Y (2008) Spike Timing–Dependent Plasticity: A Hebbian Learning Rule. Annu Rev Neurosci 31:25–46.

Caputi A, Melzer S, Michael M, Monyer H (2013) The long and short of GABAergic neurons. Curr Opin Neurobiol 23:179–186.

Carroll RC, Beattie EC, Xia H, Lüscher C, Altschuler Y, Nicoll RA, Malenka RC, von Zastrow M (1999) Dynamin-dependent endocytosis of ionotropic glutamate receptors. Proc Natl Acad Sci U S A 96:14112–14117.

Carroll RC, Beattie EC, von Zastrow M, Malenka RC (2001) Role of AMPA receptor endocytosis in synaptic plasticity. Nat Rev Neurosci 2:315–324.

Caspi A, Sugden K, Moffitt TE, Taylor A, Craig IW, Harrington H, McClay J, Mill J, Martin J, Braithwaite A, Poulton R (2003) Influence of life stress on depression: moderation by a polymorphism in the 5-HTT gene. Science 301:386–389.

Castillo PE, Janz R, Südhof TC, Tzounopoulos T, Malenka RC, Nicoll RA (1997) Rab3A is essential for mossy fibre long-term potentiation in the hippocampus. Nature 388:590–593.

Castillo PE, Schoch S, Schmitz F, Südhof TC, Malenka RC (2002) RIM1alpha is required for presynaptic long-term potentiation. Nature 415:327–330.

Chen A, Hough CJ, Li H (2003) Serotonin type II receptor activation facilitates synaptic plasticity via n-methyl-d-aspartate-mediated mechanism in the rat basolateral amygdala. Neuroscience 119:53–63.

Cheng L-L, Wang S-J, Gean P-W (1998) Serotonin depresses excitatory synaptic transmission and depolarization-evoked Ca2+ influx in rat basolateral amygdala via 5-HT1A receptors. Eur J Neurosci 10:2163–2172.

Ciocchi S, Herry C, Grenier F, Wolff SBE, Letzkus JJ, Vlachos I, Ehrlich I, Sprengel R,

Deisseroth K, Stadler MB, Müller C, Lüthi A (2010) Encoding of conditioned fear in central amygdala inhibitory circuits. Nature 468:277–282.

Ciocchi S, Passecker J, Malagon-Vina H, Mikus N, Klausberger T (2015) Brain computation. Selective information routing by ventral hippocampal CA1 projection neurons. Science 348:560–563.

Cirelli C, Pompeiano M, Tononi G (1995) Sleep deprivation and c-fos expression in the rat brain. J Sleep Res 4:92–106.

Citri A, Malenka RC (2008) Synaptic Plasticity: Multiple Forms, Functions, and Mechanisms. Neuropsychopharmacology 33:18–41.

Cohen JY, Amoroso MW, Uchida N (2015) Serotonergic neurons signal reward and punishment on multiple timescales. Elife 4:e06346.

Collins DR, Paré D (2000) Differential fear conditioning induces reciprocal changes in the sensory responses of lateral amygdala neurons to the CS+ and CS−. Learn Mem 7:97–103.

Connors BW, Malenka RC, Silva LR (1988) Two inhibitory postsynaptic potentials, and GABAA and GABAB receptor-mediated responses in neocortex of rat and cat. J Physiol 406:443–468.

Courtin J, Chaudun F, Rozeske RR, Karalis N, Gonzalez-Campo C, Wurtz H, Abdi A, Baufreton J, Bienvenu TCM, Herry C (2014) Prefrontal parvalbumin interneurons shape neuronal activity to drive fear expression. Nature 505:92–96.

Cousens G, Otto T (1998) Both pre- and posttraining excitotoxic lesions of the basolateral amygdala abolish the expression of olfactory and contextual fear conditioning. Behav Neurosci 112:1092–1103.

Csicsvari J, Hirase H, Czurko A, Mamiya A, Buzsaki G (1999) Oscillatory coupling of hippocampal pyramidal cells and interneurons in the behaving rat. J Neurosci 19:274–

287.

Cui N, Mckillop LE, Fisher SP, Oliver PL, Vyazovskiy V V (2014) Long-term history and immediate preceding state affect EEG slow wave characteristics at NREM sleep onset in C57BL/6 mice. Arch Ital Biol 152:156–168.

Cummings JA, Mulkey RM, Nicoll RA, Malenka RC (1996) Ca2+ Signaling Requirements for Long-Term Depression in the Hippocampus. Neuron 16:825–833.

Davies CH, Davies SN, Collingridge GL (1990) Paired-pulse depression of monosynaptic GABA-mediated inhibitory postsynaptic responses in rat hippocampus. J Physiol 424:513–531.

Davis M, Falls WA, Campeau S, Kim M (1993) Fear-potentiated startle: a neural and pharmacological analysis. Behav Brain Res 58:175–198.

Davis M, Gendelman DS, Tischler MD, Gendelman PM (1982) A primary acoustic startle circuit: lesion and stimulation studies. J Neurosci 2:791–805.

Dilgen J, Tejeda HA, O'Donnell P (2013) Amygdala inputs drive feedforward inhibition in the medial prefrontal cortex. J Neurophysiol 110:221–229.

Dittrich L, Morairty SR, Warrier DR, Kilduff TS (2014) Homeostatic sleep pressure is the primary factor for activation of cortical nNOS/NK1 neurons. Neuropsychopharmacology 40:1–26.

Dobrunz LE, Stevens CF (1997) Heterogeneity of Release Probability, Facilitation, and Depletion at Central Synapses. Neuron 18:995–1008.

Doyère V, Schafe GE, Sigurdsson T, LeDoux JE (2003) Long-term potentiation in freely moving rats reveals asymmetries in thalamic and cortical inputs to the lateral amygdala. Eur J Neurosci 17:2703–2715.

Dudek SM, Bear MF (1992) Homosynaptic long-term depression in area CAl of hippocampus

and effects of N-methyl-D-aspartate receptor blockade. Neurobiology 89:4363–4367.

Duvarci S, Paré D (2014) Amygdala microcircuits controlling learned fear. Neuron 82:966–980.

Ebner K, Singewald N (2006) The role of substance P in stress and anxiety responses. Amino Acids 31:251–272.

Ehrlich I, Humeau Y, Grenier F, Ciocchi S, Herry C, Lüthi A (2009) Amygdala inhibitory circuits and the control of fear memory. Neuron 62:757–771.

Elzinga BM, Bremner JD (2002) Are the neural substrates of memory the final common pathway in posttraumatic stress disorder (PTSD)? J Affect Disord 70:1–17.

Emiliani V, Cohen AE, Deisseroth K, Häusser M (2015) All-optical interrogation of neural circuits. J Neurosci 35:13917–13926.

Epsztein J, Brecht M, Lee AK (2011) Intracellular Determinants of Hippocampal CA1 Place and Silent Cell Activity in a Novel Environment. Neuron 70:109–120.

Fanselow MS (2010) From contextual fear to a dynamic view of memory systems. Trends Cogn Sci 14:7–15.

Farb CR, LeDoux JE (1997) NMDA and AMPA receptors in the lateral nucleus of the amygdala are postsynaptic to auditory thalamic afferents. Synapse 27:106–121.

Farb CR, Ledoux JE (1999) Afferents from rat temporal cortex synapse on lateral amygdala neurons that express NMDA and AMPA receptors. Synapse 33:218–229.

Farrant M, Nusser Z (2005) Variations on an inhibitory theme: phasic and tonic activation of GABA(A) receptors. Nat Rev Neurosci 6:215–229.

Fatt P, Katz B (1952) Spontaneous subthreshold activity at motor nerve endings. J Physiol 117:109–128.

Felix-Ortiz AC, Beyeler A, Seo C, Leppla CA, Wildes CP, Tye KM (2013) BLA to vHPC inputs modulate anxiety-related behaviors. Neuron 79:658–664.

Férézou I, Cauli B, Hill EL, Rossier J, Hamel E, Lambolez B (2002) 5-HT3 receptors mediate serotonergic fast synaptic excitation of neocortical vasoactive intestinal peptide/cholecystokinin interneurons. J Neurosci 22:7389–7397.

Fourcaudot E, Gambino F, Casassus G, Poulain B, Humeau Y, Lüthi A (2009) L-type voltage-dependent Ca(2+) channels mediate expression of presynaptic LTP in amygdala. Nat Neurosci 12:1093–1095.

Freese JL, Amaral DG (2009) Neuroanatomy of the primate amygdala. In: The human amygdala (Whalen P, Phelps EA, eds), pp.3–42. The Guilford Press, New York, NY.

Fuentealba P, Begum R, Capogna M, Jinno S, Márton LF, Csicsvari J, Thomson A, Somogyi P, Klausberger T (2008) Ivy cells: a population of nitric-oxide-producing, slow-spiking GABAergic neurons and their Involvement in hippocampal network activity. Neuron 57:917–929.

Gabernet L, Jadhav SP, Feldman DE, Carandini M, Scanziani M (2005) Somatosensory integration controlled by dynamic thalamocortical feed-forward inhibition. Neuron 48:315–327.

Gähwiler BH, Brown DA (1985) GABAB-receptor-activated K+ current in voltage-clamped CA3 pyramidal cells in hippocampal cultures. Proc Natl Acad Sci U S A 82:1558–1562.

Galvez T, Urwyler S, Prézeau L, Mosbacher J, Joly C, Malitschek B, Heid J, Brabet I, Froestl W, Bettler B, Kaupmann K, Pin JP (2000) Ca(2+) requirement for high-affinity gamma-aminobutyric acid (GABA) binding at GABA(B) receptors: involvement of serine 269 of the GABA(B)R1 subunit. Mol Pharmacol 57:419–426.

Gao J, Zhang J-X, Xu T-L (2002) Modulation of serotonergic projection from dorsal raphe nucleus to basolateral amygdala on sleep–waking cycle of rats. Brain Res 945:60–70.

Garpenstrand H, Annas P, Ekblom J, Oreland L, Fredrikson M (2001) Human fear

conditioning is related to dopaminergic and serotonergic biological markers. Behav Neurosci 115:358–364.

Gelman DM, Martini FJ, Nóbrega-Pereira S, Pierani A, Kessaris N, Marín O (2009) The embryonic preoptic area is a novel source of cortical GABAergic interneurons. J Neurosci 29:9380–9389.

Gerashchenko D, Wisor JP, Burns D, Reh RK, Shiromani PJ, Sakurai T, de la Iglesia HO, Kilduff TS (2008) Identification of a population of sleep-active cerebral cortex neurons. Proc Natl Acad Sci U S A 105:10227–10232.

Ghosh KK, Burns LD, Cocker ED, Nimmerjahn A, Ziv Y, Gamal A El, Schnitzer MJ (2011) Miniaturized integration of a fluorescence microscope. Nat Methods 8:871–878.

Glykys J, Mody I (2007) The main source of ambient GABA responsible for tonic inhibition in the mouse hippocampus. J Physiol 582:1163–1178.

Goosens KA, Hobin JA, Maren S (2003) Auditory-evoked spike firing in the lateral amygdala and pavlovian fear conditioning. Neuron 40:1013–1022.

Gore F, Schwartz EC, Brangers BC, Aladi S, Stujenske JM, Likhtik E, Russo MJ, Gordon JA, Salzman CD, Axel R (2015) Neural representations of unconditioned stimuli in basolateral amygdala mediate innate and learned responses. Cell 162:134–145.

Graves LA, Heller EA, Pack AI, Abel T (2003) Sleep deprivation selectively impairs memory consolidation for contextual fear conditioning. Learn Mem 10:168–176.

Greenberg BD, Tolliver TJ, Huang SJ, Li Q, Bengel D, Murphy DL (1999) Genetic variation in the serotonin transporter promoter region affects serotonin uptake in human blood platelets. Am J Med Genet 88:83–87.

Greenwood BN, Strong P V, Loughridge AB, Day HEW, Clark PJ, Mika A, Hellwinkel JE, Spence KG, Fleshner M (2012) 5-HT2C receptors in the basolateral amygdala and dorsal striatum are a novel target for the anxiolytic and antidepressant effects of exercise. PLoS

One 7:e46118.

Gross C, Zhuang X, Stark K, Ramboz S, Oosting R, Kirby L, Santarelli L, Beck S, Hen R (2002) Serotonin1A receptor acts during development to establish normal anxiety-like behaviour in the adult. Nature 416:396–400.

Gründemann J, Lüthi A (2015) Ensemble coding in amygdala circuits for associative learning. Curr Opin Neurobiol 35:200–206.

Gulledge AT, Stuart GJ (2003) Excitatory Actions of GABA in the Cortex. Neuron 37:299–309.

Hariri AR, Drabant EM, Munoz KE, Kolachana BS, Mattay VS, Egan MF, Weinberger DR (2005) A susceptibility gene for affective disorders and the response of the human amygdala. Arch Gen Psychiatry 62:146–152.

Hariri AR, Mattay VS, Tessitore A, Kolachana B, Fera F, Goldman D, Egan MF, Weinberger DR (2002) Serotonin transporter genetic variation and the response of the human amygdala. Science 297:400–403.

Harvey CD, Collman F, Dombeck D a, Tank DW (2009) Intracellular dynamics of hippocampal place cells during virtual navigation. Nature 461:941–946.

Heinbockel T, Pape HC (2000) Input-specific long-term depression in the lateral amygdala evoked by theta frequency stimulation. J Neurosci 20:RC68.

Hensler JG (2006) Serotonergic modulation of the limbic system. Neurosci Biobehav Rev 30:203–214.

Herry C, Ciocchi S, Senn V, Demmou L, Müller C, Lüthi A (2008) Switching on and off fear by distinct neuronal circuits. Nature 454:600–606.

Hirata T, Li P, Lanuza GM, Cocas L a, Huntsman MM, Corbin JG (2009) Identification of distinct telencephalic progenitor pools for neuronal diversity in the amygdala. Nat

Neurosci 12:141–149.

Huang Y-Y et al. (1998) Postsynaptic Induction and PKA-Dependent Expression of LTP in the Lateral Amygdala. Neuron 21:169–178.

Huang Y-Y, Kandel ER (2007) 5-Hydroxytryptamine induces a protein kinase A/mitogen-activated protein kinase-mediated and macromolecular synthesis-dependent late phase of long-term potentiation in the amygdala. J Neurosci 27:3111–3119.

Huber R, Deboer T, Tobler I (2000) Topography of EEG dynamics after sleep deprivation in mice. J Neurophysiol 84:1888–1893.

Hübner C, Bosch D, Gall A, Lüthi A, Ehrlich I (2014) Ex vivo dissection of optogenetically activated mPFC and hippocampal inputs to neurons in the basolateral amygdala: implications for fear and emotional memory. Front Behav Neurosci 8:64.

Huguenard JR, Alger BE (1986) Whole-cell voltage-clamp study of the fading of GABA-activated currents in acutely dissociated hippocampal neurons. J Neurophysiol 56:1–18.

Humeau Y, Herry C, Kemp N, Shaban H, Fourcaudot E, Bissière S, Lüthi A (2005) Dendritic spine heterogeneity determines afferent-specific Hebbian plasticity in the amygdala. Neuron 45:119–131.

Humeau Y, Shaban H, Bissière S, Lüthi A (2003) Presynaptic induction of heterosynaptic associative plasticity in the mammalian brain. Nature 426:841–845.

Hyman SE (2014) Revitalizing psychiatric therapeutics. Neuropsychopharmacology 39:220–229.

Ibáñez-Sandoval O, Tecuapetla F, Unal B, Shah F, Koós T, Tepper JM (2011) A novel functionally distinct subtype of striatal neuropeptide Y interneuron. J Neurosci 31:16757–16769.

Janak PH, Tye KM (2015) From circuits to behaviour in the amygdala. Nature 517:284–292.

Jasnow AM, Ressler KJ, Hammack SE, Chhatwal JP, Rainnie DG (2009) Distinct subtypes of

cholecystokinin (CCK)-containing interneurons of the basolateral amygdala identified using a CCK promoter-specific lentivirus. J Neurophysiol 101:1494–1506.

Jennings KA, Lesch K-P, Sharp T, Cragg SJ (2010) Non-linear relationship between 5-HT transporter gene expression and frequency sensitivity of 5-HT signals. J Neurochem 115:965–973.

Jennings KA, Loder MK, Sheward WJ, Pei Q, Deacon RMJ, Benson MA, Olverman HJ, Hastie ND, Harmar AJ, Shen S, Sharp T (2006) Increased expression of the 5-HT transporter confers a low-anxiety phenotype linked to decreased 5-HT transmission. J Neurosci 26:8955–8964.

Jennings KA, Sheward WJ, Harmar AJ, Sharp T (2008) Evidence that genetic variation in 5-HT transporter expression is linked to changes in 5-HT2A receptor function. Neuropharmacology 54:776–783.

Jiang X, Xing G, Yang C, Verma A, Zhang L, Li H (2009) Stress impairs 5-HT2A receptor-mediated serotonergic facilitation of GABA release in juvenile rat basolateral amygdala. Neuropsychopharmacology 34:410–423.

Jin J, Maren S (2015) Fear renewal preferentially activates ventral hippocampal neurons projecting to both amygdala and prefrontal cortex in rats. Sci Rep 5:8388.

Jones et al. (1998) GABA(B) receptors function as a heteromeric assembly of the subunits GABA(B)R1 and GABA(B)R2. Nature 396:674–679.

Kaila K, Voipio J, Paalasmaa P, Pasternack M, Deisz RA (1993) The role of bicarbonate in GABAA receptor-mediated IPSPs of rat neocortical neurones. J Physiol 464:273–289.

Kamiya H, Umeda K, Ozawa S, Manabe T (2002) Presynaptic Ca2+ entry is unchanged during hippocampal mossy fiber long-term potentiation. J Neurosci 22:10524–10528.

Kaneda M, Farrant M, Cull-Candy SG (1995) Whole-cell and single-channel currents

activated by GABA and glycine in granule cells of the rat cerebellum. J Physiol 485:419–435.

Karalis N, Dejean C, Chaudun F, Khoder S, Rozeske RR, Wurtz H, Bagur S, Benchenane K, Sirota A, Courtin J, Herry C (2016) 4-Hz oscillations synchronize prefrontal–amygdala circuits during fear behavior. Nat Neurosci 19:605–612.

Kasugai Y, Swinny JD, Roberts JDB, Dalezios Y, Fukazawa Y, Sieghart W, Shigemoto R, Somogyi P (2010) Quantitative localisation of synaptic and extrasynaptic GABAA receptor subunits on hippocampal pyramidal cells by freeze-fracture replica immunolabelling. Eur J Neurosci 32:1868–1888.

Kawaguchi Y (1993) Physiological, morphological, and histochemical characterization of three classes of interneurons in rat neostriatum. J Neurosci 13:4908–4923.

Kilduff TS, Cauli B, Gerashchenko D (2011) Activation of cortical interneurons during sleep: an anatomical link to homeostatic sleep regulation? Trends Neurosci 34:10–19.

Kim JJ, DeCola JP, Landeira-Fernandez J, Fanselow MS (1991) N-methyl-D-aspartate receptor antagonist APV blocks acquisition but not expression of fear conditioning. Behav Neurosci 105:126–133.

Kim JJ, Fanselow MS (1992) Modality-specific retrograde amnesia of fear. Science 256:675–677.

Kishi T, Tsumori T, Yokota S, Yasui Y (2006) Topographical projection from the hippocampal formation to the amygdala: a combined anterograde and retrograde tracing study in the rat. J Comp Neurol 496:349–368.

Kjelstrup KB, Solstad T, Brun VH, Hafting T, Leutgeb S, Witter MP, Moser EI, Moser M-B (2008) Finite scale of spatial representation in the hippocampus. Science 321:140–143.

Klausberger T, Magill PJ, Márton LF, Roberts JDB, Cobden PM, Buzsáki G, Somogyi P (2003) Brain-state- and cell-type-specific firing of hippocampal interneurons in vivo.

Nature 421:844–848.

Klausberger T, Somogyi P (2008) Neuronal diversity and temporal dynamics: the unity of hippocampal circuit operations. Science 321:53–57.

Kocsis B, Vertes RP (1992) Dorsal raphe neurons: synchronous discharge with the theta rhythm of the hippocampus in the freely behaving rat. J Neurophysiol 68:1463–1467.

Köhler C, Swanson LW, Haglund L, J-Yen W (1985) The cytoarchitecture, histochemistry and projections of the tuberomammillary nucleus in the rat. Neuroscience 16:85–110.

Kreitzer AC, Regehr WG (2001) Retrograde Inhibition of Presynaptic Calcium Influx by Endogenous Cannabinoids at Excitatory Synapses onto Purkinje Cells. Neuron 29:717–727.

Krettek JE, Price JL (1977a) Projections from the amygdaloid complex to the cerebral cortex and thalamus in the rat and cat. J Comp Neurol 172:687–722.

Krettek JE, Price JL (1977b) Projections from the amygdaloid complex and adjacent olfactory structures to the entorhinal cortex and to the subiculum in the rat and cat. J Comp Neurol 172:723–752.

Krettek JE, Price JL (1978) Amygdaloid projections to subcortical structures within the basal forebrain and brainstem in the rat and cat. J Comp Neurol 178:225–254.

Kubota Y, Shigematsu N, Karube F, Sekigawa A, Kato S, Yamaguchi N, Hirai Y, Morishima M, Kawaguchi Y (2011) Selective coexpression of multiple chemical markers defines discrete populations of neocortical GABAergic neurons. Cereb Cortex 21:1803–1817.

Kulik A, Vida I, Luján R, Haas CA, López-Bendito G, Shigemoto R, Frotscher M (2003) Subcellular localization of metabotropic GABA(B) receptor subunits GABA(B1a/b) and GABA(B2) in the rat hippocampus. J Neurosci 23:11026–11035.

Kumar T, Jha SK (2012) Sleep deprivation impairs consolidation of cued fear memory in rats.

PLoS One 7:e47042.

Kvitsiani D, Ranade S, Hangya B, Taniguchi H, Huang JZ, Kepecs A (2013) Distinct behavioural and network correlates of two interneuron types in prefrontal cortex. Nature 498:363–366.

LaBar KS, Gatenby JC, Gore JC, LeDoux JE, Phelps EA (1998) Human amygdala activation during conditioned fear acquisition and extinction: a mixed-trial fMRI study. Neuron 20:937–945.

LaBar KS, LeDoux JE, Spencer DD, Phelps EA (1995) Impaired fear conditioning following unilateral temporal lobectomy in humans. J Neurosci 15:6846–6855.

Labrakakis C, Rudolph U, De Koninck Y (2014) The heterogeneity in GABAA receptor-mediated IPSC kinetics reflects heterogeneity of subunit composition among inhibitory and excitatory interneurons in spinal lamina II. Front Cell Neurosci 8:424.

LaLumiere RT, Buen T-V, McGaugh JL (2003) Post-training intra-basolateral amygdala infusions of norepinephrine enhance consolidation of memory for contextual fear conditioning. J Neurosci 23:6754–6758.

Lange MD, Doengi M, Lesting J, Pape HC, Jüngling K (2012) Heterosynaptic long-term potentiation at interneuron-principal neuron synapses in the amygdala requires nitric oxide signalling. J Physiol 590:131–143.

LeDoux J, Farb C, Ruggiero D (1990a) Topographic organization of neurons in the acoustic thalamus that project to the amygdala. J Neurosci 10:1043–1054.

LeDoux JE (2000) Emotion circuits in the brain. Annu Rev Neurosci 23:155–184.

LeDoux JE, Cicchetti P, Xagoraris A, Romanski LM (1990b) The lateral amygdaloid nucleus: sensory interface of the amygdala in fear conditioning. J Neurosci 10:1062–1069.

LeDoux JE, Farb CR, Milner TA (1991) Ultrastructure and synaptic associations of auditory thalamo-amygdala projections in the rat. Exp brain Res 85:577–586.

LeDoux JE, Iwata J, Cicchetti P, Reis DJ (1988) Different projections of the central amygdaloid nucleus mediate autonomic and behavioral correlates of conditioned fear. J Neurosci 8:2517–2529.

Lee H-J, Lee M-S, Kang R-H, Kim H, Kim S-D, Kee B-S, Kim YH, Kim Y-K, Kim JB, Yeon BK, Oh KS, Oh B-H, Yoon J-S, Lee C, Jung HY, Chee I-S, Paik IH (2005) Influence of the serotonin transporter promoter gene polymorphism on susceptibility to posttraumatic stress disorder. Depress Anxiety 21:135–139.

Lee H-K et al. (1998) NMDA Induces Long-Term Synaptic Depression and Dephosphorylation of the GluR1 Subunit of AMPA Receptors in Hippocampus. Neuron 21:1151–1162.

Lee J-E, Jeon C-J (2005) Immunocytochemical localization of nitric oxide synthase-containing neurons in mouse and rabbit visual cortex and co-localization with calcium-binding proteins. Mol Cells 19:408–417.

Lesch KP, Bengel D, Heils A, Sabol SZ, Greenberg BD, Petri S, Benjamin J, Müller CR, Hamer DH, Murphy DL (1996) Association of anxiety-related traits with a polymorphism in the serotonin transporter gene regulatory region. Science 274:1527–1531.

Lesting J, Narayanan RT, Kluge C, Sangha S, Seidenbecher T, Pape H-C (2011) Patterns of coupled theta activity in amygdala-hippocampal-prefrontal cortical circuits during fear extinction. PLoS One 6:e21714.

Li Q, Wichems CH, Ma L, Van de Kar LD, Garcia F, Murphy DL (2003) Brain region-specific alterations of 5-HT2A and 5-HT2C receptors in serotonin transporter knockout mice. J Neurochem 84:1256–1265.

Likhtik E, Stujenske JM, Topiwala MA, Harris AZ, Gordon JA (2014) Prefrontal entrainment

of amygdala activity signals safety in learned fear and innate anxiety. Nat Neurosci 17:106–113.

Lin HC, Wang SJ, Luo MZ, Gean PW (2000) Activation of group II metabotropic glutamate receptors induces long-term depression of synaptic transmission in the rat amygdala. J Neurosci 20:9017–9024.

Line SJ, Barkus C, Rawlings N, Jennings K, McHugh S, Sharp T, Bannerman DM (2014) Reduced sensitivity to both positive and negative reinforcement in mice over-expressing the 5-hydroxytryptamine transporter. Eur J Neurosci 40:3735–3745.

Linke R, Braune G, Schwegler H (2000) Differential projection of the posterior paralaminar thalamic nuclei to the amygdaloid complex in the rat. Exp brain Res 134:520–532.

Lisman J (1989) A mechanism for the Hebb and the anti-Hebb processes underlying learning and memory. Proc Natl Acad Sci U S A 86:9574–9578.

Liu X, Ramirez S, Tonegawa S (2014) Inception of a false memory by optogenetic manipulation of a hippocampal memory engram. Philos Trans R Soc Lond B Biol Sci 369:20130142.

Lonsdorf TB, Weike AI, Nikamo P, Schalling M, Hamm AO, Ohman A (2009) Genetic gating of human fear learning and extinction: possible implications for gene-environment interaction in anxiety disorder. Psychol Sci 20:198–206.

López-Bendito G, Shigemoto R, Kulik A, Vida I, Fairén A, Luján R (2004) Distribution of metabotropic GABA receptor subunits GABAB1a/b and GABAB2 in the rat hippocampus during prenatal and postnatal development. Hippocampus 14:836–848.

Lovett-Barron M, Kaifosh P, Kheirbek MA, Danielson N, Zaremba JD, Reardon TR, Turi GF, Hen R, Zemelman B V, Losonczy A (2014) Dendritic inhibition in the hippocampus supports fear learning. Science 343:857–863.

Luo AH, Tahsili-Fahadan P, Wise R a, Lupica CR, Aston-Jones G (2011) Linking context

with reward: a functional circuit from hippocampal CA3 to ventral tegmental area. Science 333:353–357.

Lüscher C, Jan LY, Stoffel M, Malenka RC, Nicoll RA (1997) G Protein-Coupled Inwardly Rectifying K+ Channels (GIRKs) Mediate Postsynaptic but Not Presynaptic Transmitter Actions in Hippocampal Neurons. Neuron 19:687–695.

Luskin MB, Price JL (1983) The topographic organization of associational fibers of the olfactory system in the rat, including centrifugal fibers to the olfactory bulb. J Comp Neurol 216:264–291.

Magee JC, Johnston D (1997) A synaptically controlled, associative signal for Hebbian plasticity in hippocampal neurons. Science 275:209–213.

Magleby KL, Zengel JE (1982) A quantitative description of stimulation-induced changes in transmitter release at the frog neuromuscular junction. J Gen Physiol 80:613–638.

Malenka RC, Nicoll RA (1993) NMDA-receptor-dependent synaptic plasticity: multiple forms and mechanisms. Trends Neurosci 16:521–527.

Malinow R, Malenka RC (2002) AMPA receptor trafficking and synaptic plasticity. Annu Rev Neurosci 25:103–126.

Manko M, Bienvenu TCM, Dalezios Y, Capogna M (2012) Neurogliaform cells of amygdala: a source of slow phasic inhibition in the basolateral complex. J Physiol 590:5611–5627.

Mapelli L, Rossi P, Nieus T, D'Angelo E (2009) Tonic activation of GABAB receptors reduces release probability at inhibitory connections in the cerebellar glomerulus. J Neurophysiol 101:3089–3099.

Marek GJ, Martin-Ruiz R, Abo A, Artigas F (2005) The selective 5-HT2A receptor antagonist M100907 enhances antidepressant-like behavioral effects of the SSRI fluoxetine. Neuropsychopharmacology 30:2205–2215.

Maren S, Fanselow MS (1995) Synaptic plasticity in the basolateral amygdala induced by hippocampal formation stimulation in vivo. J Neurosci 15:7548–7564.

Maren S, Phan KL, Liberzon I (2013) The contextual brain: implications for fear conditioning, extinction and psychopathology. Nat Rev Neurosci 14:417–428.

Markram H, Lübke J, Frotscher M, Sakmann B (1997) Regulation of synaptic efficacy by coincidence of postsynaptic APs and EPSPs. Science 275:213–215.

Marowsky A, Fritschy J-M, Vogt KE (2004) Functional mapping of GABAA receptor subtypes in the amygdala. Eur J Neurosci 20:1281–1289.

Marowsky A, Yanagawa Y, Obata K, Vogt KE (2005) A specialized subclass of interneurons mediates dopaminergic facilitation of amygdala function. Neuron 48:1025–1037.

Mascagni F, McDonald AJ (2003) Immunohistochemical characterization of cholecystokinin containing neurons in the rat basolateral amygdala. Brain Res 976:171–184.

Mascagni F, McDonald AJ (2007) A novel subpopulation of 5-HT type 3A receptor subunit immunoreactive interneurons in the rat basolateral amygdala. Neuroscience 144:1015–1024.

Massou JM, Trichard C, Attar-Levy D, Feline A, Corruble E, Beaufils B, Martinot JL (1997) Frontal 5-HT 2A receptors studied in depressive patients during chronic treatment by selective serotonin reuptake inhibitors. Psychopharmacology (Berl) 133:99–101.

Mathews TA, Fedele DE, Coppelli FM, Avila AM, Murphy DL, Andrews AM (2004) Gene dose-dependent alterations in extraneuronal serotonin but not dopamine in mice with reduced serotonin transporter expression. J Neurosci Methods 140:169–181.

McDonald AJ (1982a) Cytoarchitecture of the central amygdaloid nucleus of the rat. J Comp Neurol 208:401–418.

McDonald AJ (1982b) Neurons of the lateral and basolateral amygdaloid nuclei: a Golgi study in the rat. J Comp Neurol 212:293–312.

McDonald AJ (1984) Neuronal organization of the lateral and basolateral amygdaloid nuclei in the rat. J Comp Neurol 222:589–606.

McDonald AJ (1989) Coexistence of somatostatin with neuropeptide Y, but not with cholecystokinin or vasoactive intestinal peptide, in neurons of the rat amygdala. Brain Res 500:37–45.

McDonald AJ (1991) Topographical organization of amygdaloid projections to the caudatoputamen, nucleus accumbens, and related striatal-like areas of the rat brain. Neuroscience 44:15–33.

McDonald AJ (1998) Cortical pathways to the mammalian amygdala. Prog Neurobiol 55:257–332.

McDonald AJ, Mascagni F (1997) Projections of the lateral entorhinal cortex to the amygdala: a Phaseolus vulgaris leucoagglutinin study in the rat. Neuroscience 77:445–459.

McDonald AJ, Mascagni F (2001a) Colocalization of calcium-binding proteins and GABA in neurons of the rat basolateral amygdala. Neuroscience 105:681–693.

McDonald AJ, Mascagni F (2001b) Localization of the CB1 type cannabinoid receptor in the rat basolateral amygdala: high concentrations in a subpopulation of cholecystokinin-containing interneurons. Neuroscience 107:641–652.

McDonald AJ, Mascagni F (2002) Immunohistochemical characterization of somatostatin containing interneurons in the rat basolateral amygdala. Brain Res 943:237–244.

McDonald AJ, Mascagni F (2004) Parvalbumin-containing interneurons in the basolateral amygdala express high levels of the ?1 subunit of the GABAA receptor. J Comp Neurol 473:137–146.

McDonald AJ, Mascagni F (2007) Neuronal localization of 5-HT type 2A receptor immunoreactivity in the rat basolateral amygdala. Neuroscience 146:306–320.

McDonald AJ, Mascagni F (2011) Neuronal localization of M2 muscarinic receptor immunoreactivity in the rat amygdala. Neuroscience 196:49–65.

McDonald AJ, Mascagni F, Guo L (1996) Projections of the medial and lateral prefrontal cortices to the amygdala: A Phaseolus vulgaris leucoagglutinin study in the rat. Neuroscience 71:55–75.

McDonald AJ, Mascagni F, Zaric V (2012) Subpopulations of somatostatin-immunoreactive non-pyramidal neurons in the amygdala and adjacent external capsule project to the basal forebrain: evidence for the existence of GABAergic projection neurons in the cortical nuclei and basolateral nuclear com. Front Neural Circuits 6:46.

McDonald AJ, Mott DD (2016) Functional neuroanatomy of amygdalohippocampal interconnections and their role in learning and memory. J Neurosci Res.

McDonald AJ, Payne DR, Mascagni F (1993) Identification of putative nitric oxide producing neurons in the rat amygdala using NADPH-diaphorase histochemistry. Neuroscience 52:97–106.

McDonald AJ, Zaric V (2015) GABAergic somatostatin-immunoreactive neurons in the amygdala project to the entorhinal cortex. Neuroscience 290:227–242.

McHugh SB, Barkus C, Lima J, Glover LR, Sharp T, Bannerman DM (2015) SERT and uncertainty: serotonin transporter expression influences information processing biases for ambiguous aversive cues in mice. Genes Brain Behav 14:330–336.

McIntire SL, Reimer RJ, Schuske K, Edwards RH, Jorgensen EM (1997) Identification and characterization of the vesicular GABA transporter. Nature 389:870–876.

McIntyre CK, Ragozzino ME, Gold PE (1998) Intra-amygdala infusions of scopolamine impair performance on a conditioned place preference task but not a spatial radial maze task. Behav Brain Res 95:219–226.

McKernan MG, Shinnick-Gallagher P (1997) Fear conditioning induces a lasting potentiation

of synaptic currents in vitro. Nature 390:607–611.

Meis S, Sosulina L, Schulz S, Höllt V, Pape H-C (2005) Mechanisms of somatostatin-evoked responses in neurons of the rat lateral amygdala. Eur J Neurosci 21:755–762.

Millhouse OE (1986) The intercalated cells of the amygdala. J Comp Neurol 247:246–271.

Millhouse OE, DeOlmos J (1983) Neuronal configurations in lateral and basolateral amygdala. Neuroscience 10:1269–1300.

Mintz IM, Bean BP (1993) GABAB Receptor Inhibition of P-type Ca2+ Channels in Central Neurons. Neuron 10:889–898.

Miserendino MJ, Sananes CB, Melia KR, Davis M (1990) Blocking of acquisition but not expression of conditioned fear-potentiated startle by NMDA antagonists in the amygdala. Nature 345:716–718.

Mitchell SJ, Silver RA (2003) Shunting Inhibition Modulates Neuronal Gain during Synaptic Excitation. Neuron 38:433–445.

Mittmann W, Koch U, Häusser M (2005) Feed-forward inhibition shapes the spike output of cerebellar Purkinje cells. J Physiol 563:369–378.

Morairty SR, Dittrich L, Pasumarthi RK, Valladao D, Heiss JE, Gerashchenko D, Kilduff TS (2013) A role for cortical nNOS/NK1 neurons in coupling homeostatic sleep drive to EEG slow wave activity. Proc Natl Acad Sci U S A 110:20272–20277.

Morales M, Bloom FE (1997) The 5-HT3 receptor is present in different subpopulations of GABAergic neurons in the rat telencephalon. J Neurosci 17:3157–3167.

Morozov A, Sukato D, Ito W (2011) Selective suppression of plasticity in amygdala inputs from temporal association cortex by the external capsule. J Neurosci 31:339–345.

Morris JS, Frith CD, Perrett DI, Rowland D, Young AW, Calder AJ, Dolan RJ (1996) A differential neural response in the human amygdala to fearful and happy facial

expressions. Nature 383:812–815.

Mulkey RM, Malenka RC (1992) Mechanisms underlying induction of homosynaptic long-term depression in area CA1 of the hippocampus. Neuron 9:967–975.

Muller JF, Mascagni F, McDonald AJ (2003) Synaptic connections of distinct interneuronal subpopulations in the rat basolateral amygdalar nucleus. J Comp Neurol 456:217–236.

Muller JF, Mascagni F, McDonald AJ (2005) Coupled networks of parvalbumin-immunoreactive interneurons in the rat basolateral amygdala. J Neurosci 25:7366–7376.

Muller JF, Mascagni F, McDonald AJ (2006) Pyramidal cells of the rat basolateral amygdala: synaptology and innervation by parvalbumin-immunoreactive interneurons. J Comp Neurol 494:635–650.

Muller JF, Mascagni F, McDonald AJ (2007a) Postsynaptic targets of somatostatin-containing interneurons in the rat basolateral amygdala. J Comp Neurol 500:513–529.

Muller JF, Mascagni F, McDonald AJ (2007b) Serotonin-immunoreactive axon terminals innervate pyramidal cells and interneurons in the rat basolateral amygdala. J Comp Neurol 505:314–335.

Muller JF, Mascagni F, McDonald AJ (2009) Dopaminergic innervation of pyramidal cells in the rat basolateral amygdala. Brain Struct Funct 213:275–288.

Müller M, Faber-Zuschratter H, Yanagawa Y, Stork O, Schwegler H, Linke R (2012) Synaptology of ventral CA1 and subiculum projections to the basomedial nucleus of the amygdala in the mouse: relation to GABAergic interneurons. Brain Struct Funct 217:5–17.

Munafò MR, Brown SM, Hariri AR (2008) Serotonin transporter (5-HTTLPR) genotype and amygdala activation: a meta-analysis. Biol Psychiatry 63:852–857.

Murphy SE, Norbury R, Godlewska BR, Cowen PJ, Mannie ZM, Harmer CJ, Munafò MR (2013) The effect of the serotonin transporter polymorphism (5-HTTLPR) on amygdala

function: a meta-analysis. Mol Psychiatry 18:512–520.

Murphy SE, Norbury R, O'Sullivan U, Cowen PJ, Harmer CJ (2009) Effect of a single dose of citalopram on amygdala response to emotional faces. Br J Psychiatry 194:535–540.

Nabavi S, Fox R, Proulx CD, Lin JY, Tsien RY, Malinow R (2014) Engineering a memory with LTD and LTP. Nature 511:348–352.

Namburi P, Beyeler A, Yorozu S, Calhoon GG, Halbert SA, Wichmann R, Holden SS, Mertens KL, Anahtar M, Felix-Ortiz AC, Wickersham IR, Gray JM, Tye KM (2015) A circuit mechanism for differentiating positive and negative associations. Nature 520:675–678.

Narayanan RT, Seidenbecher T, Kluge C, Bergado J, Stork O, Pape H-C (2007) Dissociated theta phase synchronization in amygdalo- hippocampal circuits during various stages of fear memory. Eur J Neurosci 25:1823–1831.

Nemeroff CB, Owens MJ (2002) Treatment of mood disorders. Nat Neurosci 5:1068–1070.

Nestler EJ, Barrot M, DiLeone RJ, Eisch AJ, Gold SJ, Monteggia LM (2002) Neurobiology of Depression. Neuron 34:13–25.

Nicoll RA et al. (1988) The current excitement in long term potentiation. Neuron 1:97–103.

Nicoll RA, Malenka RC (1995) Contrasting properties of two forms of long-term potentiation in the hippocampus. Nature 377:115–118.

Nusser Z, Sieghart W, Somogyi P (1998) Segregation of different GABAA receptors to synaptic and extrasynaptic membranes of cerebellar granule cells. J Neurosci 18:1693–1703.

O'Keefe J (1976) Place units in the hippocampus of the freely moving rat. Exp Neurol 51:78–109.

O'Keefe J, Dostrovsky J (1971) The hippocampus as a spatial map. Preliminary evidence

from unit activity in the freely-moving rat.

Oh SW et al. (2014) A mesoscale connectome of the mouse brain. Nature 508:207–214.

Ohno-Shosaku T, Maejima T, Kano M (2001) Endogenous Cannabinoids Mediate Retrograde Signals from Depolarized Postsynaptic Neurons to Presynaptic Terminals. Neuron 29:729–738.

Orsini CA, Kim JH, Knapska E, Maren S (2011) Hippocampal and prefrontal projections to the basal amygdala mediate contextual regulation of fear after extinction. J Neurosci 31:17269–17277.

Ota KT, Pierre VJ, Ploski JE, Queen K, Schafe GE (2008) The NO-cGMP-PKG signaling pathway regulates synaptic plasticity and fear memory consolidation in the lateral amygdala via activation of ERK/MAP kinase. Learn Mem 15:792–805.

Packer AM, Russell LE, Dalgleish HWP, Häusser M (2014) Simultaneous all-optical manipulation and recording of neural circuit activity with cellular resolution in vivo. Nat Methods 12:140–146.

Palchykova S, Winsky-Sommerer R, Meerlo P, Dürr R, Tobler I (2006) Sleep deprivation impairs object recognition in mice. Neurobiol Learn Mem 85:263–271.

Pan B-X, Dong Y, Ito W, Yanagawa Y, Shigemoto R, Morozov A (2009) Selective gating of glutamatergic inputs to excitatory neurons of amygdala by presynaptic GABAb receptor. Neuron 61:917–929.

Panula P, Pirvola U, Auvinen S, Airaksinen MS (1989) Histamine-immunoreactive nerve fibers in the rat brain. Neuroscience 28:585–610.

Pape H-C, Driesang RB (1998) Ionic mechanisms of intrinsic oscillations in neurons of the basolateral amygdaloid complex. J Neurophysiol 79:217–226.

Pape H-C, Paré D (2010) Plastic synaptic networks of the amygdala for the acquisition, expression, and extinction of conditioned fear. Physiol Rev 90:419–463.

Paré D, Collins DR (2000) Neuronal correlates of fear in the lateral amygdala: multiple extracellular recordings in conscious cats. J Neurosci 20:2701–2710.

Paré D, Gaudreau H (1996) Projection cells and interneurons of the lateral and basolateral amygdala: distinct firing patterns and differential relation to theta and delta rhythms in conscious cats. J Neurosci 16:3334–3350.

Paré D, Pape HC, Dong J (1995) Bursting and oscillating neurons of the cat basolateral amygdaloid complex in vivo: electrophysiological properties and morphological features. J Neurophysiol 74:1179–1191.

Pastalkova E, Itskov V, Amarasingham A, Buzsáki G (2008) Internally generated cell assembly sequences in the rat hippocampus. Science 321:1322–1327.

Penzo MA, Robert V, Li B (2014) Fear conditioning potentiates synaptic transmission onto long-range projection neurons in the lateral subdivision of central amygdala. J Neurosci 34:2432–2437.

Pezawas L, Meyer-Lindenberg A, Drabant EM, Verchinski B, Munoz KE, Kolachana BS, Egan MF, Mattay VS, Hariri AR, Weinberger DR (2005) 5-HTTLPR polymorphism impacts human cingulate-amygdala interactions: a genetic susceptibility mechanism for depression. Nat Neurosci 8:828–834.

Pfeffer CK, Xue M, He M, Huang ZJ, Scanziani M (2013) Inhibition of inhibition in visual cortex: the logic of connections between molecularly distinct interneurons. Nat Neurosci 16:1068–1076.

Phelps EA (2004) Human emotion and memory: interactions of the amygdala and hippocampal complex. Curr Opin Neurobiol 14:198–202.

Phillips RG, LeDoux JE (1992) Differential contribution of amygdala and hippocampus to cued and contextual fear conditioning. Behav Neurosci 106:274–285.

Picardo MA, Guigue P, Bonifazi P, Batista-Brito R, Allene C, Ribas A, Fishell G, Baude A, Cossart R (2011) Pioneer GABA cells comprise a subpopulation of hub neurons in the developing hippocampus. Neuron 71:695–709.

Pikkarainen M, Rönkkö S, Savander V, Insausti R, Pitkänen A (1999) Projections from the lateral, basal, and accessory basal nuclei of the amygdala to the hippocampal formation in rat. J Comp Neurol 403:229–260.

Pinard CR, Muller JF, Mascagni F, McDonald AJ (2008) Dopaminergic innervation of interneurons in the rat basolateral amygdala. Neuroscience 157:850–863.

Pinault D (1996) A novel single-cell staining procedure performed in vivo under electrophysiological control: morpho-functional features of juxtacellularly labeled thalamic cells and other central neurons with biocytin or Neurobiotin. J Neurosci Methods 65:113–136.

Pitkänen A (2000) Connectivity of the rat amygdaloid complex. In: The Amygdala: A Functional Analysis (Aggleton JP, ed), pp.31–115. Oxford, UK: Oxford Univ. Press.

Pitkänen A, Pikkarainen M, Nurminen N, Ylinen A (2000) Reciprocal connections between the amygdala and the hippocampal formation, perirhinal cortex, and postrhinal cortex in rat. A review. Ann N Y Acad Sci 911:369–391.

Pitkänen A, Savander V, LeDoux JE (1997) Organization of intra-amygdaloid circuitries in the rat: an emerging framework for understanding functions of the amygdala. Trends Neurosci 20:517–523.

Popa D, Duvarci S, Popescu AT, Léna C, Paré D (2010) Coherent amygdalocortical theta promotes fear memory consolidation during paradoxical sleep. Proc Natl Acad Sci U S A 107:6516–6519.

Popescu AT, Paré D (2011) Synaptic interactions underlying synchronized inhibition in the basal amygdala: evidence for existence of two types of projection cells. J Neurophysiol

105:687–696.

Popescu AT, Popa D, Paré D (2009) Coherent gamma oscillations couple the amygdala and striatum during learning. Nat Neurosci 12:801–807.

Portas CM, Bjorvatn B, Fagerland S, Grønli J, Mundal V, Sørensen E, Ursin R (1998) On-line detection of extracellular levels of serotonin in dorsal raphe nucleus and frontal cortex over the sleep/wake cycle in the freely moving rat. Neuroscience 83:807–814.

Portas CM, Bjorvatn B, Ursin R (2000) Serotonin and the sleep/wake cycle: special emphasis on microdialysis studies. Prog Neurobiol 60:13–35.

Pouille F, Scanziani M (2001) Enforcement of temporal fidelity in pyramidal cells by somatic feed-forward inhibition. Science 293:1159–1163.

Puig MV, Gener T (2015) Serotonin modulation of prefronto-hippocampal rhythms in health and disease. ACS Chem Neurosci.

Rainnie DG (1999) Serotonergic modulation of neurotransmission in the rat basolateral amygdala. J Neurophysiol 82:69–85.

Rainnie DG, Mania I, Mascagni F, McDonald AJ (2006) Physiological and morphological characterization of parvalbumin-containing interneurons of the rat basolateral amygdala. J Comp Neurol 498:142–161.

Ressler KJ, Mayberg HS (2007) Targeting abnormal neural circuits in mood and anxiety disorders: from the laboratory to the clinic. Nat Neurosci 10:1116–1124.

Richardson MP, Strange B a, Dolan RJ (2004) Encoding of emotional memories depends on amygdala and hippocampus and their interactions. Nat Neurosci 7:278–285.

Richmond MA, Murphy CA, Pouzet B, Schmid P, Rawlins JNP, Feldon J (1998) A computer controlled analysis of freezing behaviour. J Neurosci Methods 86:91–99.

Robbins TW (1997) Arousal systems and attentional processes. Biol Psychol 45:57–71.

Rogan MT, Stäubli U V, LeDoux JE (1997) Fear conditioning induces associative long-term potentiation in the amygdala. Nature 390:604–607.

Romanski LM, Clugnet MC, Bordi F, LeDoux JE (1993) Somatosensory and auditory convergence in the lateral nucleus of the amygdala. Behav Neurosci 107:444–450.

Rosen ZB, Cheung S, Siegelbaum SA (2015) Midbrain dopamine neurons bidirectionally regulate CA3-CA1 synaptic drive. Nat Neurosci 18:1763–1771.

Rosenkranz JA, Grace AA (2002) Dopamine-mediated modulation of odour-evoked amygdala potentials during pavlovian conditioning. Nature 417:282–287.

Roux L, Stark E, Sjulson L, Buzsáki G (2014) In vivo optogenetic identification and manipulation of GABAergic interneuron subtypes. Curr Opin Neurobiol 26:88–95.

Royer S, Sirota A, Patel J, Buzsáki G (2010) Distinct representations and theta dynamics in dorsal and ventral hippocampus. J Neurosci 30:1777–1787.

Ruiz A, Campanac E, Scott RS, Rusakov DA, Kullmann DM (2010) Presynaptic GABAA receptors enhance transmission and LTP induction at hippocampal mossy fiber synapses. Nat Neurosci 13:431–438.

Ryan SJ, Ehrlich DE, Jasnow AM, Daftary S, Madsen TE, Rainnie DG (2012) Spike-timing precision and neuronal synchrony are enhanced by an interaction between synaptic inhibition and membrane oscillations in the amygdala. PLoS One 7:e35320.

Sah P, Faber ESL, Lopez De Armentia M, Power J (2003) The amygdaloid complex: anatomy and physiology. Physiol Rev 83:803–834.

Sah P, Mahanty NK (1998) Calcium-permeable AMPA receptors mediate long-term potentiation in interneurons in the amygdala. Nature 394:683–687.

Saha S, Gamboa-Esteves FO, Batten TFC (2010) Differential distribution of 5-HT 1A and 5-HT 1B-like immunoreactivities in rat central nucleus of the amygdala neurones projecting to the caudal dorsomedial medulla oblongata. Brain Res 1330:20–30.

Sakai K (2011) Sleep-waking discharge profiles of dorsal raphe nucleus neurons in mice. Neuroscience 197:200–224.

Samson RD, Dumont EC, Paré D (2003) Feedback inhibition defines transverse processing modules in the lateral amygdala. J Neurosci 23:1966–1973.

Samson RD, Paré D (2006) A spatially structured network of inhibitory and excitatory connections directs impulse traffic within the lateral amygdala. Neuroscience 141:1599–1609.

Sarkar A, Chachra P, Vaidya VA (2014) Postnatal fluoxetine-evoked anxiety is prevented by concomitant 5-HT2A/C receptor blockade and mimicked by postnatal 5-HT2A/C receptor stimulation. Biol Psychiatry 76:858–868.

Savander V, Go CG, LeDoux JE, Pitkänen A (1995) Intrinsic connections of the rat amygdaloid complex: projections originating in the basal nucleus. J Comp Neurol 361:345–368.

Scanziani M (2000) GABA Spillover Activates Postsynaptic GABAB Receptors to Control Rhythmic Hippocampal Activity. Neuron 25:673–681.

Schafe GE, Bauer EP, Rosis S, Farb CR, Rodrigues SM, LeDoux JE (2005) Memory consolidation of Pavlovian fear conditioning requires nitric oxide signaling in the lateral amygdala. Eur J Neurosci 22:201–211.

Scholz KP, Miller RJ (1991) GABAB receptor-mediated inhibition of Ca2+ currents and synaptic transmission in cultured rat hippocampal neurones. J Physiol 444:669–686.

Schweimer J V, Ungless MA (2010) Phasic responses in dorsal raphe serotonin neurons to noxious stimuli. Neuroscience 171:1209–1215.

Segal M, Barker JL (1984) Rat hippocampal neurons in culture: voltage-clamp analysis of inhibitory synaptic connections. J Neurophysiol 52:469–487.

Seidenbecher T, Laxmi TR, Stork O, Pape H-C (2003) Amygdalar and hippocampal theta rhythm synchronization during fear memory retrieval. Science 301:846–850.

Selden NRW, Everitt BJ, Jarrard LE, Robbins TW (1991) Complementary roles for the amygdala and hippocampus in aversive conditioning to explicit and contextual cues. Neuroscience 42:335–350.

Selig DK, Hjelmstad GO, Herron C, Nicoll RA, Malenka RC (1995) Independent mechanisms for long-term depression of AMPA and NMDA responses. Neuron 15:417–426.

Semba K, Pastorius J, Wilkinson M, Rusak B (2001) Sleep deprivation-induced c-fos and junB expression in the rat brain: effects of duration and timing. Behav Brain Res 120:75–86.

Senn V, Wolff SBE, Herry C, Grenier F, Ehrlich I, Gründemann J, Fadok JP, Müller C, Letzkus JJ, Lüthi A (2014) Long-range connectivity defines behavioral specificity of amygdala neurons. Neuron 81:428–437.

Shaban H, Humeau Y, Herry C, Cassasus G, Shigemoto R, Ciocchi S, Barbieri S, van der Putten H, Kaupmann K, Bettler B, Lüthi A (2006) Generalization of amygdala LTP and conditioned fear in the absence of presynaptic inhibition. Nat Neurosci 9:1028–1035.

Shen RY, Andrade R (1998) 5-Hydroxytryptamine2 receptor facilitates GABAergic neurotransmission in rat hippocampus. J Pharmacol Exp Ther 285:805–812.

Shi C, Davis M (2001) Visual pathways involved in fear conditioning measured with fear-potentiated startle: behavioral and anatomic studies. J Neurosci 21:9844–9855.

Shi CJ, Cassell MD (1997) Cortical, thalamic, and amygdaloid projections of rat temporal cortex. J Comp Neurol 382:153–175.

Shi CJ, Cassell MD (1998a) Cortical, thalamic, and amygdaloid connections of the anterior and posterior insular cortices. J Comp Neurol 399:440–468.

Shi CJ, Cassell MD (1998b) Cascade projections from somatosensory cortex to the rat basolateral amygdala via the parietal insular cortex. J Comp Neurol 399:469–491.

Shi CJ, Cassell MD (1999) Perirhinal cortex projections to the amygdaloid complex and hippocampal formation in the rat. J Comp Neurol 406:299–328.

Shin LM, Liberzon I (2010) The neurocircuitry of fear, stress, and anxiety disorders. Neuropsychopharmacology 35:169–191.

Shin LM, Rauch SL, Pitman RK (2006) Amygdala, medial prefrontal cortex, and hippocampal function in PTSD. Ann N Y Acad Sci 1071:67–79.

Sigurdsson T, Doyère V, Cain CK, LeDoux JE (2007) Long-term potentiation in the amygdala: a cellular mechanism of fear learning and memory. Neuropharmacology 52:215–227.

Silva AJ, Paylor R, Wehner JM, Tonegawa S (1992) Impaired spatial learning in alpha-calcium-calmodulin kinase II mutant mice. Science 257:206–211.

Silva RH, Kameda SR, Carvalho RC, Takatsu-Coleman AL, Niigaki ST, Abílio VC, Tufik S, Frussa-Filho R (2004) Anxiogenic effect of sleep deprivation in the elevated plus-maze test in mice. Psychopharmacology (Berl) 176:115–122.

Silvestri AJ (2005) REM sleep deprivation affects extinction of cued but not contextual fear conditioning. Physiol Behav 84:343–349.

Sinfield JL, Collins DR (2006) Induction of synchronous oscillatory activity in the rat lateral amygdala in vitro is dependent on gap junction activity. Eur J Neurosci 24:3091–3095.

Smiley JF, McGinnis JP, Javitt DC (2000) Nitric oxide synthase interneurons in the monkey cerebral cortex are subsets of the somatostatin, neuropeptide Y, and calbindin cells. Brain Res 863:205–212.

Smith Y, Paré D (1994) Intra-amygdaloid projections of the lateral nucleus in the cat: PHA-L

anterograde labeling combined with postembedding GABA and glutamate immunocytochemistry. J Comp Neurol 342:232–248.

Soghomonian JJ, Martin DL (1998) Two isoforms of glutamate decarboxylase: Why? In: Trends in Pharmacological Sciences, pp.500–505. Elsevier.

Somogyi P, Takagi H, Richards JG, Mohler H (1989) Subcellular localization of benzodiazepine/GABAA receptors in the cerebellum of rat, cat, and monkey using monoclonal antibodies. J Neurosci 9:2197–2209.

Sosulina L, Meis S, Seifert G, Steinhäuser C, Pape H-C (2006) Classification of projection neurons and interneurons in the rat lateral amygdala based upon cluster analysis. Mol Cell Neurosci 33:57–67.

Sosulina L, Schwesig G, Seifert G, Pape H-C (2008) Neuropeptide Y activates a G-protein-coupled inwardly rectifying potassium current and dampens excitability in the lateral amygdala. Mol Cell Neurosci 39:491–498.

Spampanato J, Polepalli J, Sah P (2011) Interneurons in the basolateral amygdala. Neuropharmacology 60:765–773.

Spannuth BM, Hale MW, Evans AK, Lukkes JL, Campeau S, Lowry CA (2011) Investigation of a central nucleus of the amygdala/dorsal raphe nucleus serotonergic circuit implicated in fear-potentiated startle. Neuroscience 179:104–119.

Sparta DR, Smithuis J, Stamatakis AM, Jennings JH, Kantak PA, Ung RL, Stuber GD (2014) Inhibition of projections from the basolateral amygdala to the entorhinal cortex disrupts the acquisition of contextual fear. Front Behav Neurosci 8:129.

Spedding M, Jay T, Costa e Silva J, Perret L (2005) A pathophysiological paradigm for the therapy of psychiatric disease. Nat Rev Drug Discov 4:467–476.

Sreepathi HK, Ferraguti F (2012) Subpopulations of neurokinin 1 receptor-expressing neurons in the rat lateral amygdala display a differential pattern of innervation from

distinct glutamatergic afferents. Neuroscience 203:59–77.

Staley KJ, Mody I (1992) Shunting of excitatory input to dentate gyrus granule cells by a depolarizing GABAA receptor-mediated postsynaptic conductance. J Neurophysiol 68:197–212.

Steinbusch HWM (1981) Distribution of serotonin-immunoreactivity in the central nervous system of the rat—Cell bodies and terminals. Neuroscience 6:557–618.

Stell BM, Rostaing P, Triller A, Marty A (2007) Activation of Presynaptic GABAA Receptors Induces Glutamate Release from Parallel Fiber Synapses. J Neurosci 27:9022–9031.

Stenman J, Toresson H, Campbell K (2003) Identification of two distinct progenitor populations in the lateral ganglionic eminence: implications for striatal and olfactory bulb neurogenesis. J Neurosci 23:167–174.

Stuber GD, Sparta DR, Stamatakis AM, van Leeuwen WA, Hardjoprajitno JE, Cho S, Tye KM, Kempadoo KA, Zhang F, Deisseroth K, Bonci A (2011) Excitatory transmission from the amygdala to nucleus accumbens facilitates reward seeking. Nature 475:377–380.

Stujenske JM, Likhtik E, Topiwala MA, Gordon JA (2014) Fear and safety engage competing patterns of theta-gamma coupling in the basolateral amygdala. Neuron 83:919–933.

Südhof TC (2004) The synaptic vesicle cycle. Annu Rev Neurosci 27:509–547.

Sur C, Betz H, Schloss P (1996a) Immunocytochemical detection of the serotonin transporter in rat brain. Neuroscience 73:217–231.

Sur C, Betz H, Schloss P (1996b) Immunocytochemical detection of the serotonin transporter in rat brain. Neuroscience 73:217–231.

Sutton MA, Schuman EM (2006) Dendritic Protein Synthesis, Synaptic Plasticity, and

Memory. Cell 127:49–58.

Swanson L, Petrovich G (1998) What is the amygdala? Trends Neurosci 21:323–331.

Syvälahti E, Penttilä J, Majasuo H, Pälvimäki E-P, Laakso A, Hietala J (2006) Combined treatment with citalopram and buspirone: effects on serotonin 5-HT2A and 5-HT2C receptors in the rat brain. Pharmacopsychiatry 39:1–8.

Szabadics J, Tamás G, Soltesz I (2007) Different transmitter transients underlie presynaptic cell type specificity of GABAA,slow and GABAA,fast. Proc Natl Acad Sci U S A 104:14831–14836.

Szabadics J, Varga C, Molnár G, Oláh S, Barzó P, Tamás G (2006) Excitatory effect of GABAergic axo-axonic cells in cortical microcircuits. Science 311:233–235.

Szinyei C, Heinbockel T, Montagne J, Pape HC (2000) Putative cortical and thalamic inputs elicit convergent excitation in a population of GABAergic interneurons of the lateral amygdala. J Neurosci 20:8909–8915.

Szinyei C, Narayanan RT, Pape H-C (2007) Plasticity of inhibitory synaptic network interactions in the lateral amygdala upon fear conditioning in mice. Eur J Neurosci 25:1205–1211.

Tamamaki N, Tomioka R (2010) Long-Range GABAergic Connections Distributed throughout the Neocortex and their Possible Function. Front Neurosci 4:202.

Taniguchi H, He M, Wu P, Kim S, Paik R, Sugino K, Kvitsiani D, Kvitsani D, Fu Y, Lu J, Lin Y, Miyoshi G, Shima Y, Fishell G, Nelson SB, Huang ZJ (2011) A resource of Cre driver lines for genetic targeting of GABAergic neurons in cerebral cortex. Neuron 71:995–1013.

Thomas GM, Huganir RL (2004) MAPK cascade signalling and synaptic plasticity. Nat Rev Neurosci 5:173–183.

Thompson SM, Capogna M, Scanziani M (1993) Presynaptic inhibition in the hippocampus.

Trends Neurosci 16:222–227.

Thompson SM, Gähwiler BH (1989) Activity-dependent disinhibition. I. Repetitive stimulation reduces IPSP driving force and conductance in the hippocampus in vitro. J Neurophysiol 61:501–511.

Tomioka R, Okamoto K, Furuta T, Fujiyama F, Iwasato T, Yanagawa Y, Obata K, Kaneko T, Tamamaki N (2005) Demonstration of long-range GABAergic connections distributed throughout the mouse neocortex. Eur J Neurosci 21:1587–1600.

Torres GE, Amara SG (2007) Glutamate and monoamine transporters: new visions of form and function. Curr Opin Neurobiol 17:304–312.

Tovote P, Fadok JP, Lüthi A (2015) Neuronal circuits for fear and anxiety. Nat Rev Neurosci 16:317–331.

Tran L, Lasher BK, Young KA, Keele NB (2013) Depletion of serotonin in the basolateral amygdala elevates glutamate receptors and facilitates fear-potentiated startle. Transl Psychiatry 3:e298.

Tricoire L, Vitalis T (2012) Neuronal nitric oxide synthase expressing neurons: a journey from birth to neuronal circuits. Front Neural Circuits 6:82.

Trouche S, Sasaki JM, Tu T, Reijmers LG (2013) Fear extinction causes target-specific remodeling of perisomatic inhibitory synapses. Neuron 80:1054–1065.

Truitt W a, Johnson PL, Dietrich a D, Fitz SD, Shekhar a (2009) Anxiety-like behavior is modulated by a discrete subpopulation of interneurons in the basolateral amygdala. Neuroscience 160:284–294.

Tsvetkov E et al. (2002) Fear Conditioning Occludes LTP-Induced Presynaptic Enhancement of Synaptic Transmission in the Cortical Pathway to the Lateral Amygdala. Neuron 34:289–300.

Tsvetkov E, Shin R-M, Bolshakov VY (2004) Glutamate Uptake Determines Pathway Specificity of Long-Term Potentiation in the Neural Circuitry of Fear Conditioning. Neuron 41:139–151.

Tukker JJ, Fuentealba P, Hartwich K, Somogyi P, Klausberger T (2007) Cell type-specific tuning of hippocampal interneuron firing during gamma oscillations in vivo. J Neurosci 27:8184–8189.

Tully K, Li Y, Tsvetkov E, Bolshakov VY (2007) Norepinephrine enables the induction of associative long-term potentiation at thalamo-amygdala synapses. Proc Natl Acad Sci U S A 104:14146–14150.

Turrigiano G (2012) Homeostatic Synaptic Plasticity: Local and Global Mechanisms for Stabilizing Neuronal Function. Cold Spring Harb Perspect Biol 4:a005736–a005736.

Tye KM (2014) Neural circuit reprogramming: a new paradigm for treating neuropsychiatric disease? Neuron 83:1259–1261.

Tye KM, Prakash R, Kim S-Y, Fenno LE, Grosenick L, Zarabi H, Thompson KR, Gradinaru V, Ramakrishnan C, Deisseroth K (2011) Amygdala circuitry mediating reversible and bidirectional control of anxiety. Nature 471:358–362.

Uher R, McGuffin P (2010) The moderation by the serotonin transporter gene of environmental adversity in the etiology of depression: 2009 update. Mol Psychiatry 15:18–22.

Usunoff KG, Itzev DE, Rolfs a, Schmitt O, Wree a (2006) Nitric oxide synthase-containing neurons in the amygdaloid nuclear complex of the rat. Anat Embryol (Berl) 211:721–737.

Varga V, Losonczy A, Zemelman B V, Borhegyi Z, Nyiri G, Domonkos A, Hangya B, Holderith N, Magee JC, Freund TF (2009) Fast synaptic subcortical control of hippocampal circuits. Science 326:449–453.

Veening JG, Swanson LW, Sawchenko PE (1984) The organization of projections from the central nucleus of the amygdala to brainstem sites involved in central autonomic regulation: a combined retrograde transport-immunohistochemical study. Brain Res 303:337–357.

Vertes RP, Fortin WJ, Crane AM (1999) Projections of the median raphe nucleus in the rat. J Comp Neurol 407:555–582.

Vicini S, Ferguson C, Prybylowski K, Kralic J, Morrow AL, Homanics GE (2001) GABA(A) receptor alpha1 subunit deletion prevents developmental changes of inhibitory synaptic currents in cerebellar neurons. J Neurosci 21:3009–3016.

Vigot R, Barbieri S, Bräuner-Osborne H, Turecek R, Shigemoto R, Zhang Y-P, Luján R, Jacobson LH, Biermann B, Fritschy J-M, Vacher C-M, Müller M, Sansig G, Guetg N, Cryan JF, Kaupmann K, Gassmann M, Oertner TG, Bettler B (2006) Differential Compartmentalization and Distinct Functions of GABAB Receptor Variants. Neuron 50:589–601.

Vouimba R-M, Yaniv D, Richter-Levin G (2007) Glucocorticoid receptors and beta-adrenoceptors in basolateral amygdala modulate synaptic plasticity in hippocampal dentate gyrus, but not in area CA1. Neuropharmacology 52:244–252.

Vyazovskiy V V, Riedner BA, Cirelli C, Tononi G (2007) Sleep homeostasis and cortical synchronization: II. A local field potential study of sleep slow waves in the rat. Sleep 30:1631–1642.

Waclaw RR, Ehrman LA, Pierani A, Campbell K (2010) Developmental origin of the neuronal subtypes that comprise the amygdalar fear circuit in the mouse. J Neurosci 30:6944–6953.

Wang H-Y, Kuo Z-C, Fu Y-S, Chen R-F, Min M-Y, Yang H-W (2015) GABAB receptor-

mediated tonic inhibition regulates the spontaneous firing of locus coeruleus neurons in developing rats and in citalopram-treated rats. J Physiol 593:161–180.

Watanabe Y, Ikegaya Y, Saito H, Abe K (1995) Roles of GABAA, NMDA and muscarinic receptors in induction of long-term potentiation in the medial and lateral amygdala in vitro. Neurosci Res 21:317–322.

Wellman CL, Izquierdo A, Garrett JE, Martin KP, Carroll J, Millstein R, Lesch K-P, Murphy DL, Holmes A (2007) Impaired stress-coping and fear extinction and abnormal corticolimbic morphology in serotonin transporter knock-out mice. J Neurosci 27:684–691.

West M (1999) Stereological methods for estimating the total number of neurons and synapses: issues of precision and bias. Trends Neurosci 22:51–61.

Whitlock JR, Heynen AJ, Shuler MG, Bear MF (2006) Learning induces long-term potentiation in the hippocampus. Science (80-) 313:1093–1097.

Wilson RI, Nicoll RA (2001) Endogenous cannabinoids mediate retrograde signalling at hippocampal synapses. Nature 410:588–592.

Wolff SBE, Gründemann J, Tovote P, Krabbe S, Jacobson G a, Müller C, Herry C, Ehrlich I, Friedrich RW, Letzkus JJ, Lüthi A (2014) Amygdala interneuron subtypes control fear learning through disinhibition. Nature 509:453–458.

Wonders CP, Anderson SA (2006) The origin and specification of cortical interneurons. Nat Rev Neurosci 7:687–696.

Woodruff AR, Sah P (2007a) Networks of parvalbumin-positive interneurons in the basolateral amygdala. J Neurosci 27:553–563.

Woodruff AR, Sah P (2007b) Inhibition and synchronization of basal amygdala principal neuron spiking by parvalbumin-positive interneurons. J Neurophysiol 98:2956–2961.

Woolf NJ, Butcher LL (1982) Cholinergic projections to the basolateral amygdala: A

combined Evans Blue and acetylcholinesterase analysis. Brain Res Bull 8:751–763.

Xiao C, Zhou C, Li K, Ye J-H (2007) Presynaptic GABAA receptors facilitate GABAergic transmission to dopaminergic neurons in the ventral tegmental area of young rats. J Physiol 580:731–743.

Xu Q, Tam M, Anderson SA (2008) Fate mapping Nkx2.1-lineage cells in the mouse telencephalon. J Comp Neurol 506:16–29.

Yamamoto R, Hatano N, Sugai T, Kato N (2014) Serotonin induces depolarization in lateral amygdala neurons by activation of TRPC-like current and inhibition of GIRK current depending on 5-HT2C receptor. Neuropharmacology 82C:49–58.

Yoo S-S, Gujar N, Hu P, Jolesz FA, Walker MP (2007) The human emotional brain without sleep--a prefrontal amygdala disconnect. Curr Biol 17:R877–R878.

Young AW, Aggleton JP, Hellawell DJ, Johnson M, Broks P, Hanley JR (1995) Face processing impairments after amygdalotomy. Brain 118:15–24.

Zanoveli JM, Carvalho MC, Cunha JM, Brandão ML (2009) Extracellular serotonin level in the basolateral nucleus of the amygdala and dorsal periaqueductal gray under unconditioned and conditioned fear states: an in vivo microdialysis study. Brain Res 1294:106–115.

Zhang C-L, Houbaert X, Lepleux M, Deshors M, Normand E, Gambino F, Herzog E, Humeau Y (2015) The hippocampo-amygdala control of contextual fear expression is affected in a model of intellectual disability. Brain Struct Funct 220:3673–3682.

Zhang J, Muller JF, McDonald AJ (2013) Noradrenergic innervation of pyramidal cells in the rat basolateral amygdala. Neuroscience 228:395–408.

Zucker RS, Regehr WG (2002) Short-Term Synaptic Plasticity. Annu Rev Physiol 64:355–405.